Electronic Thesis and Dissertation Repository

3-6-2020 2:00 PM

Paleoproductivity of Late Holocene Lake Huron

Jamal Khaled Nigim, *The University of Western Ontario*

Supervisor: Longstaffe, Fred, *The University of Western Ontario*
A thesis submitted in partial fulfillment of the requirements for the Master of Science degree in Geology
© Jamal Khaled Nigim 2020

Recommended Citation

Nigim, Jamal Khaled, "Paleoproductivity of Late Holocene Lake Huron" (2020). *Electronic Thesis and Dissertation Repository*. 6907.
https://ir.lib.uwo.ca/etd/6907

ABSTRACT

The paleolimnology of North America's Lake Huron is described using lead-210 dating, mineralogy, magnetic susceptibility, total organic carbon (TOC), total nitrogen (TN), carbon:nitrogen (C/N) ratio, grain size, and the $\delta^{13}C_{OM}$ and $\delta^{15}N_{TN}$ of organic matter. Sediment cores from Lake Huron's 6 depositional basins and Georgian Bay span the Medieval Warm Period, Little Ice Age, and Canadian-European settlement. The main organic matter source is lacustrine algae, as indicated by $\delta^{13}C_{OM}$, $\delta^{15}N_{TN}$ and C/N. Prior to the 19th century, primary production changes are reflected only by small variations in TOC and TN. A gradual increase in $\delta^{15}N_{TN}$ (~1.1 ‰) suggests an increase in primary production since the start of the Industrial Revolution, likely due to warming and rising nutrient input. Deforestation, primarily during the 19th century, contributed to a rise in TOC in the Huron basin. Further land clearance likely caused a prominent increase in magnetic susceptibility during the early- to mid-20th century.

SUMMARY FOR LAY AUDIENCE

The environmental history of Lake Huron and Georgian Bay was reconstructed by measuring different components preserved in sediment cores. The sediment cores were collected from 7 different locations in the lake. The sediment records periods of natural climate change, including the Medieval Warm Period and the Little Ice Age. The impact of human activity since the Industrial Revolution is also recorded in the sediment. The main contributor of organic matter in the sediment is algae, which was indicated by the isotope composition and the ratio of carbon to nitrogen. Increasing temperature and rising nutrient input since the Industrial Revolution likely increased the quantity of algae being produced. Deforestation, primarily during the 19th century, contributed to a rise in organic carbon. Further land clearance due to human settlement and urbanization caused a significant increase in material, including magnetic minerals, entering Lake Huron during the early- to mid-20th century.

ACKNOWLEDGEMENTS

TABLE OF CONTENTS

LIST OF TABLES

LIST OF FIGURES

LIST OF APPENDICES

Chapter 1

1   Introduction

1.1   Overview

The Laurentian Great Lakes (LGL) watershed (Figure 1.1) covers an area about 765,990

km^2 and is home to one-third of all Canadians (Larson and Schaetzl 2001). The LGL are a

system of interconnected lakes, inflowing, outflowing and connecting rivers, surrounding

wetlands, and smaller water bodies. They represent the largest freshwater system in the world by

surface area and second largest by volume (Gronewold et al. 2013). Lake Superior lies at the

head of the LGL and is the largest by volume. Lake Huron is hydrologically connected to Lake

Michigan and receives the water of Lake Michigan via the Straits of Mackinac and Lake

Superior via the St. Mary River. Lake Huron discharges via the St. Clair River to Lake St. Clair

and the Detroit River, which then drains into Lake Erie and afterwards Lake Ontario. Lake

Ontario's outflow is via the 1,200 km-long St. Lawrence River, which flows into the Atlantic

Ocean (International Upper Great Lakes Study Board 2012).

The Huron basin covers an area of 59,600 km^2, has an average depth of 59 m, and a

volume of 3,540 km^3 (Colborn et al. 1990). It also shares an international border between Canada

(Ontario) and the United States of America (Michigan). The lake is separated from Georgian Bay

by a submerged bedrock sill. The North Channel lies north of Manitoulin, Drummond, and

Cockburn Islands. Georgian Bay and the North Channel have separate sediment regimes from

the Lake Huron basins (Thomas et al. 1973). Lake Huron's watershed (118,000 km^2) and long

resident time (22 years) make it vulnerable to water quality impacts that originate in its

watershed. Upland areas represent much of the current watershed and include both natural

habitats and developed areas. Remnants of Carolinian forest still exist in the southern-most sub-

watersheds and large areas of Great Lakes St. Lawrence mixed-wood forest are found in parts of Michigan and Ontario (Environment and Climate Change Canada and the U.S. Environmental Protection Agency 2018).

The Lake Huron watershed was initially inhabited by several Native American tribes prior to European settlement. Europeans first visited the area in the early 16th century. The earliest permanent European settlement on the Great Lakes was established at Ste. Marie on the banks of the Wye River near Georgian Bay in 1639 CE. This settlement was founded by French Jesuit missionaries as a central base for missions with the Huron Nation ("Ste. Marie Among the Hurons" 2005). By the 1800s, small villages began to arise near fur trade posts in the vicinity of Lake Huron and Georgian Bay. As the fur trade declined, early settlers turned to fishing and lumber operations (Riley 2013).

Presently, Lake Huron provides about 1.5 million L of freshwater per day to the public, and agricultural, industrial, and thermoelectric power industries. Agricultural operations are most dense on Ontario's southeast shores of Lake Huron and in Michigan's Saginaw Bay area. High-density confined animal feeding operations in the watershed can generate large quantities of animal waste and excess nutrients which may enter Lake Huron (Environment and Climate Change Canada and the U.S. Environmental Protection Agency 2018). Residential, urban, and development along the shores of Lake Huron and Georgian Bay can disrupt natural water flows, generate nutrients from fertilizers, and cause sediment pollution from land clearing and road development. Moreover, septic systems that are failing can contribute bacteria and phosphorus to the waterways (Environment and Climate Change Canada and the U.S. Environmental Protection Agency 2018). An increase in nutrient input can lead to eutrophication. This may result in changes to plant and animal biomass, turbidity, sedimentation rates, oxygen concentrations, and

the release of nutrients and other chemicals from sediments into the water column. Changes to the lake arising from eutrophication such as algal blooms, water taste and odour changes, and aquatic macrophyte growth can negatively impact humans.

The LGL have undergone several natural and anthropogenic shifts in climate during the Late Holocene. Generally warm conditions were recorded between 800 and 1100 CE (Common Era) during the Medieval Warm Period (MWP). Cool conditions were recorded between 1600 and 1850 CE during the Little Ice Age (LIA). The timing and nature of these regimes, however, varies between regions (PAGES 2k Consortium 2013). More recently, on a global scale, warming from pre-industrial levels to the 2006–2015 decade is assessed to be 0.87°C (IPCC 2019). Summer surface water temperatures in Lake Huron have increased 2.9°C between 1968 and 2002 CE (Dobiez and Lester 2009). Furthermore, annual lake ice coverage decreased on average about 2% per year between 1973 and 2010 (Austin and Colman 2007; Wang et al. 2012).

Lake Huron's environmental response to changing climatic conditions and anthropogenic impacts, as recorded in the organic matter (OM) of its sediments, has not previously been examined. By examining how OM within Lake Huron changed throughout its history, a better understanding of how production and OM sources within Lake Huron have changed in relation to past and future climate change and human activities can be developed. Moreover, a useful frame of reference for anticipating the consequences of future climate change and anthropogenic impacts can be established.
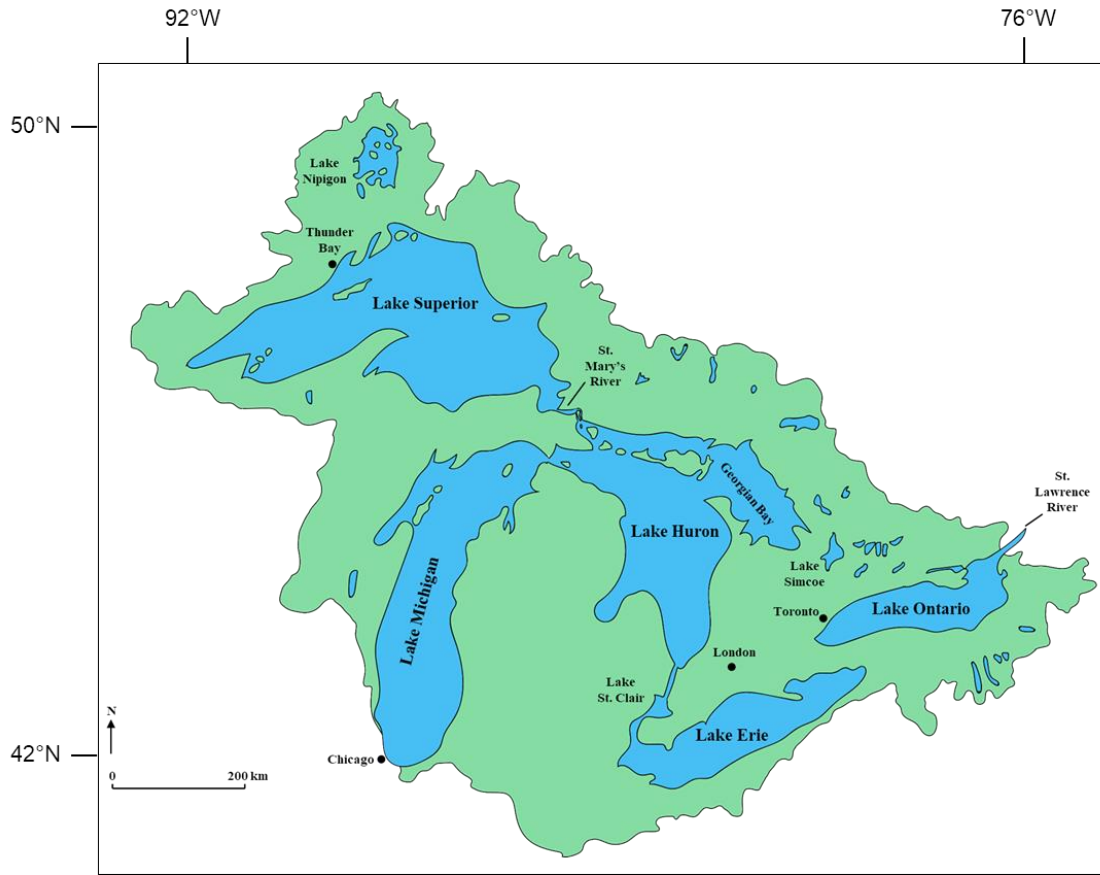
Figure 1.1. Map of the Great Lakes watershed. Significant rivers and cities are also shown.

1.2   Research Questions

This study aims to reconstruct the paleoproduction of Lake Huron and Georgian Bay using a variety of proxies preserved in sediment cores that span the last ~2000 cal BP. This study specifically focuses on the last two hundred years, when anthropogenic impacts, particularly since the onset of the industrial revolution, have affected the lake. My research questions are:

i. How has primary production and the source of the organic matter (OM) in the Huron basin changed over the last 2000 years, and how are these changes related to shifts in climate and to anthropogenic impacts?

ii. How has the mineralogy and physical properties of the sediment in the Huron basin changed over the last 2000 years, and how are these changes related to shifts in climate and to anthropogenic impacts?

iii. Is there any evidence of human activity preserved in the sediments of Lake Huron? What effect has human activity, such as agriculture and forest clear-cutting, had on the OM contribution in Lake Huron?

To answer these research questions, the Total Organic Carbon (TOC), Total Nitrogen (TN), Carbon/Nitrogen (C/N) ratios, and the stable carbon-isotope ($\delta^{13}C_{OM}$) and nitrogen-isotope ($\delta^{15}N_{OM}$) compositions of bulk sediment OM, were measured. In addition, grain size, mineralogical, and magnetic susceptibility analysis was performed and, where possible, an age-depth model was constructed, largely using ^{210}Pb dating, but also one radiocarbon date available

for the Goderich basin. Human activity such as the establishment of settlements, agriculture, forest-clear cutting, and population growth around Lake Huron has been examined to identify any possible correlations. This multi-proxy approach provides an estimate of primary production and/or OM source changes to Lake Huron (Meyers 2003).

1.3   Research Context

1.3.1   Laurentian Great Lakes

The LGL is a by-product of multiple glaciations during the late Cenozoic (Larson and Schaetzl 2001). Moreover, redirected drainage, in particular during the retreat of the LIS, contributed to the origin of the Great Lakes watershed (Larson and Schaetzl 2001). The Great Lakes watershed can be divided into two main regions: (i) a southern, lowland region underlain by relatively gently-dipping sedimentary rocks of Paleozoic age, and (ii) a northern, upland region underlain by granitic rocks, gneiss, and metamorphosed volcanic and sedimentary rocks of Precambrian age (Fenneman 1938; Hough 1958; Dickas 1986). In general, the lowland region is covered by a continuous layer of glacial sediments that are commonly greater than 50 m in thickness and occasionally reach up to 350 m (Rieck and Winters 1993; Soller 1998). The Huron basin, which includes Georgian Bay and the Nipissing lowland, resides in the lowland region.

The Superior, Michigan, Huron, Ontario, and Erie basins originated primarily from the channeling of ice flow along major bedrock valley systems that predate glaciation, and from an increase in erosion and glacial scouring of weak bedrock (Fenneman 1938; Hough 1958; Cvancara and Melik 1961; Wold et al. 1981). The ancestral Great Lakes were shallower than the present Great Lakes, which have been deepened by glacial scour (Rieck and Winters 1982). The degree of scour, however, varies across the basins and within individual basins. The Huron basin,

for example, tends to be irregular due to the presence of resistant bedrock layers. The Huron basin is underlain by Quaternary sediments with varying thickness that can exceed 100 m (Soller 1993, 1998). Overall, the lake floor topography is the product of glacial erosion and glacial and post-glacial deposition.

The Great Lakes watershed has undergone multiple glaciations. The last glaciation, which reached its maximum extent at about 18 to 21 ^{14}C ka, is referred to as the Wisconsin glaciation (Dyke et al. 2003). During the Wisconsin glaciation, the LIS, which was centered in northern and eastern Canada, extended southward and eventually covered the Great Lakes watershed. The retreat of the southern margin of the LIS allowed for the formation of large proglacial lakes between the ice margin to the north and the high topography to the south. By about 9 ^{14}C ka the ice margin had completely withdrawn from the Great Lakes watershed (Karrow et al. 2000). Isostatic uplift, however, continued to affect the development of the Great Lakes. The current configuration of the Great Lakes and their connecting channels was established when all drainage from the upper Great Lakes was captured by the St. Clair River at Port Huron-Sarnia after 5 ^{14}C ka (Lewis et al. 2007).

1.3.2 Glacial Lake Agassiz and its Effect on the Huron Basin

Glacial Lake Agassiz formed about 11.7 ^{14}C ka as the margin of the LIS retreated northward into the Hudson Bay watershed (Fenton et al. 1983; Teller 1985). At its maximum extent, Lake Agassiz covered an area about 350,000 km^2, making it the largest of the proglacial lakes that formed following the retreat of the LIS (Teller 1995). The low δ^{18}O and low salinity of Lake Agassiz suggests that it was dominated by glacial meltwater (Buhay and Betcher 1998; Moore et al. 2000). It has been proposed that glacial Lake Agassiz drained to the south via the

Mississippi River to the Gulf of Mexico. It is also suggested that the onset of the Younger Dryas cooling event at 12,000 cal BP was caused by a change in meltwater routing to an eastern outlet that flowed through the Great Lakes and into the North Atlantic Ocean (Broecker et al. 1989). Meltwater entering the North Atlantic Ocean via the St. Lawrence River suppressed thermohaline circulation causing an abrupt change in climate (Broecker et al. 1989). In an alternative model, Murton et al. (2010) identified gravels and regional erosion surfaces throughout the Mackenzie River system and suggest that Lake Agassiz instead drained through a northwest outlet into the Arctic Ocean. Still others, however, suggest that Lake Agassiz did not drain into the North Atlantic or Arctic Ocean, at least not significantly, but instead evaporated (Birks et al. 2007; Fisher and Lowell 2012). Following the collapse of the LIS and drainage of GLA and glacial Lake Ojibway to Hudson Bay after 9 ka BP, the water supply to the Huron basin was limited to local sources and subsequently lake levels fell (Lewis et al. 1994). During the final stages of deglaciation, proglacial lake waters inundated the Huron basin (Hansel et al. 1985; Eschman and Karrow 1985; Karrow 1987; Lewis and Anderson 1989).

1.3.2 Modern Sedimentation in Lake Huron

It is important to understand present-day rates of sedimentation as sediments act as major sinks for incoming material, including OM. Lake Huron can be separated into depositional and non-depositional zones (Figure 1.2). In depositional basins, fine-grained sediments (mainly clay- and silt-sized particles) are actively accumulating. Non-depositional zones, alternatively, are composed of bedrock, till, and glaciolacustrine clay or sand (Kemp and Harper 1977). Modern sediment accumulation in Lake Huron occurs in the Mackinac, Manitoulin, Alpena, Saginaw, Port Huron, and Goderich basins. It is also occurring in the Flowerpot, Cabot, Nottawasaga, and

French River basins, and the Lion's and Owen Sound troughs of Georgian Bay (Kemp and Harper 1977).

The Mackinac and Manitoulin basins are characterized by a complex undulating topography and discontinuous mud deposits. By comparison, the Alpena, Saginaw, Port Huron, and Goderich basins are characterized by gentle relief and continuous sediment deposits (Thomas et al. 1973; Kemp and Harper 1977). In the Mackinac basin, sediment is continuously deposited in most of the basin except in zones where the undulations have large relief or are steep-sided. The Manitoulin basin, the largest in Lake Huron, has a more complex undulating topography (Thomas et al. 1973). The irregular bathymetry of the Manitoulin and Mackinac basins is closely related to bed-rock features. The troughs may have resulted from post-Silurian solution weathering and collapse of Salina Formation gypsum and salt beds that overlie Guelph dolomites. The peaks may be controlled by patch and pinnacle reefs that developed in the Middle Silurian Guelph Formation (Thomas et al. 1973).

The sediments of Lake Huron are derived from several sources, including river and stream input, shoreline erosion, and bottom erosion in high energy, shallow water regions (Thomas et al. 1973). Approximately two thirds of the sediment entering Lake Huron is derived from the erosion of shorelines and bluffs (Rea et al. 1981). Tributaries and aeolian particulate matter are relatively minor contributors to sediment compared to shoreline erosion (Rae et al. 1981). Moreover, the resuspension of surface sediments in the Great Lakes, which contain large quantities of nutrients and contaminants deposited over the last few decades, results in larger fluxes to the water column than from external inputs (Eadie and Robbins 2005).

Sediment particles and organic compounds are predominantly transferred within the coastal zone of large lakes in episodic pules, such as storms and spring runoff (Eadie and

Robbins 2005). The effect of waves on sedimentation is seasonable in Lake Huron. Sediments

transported to Lake Huron by rivers in the winter and spring are deposited nearshore in shallow

water. Waves and currents during this time of year produce high-turbidity events which transport

the recently deposited sediment to deeper water (Chambers and Eadie 1981; Lick 1982). Wind

intensity and direction can influence the size of surface waves and the depth that wave scour

affects sedimentation on the lake bottom. Variations in rainfall can also influence the input of

terrigenous sediment (Johnson 1984).

The ragweed (*Ambrosia*) pollen rise in sediments provides a date for extensive land

clearance and European settlement. During this period, the rate of sedimentation increased due to

upland erosion and siltation (McAndrews and Power 1973). Sedimentation rates were calculated

in the main basin of Lake Huron (average ~1.32 mm/year; n = 10) using the thickness of the

ragweed zone (Kemp and Harper 1977). Although ragweed-rich sediments only exist in

relatively thin and patchy sequences in Georgian Bay (McCarthy et al. 2007), sedimentation

rates were also calculated (average ~0.27 mm/year; n = 3) using the thickness of the ragweed

zone (Kemp and Harper 1977).
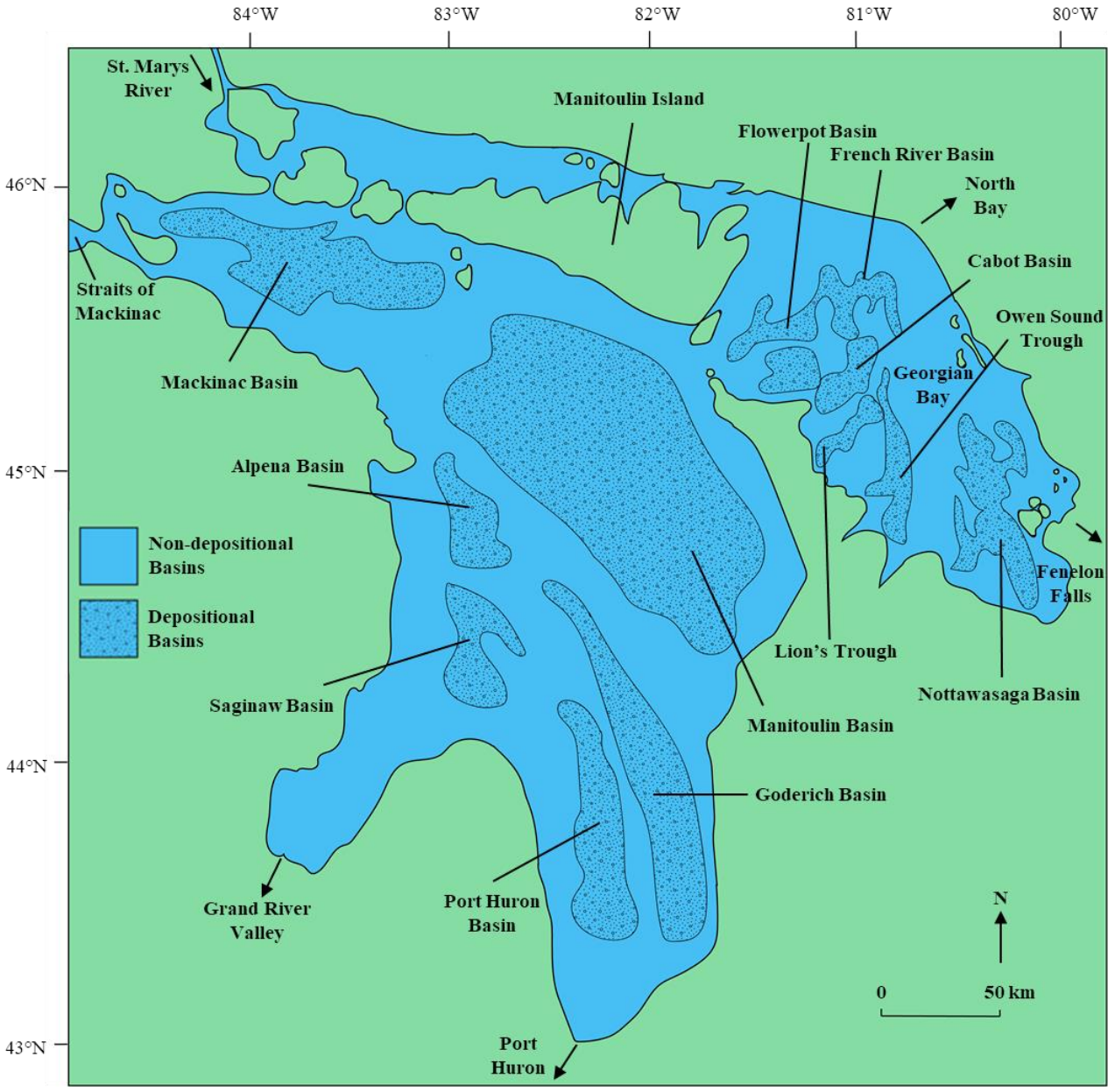
Figure 1.2. Map of the Lake Huron watershed showing non-depositional basins (blue) and depositional basins (spotted) in Lake Huron and Georgian Bay. Inlets, outlets, and Manitoulin Island are also shown (Modified from Kemp and Harper 1977).

1.4   Thesis Structure

The objectives of this thesis and a review of relevant literature are presented in Chapter 1. The review covers an overview of the Laurentian Great Lakes and their formation, as well as sedimentation in Late Holocene Lake Huron.

Chapter 2 describes the rationale for investigating changes in paleoproduction and source matter changes using bulk OM, stable isotope geochemistry, mineralogy, magnetic susceptibility, and grain size.

Chapter 3 describes the methodology used in this study. Methodology is divided into two main categories: sample collection and laboratory analyses. Samples are sediments collected in seven benthos cores. Changes to primary production and OM source is evaluated using the TOC, TN, C/N ratios, δ^{13}C, and δ^{15}N of OM. Other measurements including magnetic susceptibility, grain size distribution and mineral abundances have been conducted to assist with interpretation.

Chapter 4 presents the results of laboratory analyses of the various samples collected from Lake Huron and Georgian Bay sediment cores.

Chapter 5 provides a discussion and interpretation of the results. First, an age-depth model is established using ^{210}Pb dates collected from three of the seven cores, and one radiocarbon date available for the Goderich basin core. Second, data collected from the proxy records preserved in the sediment cores is used to interpret climatic changes and anthropogenic impacts, as well as their effects on production and OM source. Finally, a cross-basin comparison is completed.

Chapter 6 summarizes the findings of this thesis and provides suggestions for future work.

Chapter 2

2 Organic Matter & Other Proxies

Physical and chemical proxy indicators preserved in lake sediments can be used to provide information about sediment and OM source, variations in primary production, and rates of sedimentation. In this chapter, proxies related to OM such as the total amount of organic carbon, total nitrogen, the carbon to nitrogen ratio, and the stable-isotope composition of OM nitrogen and carbon are examined. Other proxies examined include magnetic susceptibility, mineralogy, and grain size.

2.1 Organic Matter Classification

Organic matter (OM) is derived from the mixture of carbohydrates, proteins, lipids, and other biochemical compounds produced by organisms living in and around the lake, such as aquatic algae and higher terrestrial plants, respectively (Meyers 2003). The primary source of OM entering lake sediments is the particulate detritus of vascular plants (e.g., trees, shrubs, grasses) and the allochthonous contribution from non-vascular plants (e.g., algae) (Meyers and Lallier-Vergès 1999). Most of the vegetation in the catchment area and littoral zone consists of vascular plants. Lake sediment OM content can be dominated by algae in some lakes and terrestrial vascular plants in others (Meyers and Lallier-Vergès 1999). The contributions of OM from these two groups to lake sediments is influenced by catchment size, lake morphology, topography, runoff, and the relative abundances of plant species (Meyers and Ishiwatari 1993).

The elemental, molecular, and isotope compositions of OM preserved in lake sediments contains information about the organisms that lived within Lake Huron and its catchment area. These organic proxies allow for the reconstruction of past environmental conditions, evaluation

of past climate change, and the assessment of anthropogenic impacts on the local ecosystem (Meyers 2003). Lake Huron sediments contain a paleoclimatic history spanning from the beginning of deglaciation in the Late Pleistocene to the present. In the present study, OM contained within Lake Huron sediments provides an opportunity to learn how post-glacial Lake Huron responded to varying climate conditions and anthropogenic impacts throughout the last 2000 years. Specifically, OM in Lake Huron sediments should contain a biochemical record of (i) its source (e.g., lacustrine or terrestrial), (ii) variations in primary production within the lake, and (iii) changes in autochthonous versus allochthonous OM contributions in response to variations in environmental conditions.

2.1.1   Carbon Isotope Composition of Organic Matter

The carbon-isotope composition (δ^{13}C) of atmospheric CO_2 is about –8.4 ‰ at present (Laskar and Mao-Chang 2016). During photosynthesis, plants preferentially take up $^{12}CO_2$ from the atmosphere, which results in a large carbon-isotope fractionation between the source and sink. The size of the fractionation is largely dependent on the photosynthesis pathway the plant uses. The Calvin-Benson cycle is used in C3 plants (e.g., wheat), the Hatch-Slack cycle in C4 plants (e.g., corn), and the Crassulacean acid metabolism (CAM) cycle in CAM plants (e.g., cacti) (Bender 1971). The δ^{13}C of modern C3 plants ranges from about –30 to –23 ‰ (Meyers and Teranes 2002), the δ^{13}C of C4 plants ranges from about –16 to –10 ‰ (O'Leary 1988), and the δ^{13}C of CAM plants spans the range of C3, averaging about –20 ‰ (O'Leary 1988). Southern Ontario and Northern Michigan are dominated by C3 plants. The δ^{13}C of modern C3 plants is lower than plants that grew prior to the Industrial Revolution by ~2 ‰; this 'Suess effect' is due to the CO_2 contribution to the atmosphere from the combustion of fossil fuels

(Keeling et al. 1979). A 'Suess effect' correction is required when comparing the δ^{13}C of modern plants versus ancient terrestrial OM preserved in Lake Huron. Verburg (2007) provided a means for estimating the effect of the changing δ^{13}C of atmospheric CO_2 on autotrophic and heterotrophic lacustrine systems for any post-industrial date. The method is based on a best fit of the δ^{13}C of atmospheric CO_2 between 1692 and 2000 (Friedli et al. 1986; Francey et al. 1999; Keeling et al. 2001; Langenfelds et al. 2002) using the following equation:

$\delta^{13}C_{atm} = 7.7738118 \times 10^{-16} \times Y^6 - 1.2222044 \times 10^{-11} \times Y^5 + 7.1612441 \times 10^{-8} \times Y^4 -$

$2.1017147 \times 10^{-4} \times Y^3 + 3.3316112 \times 10^{-1} \times Y^2 - 273.71502 \times Y + 91703.261$ [Equation 2.1]

where Y is the calendar year.

Freshwater algae are C3 eukaryotic organisms with δ^{13}C that typically ranges from –29 to –25 ‰ (Meyers and Ishiwatari 1993). The δ^{13}C of algae is largely controlled by the composition of the dissolved inorganic carbon (DIC) reservoir and the level of photosynthetic activity (McKenzie 1985; Hodell and Schelske 1998; Wolfe et al. 2002). Changes in the δ^{13}C of the DIC reservoir are reflected in the composition of algal OM ($\delta^{13}C_{OM}$) as the majority of lacustrine algae utilize dissolved CO_2 (O'Leary 1998; Wolfe et al. 2002). The δ^{13}C of DIC varies with changes in the composition of atmospheric CO_2, the degree of gas exchange between atmospheric and dissolved CO_2, the flux of soil CO_2 into the lake (Meyers 2003), the decay rate of OM buried in the sediment (Hayes 1993), and the dissolution of carbonate detritus (Meyers 2003). Although minor changes do occur during oxidative decay, the $\delta^{13}C_{OM}$ in shallow sediments generally has a value characteristic of its source (Sharp 2007). Freshwater algae typically produce OM using dissolved CO_2 in isotopic equilibrium with the atmosphere (Meyers 2003). During periods of high production, however, the availability of dissolved CO_2 becomes diminished (Keeley and Sandquist 1992; Hollander and McKenzie 1991; Bernasconi et al. 1997),

and algae begin to use dissolved HCO_3^- as their source of carbon (Meyers 2003). As a result, their carbon-isotope composition becomes higher than those of C3 land plants, which typically have a $\delta^{13}C$ indistinguishable from lake derived OM produced by algae (Meyers 2003).

Values of $\delta^{13}C_{OM}$ are useful in determining variations in primary production and OM sources and identifying changes in the availability of nutrients in surface waters (Meyers 2003; Schelske and Hodell 1995). Reconstruction of primary production is based on the premise that increases in lacustrine production will yield increases in the deposition of TOC and changes in the carbon- and nitrogen-isotope compositions of the OM. In particular, an increase in $\delta^{13}C_{OM}$ has previously been used as an indicator of enhanced aquatic production in lakes (Hollander and McKenzie 1991; Hollander et al. 1992; Hodell and Schelske 1998; Brenner et al. 1999; Hyodo and Longstaffe 2011; Hladyniuk and Longstaffe 2015; O'Beirne et al. 2017). Lake algae preferentially utilize ^{12}C to produce OM that is more depleted of ^{13}C than their DIC source. The $^{13}C/^{12}C$ ratio of the remaining DIC increases, which leads to a subsequent increase in the $\delta^{13}C_{OM}$ of newly produced material (O'Leary 1988; Wolfe et al. 2002; Meyers 2003).

2.1.2   Nitrogen Isotope Composition of Organic Matter

The $\delta^{15}N$ of atmospheric N_2 is homogenous and defined to be 0 ‰. Nitrogen-isotope fractionation occurs as N_2 gas moves through the nitrogen cycle. Nitrogen-fixing bacteria can convert nitrogen into ammonium (NH_4^+) and ammonia (NH_3) (Sournia 1986; Hopkins et al. 2004), and subsequent nitrification can produce nitrite (NO_2^-) and nitrate (NO_3^-) (Kendall 1988). These species are assimilated by plants and algae that produce organic compounds containing nitrogen, such as amino acids. The most abundant nitrogen source for plants is nitrate, but ammonium can predominate under waterlogged or acidic soil conditions (Yoneyama et al. 2003;

Pilbeam 2010). Atmospheric molecular nitrogen is also a source of nitrogen for some plants, such as legumes (Meyers and Lallier-Vergès 1999; Szpak et al. 2013).

The δ^{15}N of dissolved nitrate (NO_3^-) in lake water is typically between +7 and +10 ‰ (Peters et al. 1978), whereas nitrate derived from atmospheric nitrogen has a δ^{15}N of –4 to +4 ‰ (Hoefs 1997). Consequently, the δ^{15}N$_{OM}$ of C3 land plants averages about +1 ‰ whereas algae have a δ^{15}N$_{OM}$ of about +8.5 ‰ (Meyers and Lallier-Vergès 1999; Meyers 2003). The δ^{15}N of the dissolved nitrate reservoir is affected by input from agricultural runoff and sewage (Peterson and Fry 1987; Hodell and Schelske 1998), denitrification (Cline and Kaplan 1975; Teranes and Bernasconi 2000), ammonia volatilization (Talbot and Laerdal 2000), leaching of soil-derived nitrate (Peters et al. 1978), and the abundance of nitrogen-fixing bacteria (Fogel and Cifuentes 1993). An increase in production will result in a relative increase in the utilization of the dissolved nitrate reservoir by algae. As such, this increases the ^{15}N/^{14}N ratio of the remaining reservoir and produces a subsequent increase in newly produced δ^{15}N$_{OM}$ (Wada and Hattori 1991; Fogel and Cifuentes 1993; Kendall 1998; Talbot and Laerdal 2000). Variations in δ^{15}N typically reflect a change in lake trophic state (Brenner et al. 1999), denitrification through microbial decomposition of OM (Talbot 2001; Woszczyk et al. 2014), and a change in nitrogen sources (Meyers and Teranes 2001).

2.1.3 TOC, TN, and C/N ratio

The total organic carbon (TOC), total nitrogen (TN), and carbon to nitrogen ratio (C/N) are useful in determining changes in the amount of OM input to lacustrine systems (Meyers and Teranes 2002). The concentration of OM in sediment is approximately twice the TOC value since OM typically contains ~50 % carbon (Meyers 2003). Relative changes in carbon and

nitrogen contents should be related to changes in Lake Huron, even though less than 10 % of organic carbon produced by photosynthesis at the water's surface remains after sinking down the water column (Eadie et al. 1984; Meyers and Eadie 1993). The TOC and TN abundances, by themselves, however, do not distinguish between autochthonous and allochthonous OM inputs to a lake.

The OM in lacustrine sediments is derived from terrestrial (vascular) plants that contain large amounts of carbon-rich cellulose and waxy hydrocarbons, and aquatic algae (non-vascular) that have low cellulose and high (N-rich) protein contents. Thus, the C/N ratio is useful to distinguish between vascular plants, which typically yield a C/N >20, and non-vascular plants, which typically yield a C/N between 4 and 10 (Meyers 1994). Partial degradation of OM during early diagenesis, however, can alter the original C/N ratios. Meyers et al. (1995) observed, for example, that the C/N of fresh wood is generally higher than those of wood that has been buried. This is the result of selective degradation of carbon-rich lipids and sugars in the wood. In contrast, the selective degradation of nitrogen-rich proteins in algal-derived OM during sinking and early sedimentation will increase the C/N ratio (Meyers and Lallier-Vergès 1999). Hladyniuk and Longstaffe (2015) observed that highly degraded OM with low C/N can be retained on soil clays transported to Lake Ontario. As such, C/N ratios should be interpreted with caution. Values of C/N are normally calculated as an atomic ratio, as follows:

$$C/N = \frac{\%TOC/12.01}{\%TN/14.01} \qquad \qquad \text{[Equation 2.2]}$$

2.2   Other Proxies

2.2.1   Magnetic Susceptibility

Magnetic susceptibility is a measure of the degree of a sediment's attraction to an applied magnetic field. Volume magnetic susceptibility (κ) is defined as the ratio between induced magnetization per volume unit of measured sample (M) and applied magnetic field intensity (H).

$$\kappa = \frac{M}{H}$$ [Equation 2.3]

The SI units of both M and H are A/m, and as such, κ is a dimensionless number. Ferromagnetic substances are magnetic materials that are capable of acquiring a magnetic remanence. Common ferromagnetic minerals, such as magnetite (Fe_3O_4) and hematite (Fe_2O_3), have crystalline structures that allow interactions between constituent metallic atom shells. A magnetic susceptibility measurement of sediment is a measure of the concentration of such ferromagnetic minerals present (Thompson et al. 1975). Paramagnetic minerals have crystal structures that allow only weak interactions between iron (Fe) atom shells, such as Fe-bearing silicates (e.g., clay minerals) and Fe-sulfides (e.g., pyrite (FeS_2)). Diamagnetic minerals display negative magnetization when a magnetic field is applied. These include minerals that do not contain Fe, such as quartz (SiO_2) and calcite ($CaCO_3$), as well as water and OM.

The magnetic susceptibility of sediments in clastic-dominated systems, such as lakes, can reflect a variety of processes, which are commonly related to changes in sediment source and/or flux. In general, the most magnetically susceptible sediments contain the highest amount of allochthonous inorganic material washed into the lake from the drainage basin. As such, changes in magnetic susceptibility over time are commonly a function of the flux of allochthonous material into the lake. Deforestation, afforestation, and agricultural changes in the drainage basin can affect the amount of material entering the lake (Wetzel 2001). Several other factors can also

20

affect sediment magnetic susceptibility, including post-depositional diagenesis (Hilton and

Lishman 1985; Hilton et al. 1986), mineral segregation resulting from wave action (Smoot and

Benson 2004), and dilution from OM and/or carbonates (Kirby et al. 2005).

Higher magnetic susceptibility values in sediment are commonly attributed to wetter

climates. This assumption is made because: (i) a wetter climate raises lake-level, which results in

increased bluff erosion and reduces the removal of magnetic minerals by wave action

winnowing; (ii) an increase in the frequency of precipitation events increases the flux of

allochthonous inorganic material into the lake (Kirby et al. 2005, 2007); and (iii) an increase in

the frequency of floods in the lake's catchment area can increase fluvial input of magnetite

(Knox 1985). Finer-grained magnetic minerals are more susceptible to diagenetic alteration

(Maher and Thompson 1999). Variations in the magnetic susceptibility of coarse-grained

sediments are therefore not likely caused by diagenetic alteration, but instead result from lake-

level changes (due to climatic variations) and the episodic flux of clastic material (due to

extreme precipitation events) (Kirby et al. 2005) or anthropogenic activities.

Post-depositional processes under specific chemical conditions can confound the primary

magnetic signal, either by enhancing or suppressing it (Hilton and Lishman 1985).

On one hand, simple dilution by organic material and carbonates may affect the magnetic

susceptibility of lake sediments; there is a strong inverse relationship between TOC and

magnetic susceptibility, and carbonate and magnetic susceptibility (Kirby et al. 2005, 2007).

Higher quantities of OM, because of increased production, may dilute the magnetic susceptibility

signal during low or lowering lake levels (Kirby et al. 2007). On the other hand, magnetic

susceptibility may be affected by enhanced diagenesis or dissolution under reducing conditions

caused by higher OM. Regardless of whether a change in sediment flux, dilution, or dissolution

is responsible for the change in magnetic susceptibility, the change is in the same direction. A wetter climate will result in higher magnetic susceptibility, and inversely a drier climate will result in a lower magnetic susceptibility.

2.2.2   Mineralogy

Minerals can be subdivided into three categories based on their origin. Allogenic (i.e., detrital) minerals are brought into the lake via surface streams, sheet flooding, shoreline erosion, mass movement, and aeolian activity. Authigenic minerals are derived by the diagenetic alteration of sediment that is already deposited in the lake, or by chemical reactions within the pore-water system of the sedimentary deposit. Endogenic minerals are those that originate within the water column of the lake, either by biologically-induced or inorganic chemical precipitation (Last 2002).

Allogenic (detrital) minerals reflect (i) basin tectonics, (ii) provenance, (iii) weathering processes within the watershed, and (iv) sediment transportation processes that brought the material into the lake. As such, allogenic minerals can typically be used to quantitatively deduce past changes in drainage basin size and morphology (e.g., Henderson and Last 1998) and variations in climate (e.g., Last and Sauchyn 1993). Endogenic minerals typically provide information about the chemical and limnological conditions at the time of formation. Carbonate minerals, such as calcite ($CaCO_3$) and dolomite ($CaMg(CO_3)_2$), are common endogenic minerals in many lakes (Dead and Fouch 1983). Authigenic minerals are more difficult to interpret, as they can originate during, shortly afterward, or long after the sediment has been deposited.

2.2.3 Grain Size

Sediment grain size generally reflects distance and energy of transported material. On one hand, finer-grained particles are typically transported farther and are more likely to settle out of calm, deep water. On the other hand, coarse-grained particles typically indicate a shorter transportation distance and higher energy depositional environment. Interpretation of particle size data is, however, controversial. For fine-grained sediments, palaeohydrological interpretations are devalued because fine particles are often deposited as larger aggregates (e.g., inorganic floccules). Individual particles will respond differently to hydrological conditions than larger aggregates. For coarse-grained sediments, the relationship between particle size, water depth and energy level can be ambiguous. An increase in grain size may represent a number of possible changes in the system that have led to greater energy level, which may or may not be directly correlated to a decrease in water depth. These include: (i) an increase in aridity, (ii) infilling by sediment, and (iii) an increase in wind strength or fetch (Teller and Last 1990). Moreover, an increase in surface runoff may produce an increase in grain size. The relationship between increased rainfall and sediment flux to the lake basin is, however, complicated in non-arid regions because of the role vegetation has in reducing sediment yield from a watershed in a wetter climate (e.g., Schumm 1965).

2.3   Summary

The carbon- and nitrogen-isotope composition of OM provides information about the source of the organic material, as well as changes in primary production. The TOC and TN are useful indicators of the amount of OM entering the lacustrine system. The C/N ratio can provide information regarding the OM source, but partial degradation of OM during early diagenesis can

alter the original value. The magnetic susceptibility signal in lacustrine sediments can be used as an indicator of changes in climate or sediment input, if the source of the sediment contains magnetic minerals. The mineralogy and grain size of the sediment provides information on the sediment source as well rate of sedimentation.

Chapter 3

3   Methodology

3.1   Sample Collections

In May 2004, the Canadian Coast Guard Ship (CCGS) LIMNOS set out on an expedition to Lake Huron and Georgian Bay to collect piston and benthos cores (Figure 3.1). The benthos cores, which represent the undisturbed sediment-water interface, are the primary interest of this study. On May 4, a piston core (15.0 m) from station 594 in the Goderich basin (43°48'02"N 82°06'57"W; water depth 88.5 m) was retrieved alongside a benthos core (0.65 m). The CCGS LIMNOS set out on another expedition, this time to Lake Huron and Lake Michigan, in late May and early June 2006. At station 181 in the Manitoulin basin (45°19'51"N, 82°29'44"W; water depth 195 m), a piston core (15.08 m) was retrieved. At station 182 in the Mackinac basin (45°39'53"N, 83°33'42"W; water depth 124 m), a piston core (15.64) was also retrieved. Approximately 1.0 m benthos cores were also collected at station 181 and 182. The benthos cores collected at stations 181, 182, and 594 by the CCGS LIMNOS were used during this study. The cores collected by the CCGS LIMNOS have been stored in a refrigerator at 4°C at The University of Western Ontario since shortly after their retrieval.

In June 2007, the CCGS GRIFFON set out on an expedition to collect video camera and bottom data from selected areas of interest in Lake Huron, as well benthos and piston cores from Lake Huron and Georgian Bay. A total of 6 benthos cores were collected from Lake Huron, as well as 2 from Georgian Bay. On June 12, at station 819 (43°31'42"N, 82°14'18"W; water depth 48 m), piston core 819 (2.66 m) was collected from the Port Huron basin, along with a benthos core (0.60 m). Although an 18 m core was suggested at this location, only 2.66 m was recovered. The benthos core that was also obtained was deemed to be too dry and in poor condition for use

in the current study. On June 13, at station 818 in the Port Huron basin (43°47'48"N, 82°22'12"W; water depth 66 m), piston core 818 (1.75 m) was collected alongside a benthos core (1.10 m). On June 14, piston core 816 (11.6 m) and benthos core 816 (0.40 m) were collected from the Alpena basin (44°47'00"N, 82°45'48"W; water depth 76.7 m). Upon further review, the benthos core was deemed to be in poor condition, as the sediment in the top portion of the core was excessively watery and thus the sediments were likely disturbed from their original position. On June 15, the expedition attempted to collect an 18 m core at station 817 in the Alpena basin (44°41'36"N, 82°53'00"W; water depth 70.9 m), but bedrock was hit at 4.5 m. As a result, no piston core was retrieved. A benthos core (1.40 m), however, was collected. On June 16, piston core 821 (7.21 m) was collected from station 821 in the Saginaw basin (44°25'21"N, 82°44'59"W; water depth 71 m). A benthos core (1.30 m) was also retrieved. On June 18, piston core 593 (7.26 m) was collected alongside a benthos core (1.80 m) from station 593 (45°16'00"N, 81°04'00"W; water depth 141 m). Later that day, piston core 41 (8.75 m) and a benthos core (1.25 m) were collected from station 41 (45°19'00"N, 81°27'00"W; water depth 96.2 m). On June 19, the ship returned to station 818 (43°47'48"N, 82°22'12"W; water depth 61.5 m) and collected piston core 818-2 (4.23 m) and a benthos core (1.15 m). The benthos cores collected at stations 817, 818, 821 and 41 by the CCGS GRIFFON were used during this study. The cores collected by the CCGS GRIFFON have been stored in a refrigerator at 4°C at The University of Western Ontario since shortly after their retrieval.
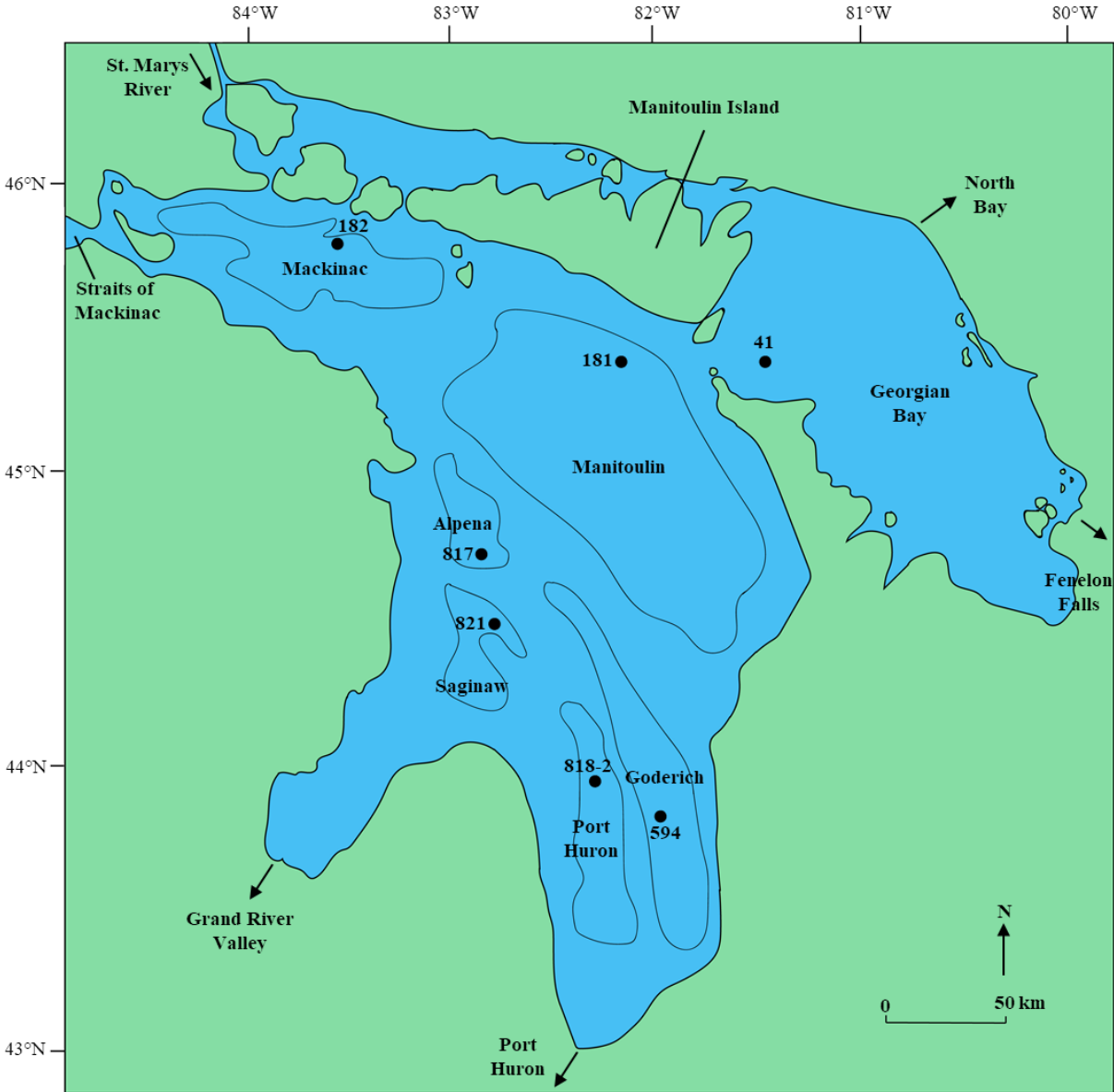
Figure 3.1. Map of Lake Huron showing basins and core locations. Major inlets and outlets, and Manitoulin Island, are also shown.

3.2 Analytical Methods

3.2.1 ^{210}Pb Dating

The ^{210}Pb dating was performed by Linda E. Kimpe at the University of Ottawa using an

Ortec High Purity Germanium Gamma Spectrometer (Oak Ridge, TN, USA). Certified

Reference Materials obtained from International Atomic Energy Association (Vienna, Austria)

were used for efficiency corrections, and results were analyzed using ScienTissiME (Barry's Bay, ON, Canada).

Lead-210 (^{210}Pb) is a natural radionuclide of the ^{238}U radioactive chain with a half-life of $T_{1/2} = 22.23 \pm 0.12$ years (Appleby 2001). There are two categories of ^{210}Pb: supported and unsupported (Figure 3.2). Supported ^{210}Pb is in equilibrium with its parent radionuclide ^{226}Ra ($T_{1/2} = 1600$ years) and occurs in systems that have remained closed for sufficient time (>150 years) (Sanchez-Cabeza and Ruiz-Fernández 2012). In sediments younger than 150 years, ^{210}Pb may not be in equilibrium with ^{226}Ra. The ^{226}Ra daughter radionuclide ^{222}Rn ($T_{1/2} = 3.8$ days) can transfer from soils to the atmosphere, and decay to ^{210}Pb, which then attaches to aerosols and deposits onto the Earth's surface by wet and dry deposition (Turekian et al. 1977). A portion of the deposited ^{210}Pb will either directly enter or be transported to aquatic ecosystems where it will attach to suspended matter in the water column and eventually be deposited in bottom sediments (Sanchez-Cabeza and Ruiz-Fernández 2012). The ^{210}Pb produced by disequilibrium with ^{226}Ra is referred to as unsupported ^{210}Pb or excess ^{210}Pb (^{210}Pb$_{ex}$). As a result of its half-life, the ^{210}Pb dating method is only applicable for sediments deposited in the last 150 years.

The total ^{210}Pb concentration in sediments can be determined by: (i) gamma spectrometry (46.5 keV line; Schelske et al. 1994) – the case in this study, (ii) alpha spectrometry (Sanchez-Cabeza et al. 1998), (iii) liquid scintillation (Vajda et al. 1997), and (iv) beta counting (Godoy et al. 1998). Radon-226 (^{226}Ra) (equal to supported ^{210}Pb) is typically determined by gamma spectrometry, primarily through the 352 keV line of ^{214}Pb in equilibrium. Unsupported ^{210}Pb is then calculated as the difference between total and supported ^{210}Pb.

Dating models are used to obtain an age model and calculate accumulation rates. The

Constant Initial Activity (CIC) model assumes that, at formation of a sediment layer i, the $^{210}Pb_{ex}$

concentration (C_0) is constant.

$$C_i = C_0e^{-\lambda ti} \qquad \text{[Equation 3.1]}$$

where t = time (generally years), C_t = activity at time t, C_0 = activity at time 0, e = 2.71828, and λ

= decay constant (^{210}Pb = 0.03118 year^{-1}). Equation 3.1 can be rearranged to:

$$t_i = \frac{1}{\lambda}\ln\frac{C_0}{C_i} \qquad \text{[Equation 3.2]}$$

The CIC model implies that fluxes to the sediment surface and mass accumulations are

proportional, which is typically false. As such, this model is rarely used. The Linear or Constant

Flux and Sedimentation (CS) model assumes flux and mass accumulation (r) are constant. The

time of layer formation can thus be calculated using the following equation:

$$t_i = \frac{m_i}{r} \qquad \text{[Equation 3.3]}$$

where m_i is the cumulative depth in dry mass of layer i. Combining equations 3.1 and 3.3 gives:

$$C_i = C_0e^{\frac{-\lambda m_i}{r}} \qquad \text{[Equation 3.4]}$$

This can be rearranged to:

$$\ln C_i = \ln C_0 - \frac{\lambda}{r}mi \qquad \text{[Equation 3.5]}$$

A linear regression of $\ln C_i$ gives the line equation y = a + bx, where a = $\ln C_0$ and b = $\frac{-\lambda}{r}$. As λ is

known, r = $\frac{-\lambda}{b}$, and the age (ti) of sediment layer (mi) can be calculated by equation 3.5. The

Constant Rate of Supply (CRS) or Constant Flux (CF) model is mostly commonly used in

paleolimnological studies. It assumes that the $^{210}Pb_{ex}$ flux to the sediment surface is constant and activity (C) and sedimentation rate (r) can vary.

$$A_i = A_0 e^{-\lambda t_i} \hspace{4cm} \text{[Equation 3.6]}$$

where A_i and A_0 is the activity per unit area at time i and 0, respectively. This can be rearranged to:

$$t_i = \frac{1}{\lambda}\ln(\frac{A_0}{A_i}) \hspace{4cm} \text{[Equation 3.7]}$$
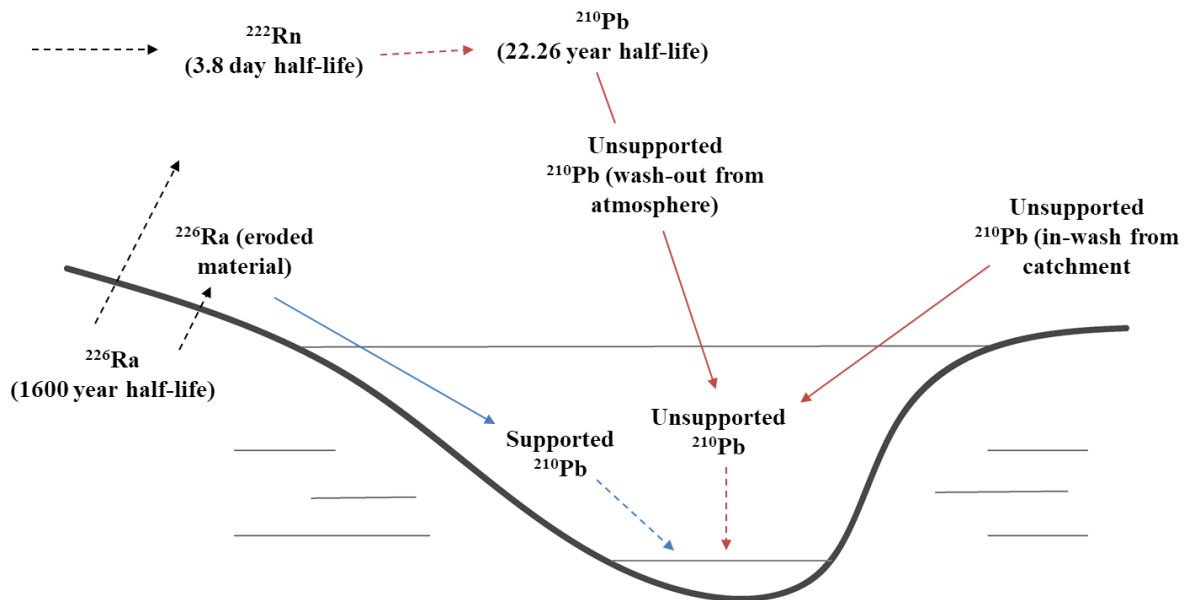
Figure 3.2. Contributions of supported and unsupported ^{210}Pb to lake sediments.

3.2.2   Magnetic Susceptibility

Magnetic susceptibility was determined at the Lakes and Reservoirs Systems Research Facility (LARS), The University of Western Ontario, using a Geotek® multi-sensor core logger (MSCL) equipped with a loop sensor (MS2C) and point sensor (MS2E). The loop sensor is used for volume susceptibility measurements of whole sediment cores, whereas the point sensor is

used for surface scanning and providing high-resolution surface measurements on split sediment cores. The loop and point sensors are electronically calibrated to measure a single standard of stable iron oxide. An oscillator circuit in the sensors produces a low intensity of about 80 A/m root mean squared (RMS) non-saturating, alternating magnetic field (0.565 kHz and 2 kHz for the loop and point sensor, respectively). Any material in the near vicinity of the sensor that has a magnetic susceptibility will produce a change in the oscillator frequency. The MSCL system will convert this pulsed frequency information into magnetic susceptibility values. The loop sensor integrates the magnetic signal over a longer segment of core than the actual length of the loop. Each data point is therefore treated as a weighted running average of the susceptibility distribution over the spatial resolution of the loop. The point sensor has a field of influence of about 1 cm in diameter. Point sensor measurements yield higher uncertainties in magnetic susceptibility values as a result of not using a normalizing volume.

Measurements were taken every 0.5 cm and, when possible, were determined using both the loop and point sensors. Point sensor measurements were taken in the shortest timeframe possible after the core was split and described to avoid possible magnetic mineral diagenesis arising from exposure to air.

3.2.3   Powder X-ray Diffraction

Powder X-ray diffraction (p-XRD) was used to characterize the mineralogy of the sediment cores. Crystalline materials give a unique X-ray diffraction pattern; thus, the study of diffraction patterns of unknown phases provides a mean of qualitative identification. Samples from the cores were first freeze-dried, then homogenized by hand-grinding with a ceramic mortar and pestle. Samples were ground into a powder to decrease the size of the individual crystallites,

which facilitates acquiring a random orientation of particles during p-XRD. To avoid contamination, the mortar and pestle were cleaned with acetone after each sample was prepared. A representative sample (~30 mg) was subsequently mounted into an Al-backpack holder in preparation for analysis. The p-XRD was performed using a high brilliance Rigaku RU-200BVH rotating anode X-ray diffractometer equipped with a Co source and a graphite monochromator (Co K-alpha radiation) and operated at 45 kV and 160 mA. The instrument is located in the Laboratory for Stable Isotope Science (LSIS) at the University of Western Ontario. Samples were scanned in step-scan mode from 2° to 82°2θ, using a step size of 0.02°2θ and a scan rate of 10°2θ/min. The abundance of each mineral phase was estimated using the background-subtracted peak height of its most intense diffraction, after counting for any peak overlaps with other minerals. Following their measurement, peak heights were adjusted for differences in crystallinity among minerals using crystallinity form factors. All minerals except for clay phases are assigned a form factor of x1, following Ignasiak et al. (1983). The 0.7 nm phase was assigned a form factor of x2, the 1.0 nm phase a form factor of x4, and the 1.4 nm phase a form factor of x2.5. Following these adjustments, the relative abundances were standardized to 100 %. As OM is not detectable by p-XRD, the abundance estimates are considered to be representative of organic-free sediment.

3.2.4 Grain Size Analyses

Grain size analysis was performed at the Control and Crystallization of Pharmaceuticals Laboratory (CCPL), the University of Western Ontario, using a Malvern Mastersizer® 2000 laser grain size analyzer. The Malvern Mastersizer® 2000 measures grain size ranging from 0.02 to 2000 μm in diameter. The analyzer assumes that grains are perfect spheres and uses the

volume of a grain to subsequently calculate the size and diameter that is equivalent to the

measured volume using an equivalent spheres technique (Xiao et al. 2009). Approximately 80

mg of sediment from 45 freeze-dried samples were disaggregated into individual grains using a

mortar and pestle. The sediment samples were treated with a dispersing agent, 10 mL of 0.1%

sodium hexametaphosphate solution, prior to grain size analysis. The solution was dispersed with

an ultrasonic probe for 1 minute at 700 watts. At the CCPL, the sample solution was added to

500 mL of distilled water and pumped into the laser diffractometer for analyses. The analyzer

produces three measurements and one weighted average per sample. The sample is considered to

have been dispersed completely if no major changes are observed in the replicate analytical

curves.

3.2.5   Bulk Organic Matter Analyses

Samples were prepared for bulk organic matter analysis at LSIS. One-centimeter-thick

samples of bulk sediment were freeze-dried and ground using a ceramic mortar and pestle in

preparation for measurements of TOC, TN and their carbon- and nitrogen-isotope compositions.

Prior to the measurement of TOC and carbon-isotope compositions, inorganic carbonates were

removed by acid fumigation (Harris et al. 2001). Quantities of sediment, ranging from 5-30 mg,

were weighed into silver capsules and placed into a sample tray. Two drops of deionized water

were added to each capsule. A glass desiccator was filled with ~500 mL of concentrated, 12 N,

hydrochloric acid (HCl), ensuring maximum surface area for the HCl to fumigate. The sample

tray was placed inside the desiccator on an elevated ceramic holder above the acid, with the lid

partially off, for 24 hours. Acid fumes dissolved into the deionized water, which created an

acidic solution that dissolved any carbonates in the sediment (Harris et al. 2001). The samples

were then dried in an oven at ~60°C for 24 hours. The dried samples were then crimped and wrapped in tin to maximize flash combustion in the elemental analyzer. Separate 5-50 mg samples that had not been subjected to acid-treatment were loaded into tin capsules for measurements of TN and nitrogen-isotope compositions. Untreated samples are required because acid-treatment can alter the original $\delta^{15}N$ (Teranes and Bernasconi 2000). The atomic C/N ratio was calculated based on TOC and TN results using Equation 2.2.

At LSIS, a Costech Elemental Combustion System coupled to a Thermo Scientific^{TM} Delta$^{®}$ Plus XL mass spectrometer (EA-IRMS) in continuous-flow (helium (He)) mode was used to determine the TOC, TN, C/N ratio, and carbon- and nitrogen-isotope compositions ($\delta^{13}C$ and $\delta^{15}N$, respectively) of OM. At the start of the analytical cycle, He carrier gas is switched to a volume of oxygen chosen by the operator, which is dependent on the size and composition of the sample. The samples are dropped sequentially into the combustion reactor prior to the arrival of oxygen by a rotating autosampler. The sample silver and/or tin capsule react with oxygen and combust at temperatures of 1700-1800°C. Carbon is converted to carbon dioxide (CO_2) and nitrogen to nitrogen gas (N_2) and oxides of nitrogen. The combustion products are swept out of the combustion chamber by an inert carrier gas (He) and passed over heated (~600°C), high purity copper. The copper removes any oxygen that is not consumed during the initial combustion and converts any oxides of nitrogen to N_2. The gases then flow through the gas chromatographic (GC) separation column. As they pass through the GC column, the gases are separated and are detected sequentially by the thermal conductivity detector (TCD). Any water produced is trapped using magnesium perchlorate. During analytical runs in which only $\delta^{15}N$ was measured, CO_2 was removed using Carbo-Sorb$^{®}$. The separated gases are then carried to the mass spectrometer, where they are bombarded by high-energy electrons to create mono-cationic

versions of the gas. The cations are then accelerated through electric plates and subsequently

deflected by a magnetic field. Ion deflection is inversely proportional to the mass-to-charge ratio:

$$\frac{m}{z} \qquad \text{[Equation 3.8]}$$

where m is the mass of the ion and z is equal to the charge. The mass spectrometer then

generates a mass spectrum for the sample.

Values of $\delta^{13}C$ and $\delta^{15}N$ are expressed in δ-notation:

$$\delta^{13}C \text{ or } \delta^{15}N = [(R_{sample} / R_{standard}) - 1] \text{ (in ‰)} \qquad \text{[Equation 3.9]}$$

where R_{sample} and $R_{standard}$ are equal to $^{13}C/^{12}C$ or $^{15}N/^{14}N$ in the sample and standard,

respectively. Values of $\delta^{13}C$ were calibrated to international standard VPDB using USGS-41a

(+37.63 ‰) and USGS-40 (–26.39 ‰) (accepted values in parentheses). The accuracy of this

calibration curve was checked using IAEA-CH-6; its average measured $\delta^{13}C$ (–10.65±0.18 ‰;

SD, n=15) compared well with the accepted value of –10.45±0.13 ‰. Laboratory standard

keratin (MP Biomedicals Inc., Cat. No. 90211, Lot No. 9966H; $\delta^{13}C$ = +24.04 ‰; $\delta^{15}N$ = +6.36

‰) was also analyzed to evaluate the accuracy and precision of analytical sessions. The average

$\delta^{13}C$ of keratin was –24.06±0.12 ‰ (SD, n=34) across all sessions, and compared well with the

accepted value of –24.04 ‰. The absolute difference in $\delta^{13}C$ between duplicate analyses of the

same sample averaged 0.05 ‰ (n=24). Values of $\delta^{15}N$ were calibrated to the international

standard AIR (Mariotti 1983) using USGS-41a (+47.57 ‰) and USGS-40 (–4.52 ‰) (accepted

values in parentheses). Laboratory standard keratin was also analyzed to evaluate the accuracy

and precision of analytical sessions. The average $\delta^{15}N$ of the keratin was +6.40±0.08 ‰ (SD,

n=23) across all sessions, and compared well with its accepted value of +6.36 ‰. The absolute

difference in $\delta^{15}N$ between duplicate analyses of the same sample averaged 0.02 ‰ (n=18).

Chapter 4

4 Results

4.1 Core 594 (Goderich Basin)

4.1.1 Core Description

Using the Munsell Color System, the wet sediment in core 594 is very dark greyish brown (10YR 3/2) throughout most of the core, changing to generally very dark grey (10YR 3/1) at the top (0 to 12 cm). The sediments are fine-grained silt and clay. There were no visible shell fragments or plant material.

4.1.2 Grain Size

Grain size measurements were made for 7 samples from core 594 (Figure 4.1a and b). Three measurements were recorded for each sample, and an average of the 3 results is presented. The d(0.1) (10% of particles are less than or equal to this value), d(0.5) (the median, where 50% of particles are less than or equal to this value), and d(0.9) (90% of particles are less than or equal to this value) values were calculated from each average. The d(0.5) results range from 3.8–5.4 μm. The d(0.5) measurements sharply increase at 40.5 cm and then reach their peak of 5.4 μm at 50.5 cm. Measurements then sharply decrease until 10.5 cm where they decrease slightly to the lowest d(0.5) value of 3.8 μm at 1.5 cm. The d(0.1) does not vary significantly throughout the core. The d(0.9) measurements show a similar trend to d(0.5), but with a larger increase at 40.5 cm.
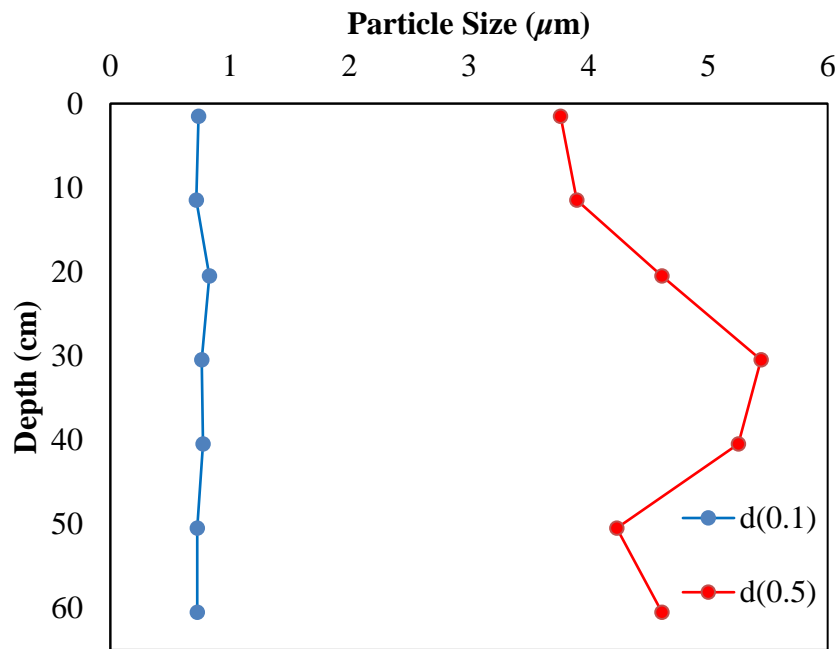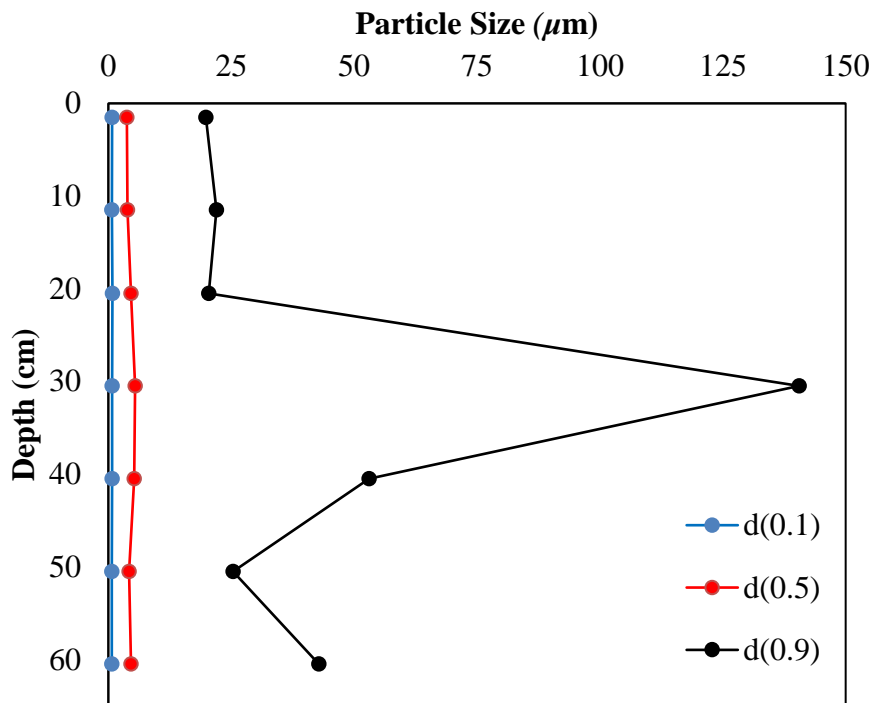
Figure 4.1. Grain size distributions for core 594: (a) d(0.1) and d(0.5) indicate that 10 % and 50 % of the sediment is finer than the size (μm) indicated; (b) d(0.9) indicates that 90 % of the sediment is finer than the size (μm) indicated.

4.1.3   Mineralogy

Minerals detected by p-XRD are quartz, K-feldspar, plagioclase, dolomite, amphibole, and clay minerals (1.4 nm – chlorite; 1.0 nm – illite; 0.7 nm – kaolinite) (Figure 4.2). In general, the mineralogy does not change much throughout the core. The majority of the core has a quartz content of 59-62 %, with an increase to 66 % at 1.5 cm. Amphibole represents 5% of the mineral content at 60.5 cm but ranges from 0-2% throughout the remainder of the core. Clay minerals are the second largest mineral fraction with chlorite, illite and kaolinite contents of 7-9 %, 8-11 %, and 4-7 %, respectively. Potassium feldspar and plagioclase contents are 4-6 % and 6-9 % respectively. Dolomite content is 2-5 %. Calcite is absent.
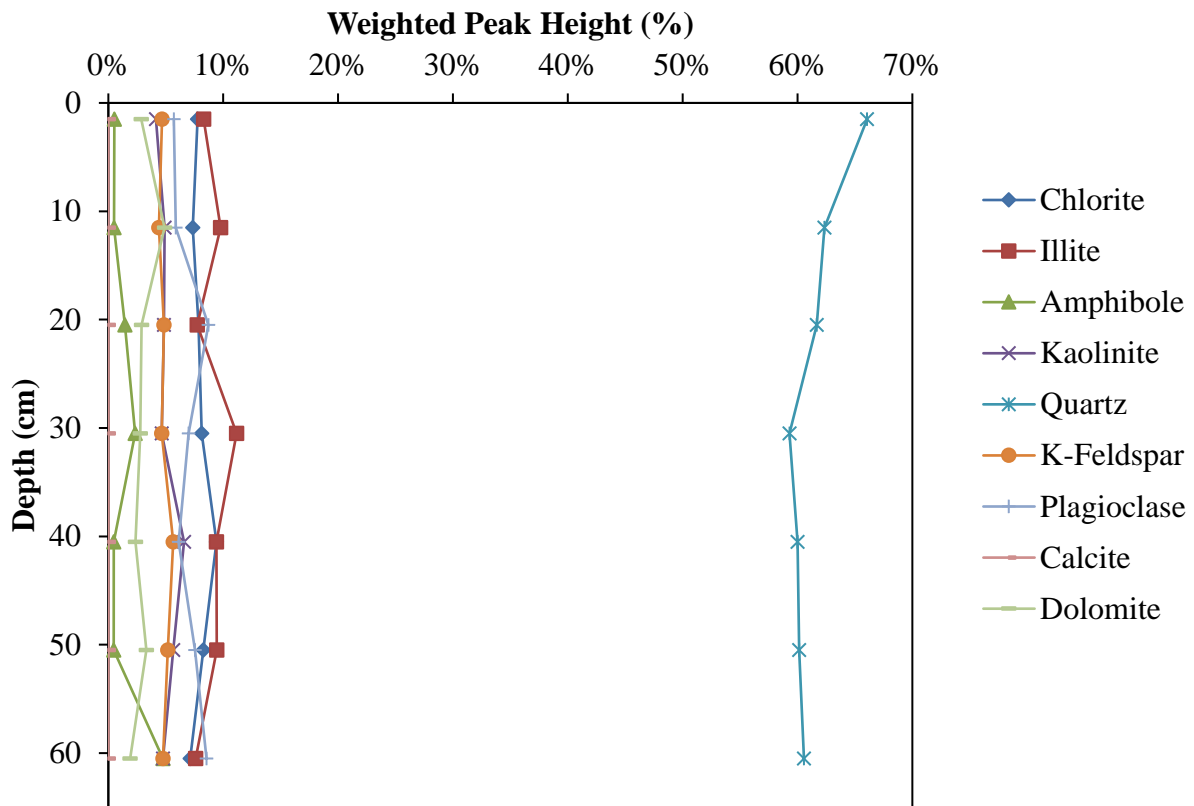
Figure 4.2. Mineral abundances for core 594. Percentages are based on weighted peak heights of the strongest diffraction for each phase, as measured by p-XRD.

4.1.4 Magnetic Susceptibility

Half-core MS signals were measured with a point sensor (Figure 4.3). Point sensor MS signals average 18.6. The point sensor MS signals are relatively constant throughout the core until ~14.5 cm. The MS signal gradually increases until 4.5 cm to a maximum value of 36. The MS signal then decreases and reaches a value similar to pre 14.5 cm measurements at 0.5 cm.
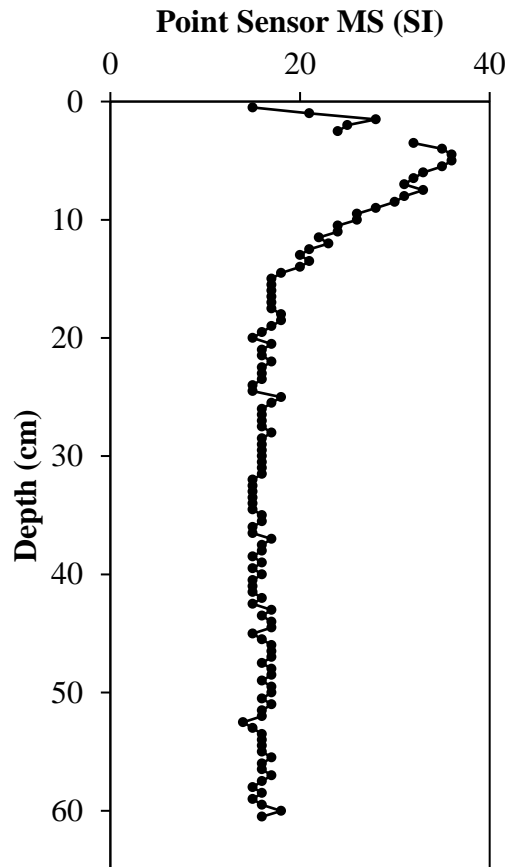
Figure 4.3. Point sensor magnetic susceptibility measurements of core 594.

4.1.5 Chronology

Activities of unsupported and supported ^{210}Pb with depth for core 594 are summarized in Table 4.1. The constant flux and sedimentation (CF:CS), constant rate of supply (CRS), and constant initial concentration (CIC) models have been applied in the interpretation of

unsupported and supported ^{210}Pb data (Figure 4.4a and Table 4.2). The CF:CS model provides the longest dating record. This model, however, assumes a constant sedimentation rate, which is typically not true for natural systems. The CIC model is discontinuous and is only reliable when the ^{210}Pb activities show a monotonic decline in the sediments, which does not occur in core 594. The CRS model accounts for variations in sedimentation rates and correlates adequately with the peak of ^{137}Cs and ^{241}Am, and as such, is considered to be the most reliable. The peak of ^{137}Cs (297.05 Bq/kg) and second-highest peak (296.88 Bq/kg) occur at 2.5 and 4.5 cm, respectively (Figure 4.4b and Table 4.3). In addition, the peak of ^{241}Am (4.65 Bq/kg) and the second-highest peak (3.89 Bq/kg) occur at 2.5 and 4.5 cm, respectively (Figure 4.4b and Table 4.3). The CRS model yields dates CE 1980.25 and 1960.88 at 2.5 and 4.5 cm, respectively (Table 4.2). These dates correspond adequately to the injection of these isotopes into the atmosphere by nuclear weapon testing that peaked in 1963 (Pennington et al. 1976; Blais et al. 1995; Benoit and Rozan 2001), and the Chernobyl reactor accident in 1986 (Bollhöfer et al. 1994; Jorhola et al. 2002).

A radiocarbon date obtained from terrestrial OM in core 594 by MacDonald (2012) is listed in Table 4.4. The calibrated date was obtained using INTCAL04 (Reimer et al. 2004) and ranges of the calibrated date were obtained using OxCal 4.1.

Cumulative Dry Mass	Midpoint Depth	Unsupported ^{210}Pb Activity	Unsupported ^{210}Pb Error	Supported ^{210}Pb Activity	Supported ^{210}Pb Error
[g/cm^2]	[cm]	[Bq/kg]	[Bq/kg]	[Bq/kg]	[Bq/kg]
0	0	568.26	55.4873	N/A	N/A
0.2144	0.5	568.26	55.4873	53.36	5.44
0.6344	1.5	416.16	55.0615	39.24	6.88
1.0493	2.5	416.6	46.2091	47.53	4.98
1.8802	4.5	300.22	36.8891	47.65	4.99
3.1642	7.5	204.42	31.3659	49.12	4.37
4.5029	10.5	64.31	24.1419	51.85	4.7
5.8001	13.5	16.87	25.9235	50.77	4.88
7.0184	16.5	33.6	21.5885	48.75	4.18
8.5329	20.5	0	21.6163	48	4.37
9.6072	23.5	0	29.1047	46.11	5.18
10.6714	26.5	0	24.9148	43.22	4.99
12.0927	30.5	44.1	24.562	37.66	4.48
13.1534	33.5	17.74	24.2497	43.83	4.33
14.236	36.5	47.04	20.8038	38.64	3.6
15.6653	40.5	4.05	21.1604	39.71	3.78

Table 4.1. Activities of unsupported ^{210}Pb and supported ^{210}Pb with depth for core 594.
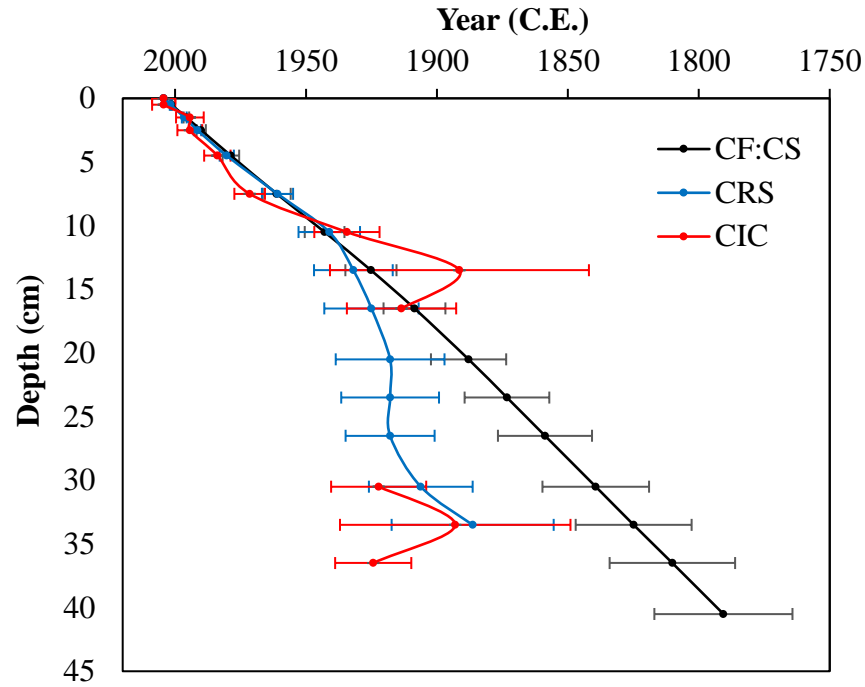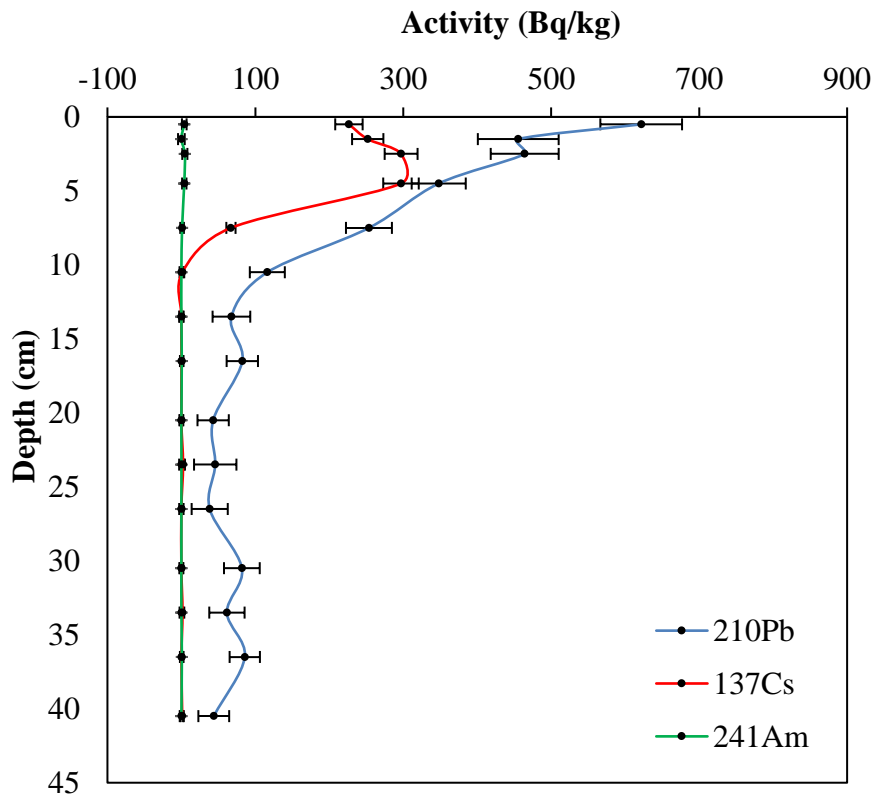
Figure 4.4. (a) Age-depth relationship for the three ^{210}Pb dating models. (b) Activities of ^{210}Pb, [137]C and [241]Am measured for core 594.

Midpoint Depth	Constant Flux & Sedimentation			Constant Rate of Supply			Constant Initial Concentration		
[cm]	Age [y]	Year [y]	Error [y]	Age [y]	Year [y]	Error [y]	Age [y]	Year [y]	Error [y]
0	0	2004.34	0	0	2004.34	0	0	2004.34	4.4345
0.5	2.9253	2001.41	0.3609	2.6934	2001.65	0.3775	0	2004.34	4.4345
1.5	8.6557	1995.68	1.0678	7.854	1996.49	0.9183	10.0035	1994.34	5.2806
2.5	14.3166	1990.02	1.7661	12.9104	1991.43	1.4069	9.9696	1994.37	4.7455
4.5	25.6533	1978.69	3.1646	24.0886	1980.25	2.7107	20.4902	1983.85	5.04
7.5	43.172	1961.17	5.3258	43.4599	1960.88	5.9522	32.8324	1971.51	5.8405
10.5	61.4371	1942.9	7.579	63.2302	1941.11	11.7423	69.9699	1934.37	12.4563
13.5	79.136	1925.2	9.7623	72.4285	1931.91	15.0222	112.943	1891.4	49.4464
16.5	95.7584	1908.58	11.8129	79.3409	1925	18.0147	90.8174	1913.52	20.87
20.5	116.4221	1887.92	14.362	86.4572	1917.88	20.7683	N/A	N/A	N/A
23.5	131.0797	1873.26	16.1702	86.4572	1917.88	18.6672	N/A	N/A	N/A
26.5	145.5996	1858.74	17.9614	86.4572	1917.88	16.9964	N/A	N/A	N/A
30.5	164.9917	1839.35	20.3536	98.1674	1906.17	19.8126	82.0848	1922.25	18.1585
33.5	179.4638	1824.88	22.1389	117.9832	1886.36	30.9408	111.328	1893.01	44.0088
36.5	194.2346	1810.1	23.9611	196.2206	1808.12	288.3074	80.0122	1924.33	14.5443
40.5	213.7359	1790.6	26.3668	N/A	N/A	N/A	N/A	N/A	N/A

Table 4.2. Summary table of radioisotope dates obtained by CF/CS, CRS and CIC models by depth for core 594.

Cumulative Dry Mass	Midpoint Depth	^{210}Pb Activity	^{210}Pb (error)	^{137}Cs Activity	^{137}Cs (error)	^{241}Am Activity	^{241}Am (error)
[g/cm^2]	[cm]	[Bq/kg]	[Bq/kg]	[Bq/kg]	[Bq/kg]	[Bq/kg]	[Bq/kg]
0.2144	0.5	621.62	55.22	226.48	18.53	3.87	3.13
0.6344	1.5	455.4	54.63	251.91	21.16	0	4.51
1.0493	2.5	464.13	45.94	297.05	22.23	4.65	3.46
1.8802	4.5	347.87	36.55	296.88	24.01	3.89	2.93
3.1642	7.5	253.54	31.06	66.98	6.22	0.92	2.5
4.5029	10.5	116.16	23.68	1.35	2.5	0	2.52
5.8001	13.5	67.64	25.46	0	2.65	0	2.79
7.0184	16.5	82.35	21.18	0.2	2.15	0.5	2.26
8.5329	20.5	42.92	21.17	0	2.43	0	2.38
9.6072	23.5	45.75	28.64	2.17	2.66	0.06	3.11
10.6714	26.5	38.28	24.41	0	2.56	0	2.69
12.0927	30.5	81.76	24.15	0	2.37	0	2.55
13.1534	33.5	61.57	23.86	1.48	2.44	0	2.5
14.236	36.5	85.68	20.49	0.09	2.09	0.63	2.27
15.6653	40.5	43.76	20.82	1.11	2.14	0	2.25

Table 4.3. Activities of ^{210}Pb, ^{137}Cs and ^{241}Am with depth for core 594.

Sample ID	Interval [cm]	$\delta^{13}C$ (VPDB, ‰)	^{14}C Date [year BP]	Accepted Date	Calibrated Date	Range
AA64477	340 - 350	–26.3	6065 ± 47	6065	6925	7155 - 6785

Table 4.4. AMS ^{14}C date for core 594 OM (plant/insect fragments) at 430 – 350 cm from MacDonald (2012). Radiocarbon date was converted to calibrated date using INTCAL04 (Reimer et al. 2004). Ranges on calibrated date were calculated using OxCal 4.1.

4.1.6   TOC, TN, and C/N ratio

The Total Organic Carbon (TOC) and Total Nitrogen (TN) contents of core 594 range between 3.70–4.05 % and 0.43–0.51 %, respectively (Figure 4.5a and b, respectively). Both patterns are characterized by a sharp decrease at 45.5 cm, which is followed by a sharp increase at 40.0 cm. The amounts then decrease at 35.5 and 30.5 cm, before increasing at 25.5 and 20.5 cm but all measurements in this interval are above average for the core. The TOC values sharply decrease at 15.5 cm, followed by a gradual increase at the top of the core. The TN values gradually decrease above 20.5 cm until 9.5 cm, after which they gradually increase up core. The C/N ratios range from 9.2–10.4 and average 9.4 (Figure 4.5c). No significant change in C/N ratio occurs from 60.5 to 15.5 cm, after which there is an increase from 15.5 to a maximum of 10.4 at 9.5 cm. The C/N ratio then gradually declines, with the ratios at 9.5 and 7.5 cm being the only measurements that exceed a C/N ratio of 10. The increase in C/N ratio between 15.5 and 9.4 cm is inversely proportional to the decrease in TN over the same interval.
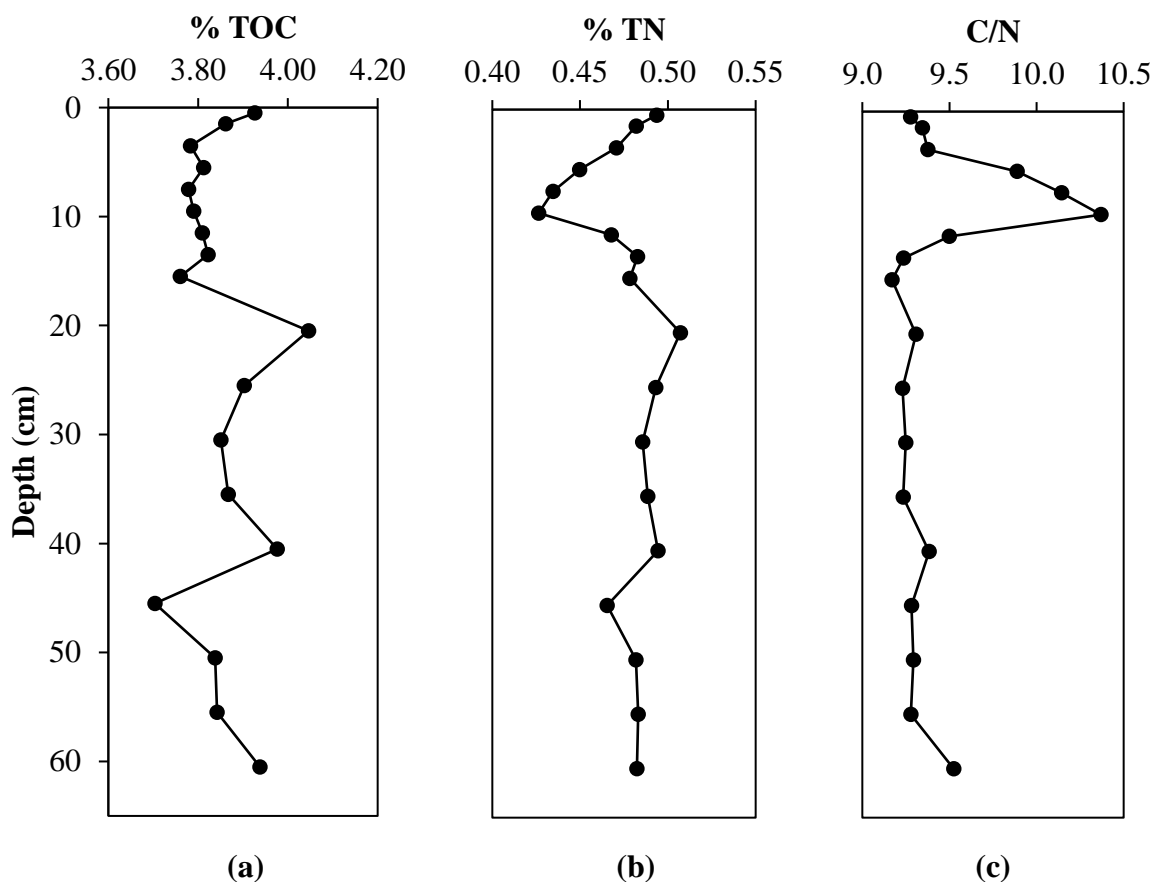
Figure 4.5. (a) TOC, (b) TN, and (c) C/N ratio for core 594.

4.1.7   Carbon- and Nitrogen-Isotope Compositions of OM

The carbon-isotope composition of OM ($\delta^{13}C_{OM}$) for core 594 ranges from –26.80 to

–26.07 ‰ (Figure 4.6a). There is little variation from 60.5 to 45.5 cm, followed by a sharp

increase at 40.5 cm. The $\delta^{13}C_{OM}$ then gradually decreases from 40.5 to 30.5 cm, before sharply

decreasing at 25.5 cm, and then gradually decreasing until reaching the core minimum of –26.80

‰ at 13.5 cm. The $\delta^{13}C_{OM}$ then sharply increases to the core's maximum of –26.07 ‰ at 9.5 cm.

A decrease in $\delta^{13}C_{OM}$ occurs at 1.5 cm, followed by a small increase to the top of the core.

The nitrogen-isotope composition of OM ($\delta^{15}N_{TN}$) ranges from +4.34 to +5.17 ‰ (Figure 4.6b). Following a sharp decrease from 60.5 to 55.5 cm, the $\delta^{15}N_{TN}$ gradually decreases until 13.5 cm, where the minimum of +4.34 ‰ is reached. An overall trend of increasing $\delta^{15}N_{TN}$ then follows to the maximum of +5.17 ‰ at 0.5 cm.
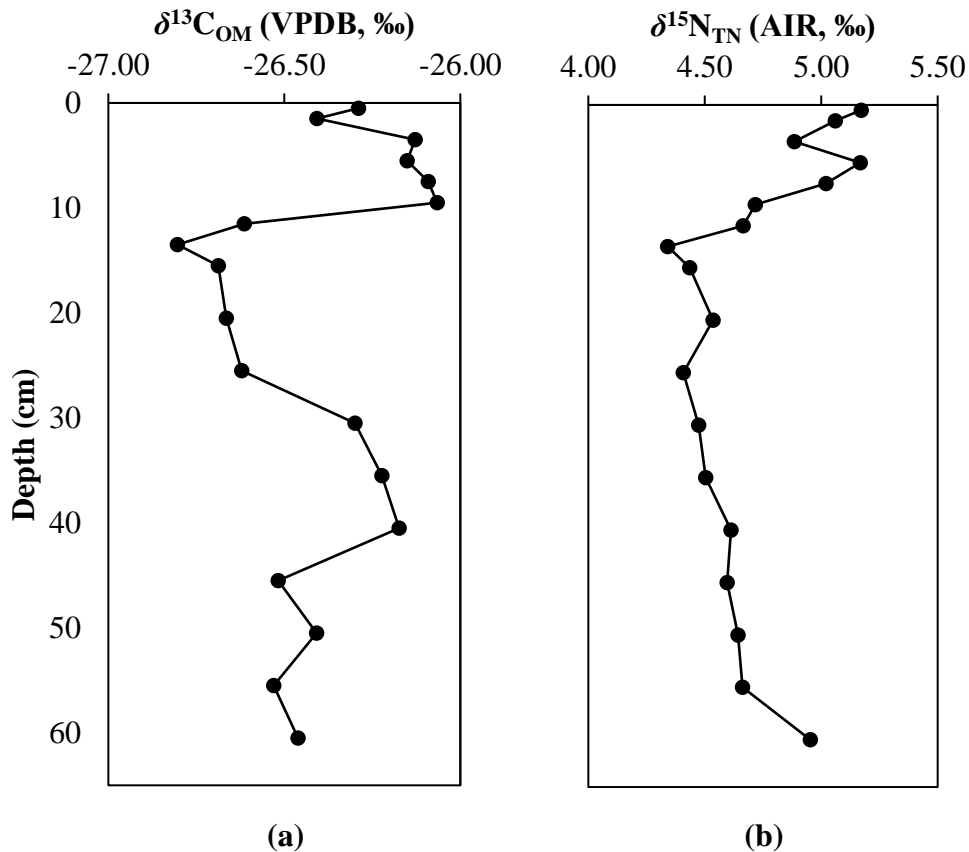
Figure 4.6. (a) $\delta^{13}C_{OM}$ and (b) $\delta^{15}N_{TN}$ for core 594.

4.2   Core 181 (Manitoulin Basin)

4.2.1   Core Description

Wet sediment in core 181 is very dark greyish brown (10YR 3/2) throughout, except for the top 20 cm, which is brown (10YR 5/3). The sediments are fine-grained silt and clay. There were no visible shell fragments or plant material.

4.2.2 Grain Size

Grain size measurements were made for 7 samples from core 181 (Figure 4.7a and b). The d(0.5) results range from 2.0–2.8 μm. Between 100.5 and 50.0 cm, the d(0.5) increases to the highest value of 2.8 μm, before decreasing to the lowest value of 2.0 μm at 40.5 cm. Grain size then generally and gradually increases to the top of the core. The d(0.1) measurements do not show any significant variations throughout the core, and d(0.9) shows a similar trend to d(0.5).

(a)
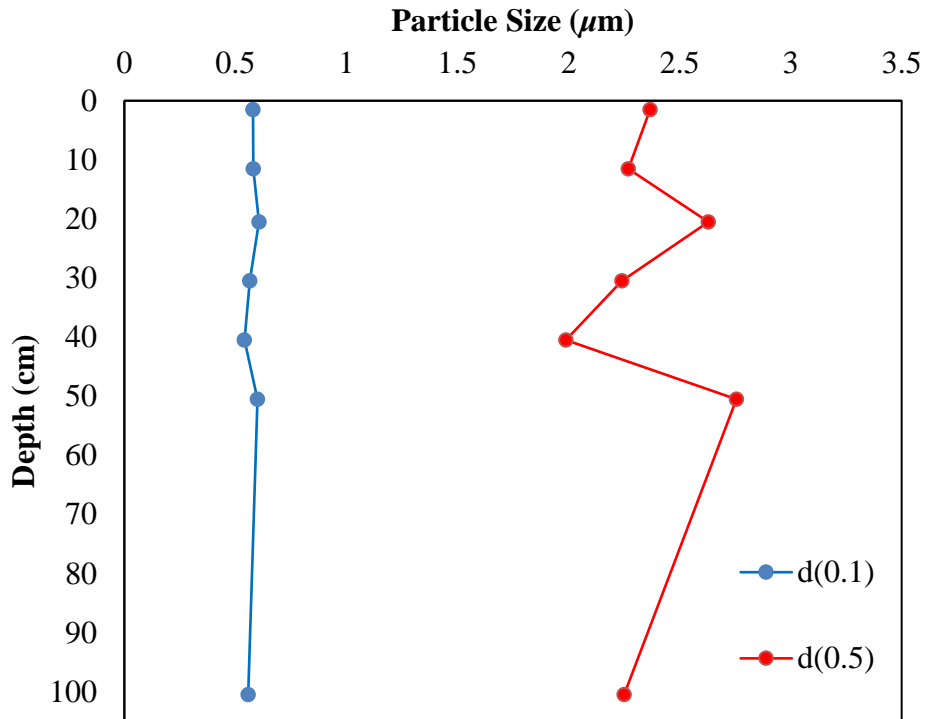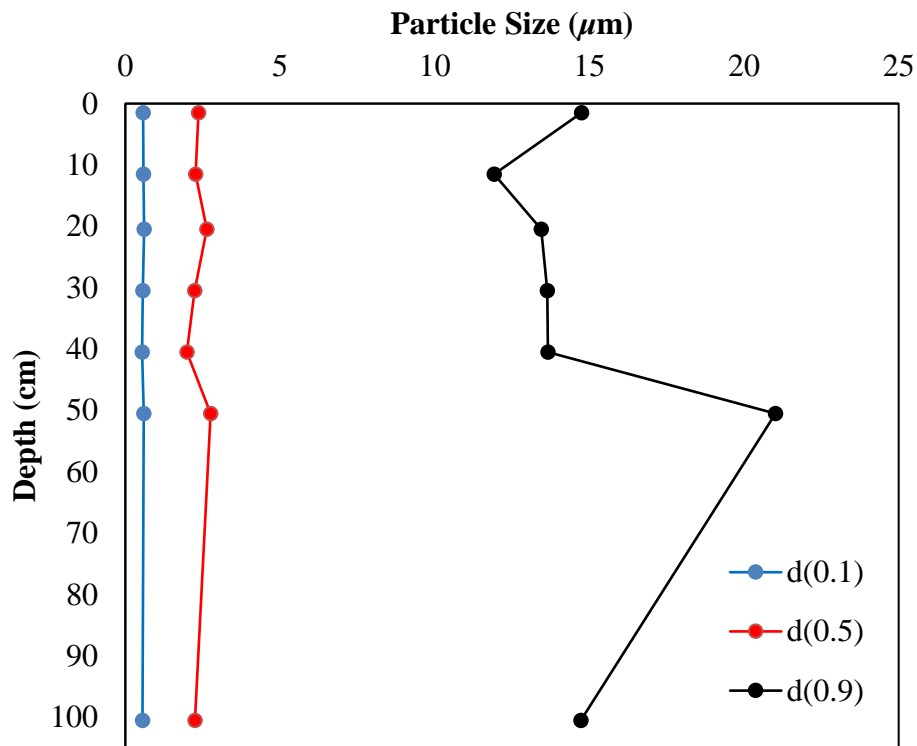
Figure 4.7. Grain size distributions for core 181: (a) d(0.1) and d(0.5) indicate that 10 % and 50 % of the sediment is finer than the size (μm) indicated; (b) d(0.9) indicates that 90 % of the sediment is finer than the size (μm) indicated.

4.2.3   Mineralogy

Minerals observed are quartz, K-feldspar, plagioclase feldspar, calcite, dolomite, amphibole, and clay minerals (1.4 nm – chlorite; 1.0 nm – illite; 0.7 nm – kaolinite) (Figure 4.8). Quartz shows the largest variation in abundance, ranging from 50-56 %. Clay mineral content does not vary significantly and represents the second largest mineral fraction, with chlorite, illite and kaolinite contents of 10-11 %, 9-11 %, and 6-7 %, respectively. Potassium feldspar and plagioclase contents are 6-7 % and 8-9 % respectively. Dolomite was detected (2%) only at 100.5 cm. Calcite content is minimal, ranging from 2-4 %.
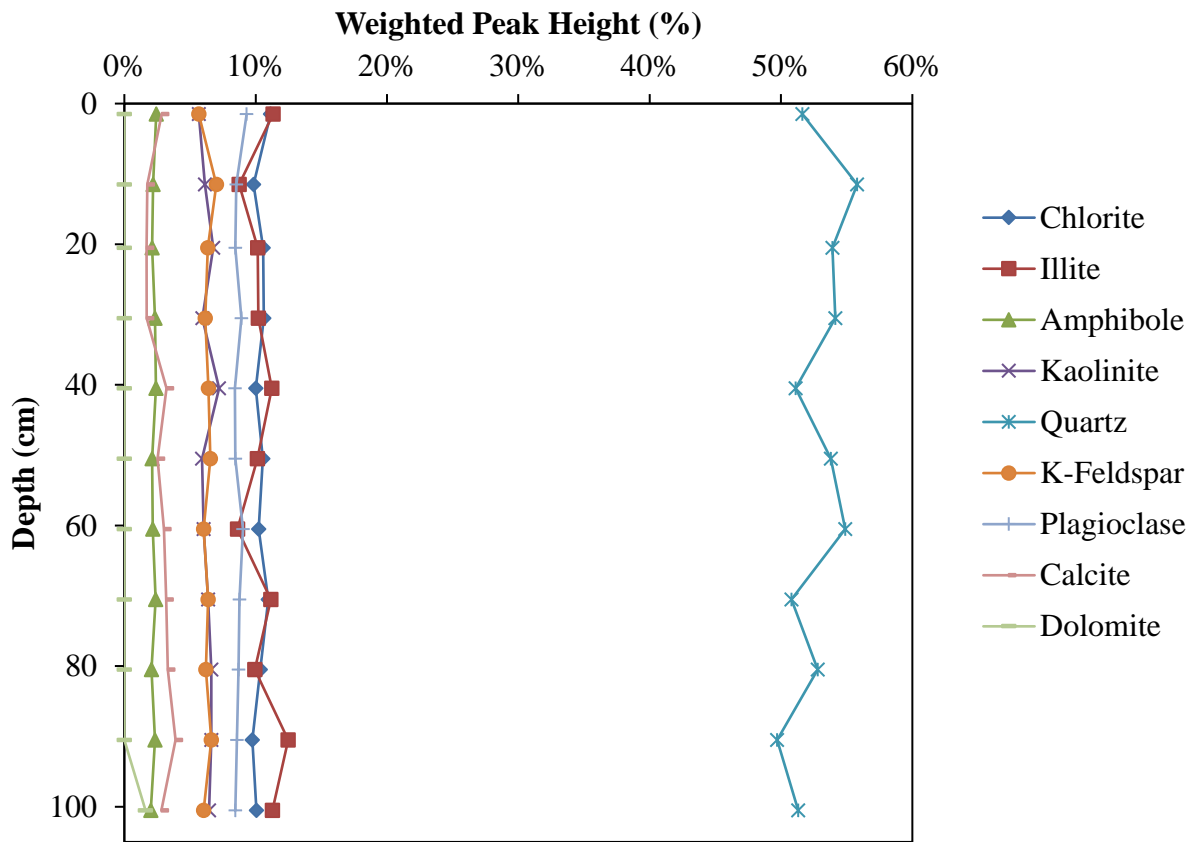
Figure 4.8. Mineral abundances for core 181. Percentages are based on weighted peak heights of the strongest diffraction for each phase, as measured by p-XRD.

4.2.4   Magnetic Susceptibility (MS)

Half-core MS signals were measured with a point sensor (Figure 4.9). Point sensor MS signals average 11. The point sensor MS signals are relatively constant throughout the core until ~40.5 cm, where a sharp decrease in MS occurs until 28 cm, after which there is a gradual increase until a maximum of 18 SI is reached at 12 and 12.5 cm. The MS signal then generally decreases towards the top of the core.
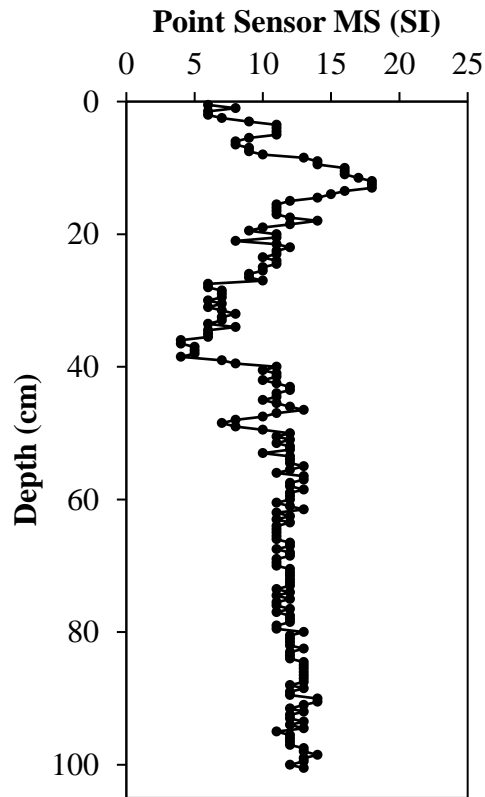
Figure 4.9. Point sensor magnetic susceptibility measurements for core 181.

4.2.5 Chronology

Activities of unsupported and supported ^{210}Pb with depth for core 181 are summarized in Table 4.5. The constant flux and sedimentation (CF:CS), constant rate of supply (CRS), and constant initial concentration (CIC) models have been applied in the interpretation of unsupported and supported ^{210}Pb data (Figure 4.10a and Table 4.6). The CF:CS model provides the longest dating record. This model, however, assumes a constant sedimentation rate, which is typically not true for natural systems. The CIC model agrees with the CF:CS model but is only reliable when ^{210}Pb activities show a monotonic decline in the sediments, which does not occur in core 181. The CRS model agrees with the CF:CS and CIC models. It also accounts for variations in sedimentation rates and correlates well with the peak of ^{137}Cs and ^{241}Am, and as

such, is considered to be the most reliable. The peak of ^{137}Cs (305.35 Bq/kg) occurs at 10.5 cm

(Figure 4.10b and Table 4.7). In addition, the peak of ^{241}Am (2.83 Bq/kg) also occurs at 10.5 cm

(Figure 4.10b and Table 4.7). The CRS model yields a date of CE 1968.49 at 10.5 cm. This date

corresponds well to nuclear testing that peaked in 1963 and the Chernobyl reactor accident in

1986.

Cumulative Dry Mass	Midpoint Depth	Unsupported ^{210}Pb Activity	Unsupported ^{210}Pb Error	Supported ^{210}Pb Activity	Supported ^{210}Pb Error
[g/cm^2]	[cm]	[Bq/kg]	[Bq/kg]	[Bq/kg]	[Bq/kg]
0	0	985.216	90.4741	N/A	N/A
0.1872	0.5	985.216	90.4741	50.234	5.446
0.5661	1.5	818.186	90.9432	50.234	5.446
0.9436	2.5	758.266	65.8456	50.234	5.446
1.6848	4.5	768.326	68.8856	50.234	5.446
2.7958	7.5	427.826	49.5403	50.234	5.446
3.9066	10.5	292.536	57.1899	50.234	5.446
5.0571	13.5	286.416	47.6522	50.234	5.446
6.2554	16.5	131.346	26.7796	50.234	5.446
7.8342	20.5	138.956	28.5149	50.234	5.446
8.9912	23.5	77.286	23.8501	50.234	5.446
10.1254	26.5	15.096	24.815	50.234	5.446
11.6016	30.5	22.376	26.4859	50.234	5.446
12.6874	33.5	55.016	23.2955	50.234	5.446
13.7737	36.5	20.486	23.8598	50.234	5.446
15.2661	40.5	25.096	23.1497	50.234	5.446

Table 4.5. Activities of unsupported ^{210}Pb and supported ^{210}Pb with depth for core 181.
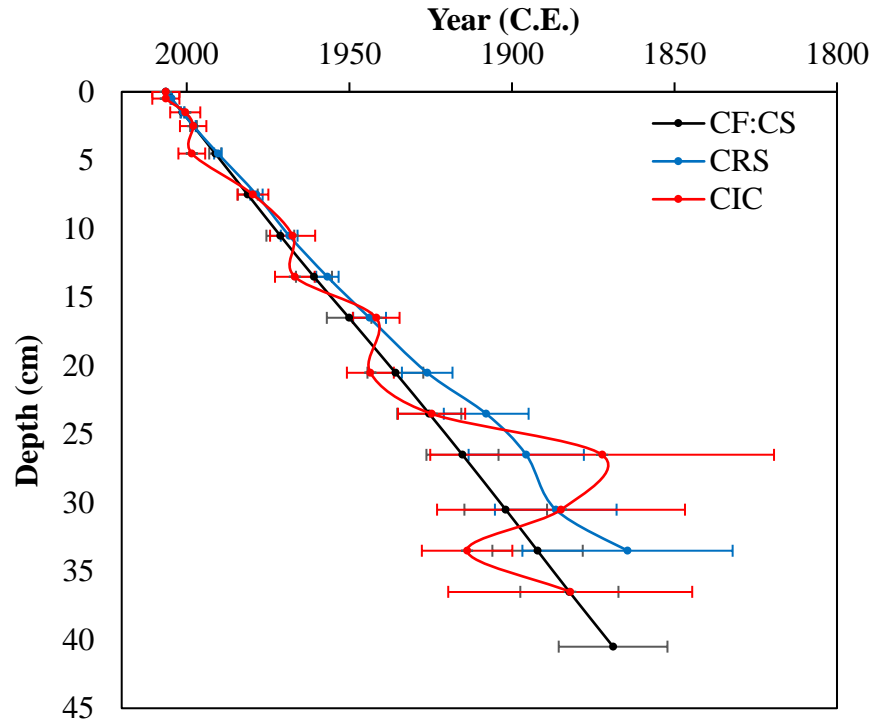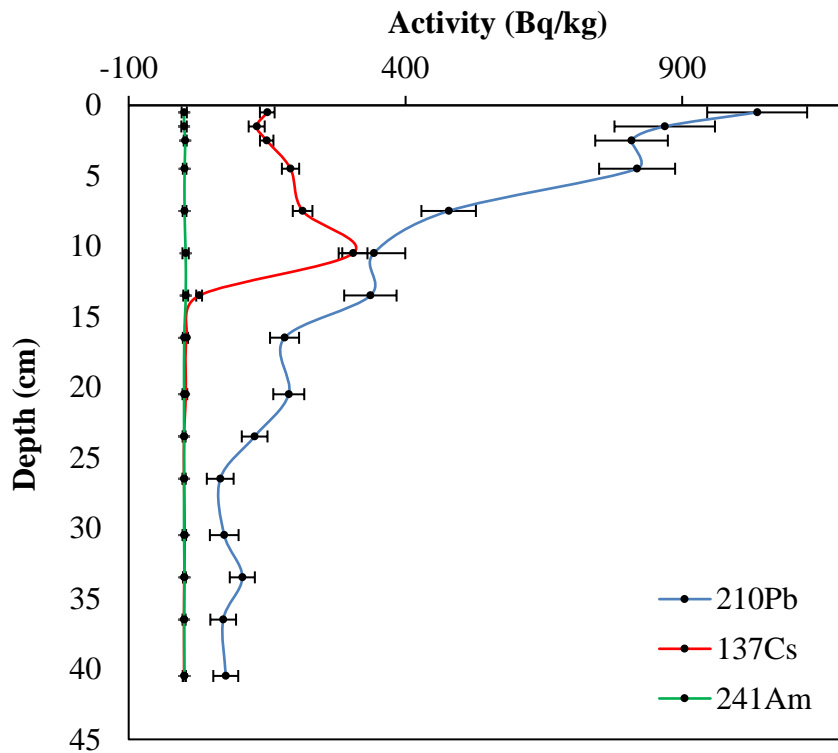
Figure 4.10. (a) Age-depth relationship for the three ^{210}Pb dating models. (b) Activities of ^{210}Pb, ^{137}C and ^{241}Am measured for core 181.

52

Midpoint Depth	Constant Flux & Sedimentation			Constant Rate of Supply			Constant Initial Concentration		
[cm]	Age [y]	Year [y]	Error [y]	Age [y]	Year [y]	Error [y]	Age [y]	Year [y]	Error [y]
0	0	2006.42	0	0	2006.42	0	0	2006.42	4.1705
0.5	1.6868	2004.74	0.2051	1.7181	2004.71	0.2105	0	2006.42	4.1705
1.5	5.101	2001.32	0.6201	5.166	2001.26	0.4901	5.9657	2000.46	4.6301
2.5	8.5025	1997.92	1.0337	8.5036	1997.92	0.6711	8.408	1998.02	4.0587
4.5	15.1813	1991.24	1.8457	16.0023	1990.42	1.155	7.9848	1998.44	4.1214
7.5	25.1922	1981.23	3.0627	27.8677	1978.56	1.9076	26.7869	1979.64	4.746
10.5	35.2013	1971.22	4.2796	37.9365	1968.49	2.5713	38.994	1967.43	6.9361
13.5	45.5681	1960.86	5.5399	49.6924	1956.73	3.4388	39.6729	1966.75	6.1026
16.5	56.3657	1950.06	6.8527	62.6605	1943.76	5.0462	64.7086	1941.72	7.1809
20.5	70.5918	1935.83	8.5822	80.3837	1926.04	7.7798	62.8999	1943.52	7.2196
23.5	81.0172	1925.41	9.8497	98.5375	1907.89	13.0432	81.7389	1924.69	10.3394
26.5	91.2372	1915.19	11.0921	110.8413	1895.58	17.7272	134.182	1872.24	52.8701
30.5	104.5388	1901.89	12.7093	119.9293	1886.5	18.7119	121.544	1884.88	38.1257
33.5	114.3227	1892.1	13.8988	141.9909	1864.43	32.3283	92.6537	1913.77	13.9138
36.5	124.111	1882.31	15.0888	248.7987	1757.63	727.5451	124.378	1882.05	37.5178
40.5	137.5586	1868.87	16.7237	N/A	N/A	N/A	N/A	N/A	N/A

Table 4.6. Summary table of radioisotope dates obtained by CF/CS, CRS and CIC models by depth for core 181.

Cumulative Dry Mass	Midpoint Depth	^{210}Pb Activity	^{210}Pb (error)	^{137}Cs Activity	^{137}Cs (error)	^{241}Am Activity	^{241}Am (error)
[g/cm^2]	[cm]	[Bq/kg]	[Bq/kg]	[Bq/kg]	[Bq/kg]	[Bq/kg]	[Bq/kg]
0.1872	0.5	1035.45	90.31	150.34	13.27	0.35	4.71
0.5661	1.5	868.42	90.78	131.24	14.49	0	4.86
0.9436	2.5	808.5	65.62	149.34	12.16	2.13	2.69
1.6848	4.5	818.56	68.67	192.4	15.61	1.03	3.22
2.7958	7.5	478.06	49.24	214.19	17.73	0.87	3.36
3.9066	10.5	342.77	56.93	305.35	26.02	2.83	5.66
5.0571	13.5	336.65	47.34	27.26	5.26	3.04	4.4
6.2554	16.5	181.58	26.22	4.61	2.59	0.33	2.48
7.8342	20.5	189.19	27.99	3.18	2.55	0	2.73
8.9912	23.5	127.52	23.22	0	2.18	0	2.39
10.1254	26.5	65.33	24.21	0	2.57	0	2.53
11.6016	30.5	72.61	25.92	1.1	2.63	0	2.77
12.6874	33.5	105.25	22.65	0.28	2.18	0.71	2.34
13.7737	36.5	70.72	23.23	0	2.21	0	2.59
15.2661	40.5	75.33	22.5	0	2.41	0.7	2.49

Table 4.7. Activities of ^{210}Pb, ^{137}Cs and ^{241}Am with depth for core 181.

4.2.6   TOC, TN, and C/N ratio

The TOC and TN for core 181 range between 2.54–2.95 % and 0.32–0.38 %, respectively (Figure 4.11a and b, respectively). TOC measurements do not vary significantly from 100.5 to 40.5 cm. From this point, TOC then increases until the maximum of 2.95 % is reached at 20.5 cm. This is followed by a decrease until 11.5 cm, and then a general increase up core. TN does not vary significantly throughout the core, but there is a slight, gradual increases from 100.5 to 25.5 cm. This is followed by a decrease until 13.5 cm, and then a gradual increase up core. The maximum TN of 0.38 % occurs at 0.5 cm. The C/N ratio ranges from 8.6–9.9 and has an average of 9.1 (Figure 4.11c). There is a gradual decrease in C/N ratio from 9.2 to 8.6 between 100.5 to 40.5 cm, followed by a sharp increase in C/N ratio until its maximum is reached at 15.5 cm. After 13.5 cm, the C/N ratio then generally decreases towards the top of the core.
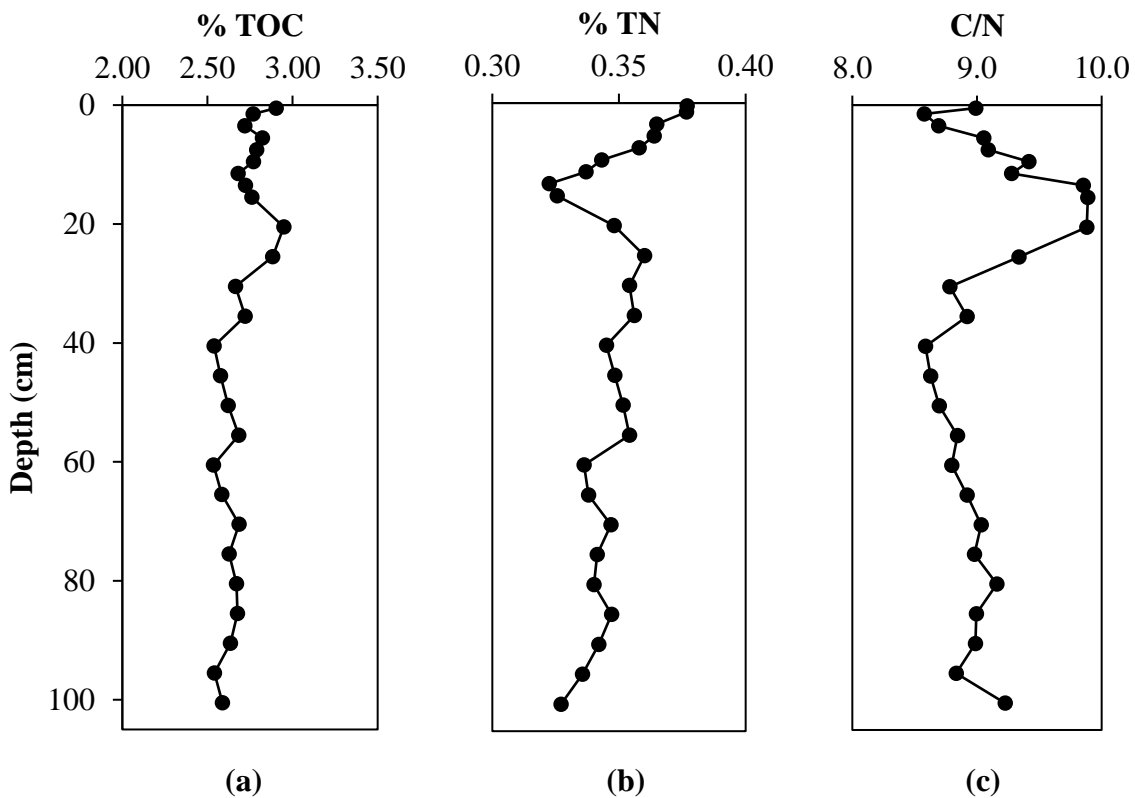
Figure 4.11. (a) TOC, (b) TN, and (c) C/N ratio for core 181.

4.2.7 Carbon- and Nitrogen-Isotope Compositions of OM

The $\delta^{13}C_{OM}$ of core 594 ranges from –27.43 to –26.40 ‰ (Figure 4.12a). The $\delta^{13}C_{OM}$ generally increases from 100.5 to 55.5 cm, where the maximum of –26.40 ‰ is reached. The $\delta^{13}C_{OM}$ then generally decreases upwards in the core to the minimum of –27.43 ‰ reached at 3.5 cm, after which there is a small increase to the top of the core.

The $\delta^{15}N_{TN}$ for core 594 ranges from +5.27 to +6.33 ‰ (Figure 4.12b), decreasing from the base of the core at 100.5 cm to the minimum of +5.27 ‰ at 40.5 cm. The $\delta^{15}N_{TN}$ then increases to +6.24 ‰ by 13.5 cm, followed by decreasing values to 7.5 cm, and then gradual increases to the top of the core, where the maximum of +6.33 ‰ is reached at 0.5 cm.
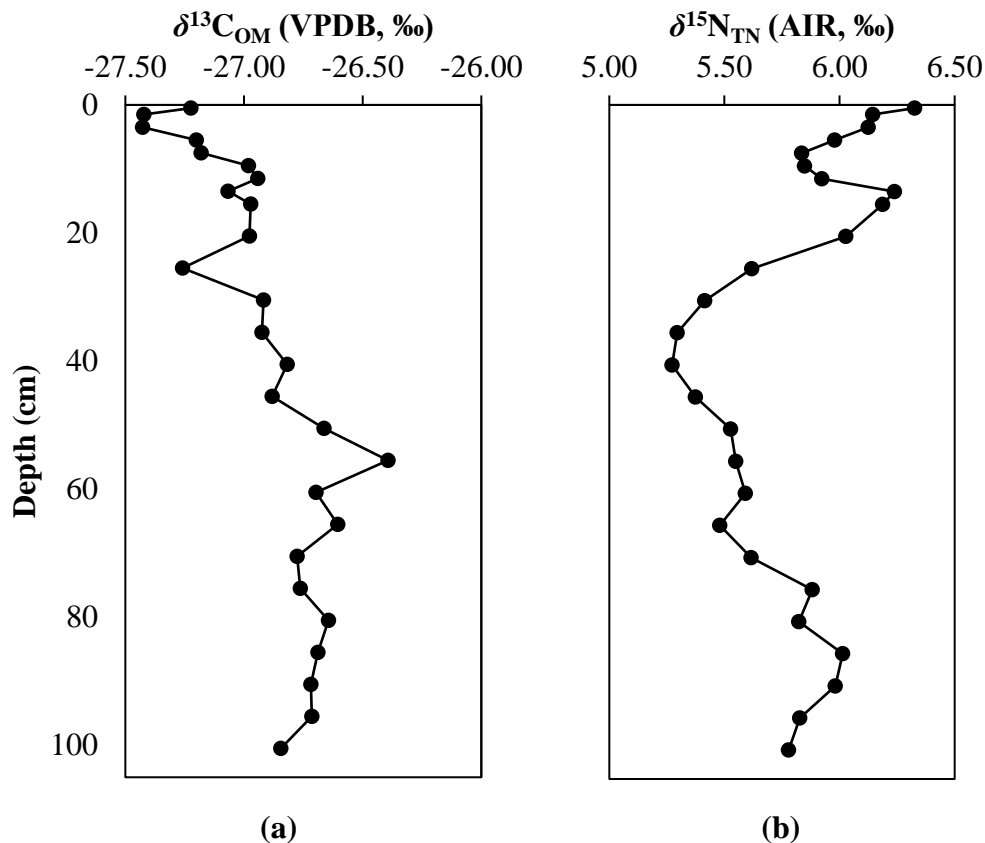
Figure 4.12. (a) $\delta^{13}C_{OM}$ and (b) $\delta^{15}N_{TN}$ for core 181.

4.3   Core 182 (Mackinac Basin)

4.3.1   Core Description

Wet sediment at the very bottom of core 182 is brown (10YR 5/3), and lighter than the rest of the core. The majority of the rest of the core is dark greyish brown (10YR 4/2), except for the top 2 cm of the core, which is very dark greyish brown (10YR 3/2). The sediments are fine-grained silt and clay. There were no visible shell fragments or plant material. A portion of the core, between 68 to 78 cm was missing, due to previous sampling.

4.3.2   Grain Size

Grain size measurements were made for samples from 7 intervals in core 182 (Figure 4.13a and b). The d(0.5) results range from 2.1–2.5 μm, with a very small upward trend of increasing grain size. The d(0.1) measurements do not vary significantly, and d(0.9) measurements show a similar trend to d(0.5).

(a)
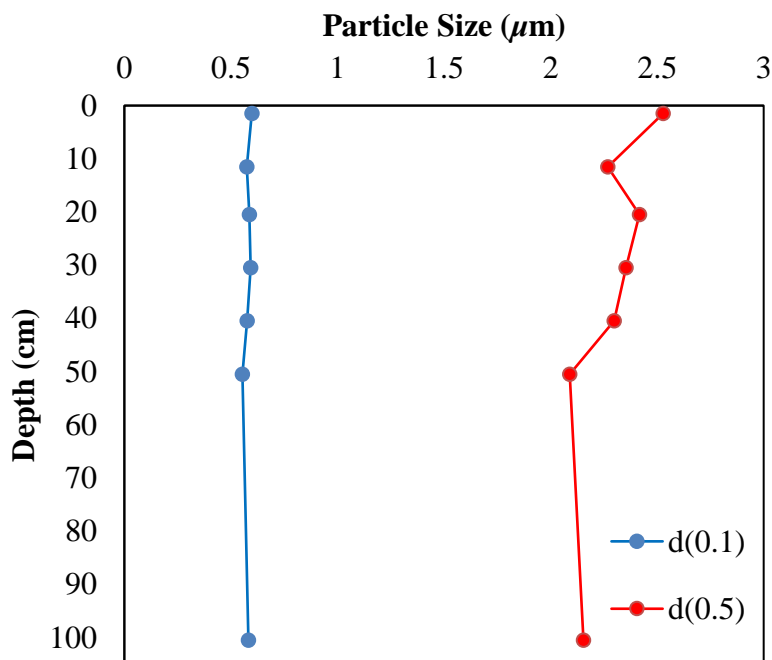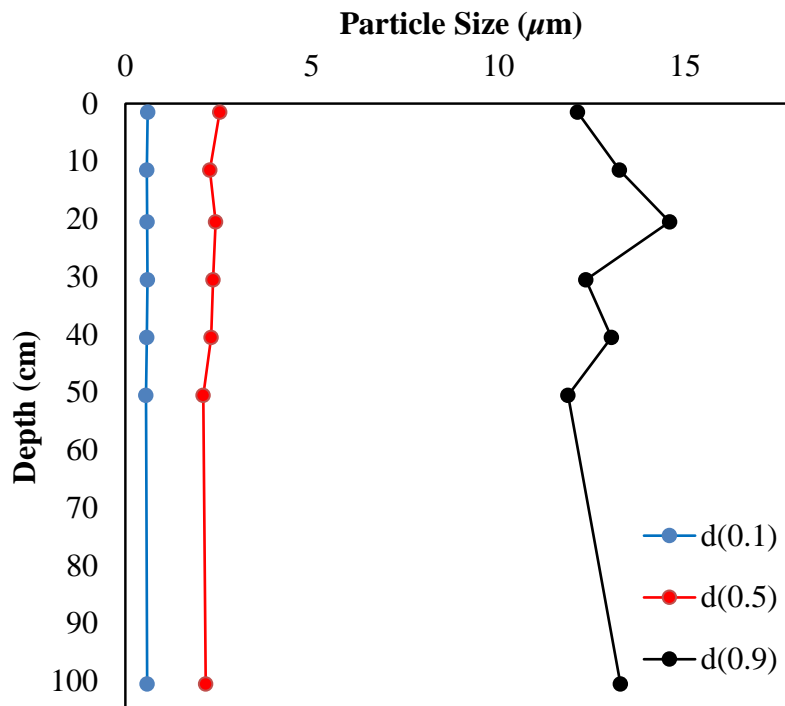
Figure 4.13. Grain size distributions for core 182: (a) d(0.1) and d(0.5) indicate that 10 % and 50 % of the sediment is finer than the size (μm) indicated; (b) d(0.9) indicates that 90 % of the sediment is finer than the size (μm) indicated.

4.3.3 Mineralogy

Minerals observed are quartz, K-feldspar, plagioclase, calcite, amphibole, and clay minerals (1.4 nm – chlorite; 1.0 nm – illite; 0.7 nm – kaolinite) (Figure 4.14). Quartz abundance varies most throughout the core (52-60 %). It is highest at the base (100.5 cm) and decreases to its lowest at 60.5 cm, above which abundances are somewhat higher (~54-58 %). Clay mineral content does not vary significantly along the core, with chlorite, illite and kaolinite contents of 8-11 %, 8-11 %, and 5-7 %, respectively. Potassium feldspar and plagioclase contents are 5-7 % and 9-11 %, respectively. Calcite abundance is relatively constant at 3%, until above 10.5 cm where it disappears. Dolomite is not present. Amphibole content is 1-2 % throughout.

57
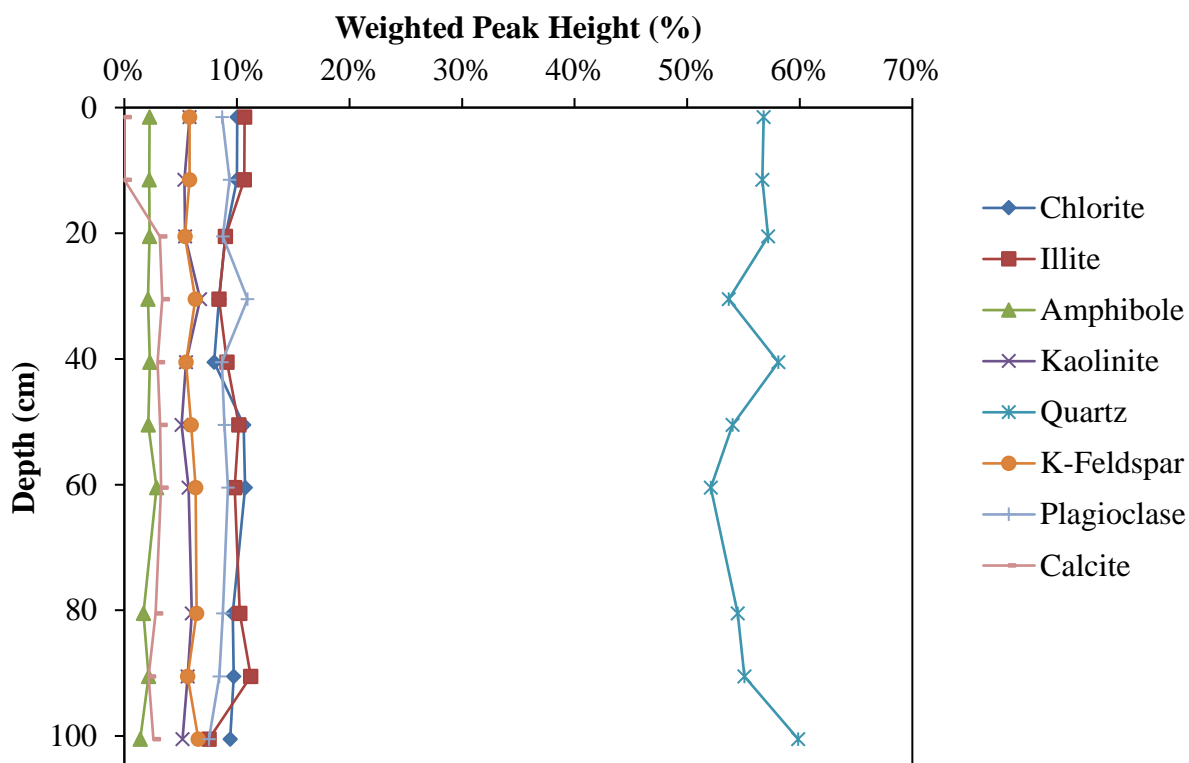
Figure 4.14. Mineral abundances for core 182. Percentages are based on weighted peak heights of the strongest diffraction for each phase, as measured by p-XRD.

4.3.4   Magnetic Susceptibility

Half-core MS signals, measured with a point sensor, averaged 11.1 (Figure 4.15). The MS signals generally decrease from the base of the core at 100.5 cm to 79.0 cm. Above the gap (missing core), the MS signal remains relatively stable until 10.5 cm. The signal then fluctuates first to higher and then lower values (at 6 cm). This is followed by a gradual increase to a maximum of 22 at 2.5 cm, which is followed by a small decrease to the top of the core.
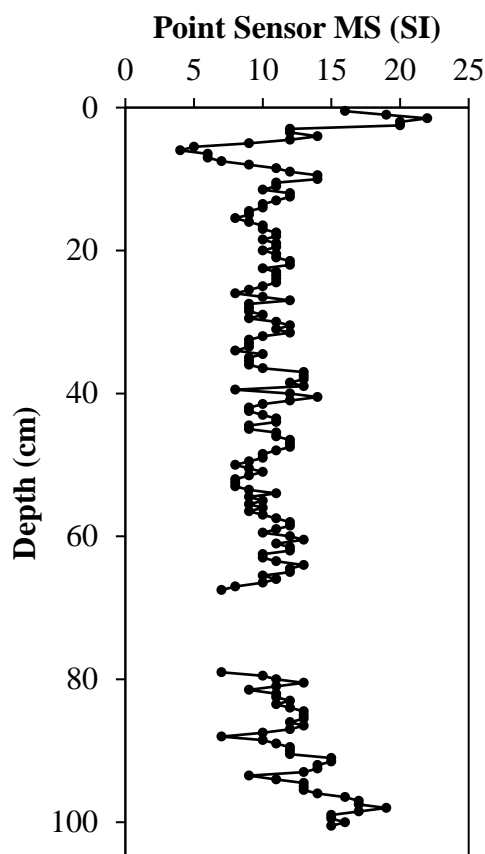
Figure 4.15. Point sensor magnetic susceptibility measurements for core 182.

4.3.5   Chronology

Activities of unsupported and supported ^{210}Pb with depth for core 182 are summarized in

Table 4.8. The constant flux and sedimentation (CF:CS), constant rate of supply (CRS), and

constant initial concentration (CIC) models have been applied in the interpretation of

unsupported and supported ^{210}Pb data (Figure 4.16a and Table 4.9). The CF:CS model provides

the longest dating record. This model, however, assumes a constant sedimentation rate, which is

typically not true for natural systems. The CIC model agrees with the CF:CS model but is only

reliable when the ^{210}Pb activities show a monotonic decline in the sediments, which does not

occur in core 182. The CRS model agrees with the CF:CS and CIC models. It also accounts for

variations in sedimentation rates. None of the models, however, agree with the peak of ^{137}Cs and

[241]Am. The peak of [137]Cs (160.44 Bq/kg) occurs at 0.5 cm (Figure 4.16b and Table 4.10). In addition, the peak of [241]Am (13.46 Bq/kg) also occurs at 0.5 cm (Figure 4.3.2b and Table 4.10). The CRS model yields a date of CE 2000.37 at 0.5 cm. In contrast, dates that would correspond adequately with nuclear testing that peaked in 1963 and the Chernobyl reactor accident in 1986 occur at 2.5 cm (1978.87) and 4.5 cm (1851.02). While the CRS model does not agree with the ^{137}Cs maximum, it is still considered to be the most reliable. The discrepancies in the dates may reflect the location of core 182 in northern Mackinac basin, south of Cockburn Island. This is an area containing many small islands, and strong currents, wave action and turbulence, which may have affected the sedimentation rate.

Cumulative Dry Mass	Midpoint Depth	Unsupported [210]Pb Activity	Unsupported [210]Pb Error	Supported [210]Pb Activity	Supported [210]Pb Error
[g/cm^2]	[cm]	[Bq/kg]	[Bq/kg]	[Bq/kg]	[Bq/kg]
0	0	344.36	45.5412	N/A	N/A
0.196	0.5	344.36	45.5412	63.1	5.88
0.5717	1.5	253.42	36.4642	44.41	5.07
0.9728	2.5	185.2	31.1482	51.17	4.51
1.8036	4.5	90.03	25.2928	47.6	4.21
2.9748	7.5	23.68	26.7979	43.23	4.77
4.1707	10.5	3.45	21.3598	41.99	3.85
5.3864	13.5	17	24.2499	49.49	4.44
6.538	16.5	33.18	26.6003	48.69	4.54
8.0486	20.5	32.81	21.3431	47.91	3.92
9.242	23.5	0	27.1177	49.75	4.51
10.4409	26.5	27.31	20.4636	54.51	3.68
12.0704	30.5	18.97	19.84	44.89	3.38
13.3039	33.5	40.76	20.7259	47.49	3.49
14.5229	36.5	16.07	22.567	46.65	3.71
16.1707	40.5	10.45	20.4776	45.72	3.81

Table 4.8. Activities of unsupported ^{210}Pb and supported ^{210}Pb with depth for core 182.
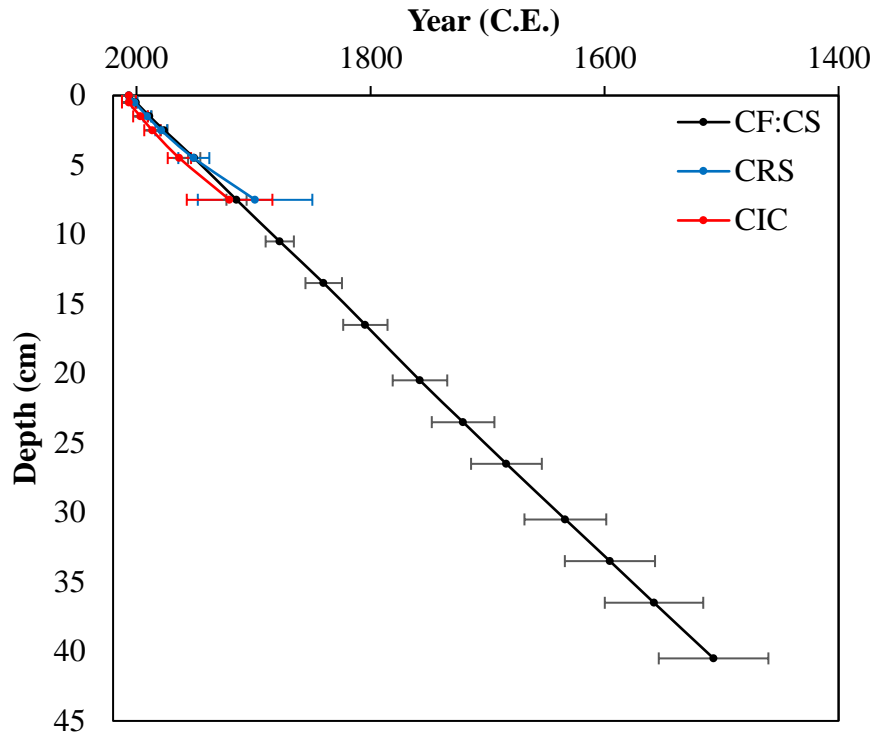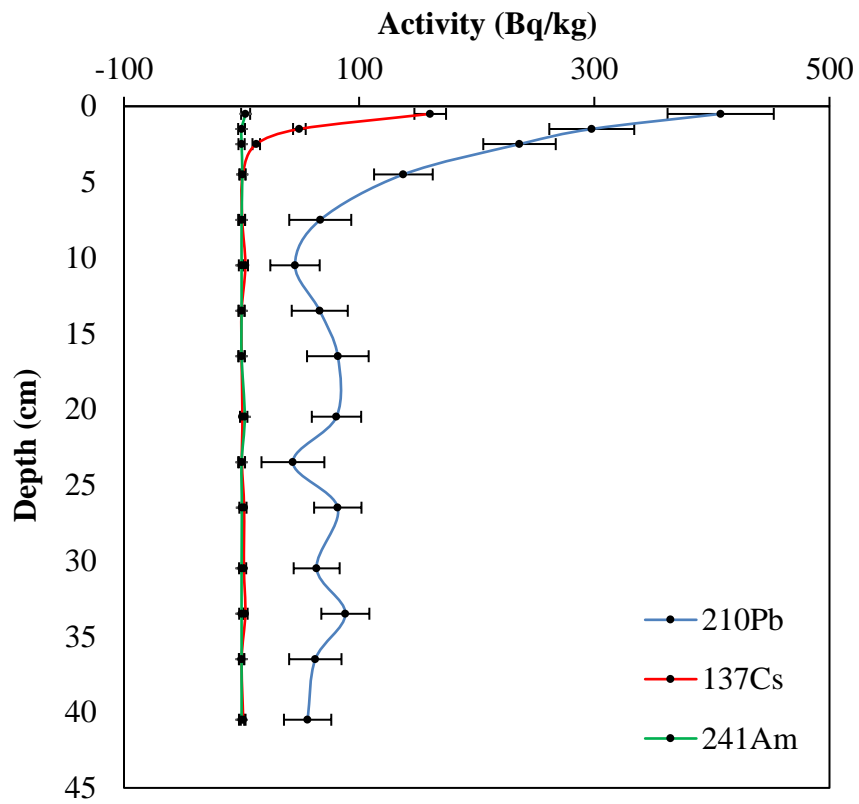
Figure 4.16. (a) Age-depth relationship for the three ^{210}Pb dating models. (b) Activities of ^{210}Pb, ^{137}C and ^{241}Am measured for core 182.

Midpoint Depth	Constant Flux & Sedimentation			Constant Rate of Supply			Constant Initial Concentration		
[cm]	Age [y]	Year [y]	Error [y]	Age [y]	Year [y]	Error [y]	Age [y]	Year [y]	Error [y]
0	0	2006.42	0	0	2006.42	2.0389	0	2006.42	6.006
0.5	6.0555	2000.37	0.5677	5.0375	2001.39	2.2341	0	2006.42	6.006
1.5	17.6628	1988.76	1.6559	15.7016	1990.72	3.1785	9.8471	1996.58	6.2759
2.5	30.0549	1976.37	2.8177	27.5494	1978.87	5.02	19.9182	1986.51	6.8707
4.5	55.7226	1950.7	5.2241	55.403	1951.02	13.2512	43.0811	1963.34	9.9714
7.5	91.9071	1914.52	8.6164	107.7527	1898.67	48.9437	85.9684	1920.46	36.5887
10.5	128.8546	1877.57	12.0803	N/A	N/A	N/A	N/A	N/A	N/A
13.5	166.4139	1840.01	15.6016	N/A	N/A	N/A	N/A	N/A	N/A
16.5	201.9928	1804.43	18.9372	N/A	N/A	N/A	N/A	N/A	N/A
20.5	248.6631	1757.76	23.3126	N/A	N/A	N/A	N/A	N/A	N/A
23.5	285.5335	1720.89	26.7693	N/A	N/A	N/A	N/A	N/A	N/A
26.5	322.5737	1683.85	30.2419	N/A	N/A	N/A	N/A	N/A	N/A
30.5	372.9175	1633.51	34.9617	N/A	N/A	N/A	N/A	N/A	N/A
33.5	411.0267	1595.4	38.5345	N/A	N/A	N/A	N/A	N/A	N/A
36.5	448.6879	1557.74	42.0653	N/A	N/A	N/A	N/A	N/A	N/A
40.5	499.5971	1506.83	46.8381	N/A	N/A	N/A	N/A	N/A	N/A

Table 4.9. Summary table of radioisotope dates obtained by CF/CS, CRS and CIC models by depth for core 182.

Cumulative Dry Mass	Midpoint Depth	^{210}Pb Activity	^{210}Pb (error)	^{137}Cs Activity	^{137}Cs (error)	^{241}Am Activity	^{241}Am (error)
[g/cm^2]	[cm]	[Bq/kg]	[Bq/kg]	[Bq/kg]	[Bq/kg]	[Bq/kg]	[Bq/kg]
0.196	0.5	407.46	45.16	160.44	13.46	3.44	3.83
0.5717	1.5	297.83	36.11	49.16	5.38	0	2.9
0.9728	2.5	236.37	30.82	12.47	3.21	0	2.64
1.8036	4.5	137.63	24.94	0.97	2.43	0.63	2.61
2.9748	7.5	66.91	26.37	0.56	2.47	0	2.89
4.1707	10.5	45.44	21.01	3.22	2.22	0	2.32
5.3864	13.5	66.49	23.84	0	2.43	0	2.61
6.538	16.5	81.87	26.21	0	2.46	0	2.81
8.0486	20.5	80.72	20.98	0.71	2.05	2.68	2.26
9.242	23.5	43.67	26.74	0.29	2.53	0	2.93
10.4409	26.5	81.82	20.13	2.14	2.06	0.22	2.14
12.0704	30.5	63.86	19.55	1.99	1.92	0	2.14
13.3039	33.5	88.25	20.43	3.2	1.93	0	2.04
14.5229	36.5	62.72	22.26	0.08	2.11	0	2.29
16.1707	40.5	56.17	20.12	1.37	2.01	0	2.2

Table 4.10. Activities of ^{210}Pb, ^{137}Cs and ^{241}Am with depth for core 182.

4.3.6 TOC, TN, and C/N ratio

The TOC and TN for core 182 range between 1.40–3.14 % and 0.16–0.39 %, respectively (Figures 4.17a and b, respectively). TOC and TN gradually increase up core. The C/N ratio ranges from 8.6–10.5 with an average of 9.4 (Figure 4.17c); it gradually decreases up core until ~9.5 cm, after which there is a steady increase to the top of the core. An exception occurs at 90.5 and 85.5 cm, where the C/N ratio increases to >10.
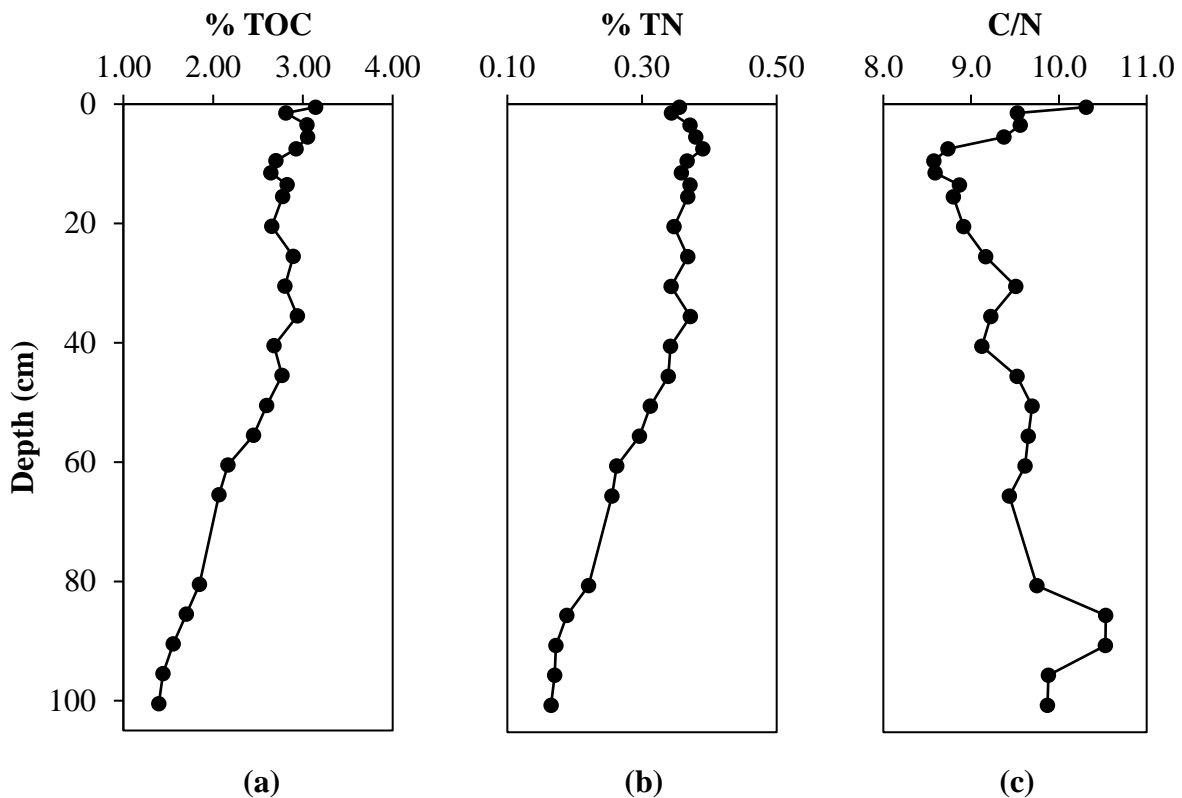
Figure 4.17. (a) TOC, (b) TN, and (c) C/N ratio for core 182.

4.3.7 Carbon- and Nitrogen-Isotope Compositions of OM

The $\delta^{13}C_{OM}$ for core 594 ranges from –26.32 to –25.71 ‰ (Figure 4.18a). The minimum value of –26.32 ‰ occurs at the base of the core (100.5 cm), and gradually increases to a maximum value of –25.71 ‰ at 85.5 cm. The $\delta^{13}C_{OM}$ then fluctuates by ±0.1 ‰ about an

average of ~ –25.9 ‰ until 5.5 cm where there is a sharp decrease to –26.28 ‰, followed by a gradual increase to the top of the core.

The $\delta^{15}N_{TN}$ ranges from +5.00 to +6.09 ‰ (Figure 4.18b). There is an initial increase in $\delta^{15}N_{TN}$ from 100.5 cm to the maximum of +6.09 ‰ at 85.5 cm. This is followed by more or less constant $\delta^{15}N_{TN}$ (~ +5.9±0.1 ‰) to 30.5 cm. There is then a steady decline in $\delta^{15}N_{TN}$ to the minimum of +5.00 ‰ at 9.5 cm, which is followed by a gradual increase to +5.79 ‰ at 1.5 cm.
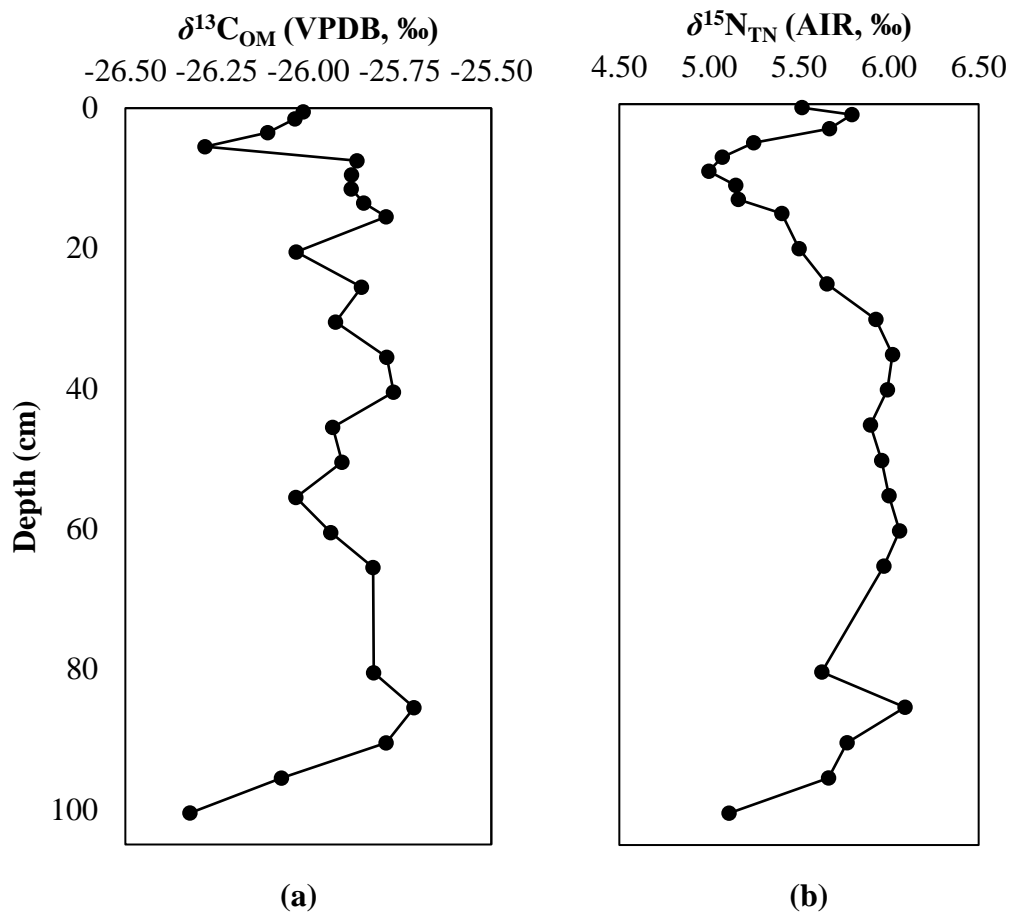
Figure 4.18. (a) $\delta^{13}C_{OM}$ and (b) $\delta^{15}N_{TN}$ for core 182.

4.4　Core 821 (Saginaw Basin)

4.4.1　Core Description

The wet sediment's colour in the basal portion of core 821 lies between dark grey (10YR 4/1) and dark greyish brown (10YR 4/2) until ~60 cm. It is brown (10YR 5/3) and pale brown (10YR 6/3) from 60 to 50 cm, brown (10YR 5/3) from 50 to 20 cm, dark greyish brown (10YR 4/2) from 20 to 2 cm, and very dark greyish brown (10YR 3/2) in the top 2 cm. The sediments are fine-grained silt and clay. There were no visible shell fragments or plant material.

4.4.2　Grain Size

Grain size measurements were made for 7 samples from core 821 (Figure 4.19a and b). The d(0.5) results range from 2.2–5.7 μm. For most of the section, the d(0.5) grain size fluctuates between 2.19 and 3.6 μm. There is a sharp increase at 1.5 cm to 5.7 μm. The d(0.1) measurements do not vary significantly, and d(0.9) measurements show a similar trend to d(0.5).

(a)

(b)
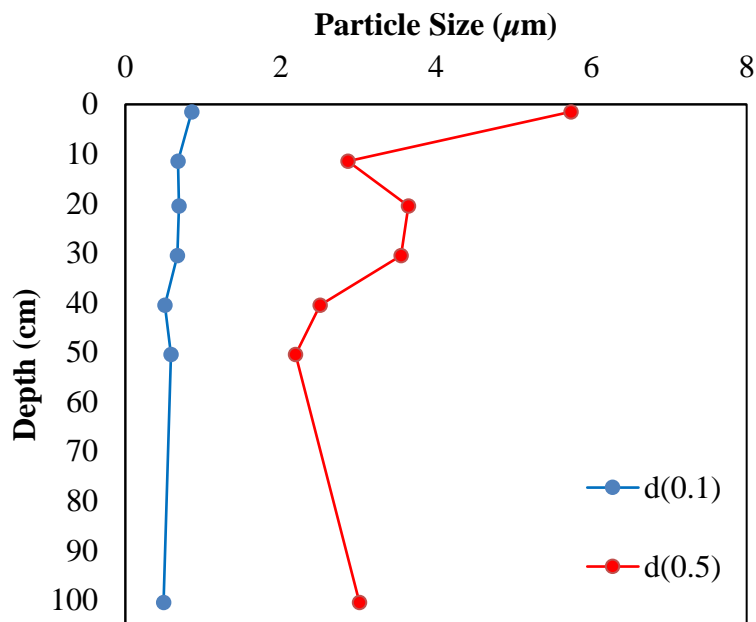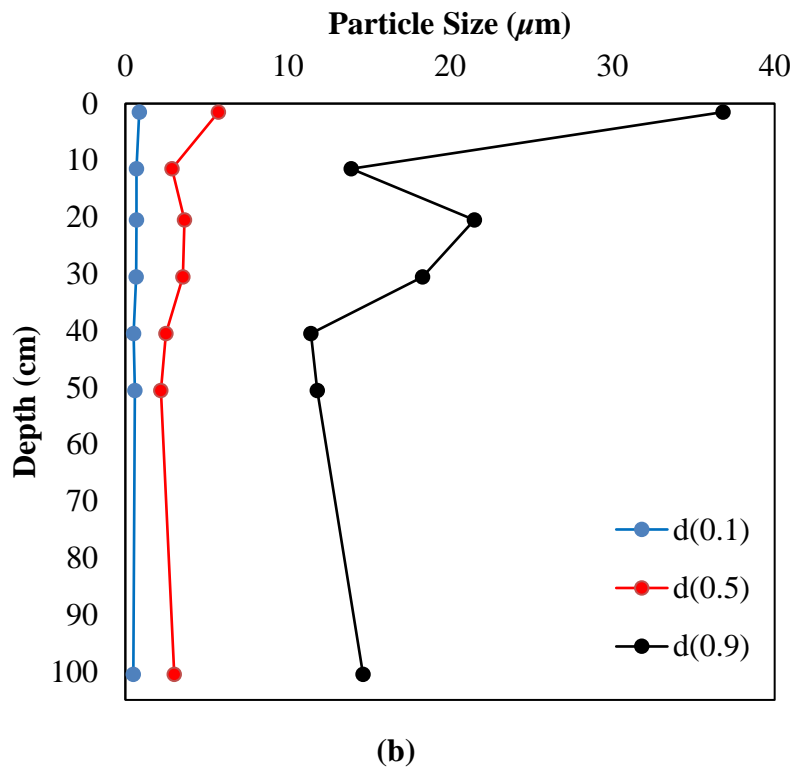
Figure 4.19. Grain size distributions for core 821: (a) d(0.1) and d(0.5) indicate that 10 % and 50 % of the sediment is finer than the size (μm) indicated; (b) d(0.9) indicates that 90 % of the sediment is finer than the size (μm) indicated.

4.4.3 Mineralogy

Minerals observed are quartz, K-feldspar, plagioclase, calcite, dolomite, amphibole, and clay minerals (1.4 nm – chlorite; 1.0 nm – illite; 0.7 nm – kaolinite) (Figure 4.20). Quartz content varies greatly throughout the core (30-72 %). The abundance of quartz is relatively constant (37-39 %) between 100.5 and 70.5 cm, before decreasing to the minimum of 30 % at 60.5 cm. Quartz then continuously rises through the rest of the core, increasing in particular from 34 % at 40.5 cm to 72 % at 1.5 cm.

Calcite and dolomite contents show significant variations throughout the core. Calcite is initially present in low amounts (3-4 %) from 100.5 to 70.5 cm but its abundance rises sharply (to 26-23 %) between 60.5 to 50.5 cm before a sharp decrease back to 3 % at 40.5 cm. Calcite

abundance then remains low until it disappears at 10.5 cm. The abundance of dolomite also begins low (3-4 %) until an increase to 12 -16 % between 60.5 to 50.5 cm. That is followed by a decrease to 3 % at 40.5 cm, before another large increase at 30.5 cm to 27 %. The abundance of dolomite then decreases to 2-4 % before disappearing at the core's top.

Chlorite, illite and kaolinite contents are 5-14 %, 7-15 %, and 2-10 %; K-feldspar and plagioclase contents range from 3-7 % and 6-10 %, respectively. Lower concentrations of clay minerals and feldspars occur in intervals with higher quartz or carbonate contents. Amphibole content ranges from 1-4 %, with higher amounts typical of the lower half of the core.
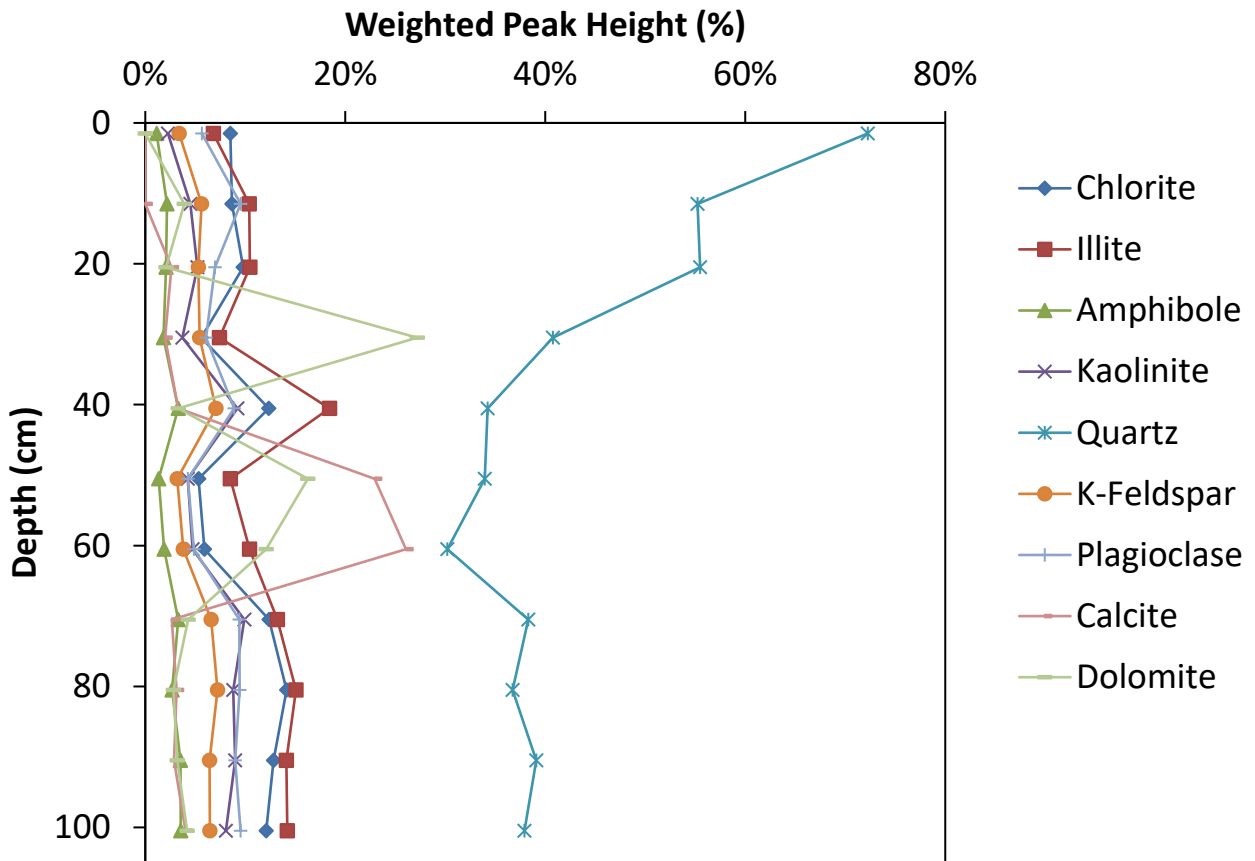
Figure 4.20. Mineral abundances for core 821. Percentages are based on weighted peak heights of the strongest diffraction for each phase, as measured by p-XRD.

4.4.4 Magnetic Susceptibility

Full core and half-core MS signals were measured with a sensor and point sensor, respectively (Figure 4.21). In general, loop sensor measurements are lower than point sensor measurements. Loop sensor MS signals average 5.9 and are relatively constant throughout the core except in the top 7 cm, where the MS signal sharply increases until 4 cm, where a maximum of 80.7 is reached. The MS signal then decreases but still remain higher than average. Point sensor MS signals average 6.7 and show a similar trend to loop sensor measurements. The point sensor MS signals are relatively constant throughout the core until ~5.5 cm, where the signal sharply increases to a maximum of 112 at 3 cm. The MS signal then decreases, and reaching pre-peak values at 0.5 cm.

(a)   (b)
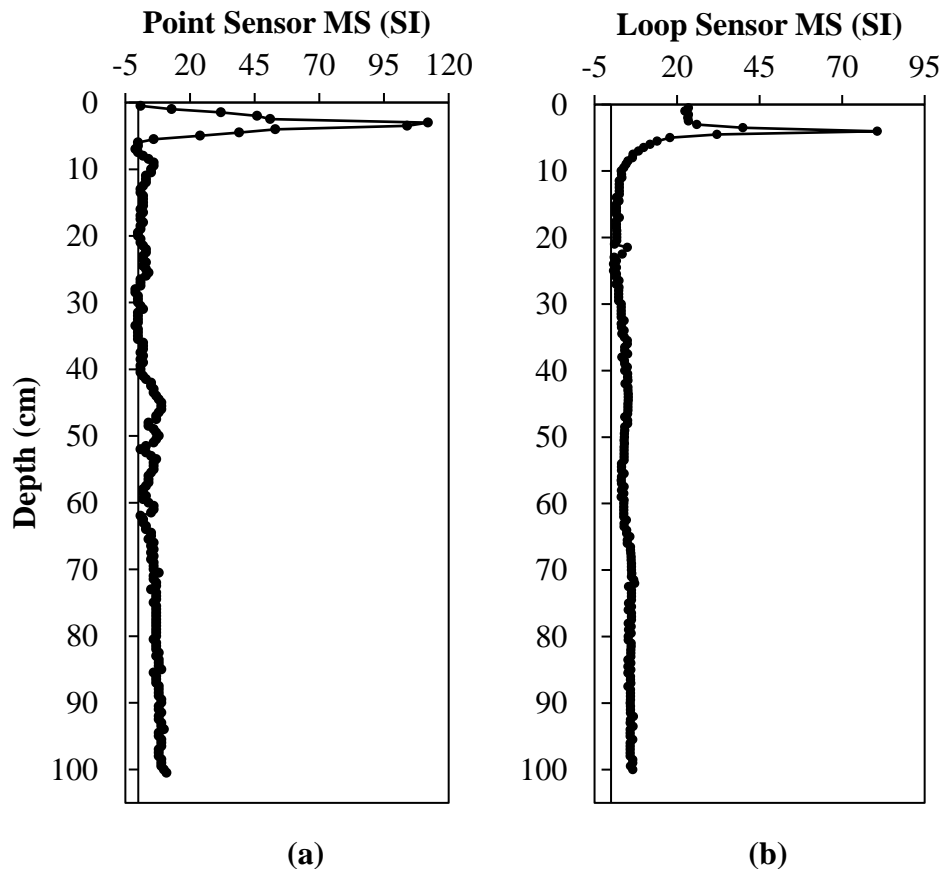
Figure 4.21. Magnetic susceptibility measurements for core 821: (a) point sensor and (b) loop sensor.

4.4.5   TOC, TN, and C/N ratio

The TOC and TN for core 821 range between 0.64–3.70 % and 0.06–0.45 %, respectively (Figure 4.22 a and b, respectively). In general, both TOC and TN exhibit very similar trends. Neither TOC nor TN vary significantly from 100.5 to 60.5 cm. A small increase reaches its maximum at 50.5 cm before decreasing once again to former values through to 35.5 cm. TOC and TN then rise again, reaching a maximum at 13.5 cm, before declining to the lowest measured values at 3.5 cm. A sharp increase in TOC and TN to the highest measured values then occurs at the core's top (1.5 – 0.5 cm). The C/N ratio ranges from 7.90–12.47, with an average of 10.85 (Figure 4.22c). This is the highest average observed for the Lake Huron and Georgian Bay cores examined in this study. The C/N ratio follows a similar pattern to that of TOC and TN. The highest C/N ratio occurs between 60.5 and 50.5 cm. The lowest C/N ratio occurs at 1.5 cm, in association with the very sharp increases in the TOC and TN for that interval.
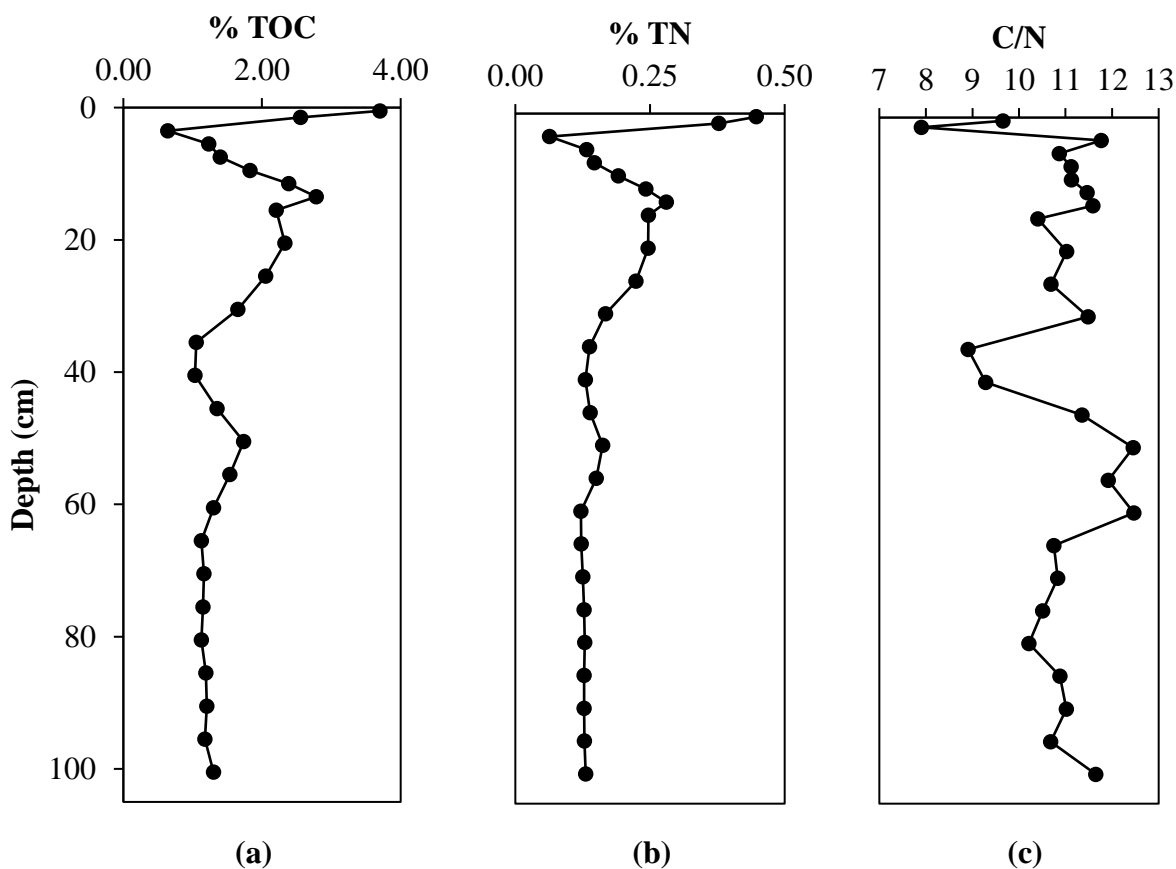
Figure 4.22. (a) TOC, (b), TN, and (c) C/N ratio for core 821.

4.4.6   Carbon- and Nitrogen-Isotope Compositions of OM

The $\delta^{13}C_{OM}$ of core 821 ranges from –27.60 to –25.26 ‰ (Figure 4.23a). A gradual

increase from 100.5 to stable, higher values between 80.5 to 70.5 cm is followed by a sharp

decrease at 65.5 cm to the core's lowest value (–27.60 ‰). A gradual increase then occurs from

65.5 to 35.5 cm, followed by a sharp decrease at 30.5 cm. A gradual increase in $\delta^{13}C_{OM}$ then

ensues to a maximum of –25.26 ‰ at 3.5 cm followed by a small decrease at 1.5 to 0.5 cm.

The $\delta^{15}N_{TN}$ for core 594 ranges from +3.31 to +6.02 ‰ (Figure 4.23b). The $\delta^{15}N_{TN}$ increases

slightly from 100.5 to 75.5 cm, followed by a decrease to a minimum of +3.31 ‰ at 60.5 cm.

The $\delta^{15}N_{TN}$ then increases between 45.5 to 35.5 cm before again declining to lower values at 30.5 to 13.5 cm. The $\delta^{15}N_{TN}$ then rises steadily to the core's maximum of +6.02 ‰ at 1.5 cm.
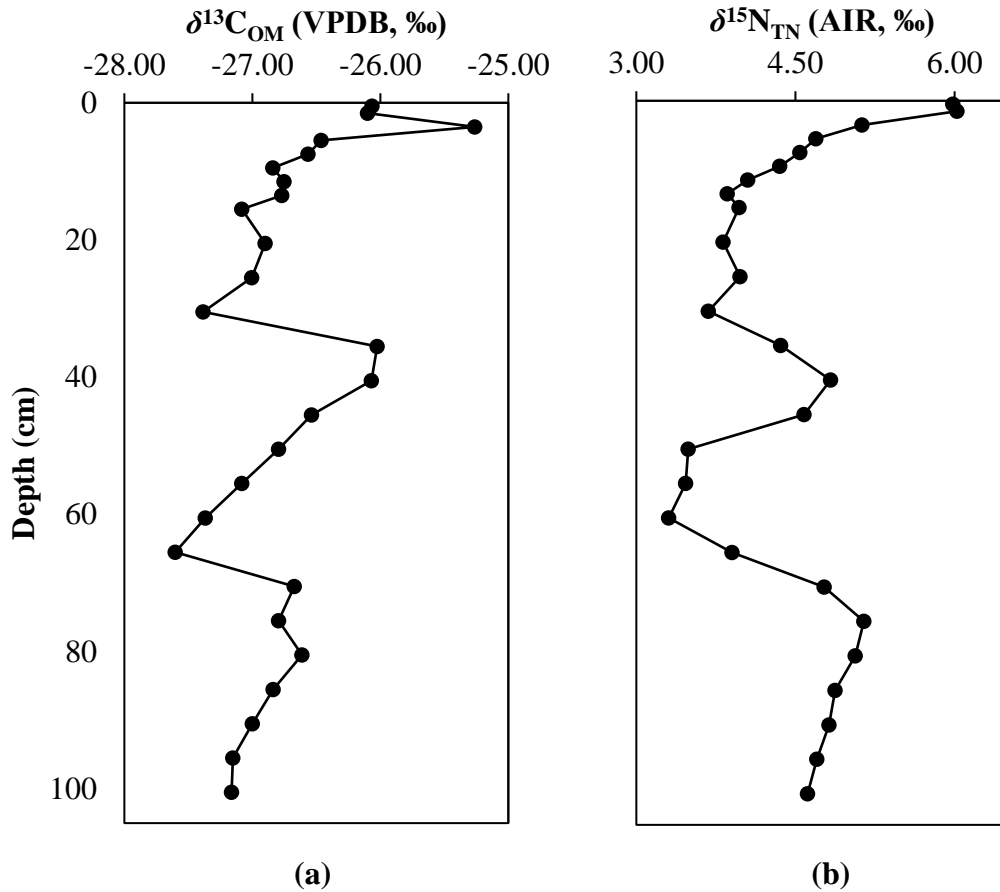
Figure 4.23. (a) $\delta^{13}C_{OM}$ and (b) $\delta^{15}N_{TN}$ for core 821.

4.5   Core 817 (Alpena Basin)

4.5.1   Core Description

Wet sediment of core 817 varies between brown (10YR 5/3) and pale brown (10YR 6/3) throughout most of the core, changing to dark greyish brown (10YR 4/2) in the top 26 cm. The sediments are generally fine-grained silt and clay, except between 29 to 32 cm, where there is also fine to coarse-grained sand. Shelly material occurs between 29 to 32 cm, with substantial amounts between 30 to 32 cm. No visible plant material was observed.

4.5.2 Grain Size

Grain size measurements were made for 7 samples from core 817 (Figure 4.24a and b). The d(0.5) results range from 1.9–7.1 μm, averaging 2-4 μm throughout most of the core, except for a very sharp increase to 7.1 μm at 30.5 cm. The d(0.1) measurements do not vary significantly. A large spike in d(0.9) occurs at 30.5. This coincides with the increase in visible shelly material and coarse-grained sand observed in the sediment.

(a)
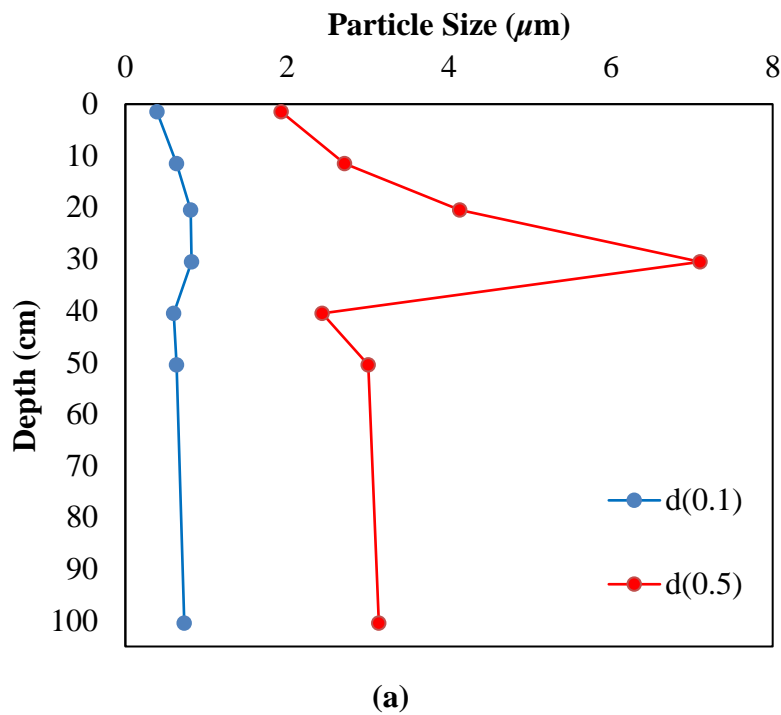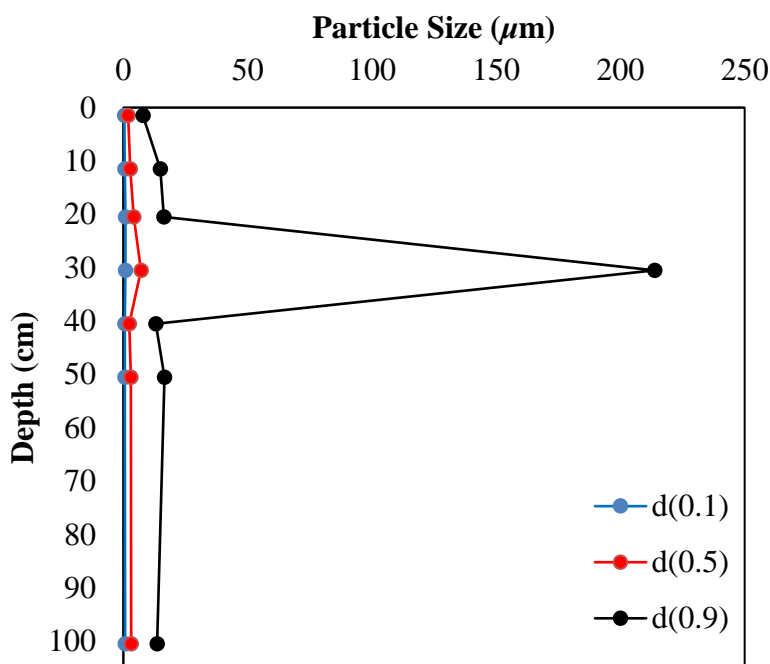
(b)

**Figure 4.24.** Grain size distributions for core 817: (a) d(0.1) and d(0.5) indicate that 10 % and 50 % of the sediment is finer than the size (*μ*m) indicated; (b) d(0.9) indicates that 90 % of the sediment is finer than the size (*μ*m) indicated.

4.5.3   Mineralogy

Minerals observed are quartz, K-feldspar, plagioclase, calcite, dolomite, amphibole, and clay minerals (1.4 nm – chlorite; 1.0 nm – illite; 0.7 nm – kaolinite) (Figure 4.25). The relative abundance of quartz shows the largest variation (39-66 %). Quartz content is lowest (39-44 ‰) in the lower half of the core (100.5 to 40.5 cm), with a sharp increase beginning at 30.5 cm to the top of the core (56-66 %). The relative abundance of chlorite, illite, and kaolinite is 7-9 %, 4-11 %, and 2-6 %, respectively. Chlorite content is relatively constant throughout the core but illite and kaolinite abundances decrease in concert with the sharp increase in quartz at 30.5 cm. Potassium feldspar contents (2-7 %) are relatively constant throughout the core except for a decrease at 30.5 cm. Plagioclase contents (5-12 %) are highest in the core's lower half until 30.5

73

cm when its abundance sharply decreases before gradually increasing upwards in the core.

Calcite occurs in low amounts (2-3 %) except at 30.5 cm, where there is a small increase to 5 %,

and above 10.5 cm where it is absent. Dolomite content ranges from 0-20 %. It is highest at the

base of the core (100.5 cm) and gradually decreases upwards, with some variation, before

disappearing above 10.5 cm. Amphibole contents are minimal (0-2 %).
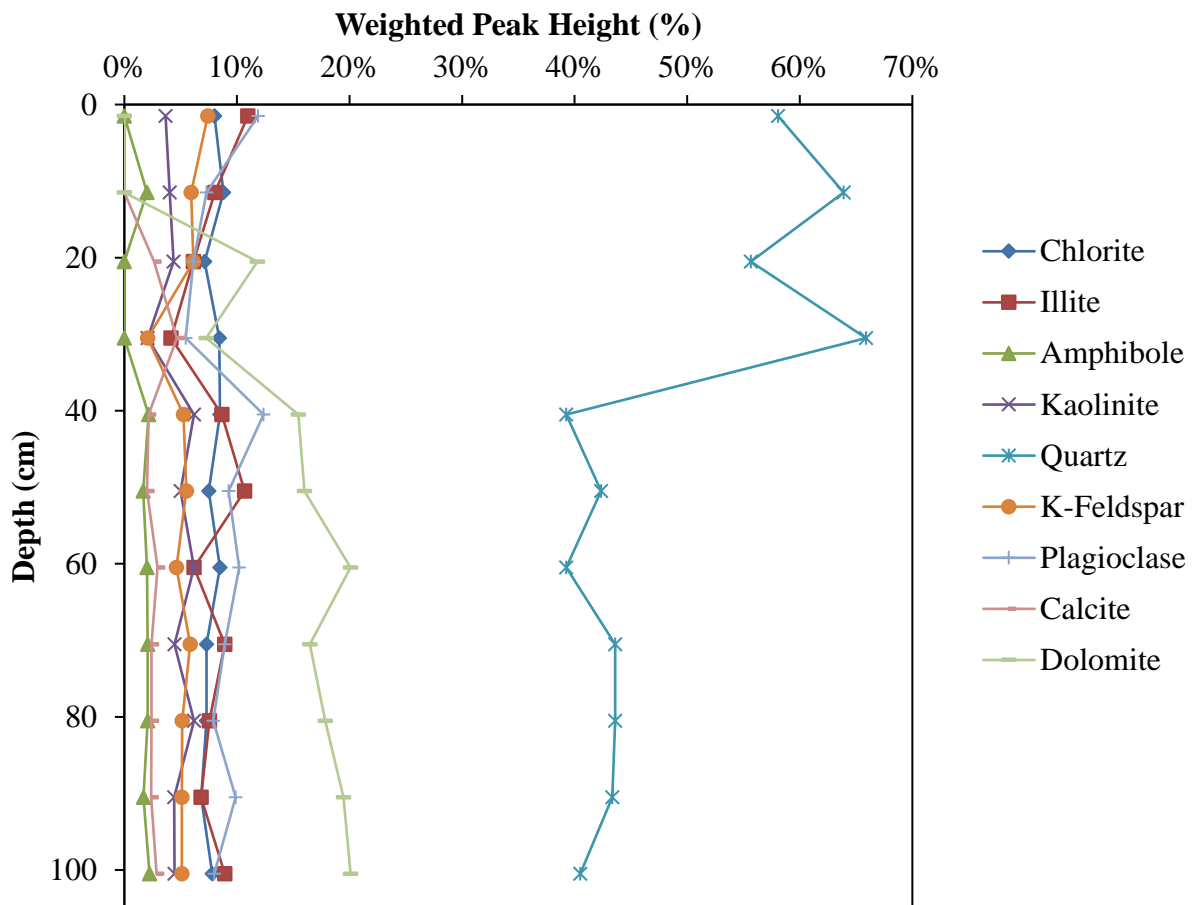

Figure 4.25. Mineral abundances for core 817. Percentages are based on weighted peak heights of the strongest diffraction for each phase, as measured by p-XRD.

4.5.4 Magnetic Susceptibility

Full core and half-core MS signals were measured with a loop sensor and point sensor, respectively (Figure 4.26). In general, loop sensor measurements are lower than point sensor

measurements. Loop sensor MS signals average 17.6. The general trend is a gradual decrease

from 100.5 to 34 cm. A sharp decrease in MS signal then occurs, with the lowest values

occurring at 9 cm, followed by a slight increase in the top 8.5 cm. Point sensor MS signals

average 23.2 and show a similar, albeit noisier, pattern to the loop sensor measurements.
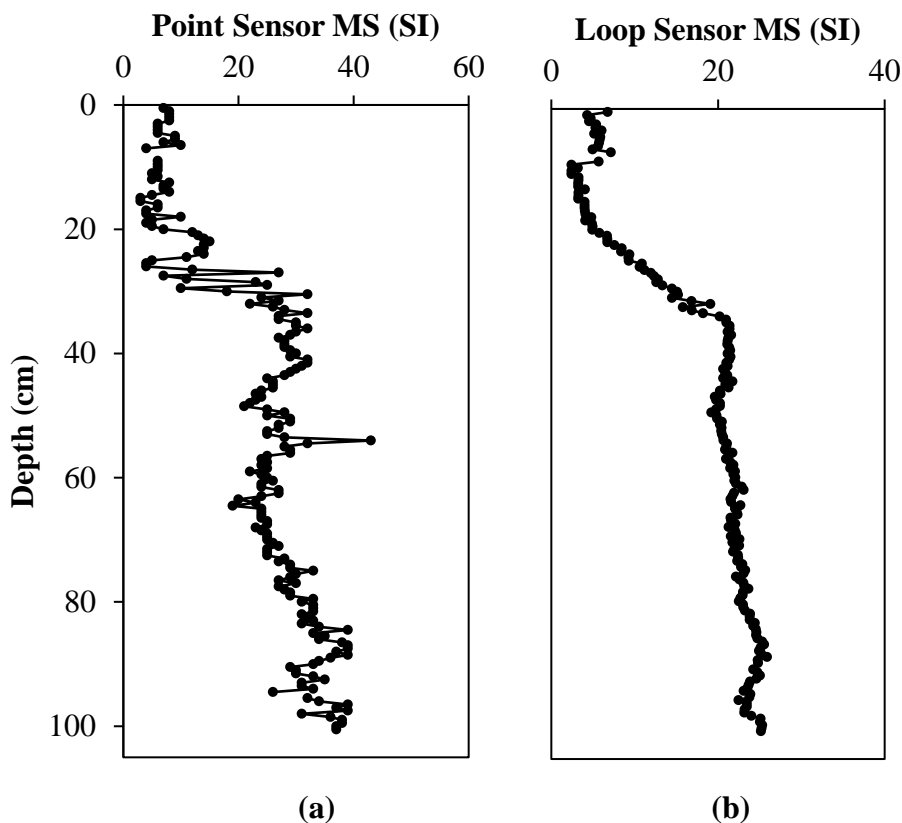
Figure 4.26. Magnetic susceptibility measurements for core 817: (a) point sensor and (b) loop sensor.

4.5.5   TOC, TN, and C/N ratio

The TOC and TN for core 817 range between 0.12–1.72 % and 0.018–0.183 %,

respectively (Figure 4.27a and b, respectively). Both TOC and TN are very low (<0.2 %) from

100.5 to 30.5 cm and do not vary significantly. This is followed by a very sharp increase over the

span 25.5 to 15.5 cm, with maximum TOC of 1.72 % occurring at 11.5 cm. This is followed by a

small decrease to 1.33 % at 3.5 cm and then an even smaller increase to the top of the core. The

pattern is very similar for TN. The C/N ratio ranges from 7.0–11.9, with an average of 9.3

(Figure 4.26c), and follows the patterns observed for TOC and TN. There is a gradual decrease

in C/N ratio from 100.5 to 30.5 cm to as low as 7.0, followed by a very sharp increase at 25.5 cm

to the maximum of 11.9. The C/N ratio then gradually decreases to the top of the core.
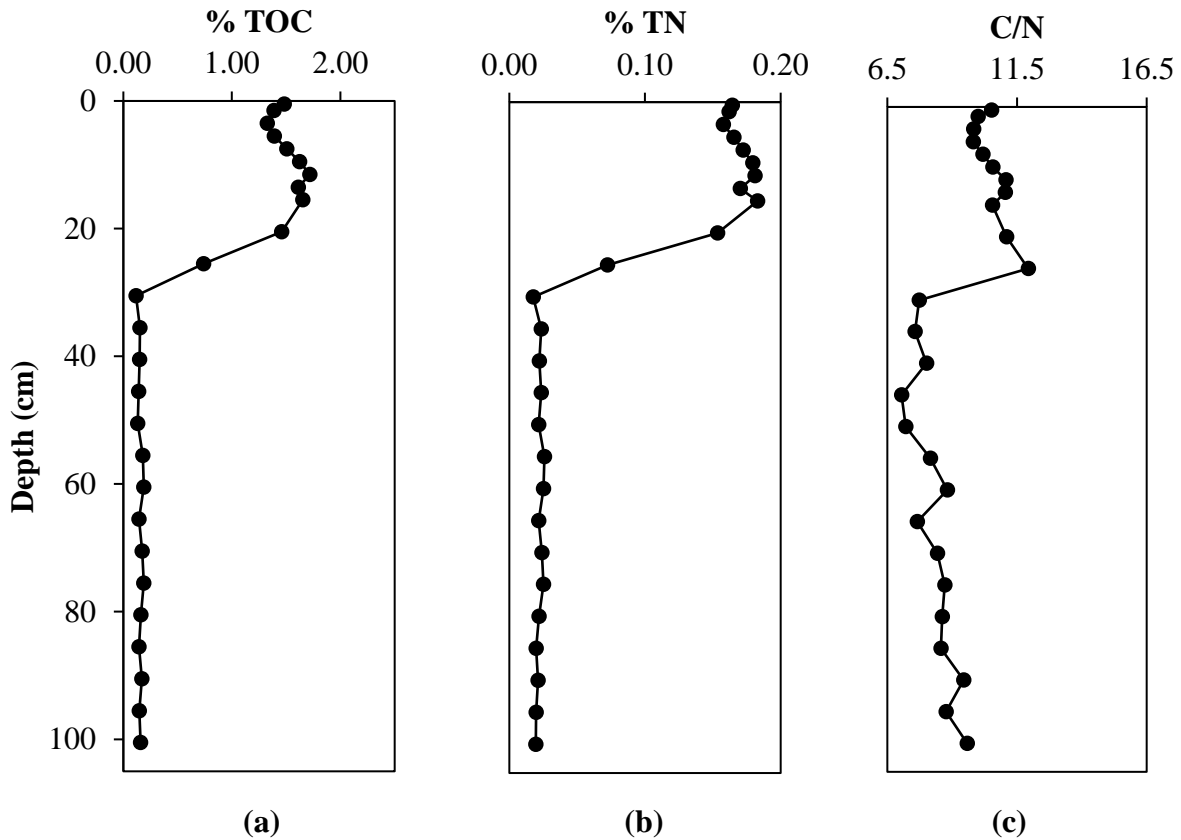
Figure 4.27. (a) TOC, (b) TN, and (c) C/N ratio for core 821.

4.5.6   Carbon- and Nitrogen-Isotope Compositions of OM

The $\delta^{13}C_{OM}$ of core 594 ranges from –28.07 to –25.21 ‰ (Figure 4.28a). While fluctuating, the

$\delta^{13}C_{OM}$ shows an overall increase from –27.56 ‰ R 100.5 to –26.61 ‰ at 55.5 cm. A sharp

decrease to the lowest observed value (–28.07 ‰) occurs over the interval 50.5 to 30.5 cm,

followed by a very sharp increase in $\delta^{13}C_{OM}$ to –26.37 ‰ at 25.5 cm. The $\delta^{13}C_{OM}$ then gradually

increases upwards in the core to the maximum of –25.21 ‰ at 0.5 cm. The $\delta^{15}N_{TN}$ of core 594

gradually increases from +4.91 ‰ at 25.5 cm to +6.05 ‰ at 0.5 cm (Figure 4.28b). Insufficient

N was available for isotopic analysis below 25.5 cm.
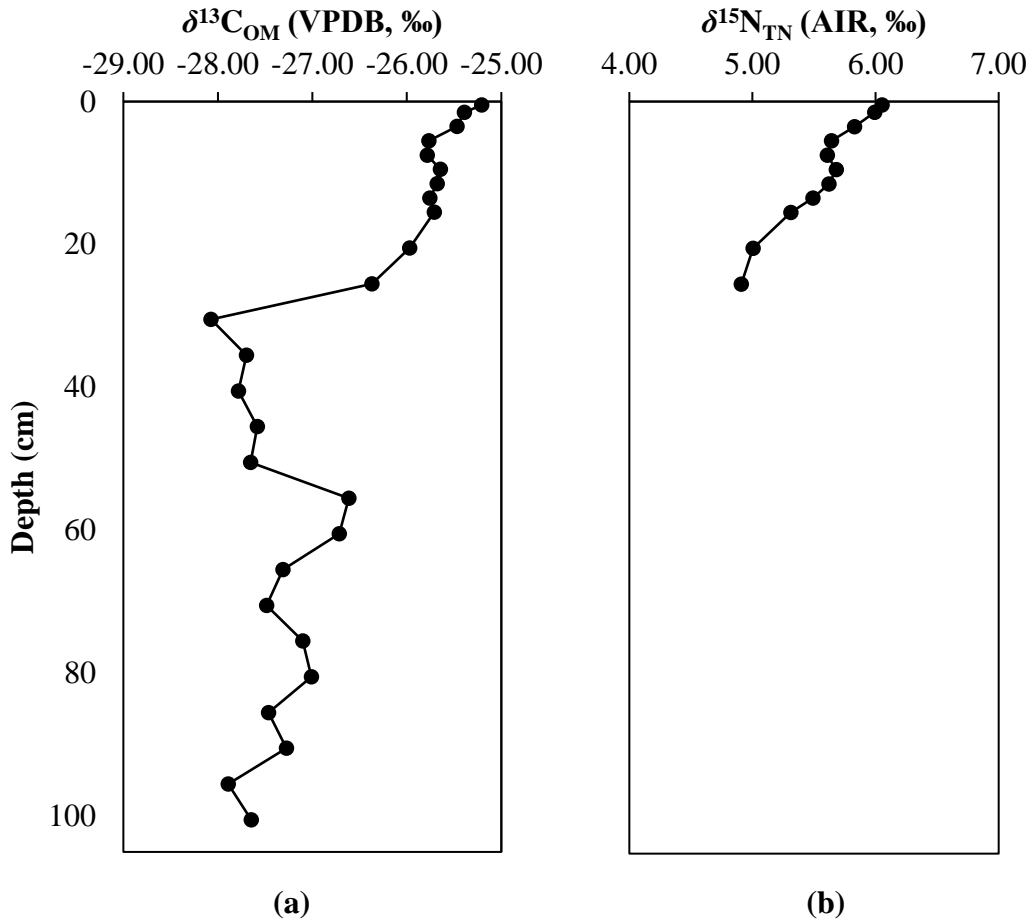
Figure 4.28. (a) $\delta^{13}C_{OM}$ and (b) $\delta^{15}N_{TN}$ for core 817.

4.6   Core 818-2 (Port Huron Basin)

4.6.1   Core Description

The top 16.5 cm of core 818-2 is unconsolidated, likely because of disturbance during

coring, and was not examined further. In the remainder of the core, the wet sediment was very

dark greyish brown (10YR 3/2). The sediments are fine-grained silt and clay. There were no

visible shell fragments or plant material.

4.6.2   Grain Size

Grain size measurements were made for 3 samples from core 818-2 (Figure 4.29a and b). The d(0.5) results range from 3.1–5.0 μm. The d(0.1) measurements gradually increase up core. The d(0.9) measurements decrease from 35.8 to 16.5 μm.
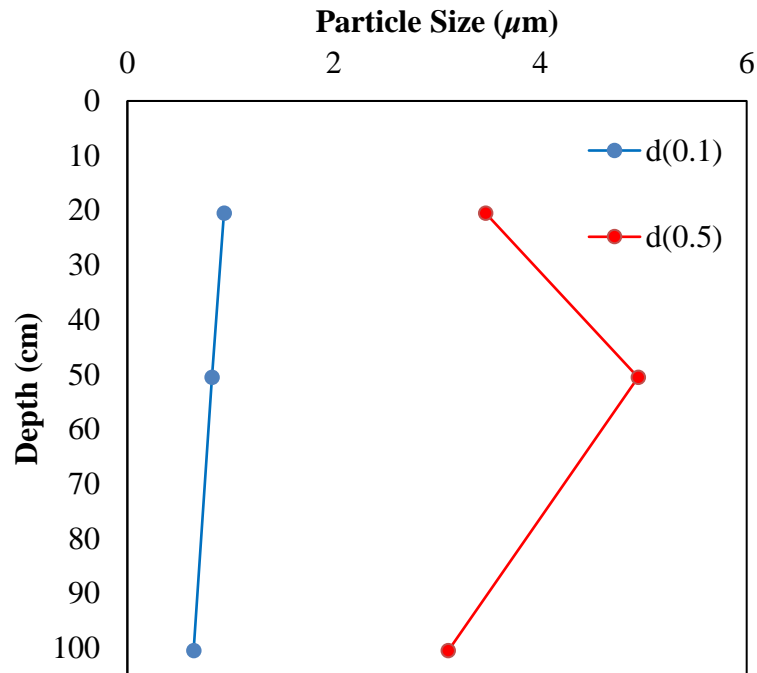
(a)
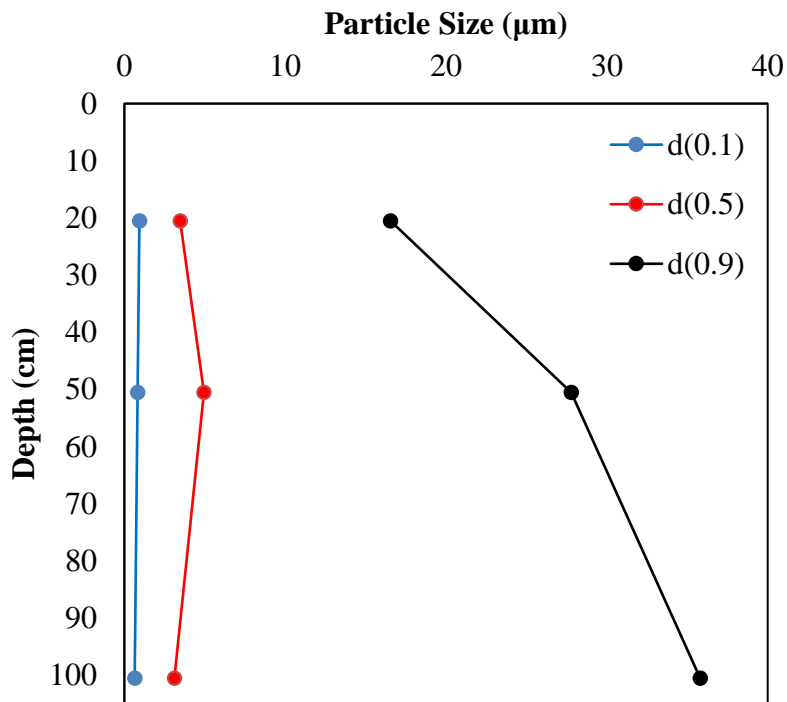
(b)

Figure 4.29. Grain size distributions for core 818-2: (a) d(0.1) and d(0.5) indicate that 10 % and 50 % of the sediment is finer than the size (μm) indicated; (b) d(0.9) indicates that 90 % of the sediment is finer than the size (μm) indicated.

4.6.3   Mineralogy

Minerals observed are quartz, K-feldspar, plagioclase, calcite, dolomite, amphibole, and clay minerals (1.4 nm – chlorite; 1.0 nm – illite; 0.7 nm – kaolinite) (Figure 4.30). Quartz contents show the largest variation (58-69 %), with the lowest values occurring at 100.5 cm and 60.5 cm. Chlorite (7-9 %) and kaolinite (4-5 %) contents are relatively constant throughout the core, with illite (4-9 %) showing more variability. Potassium feldspar contents are relatively constant (4-6 %) with plagioclase showing more variability (5-11 ‰). Calcite is present only in small amounts (2-3 %) at 100.5, 60.5, and 50.5 cm, and is not present elsewhere. Dolomite is present at low concentrations (2-5 %) except at 50.5, 40.5, and 20.5 cm, where it is absent.
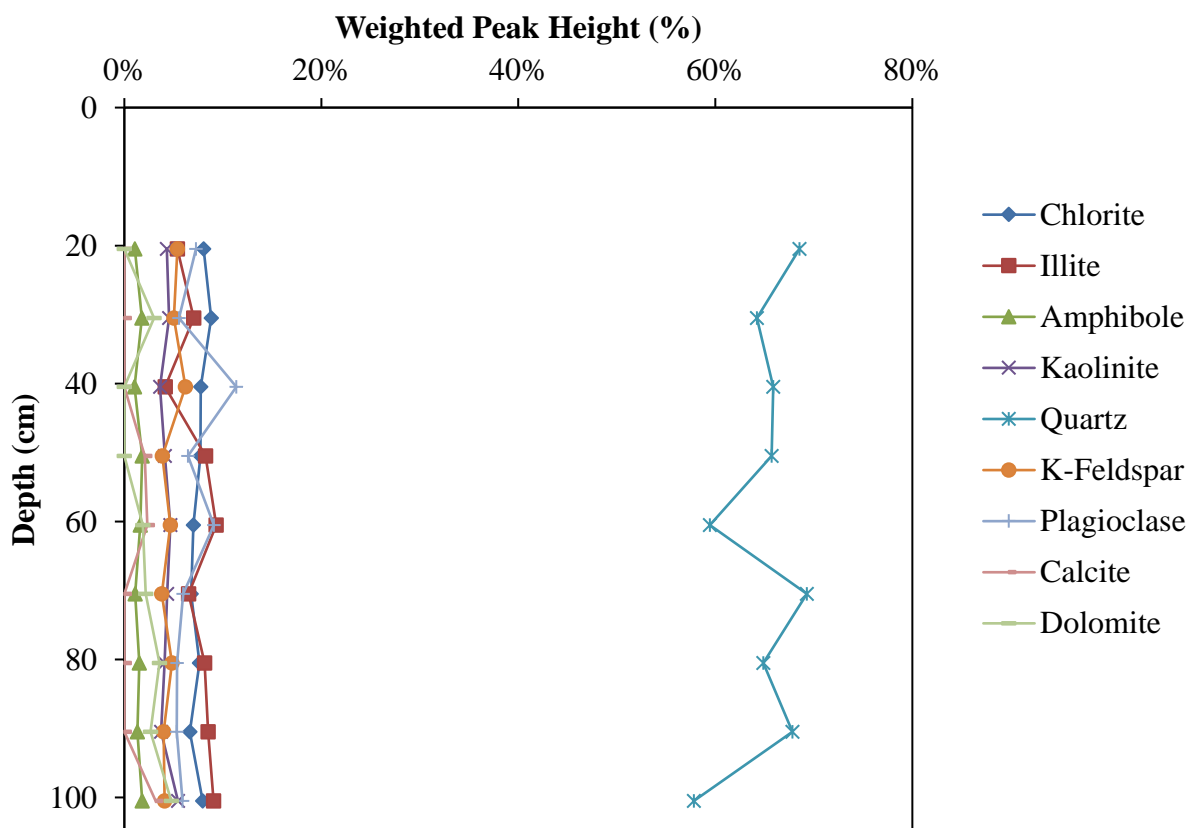
Figure 4.30. Mineral abundances for core 818-2. Percentages are based on weighted peak heights of the strongest diffraction for each phase, as measured by p-XRD.

4.6.4   Magnetic Susceptibility

Full core and half-core MS signals were measured with a loop sensor and point sensor, respectively (Figure 4.31). In general, loop sensor measurements (average 6.0) are lower than point sensor measurements (average 10.7). Neither vary significantly throughout the core.
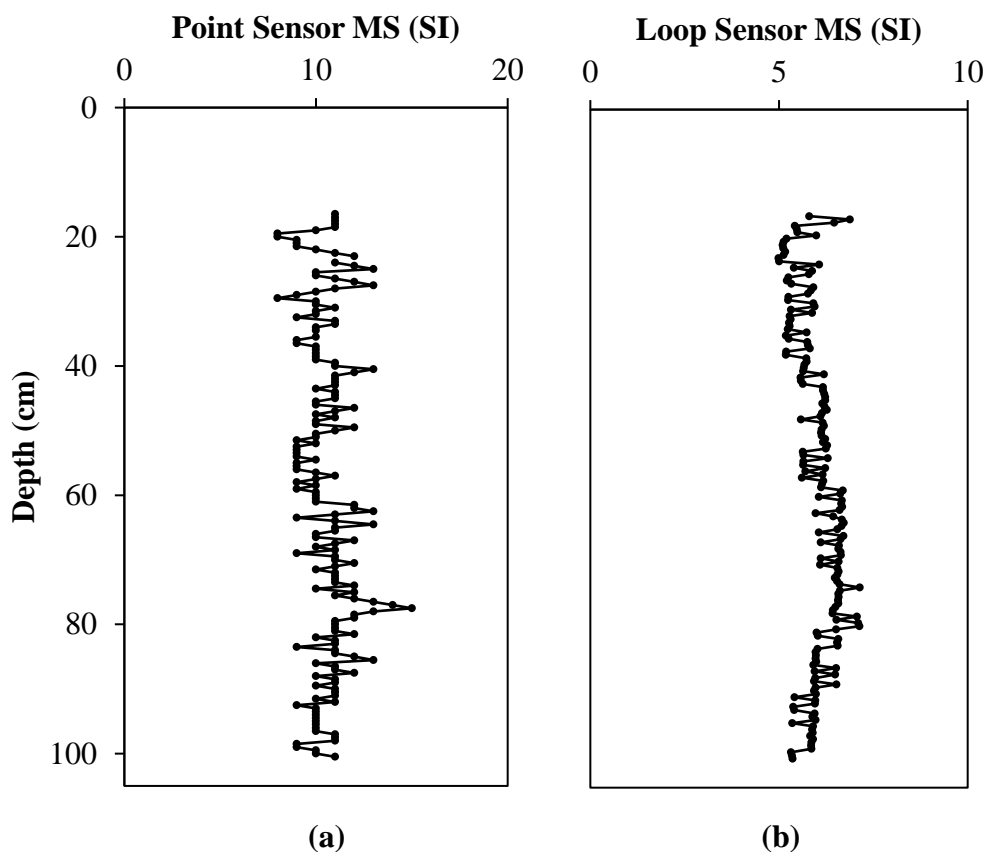
Figure 4.31. Magnetic susceptibility measurements for core 818-2: (a) point sensor and (b) loop sensor.

4.6.5   TOC, TN, and C/N ratio

The TOC and TN for core 818-2 range between 2.06–4.35 % and 0.29–0.56 %, respectively (Figure 4.32a and b, respectively). Both gradually increase up core, except for small reversals at 40.5 and 25.5 cm. The C/N ratio ranges from 8.13–10.03, with an average of 9.11 (Figure 4.32c). A sharp increase to the maximum C/N ratio (10.03) occurs at 95.5 cm. This is followed by a gradual decline to 8.44 at 70.5 cm, and then an increase to ~9.5 ending at 45.5 cm. A decrease to 8.13 at 40.5 cm is then followed by higher and near constant C/N ratios (~9) from 35.5 to 20.5 cm.
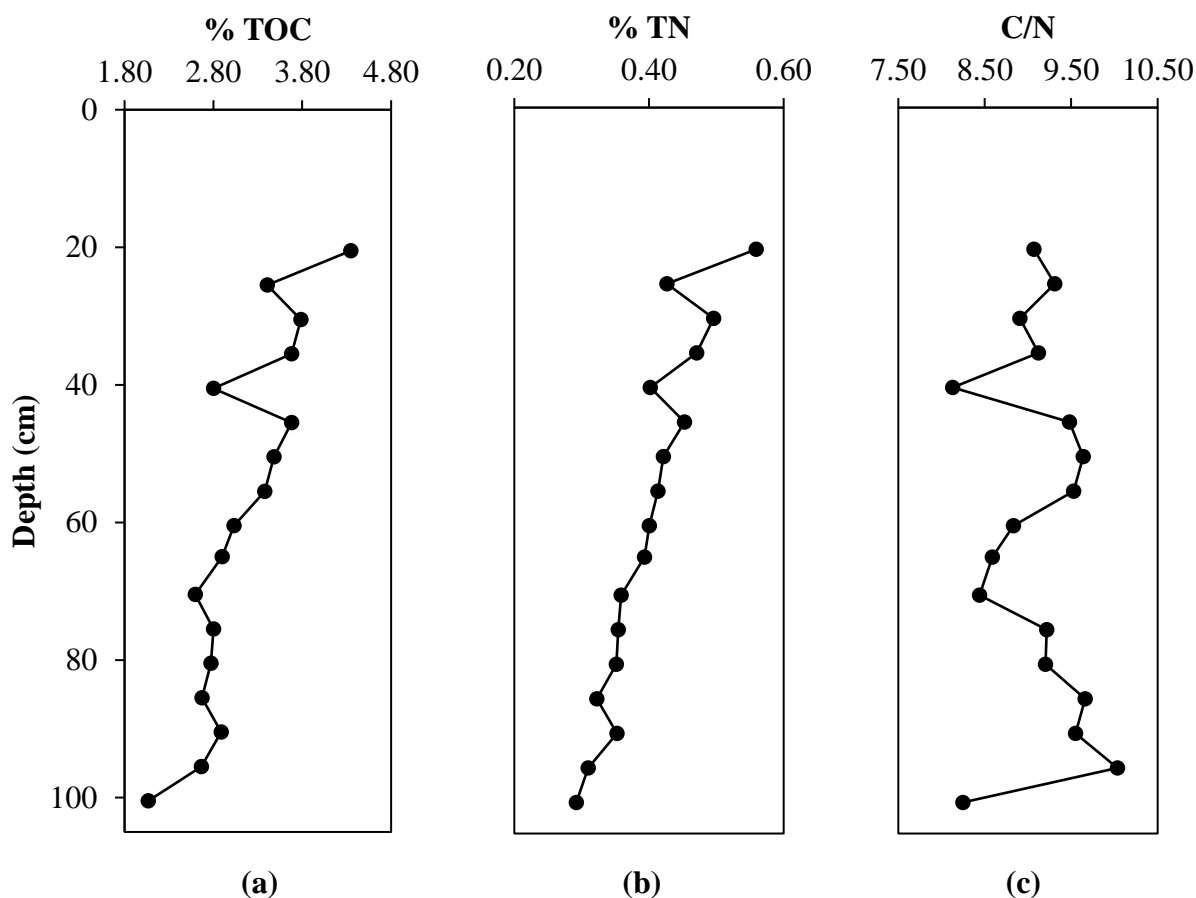
Figure 4.32. (a) TOC, (b) TN, and C/N ratio for core 818-2.

4.6.6 Carbon- and Nitrogen-Isotope Compositions of OM

The $\delta^{13}C_{OM}$ of core 818-2 varies within a narrow range from –26.23 to –25.50 ‰ (Figure 4.33a). Values fluctuate between –26.23 and –25.88 ‰ from 100.5 to 40.5 cm before rising to the maximum $\delta^{13}C_{OM}$ (–25.50 ‰) at 20.5 cm. The $\delta^{15}N_{TN}$ also fluctuates within a narrow range (+4.46 to +4.94 ‰), while trending to higher values upwards in the core (Figure 4.33b). The minimum $\delta^{15}N_{TN}$ (+4.46 ‰) occurs at 100.5 cm, which rises to +4.83 ‰ at 85.5 cm before declining to +4.49 ‰ at 70.5 cm. The $\delta^{15}N_{TN}$ then gradually rises upwards in the core, albeit with some fluctuation, to its maximum (+4.89 ‰) at 20.5 cm.
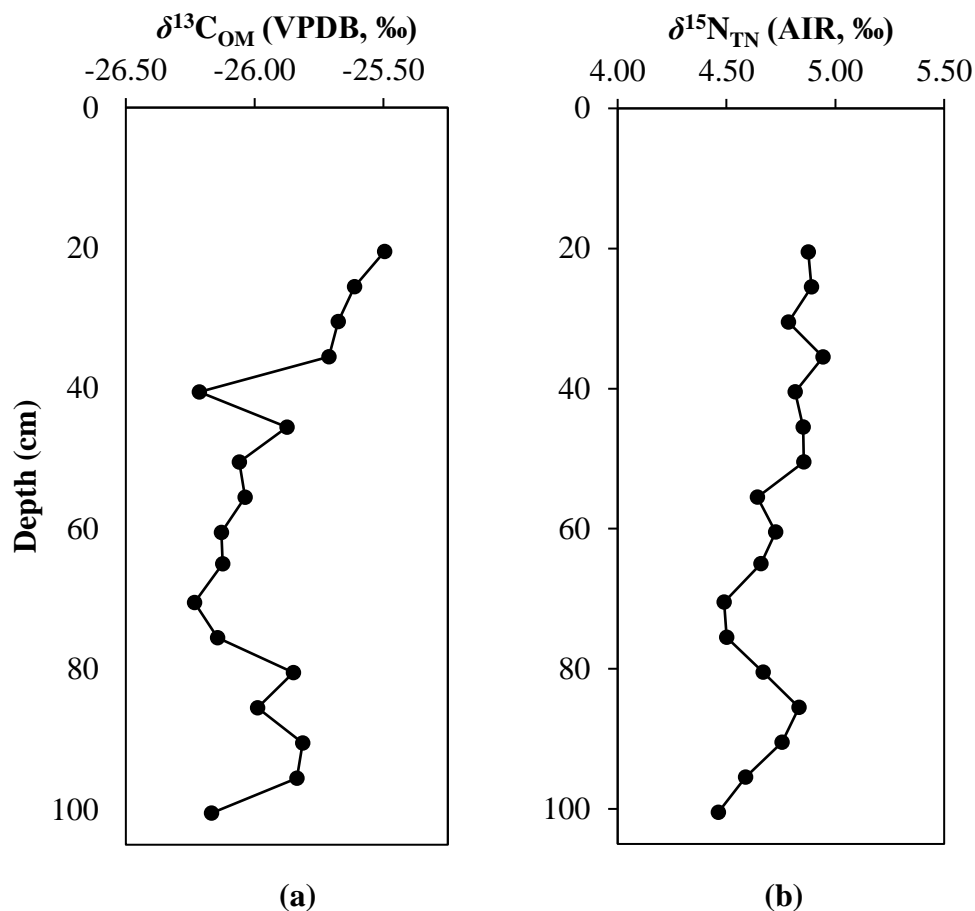
Figure 4.33. (a) $\delta^{13}C_{OM}$ and (b) $\delta^{15}N_{TN}$ for core 818-2.

4.7   Core 41 (Georgian Bay)

4.7.1   Core Description

Wet sediment in core 41 is dark greyish brown (10YR 4/2), except for the top 0 to 22 cm, which is very dark grey (10YR 3/1). The sediments are fine-grained silt and clay. There were no visible shell fragments or plant material.

4.7.2   Grain Size

Grain size measurements were made for 7 sample from core 41 (Figure 4.34a and b). The d(0.5) results are very tightly clustered from 2.5–3.1 μm. The d(0.1) measurements do not vary

significantly throughout the core. The d(0.9) measurements range from 19.6 to 16.1 μm, and

have a gradually decreasing trend from 50.5 to 1.5 cm.

(a)

Particle Size (μm)
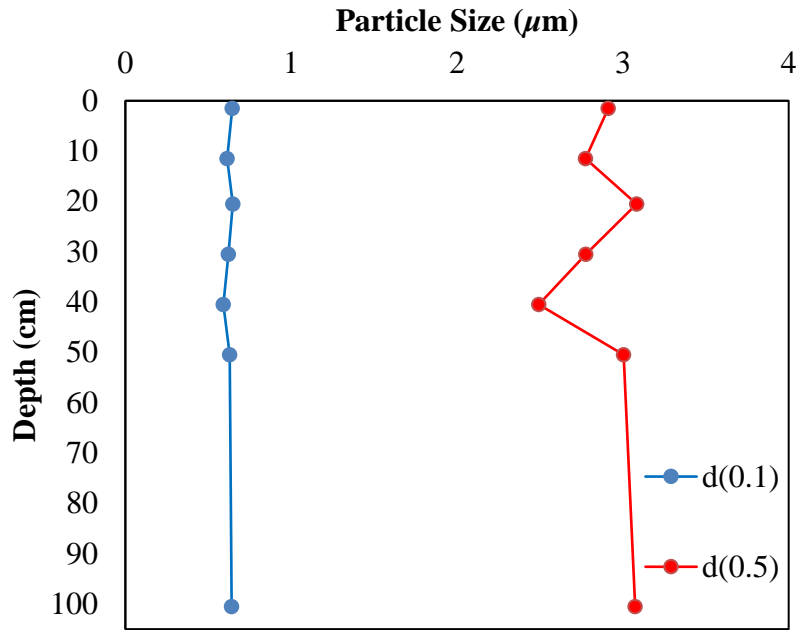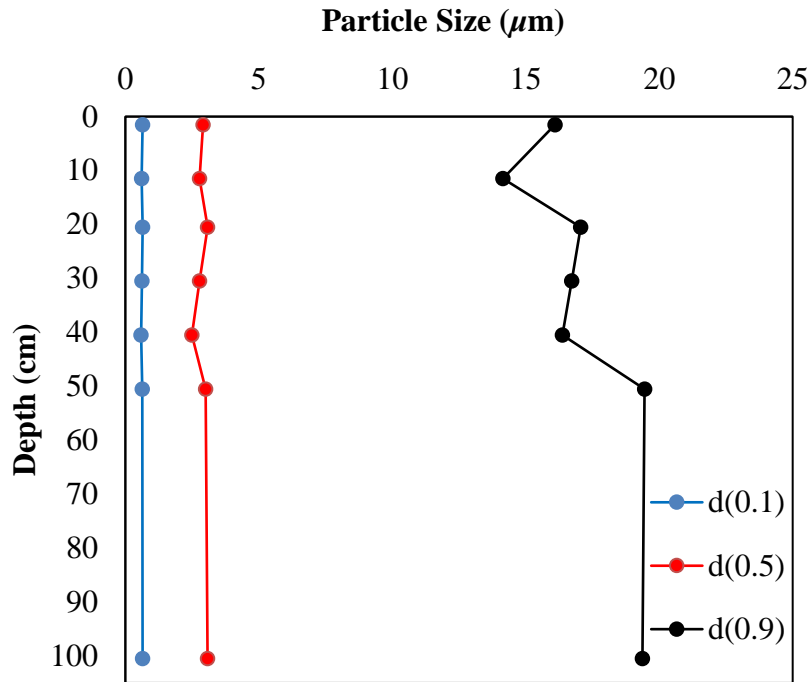
(b)

Figure 4.34. Grain size distributions for core 41: (a) d(0.1) and d(0.5) indicate that 10 % and 50 % of the sediment is finer than the size (μm) indicated; (b) d(0.9) indicates that 90 % of the sediment is finer than the size (μm) indicated.

4.7.3   Mineralogy

Minerals observed are quartz, K-feldspar, plagioclase, calcite, dolomite, amphibole, and clay minerals (1.4 nm – chlorite; 1.0 nm – illite; 0.7 nm – kaolinite) (Figure 4.35). Quartz content varies the most (44-50%), generally increasing from 100.5–60.5 cm, before declining at 50.5 cm and then increasing up core. Illite and kaolinite contents range from 10-13 %, and 6-8 %, respectively. Chlorite (10-16 %) is most abundant at the base of the core (100.5 to 90.5 cm). K-feldspar content is 6-7%, while plagioclase content is typically 9-11% with a maximum of 15% at 80.5 cm. Calcite (3-4%) occurs throughout the core until its disappearance at 1.5 cm. Dolomite (3 %) is only present at 20.5 and 10.5 cm. Amphibole (2-3%) is present throughout the core.
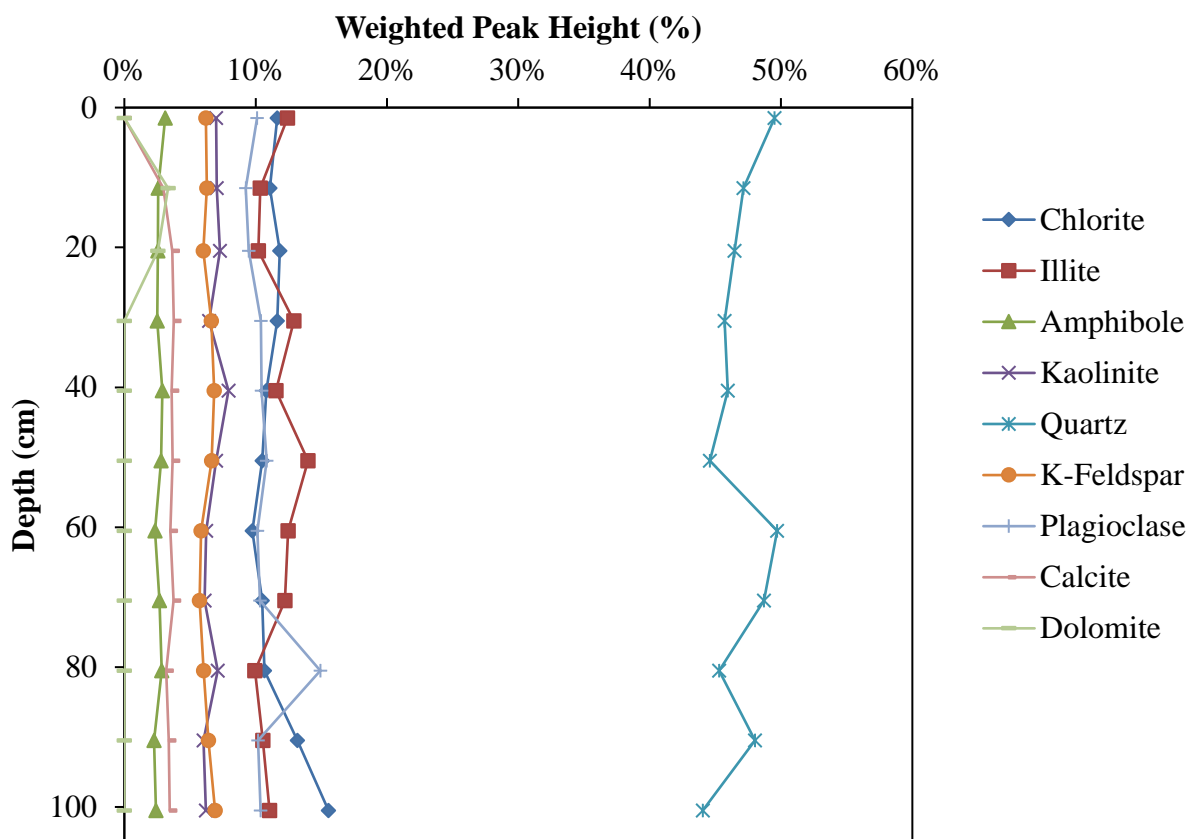
Figure 4.35. Mineral abundances for core 41. Percentages are based on weighted peak heights of the strongest diffraction for each phase, as measured by p-XRD.

4.7.4 Magnetic Susceptibility

Full core and half-core MS signals were measured with a loop sensor and point sensor, respectively (Figure 4.36). In general, loop sensor measurements (average 9) are lower than point sensor (average 11.5) measurements. Loop sensor MS signals are relatively constant throughout the core except in the upper 19 cm. There, the MS signal gradually increases until ~9 cm, and then sharply increases to 21 at 5.5 cm, before decreasing to 11-12) at the core's top. Point sensor MS signals show a similar pattern. They are relatively constant until ~22 cm, increase gradually until 10 cm and then more sharply to a maximum of 17 at 7.5 cm, and then decrease towards the top of the core.
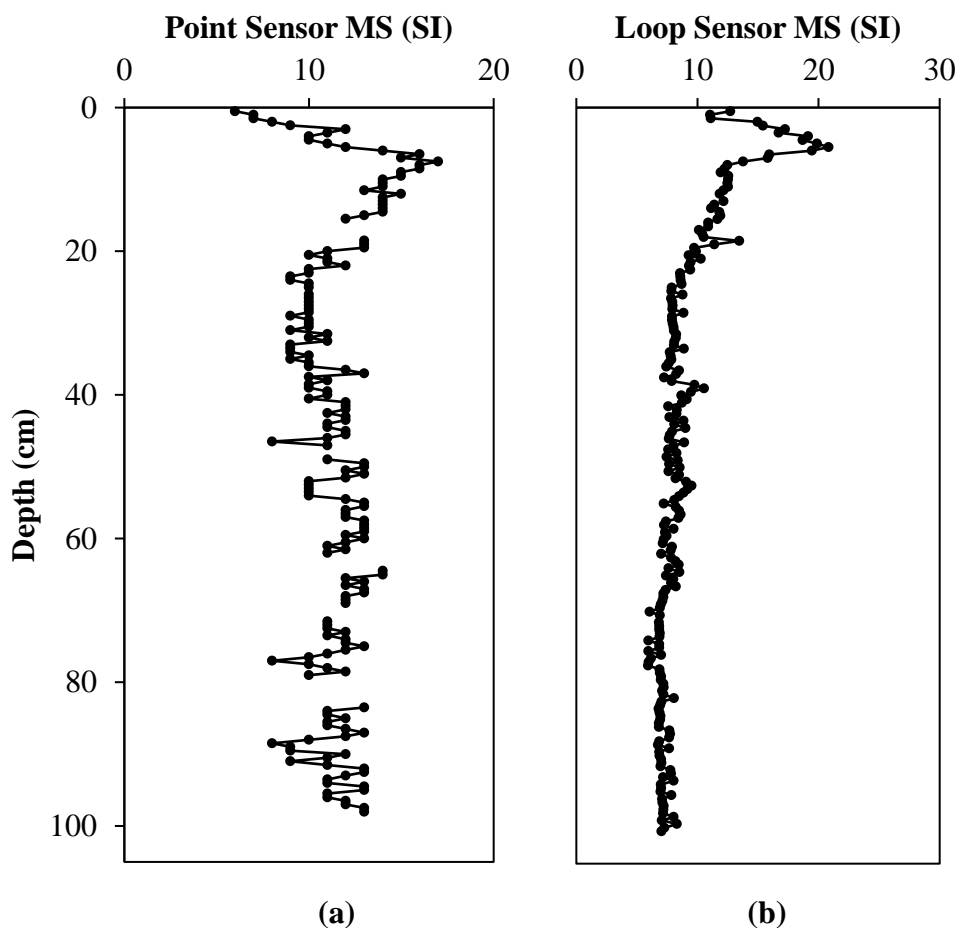
Figure 4.36. Magnetic susceptibility measurements of core 41: (a) point sensor and (b) loop sensor.

4.7.5   TOC, TN, and C/N ratio

The TOC and TN for core 41 range between 2.18–3.50 % and 0.29–0.40 %, respectively (Figure 4.37a and b, respectively) and display similar patterns. Values vary slightly from 100.5 to 60.5 cm, increase modestly from 55.5 to 45.5 cm, decrease slightly from 40.5 to 30.5 cm, and then gradually increase to maximum values at the top of the core. The C/N ratio ranges from 8.4–9.7, with an average of 8.9 (Figure 4.37c). The C/N ratio remains relatively consistent from 100.5 to 60.5 cm, followed by an increase between 55.5 to 45.5 cm, and then a gradual decrease

ending at its minimum (8.4) at 30.5 cm. The C/N ratio then rises to its maximum (9.7) at 13.5 to

7.5 cm, before declining to 8.4 at the top of the core.
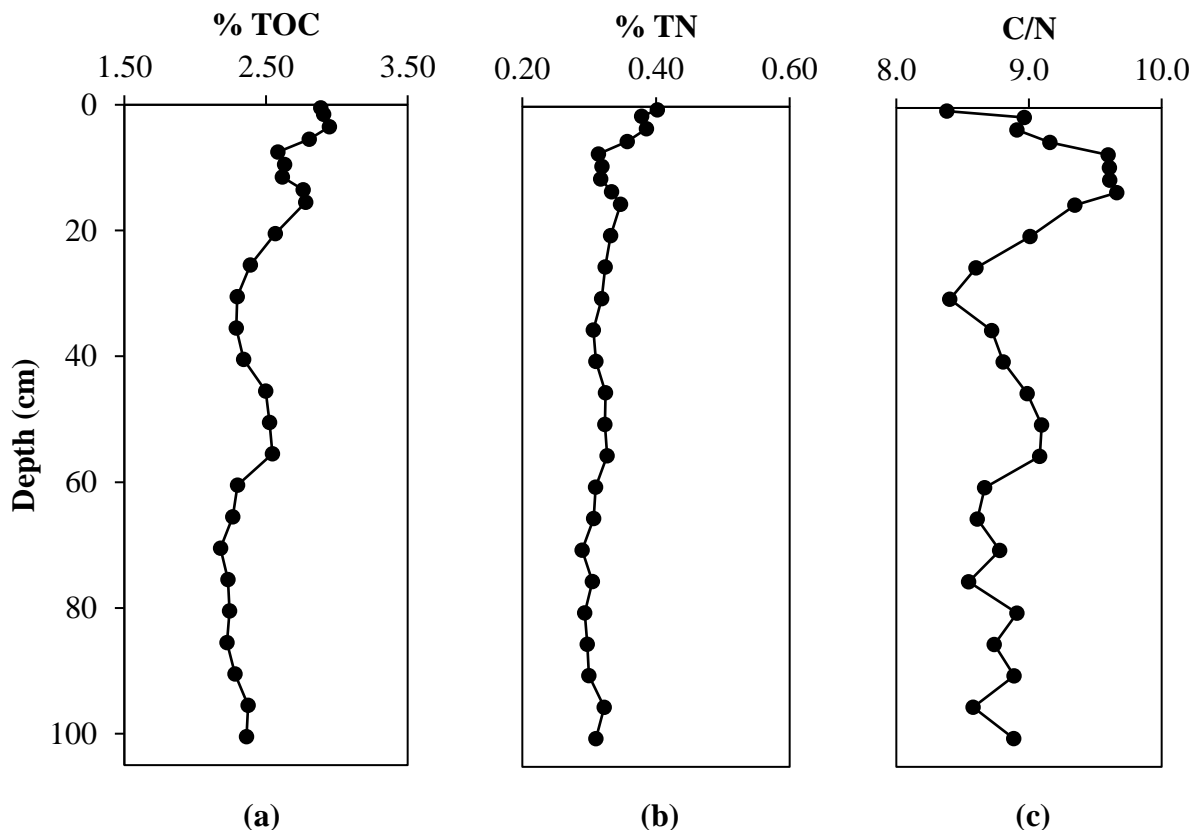
Figure 4.37. (a) TOC, (b) TN, and (c) C/N ratio for core 41.

4.7.6   Carbon- and Nitrogen-Isotope Compositions of OM

The $\delta^{13}C_{OM}$ for core 41 ranges from –26.77 to –25.53 ‰ (Figure 4.38a). The $\delta^{13}C_{OM}$ is

more or less constant (~ –25.6 ‰) from 100.5 to 40.5 cm. A small step decrease in $\delta^{13}C_{OM}$ to –

25.95 ‰ follows at 35.5 to 5.5 cm, succeeded by a decrease to the core's lowest values at its top.

The $\delta^{15}N_{TN}$ ranges from +4.28 to +5.65 ‰ (Figure 4.38b). Values remain more or less constant

(~+5.2 ‰) from 100.5 to 65.5 cm, followed by a gradual decrease to +4.28 ‰ at 40.5 cm. An

increase in $\delta^{15}N_{TN}$ to the core's maximum (+5.65 ‰) at 13.5 to 7.5 cm ensues, followed by a

decrease to ~+5.0 ‰ the core's top.
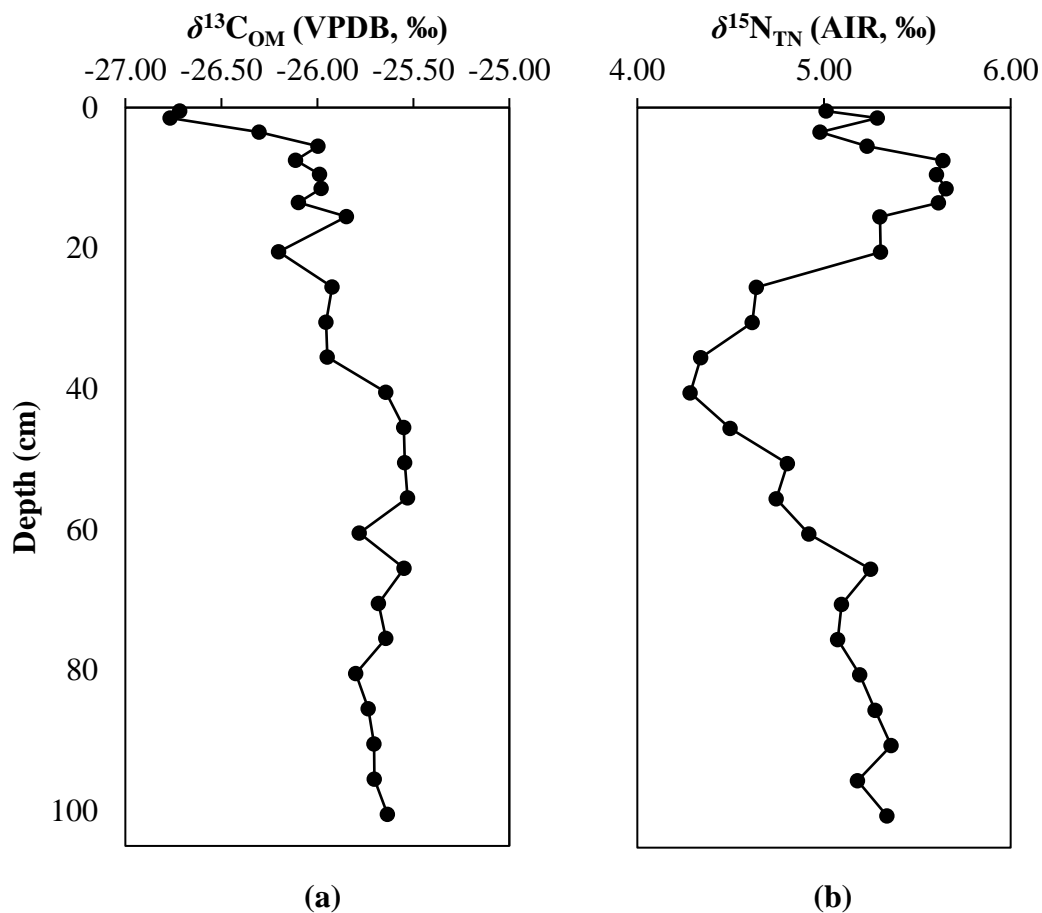
Figure 4.38. (a) $\delta^{13}C_{OM}$ and (b) $\delta^{15}N_{TN}$ for core 41.

4.8   Cross-Basin Comparison

4.8.1   Carbon-Isotope Composition versus C/N Ratio

The $\delta^{13}C_{OM}$ versus C/N results (Figure 4.39) for the Port Huron, Manitoulin, Mackinac and Goderich basins, and Georgian Bay (cores 818-2, 181, 182, 594, and 41) are predominantly within the lacustrine algae range. Results for the Alpena basin (core 817), however, lie both within and just outside the range for lacustrine algae and most of the values for the Saginaw basin (core 821) lie just outside of the lacustrine range.
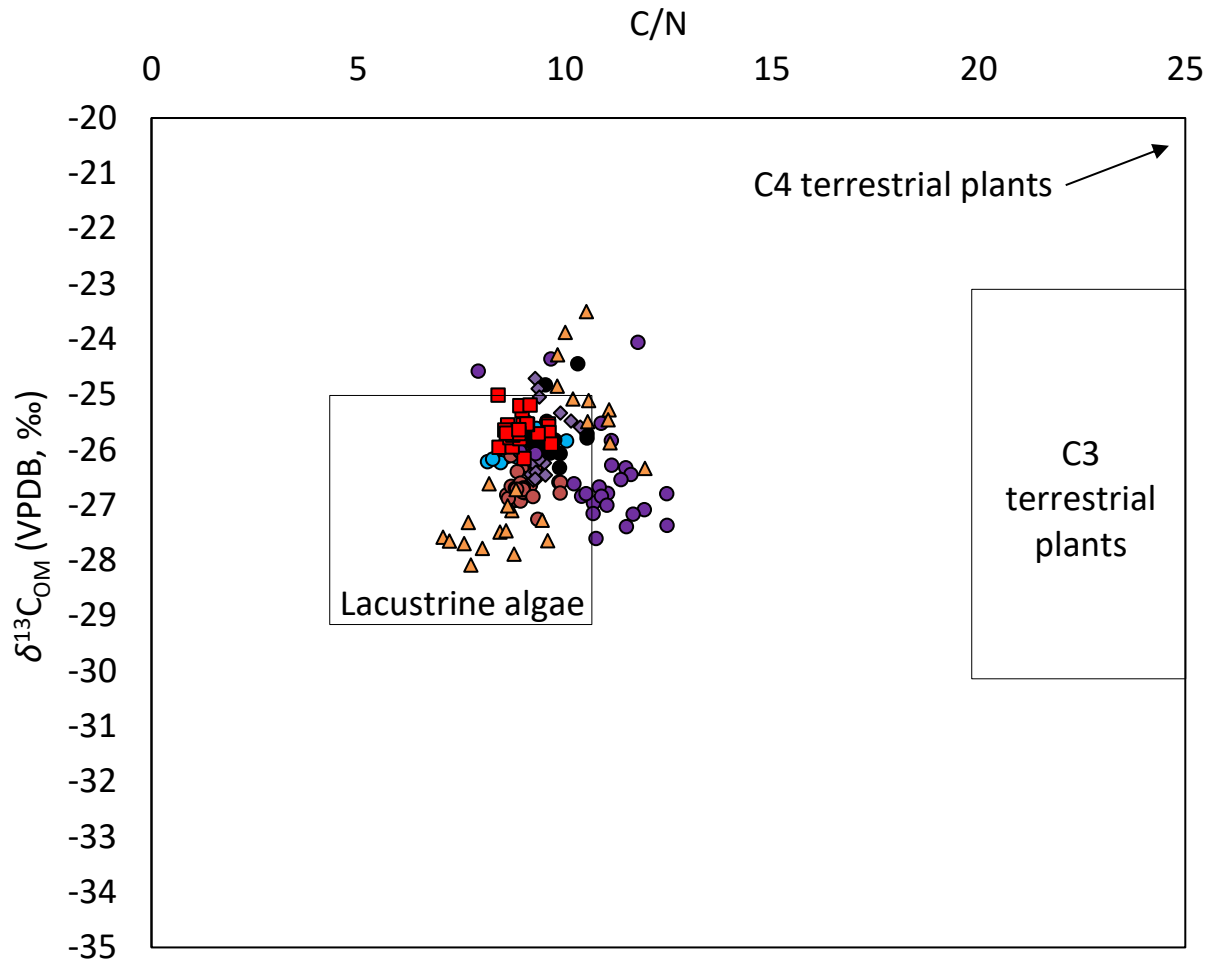
Figure 4.39. $\delta^{13}C_{OM}$ versus C/N for cores 818-2 (Port Huron basin), 181 (Manitoulin basin), 182 (Mackinac basin), 594 (Goderich basin), 821 (Saginaw basin), 817 (Alpena basin), and 41 (Georgian Bay). See Figure 3.1 for core locations.

Chapter 5

5 Discussion

Here, the age-depth models used in this study are developed. This is followed by an interpretation of climate conditions and the impact of anthropogenic activities on the lake sediments in the seven cores that were studied. The significance of the similarities and differences observed among the various cores is also discussed.

5.1 Age-depth Models

Age-depth models for cores 594 (Figure 5.1), 181 (Figure 5.2), and 182 (Figure 5.3) have been established using the Bayesian age-depth modeling program Bacon (Blaauw and Christén, 2011). All dates used in the age-depth models are summarized in Tables 5.1, 5.2, and 5.3 for cores 594, 181, and 182, respectively. The Bacon software was used to interpolate between dated horizons to assign ages to depths. As ^{210}Pb dating was not completed on cores 821, 817, 818-2, and 41, the start of the significant increase in % TOC and % TN typically observed between 20–40 cm is interpreted to indicate the start of European settlement and deforestation that occurred in the 19th century. Above this point, a sedimentation rate similar to what is observed post-1850 in the ^{210}Pb dated cores is used. Prior to this point, a sedimentation rate similar to what is observed in the older sediments of core 594, which is underpinned by an AMS ^{14}C date, is used. The AMS ^{14}C date was also used to constrain the lower boundary of core 181 and core 182 (Figure 5.2b and 5.3b, respectively).

Samples	Age (year before 1950)	Error (y)	Depth (cm)
surface	-54	0	0
lead1	-52	0.3775	0.5
lead2	-46	0.9183	1.5
lead3	-41	1.4069	2.5
lead4	-30	2.7107	4.5
lead5	-11	5.9522	7.5
lead6	9	11.7423	10.5
lead7	18	15.0222	13.5
lead8	25	18.0147	16.5
lead9	32	20.7683	20.5
lead10	32	18.6672	23.5
lead11	32	16.9964	26.5
lead12	44	19.8126	30.5
lead13	64	30.9408	33.5
lead14	142	288.3074	36.5
radiocarbon1	6065	47	350

Table 5.1. Age constraints and uncertainties for core 594 (Goderich basin).

Samples	Age (year before 1950)	Error (y)	Depth (cm)
surface	-56	0	0
lead1	-55	1.7181	0.5
lead2	-51	5.166	1.5
lead3	-48	8.5036	2.5
lead4	-40	16.0023	4.5
lead5	-29	27.8677	7.5
lead6	-18	37.9365	10.5
lead7	-7	49.6924	13.5
lead8	6	62.6605	16.5
lead9	24	80.3837	20.5
lead10	42	98.5375	23.5
lead11	54	110.8413	26.5
lead12	64	119.9293	30.5
lead13	86	141.9909	33.5
lead14	192	248.7987	36.5
radiocarbon1	6065	47	350

Table 5.2. Age constraints and uncertainties for core 181 (Manitoulin basin).

Samples	Age (year before 1950)	Error (y)	Depth (cm)
surface	-56	2.0389	0
lead1	-51	2.2341	0.5
lead2	-41	3.1785	1.5
lead3	-29	5.0200	2.5
lead4	-1	13.2512	4.5
lead5	51	48.9437	7.5

Table 5.3. Age constraints and uncertainties for core 182 (Mackinac basin).
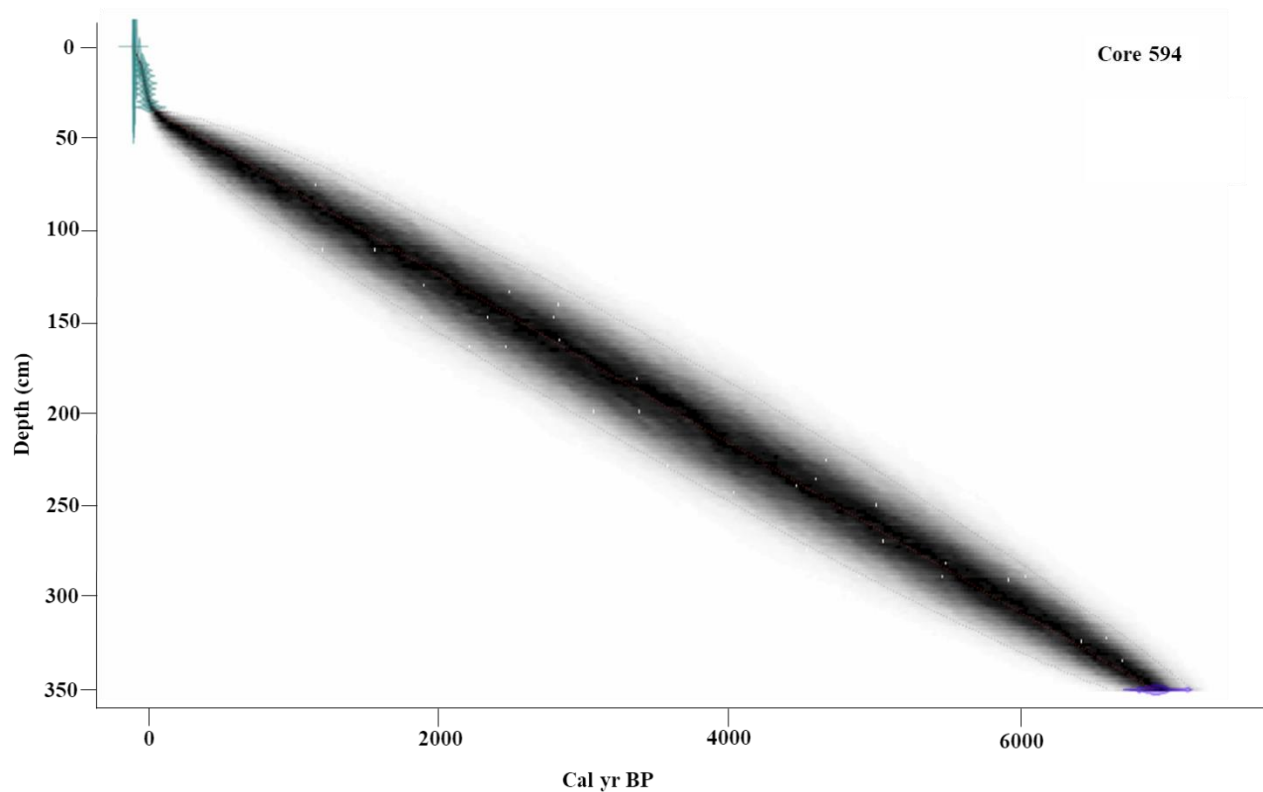
Figure 5.1. Bacon age-depth model (Blaauw and Christén, 2011) for core 594 (Goderich basin) based on fourteen ^{210}Pb dates and one AMS ^{14}C date. The 95 % confidence intervals are shown by grey dots and the potential distribution is shown in grey shading. The denser shading indicates the most likely age.
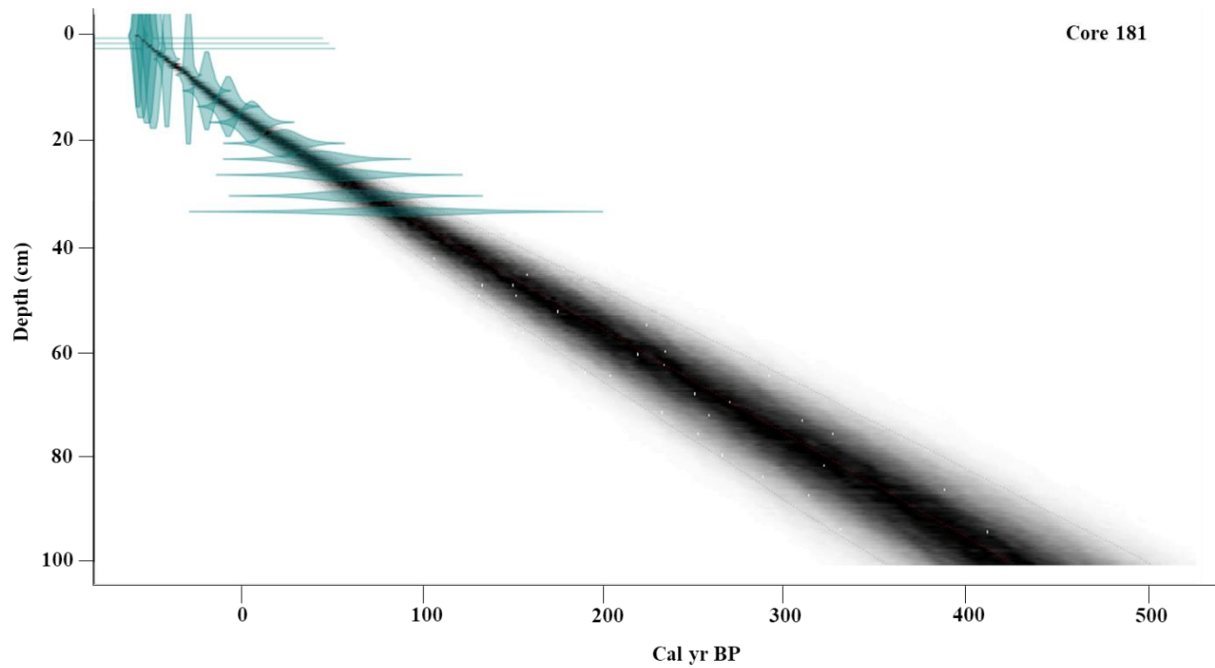
(a)
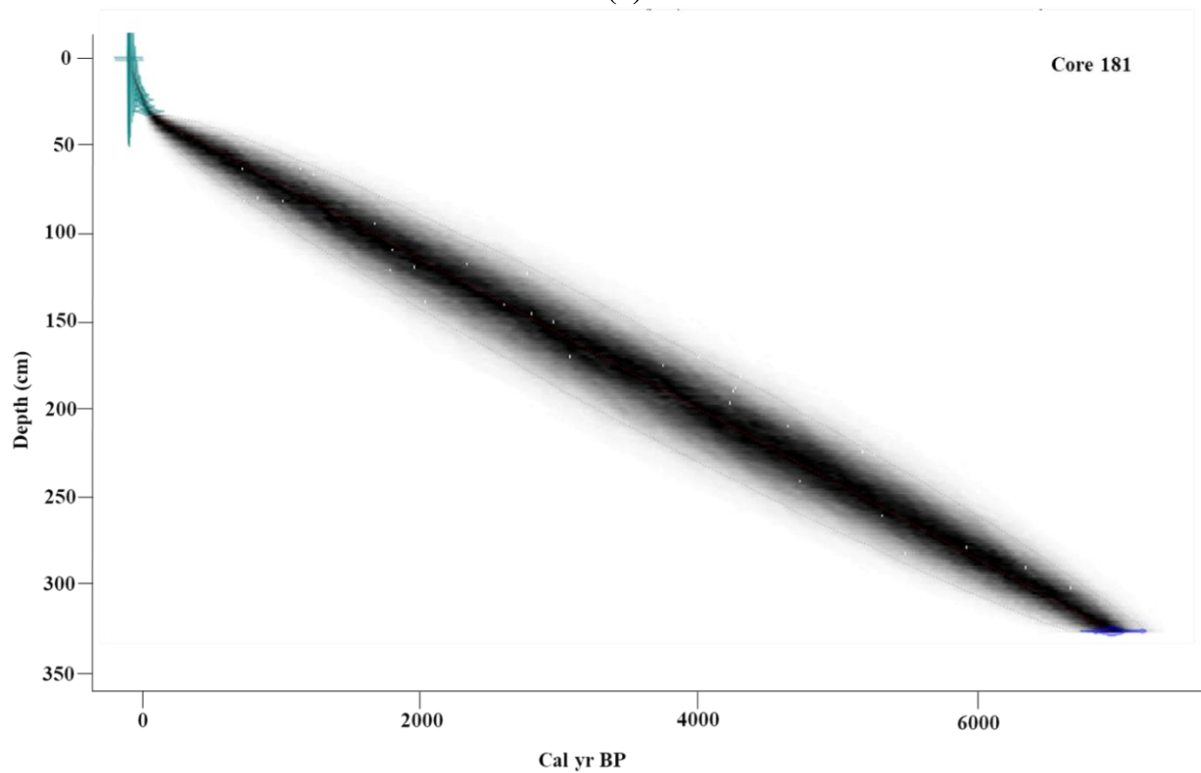
(b)

Figure 5.2. Bacon age-depth model (Blaauw and Christén, 2011) for core 181 (Manitoulin basin) based on (a) fourteen ^{210}Pb dates, and (b) fourteen ^{210}Pb dates and one AMS ^{14}C date. The 95 % confidence intervals are shown by grey dots and the potential distribution is shown in grey shading. The denser shading indicates the most likely age.
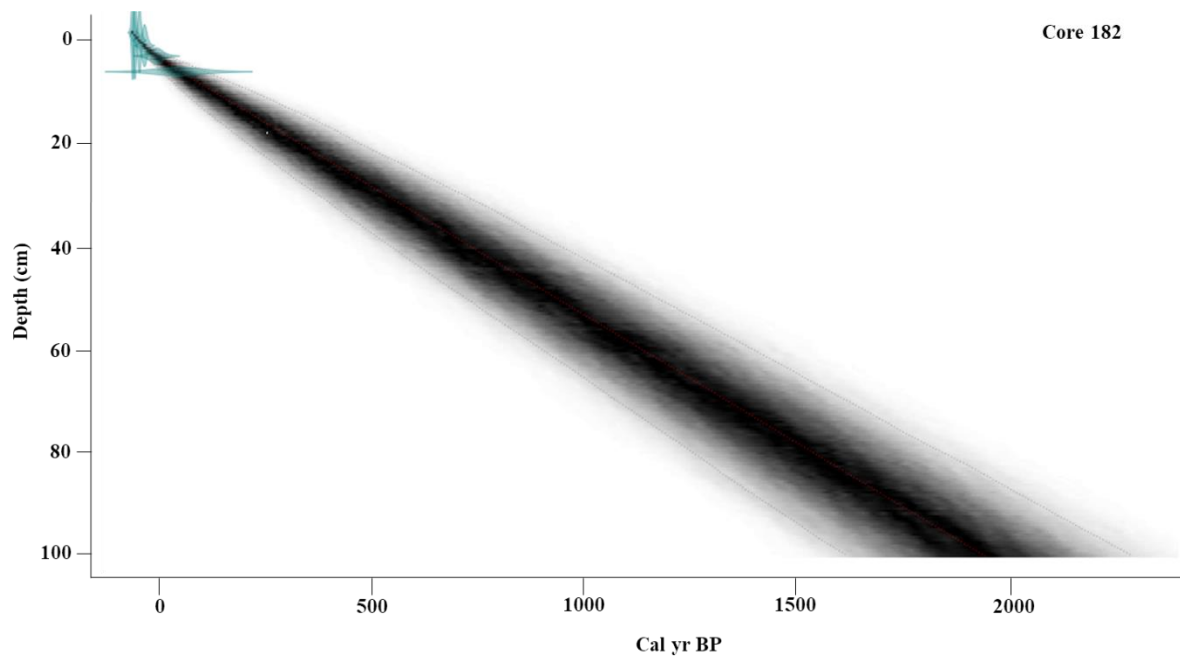
(a)
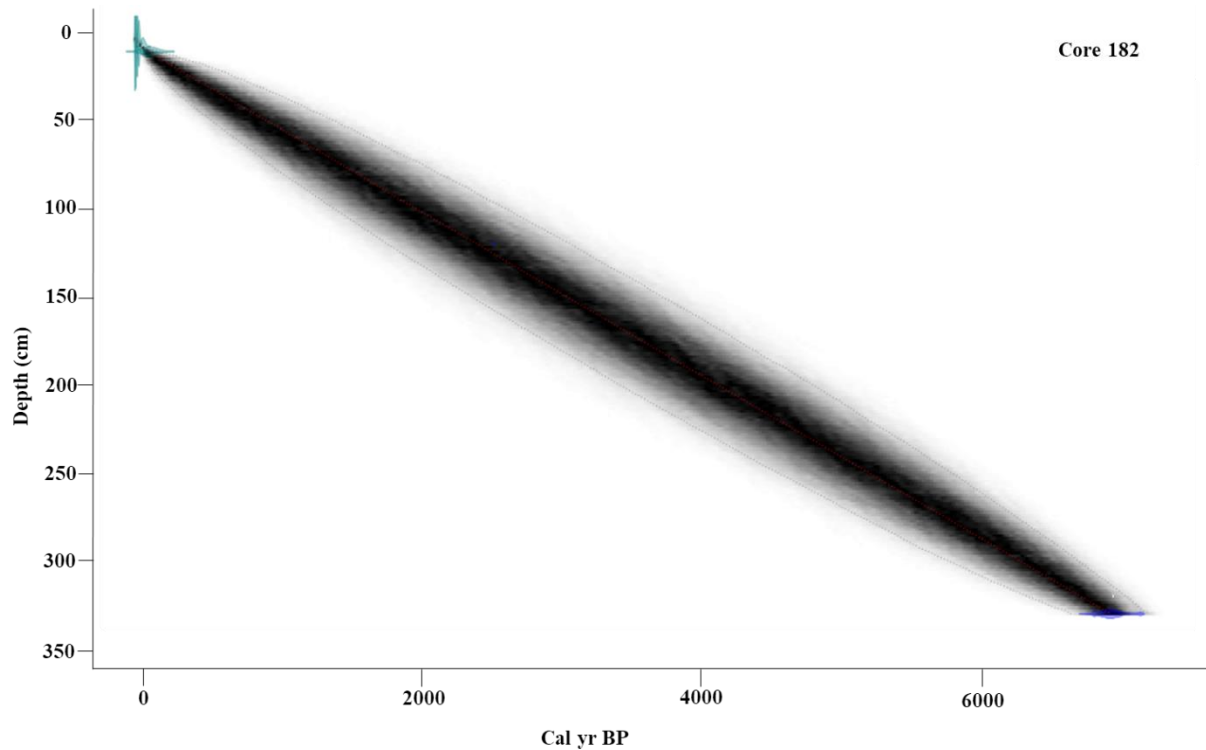
(b)

Figure 5.3. Bacon age-depth model (Blaauw and Christén, 2011) for core 182 (Mackinac basin) based on (a) five ^{210}Pb dates, and (b) five ^{210}Pb dates and one AMS ^{14}C date. The 95 % confidence intervals are shown by grey dots and the potential distribution is shown in grey shading. The denser shading indicates the most likely age.

5.2   Environmental History of Lake Huron

This section explores the environmental history of Lake Huron based on the age-depth models and information collected from the various proxies described previously. The history is presented in intervals separated based on significant shifts in proxy measurements.

5.2.1   Core 594 (Goderich Basin)

Interval I in core 594 (Figure 5.4) spans depths from 60.5 to 40.5 cm and represents 1306 to 1743 CE, according to the age-depth model. During this time period, the shores of Lake Huron were sparsely populated, with the establishment of counties and settlement focused in Quebec, eastern Ontario, and the shores of Lake Ontario. Most proxies analysed for this interval do not show substantial variations, but % TOC and % TN show a small gradual decrease. The LIA, which was a period of moderately cooler Northern Hemisphere temperatures from about 1600 and 1850 CE (PAGES 2k Consortium 2013), occurred during this interval. Moreover, Buhay and Edwards (1995) measured oxygen and hydrogen isotopes in wood cellulose and cellulose-nitrate from trees in southwestern Ontario to develop an isotope model for climate inference (Figure 5.6). Their model inferred that between 1600 and 1750 CE, cool-dry conditions existed in southwestern Ontario. The lower temperatures and precipitation likely resulted in a decrease in primary production and allochthonous input, leading to a reduction in % TOC and % TN.

Interval II spans depths from 40.5 to 15.5 cm and represents 1743 to 1932 CE. Following the American Revolutionary War in 1783, about 30,000 United Empire Loyalist refugees came to the remaining British colonies in North America. These refugees demanded new lands for settlement which encouraged colonial administrators to begin land surrender treaty negotiations

with the Aboriginal peoples. Between 1783 and 1812 CE, fifteen land surrender treaties were concluded in the Upper Canadian peninsula ("Upper Canada Land Surrenders and the Williams Treaties (1764-1862/1923)" 2013). Following the War of 1812, immigrants arriving from Europe came in increasingly large numbers to Upper Canada to settle. With peace established between Britain and the United States, the influence of Aboriginal peoples over British officials waned, and the pace of land surrenders increased to provide European settlers with land ("Upper Canada Land Surrenders and the Williams Treaties (1764-1862/1923)" 2013). Settlement in Ontario expanded, and many townships were established on the eastern shores of Lake Huron (Figure 5.5) (Dean and Matthews 1969). The treaties conducted between 1815 and 1860 CE procured all the remaining lands in Upper Canada, and by the end of the 19th century, townships had been established along the majority of Lake Huron and Georgian Bay's shores (Dean and Matthews 1969).

This interval is characterized by a significant increase in % TOC, % TN, and grain size. The increase in % TOC and % TN was likely the result of warmer climate conditions following the end of the LIA (e.g., Moore et al. 2001), as well as deforestation by European settlers. The climate during much of this interval varied between warm-moist and cool-dry (Buhay and Edwards 1995) and lake levels were usually high until they began to decrease in 1887 CE (Figure 5.7). Warmer climate conditions can lead to an increase in algal primary production (Konopoka and Brock 1978), which would have increased the % TOC and % TN. Furthermore, an increase in terrestrial OM, and subsequently % TOC and % TN, is likely to have occurred due to the extensive deforestation. Prior to European settlement, southern Ontario was continuously forested, with as much as 90 % forest cover. Today, southern Ontario has only about 25 % forest cover, with much of it having been cleared by settlers for farms and communities

(Environmental Protection Report 2018). The C/N ratio of the sediment OM, however, does not vary widely, indicating that the ratio of lacustrine and terrestrial sourced OM remained steady. Moreover, the magnetic susceptibility signal also does not vary widely, suggesting that the increase in terrestrial material expected from land clearance was either not significant enough to increase the signal, or, that the source of the terrestrial material did not contain an abundance of magnetic minerals.

Water level variations occur on a variety of temporal scales. Long-term variations (years, decades) are related to changes in climate (Bishop 1990), which suggests that the high water levels known for much of this interval are the result of the increased precipitation during the warm-moist period between 1750 and 1775 CE, and the warm and moist period between 1800 and 1850 CE (Buhay and Edwards 1995). The decrease in water level that began in 1887 CE has been suggested to be caused by dredging at the outlet of Lake Huron and in the St. Clair River between 1893 and 1899 CE which caused a 0.20 m permanent lowering of lake level (Quinn and Croley 1981). Further dredging between 1908 and 1925 CE, and continued navigation improvements between 1933 and 1962 CE, are estimated to have also produced a permanent 0.27 m lowering of lake levels (Derecki 1982). Local land clearance and a lowering of lake level would have contributed to the increase in grain size observed during this interval, as it would have allowed for a shorter sediment transportation time prior to deposition.

Interval III spans depths from 15.5 to 3.5 cm and represents 1932 to 1986 CE. The interval is characterized by an increase in $\delta^{13}C_{OM}$ and $\delta^{15}N_{TN}$, a decrease in OM compared to *Interval II*, an increase in the C/N ratio followed by a gradual decrease, and a sharp increase in magnetic susceptibility also followed by a decrease. Continuous and increased land clearance

following WWII for agriculture and urban development produced the significant changes observed in the proxies. The increase in magnetic susceptibility and the C/N ratio was likely caused by an increase in the flux of allochthonous material entering the Goderich basin. Moreover, the total annual precipitation in the Great Lakes region increased by 10.7 cm between 1955–2005 (Andresen et al. 2002; Hodgkins et al. 2007), which may have further facilitated the delivery of allochthonous material into the basin. The decrease in the C/N ratio and magnetic susceptibility that followed the increase reflects the reduction in allochthonous inputs after most land clearance had occurred. The % TOC decreased sharply from the maximum observed at 20.5 cm depth in *Interval II*, but then remained steady throughout *Interval III*. The initial decrease in % TOC and % TN was likely caused by turbidity due to the increased input of allochthonous material causing a decrease in primary production. The % TN trend shows a sharper initial decrease because terrestrial plant material has a greater proportion of carbon-rich cellulose and waxy hydrocarbons than algal OM (Meyers 1994). The increase in $\delta^{13}C_{OM}$ and $\delta^{15}N_{TN}$ suggests that primary production was increasing. This is also reflected in that % TOC and % TN began to gradually increase following their decrease. As land clearance waned, turbidity was no longer inhibiting primary production. Urbanization and nitrogen sourced from septic waste (Heaton 1986) and soil nitrate of organic origin from agriculture (Hodell and Schelske 1988), in addition to continually warming temperatures, may have contributed to the sharp increase in $\delta^{15}N_{TN}$. The small decrease in $\delta^{15}N_{TN}$ in 1986 CE may be a response to decrease P loading in the 1970s and 1980s, which can decrease lacustrine production (Schelske and Hodell 1995). Prior to efforts to reduce P loading, anthropogenic inputs of P would have also contributed to an increase in primary production (Kemp et. al 1972, 1974; Kemp and Thomas 1976).

Interval IV spans depths from 3.5 to 0 cm and represents 1986 to 2004 CE. This interval is characterized by a continued increase in $\delta^{13}C_{OM}$ and $\delta^{15}N_{TN}$, and an increase in % TOC and % TN. The increase in OM and continued increase in $\delta^{13}C_{OM}$ and $\delta^{15}N_{TN}$ suggests that primary production was continuously increasing. Higher temperatures and reduced ice cover of Lake Huron water may have contributed to the trends observed for *Intervals III* and *IV*. Warming from pre-industrial levels to the 2006–2015 decade is assessed to be 0.87°C, according to the Intergovernmental Panel on Climate Change (IPCC 2019).
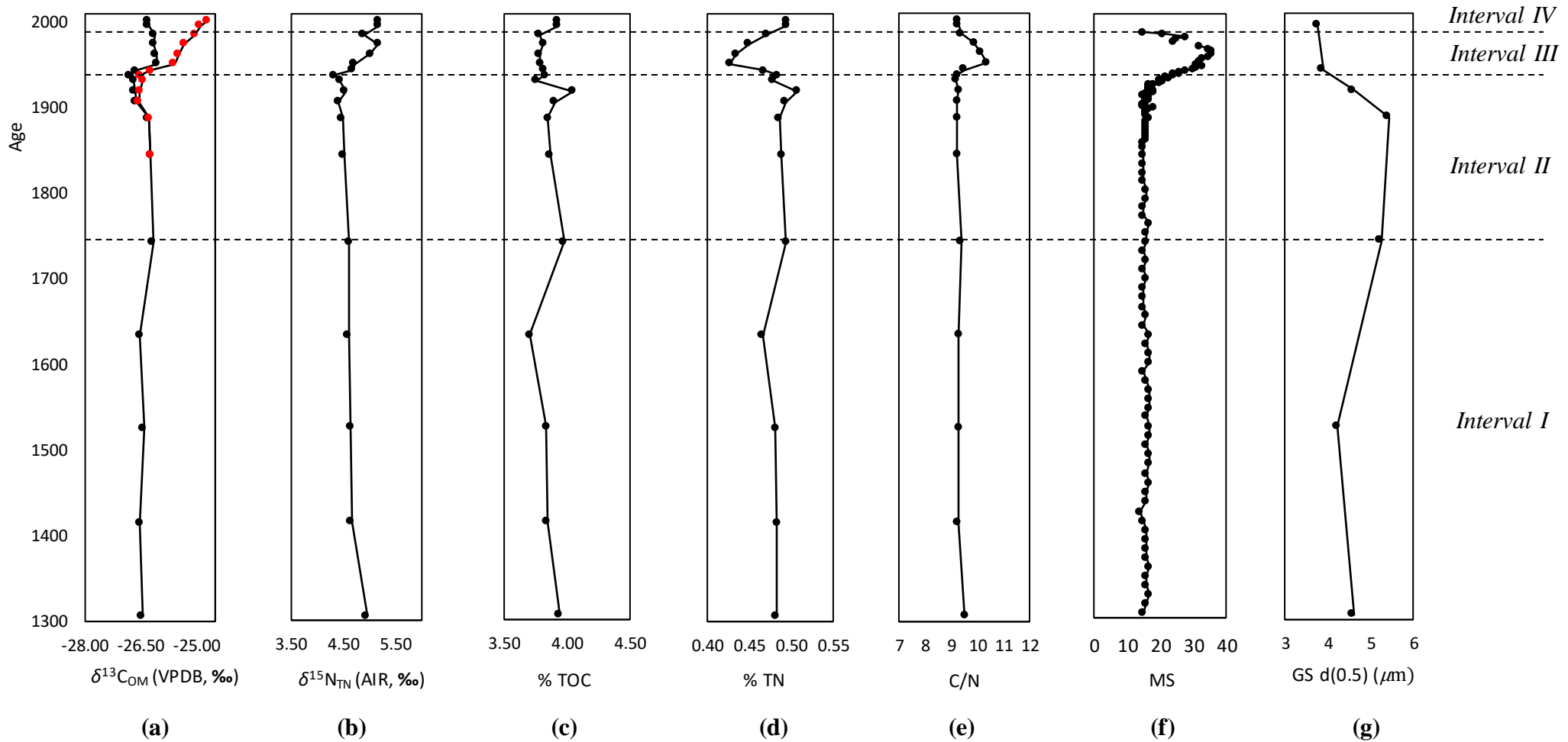
Figure 5.4. Age versus: (a) $\delta^{13}C_{OM}$. Measured $\delta^{13}C_{OM}$ is shown in black, and Suess-corrected $\delta^{13}C_{OM}$ (applied to years after 1850 CE) is shown in red. (b) $\delta^{15}N_{TN}$. (c) Total organic carbon content. (d) Total nitrogen content. (e) C/N ratio. (f) Magnetic susceptibility. (g) Grain size. All curves are from core 594 (Goderich basin).
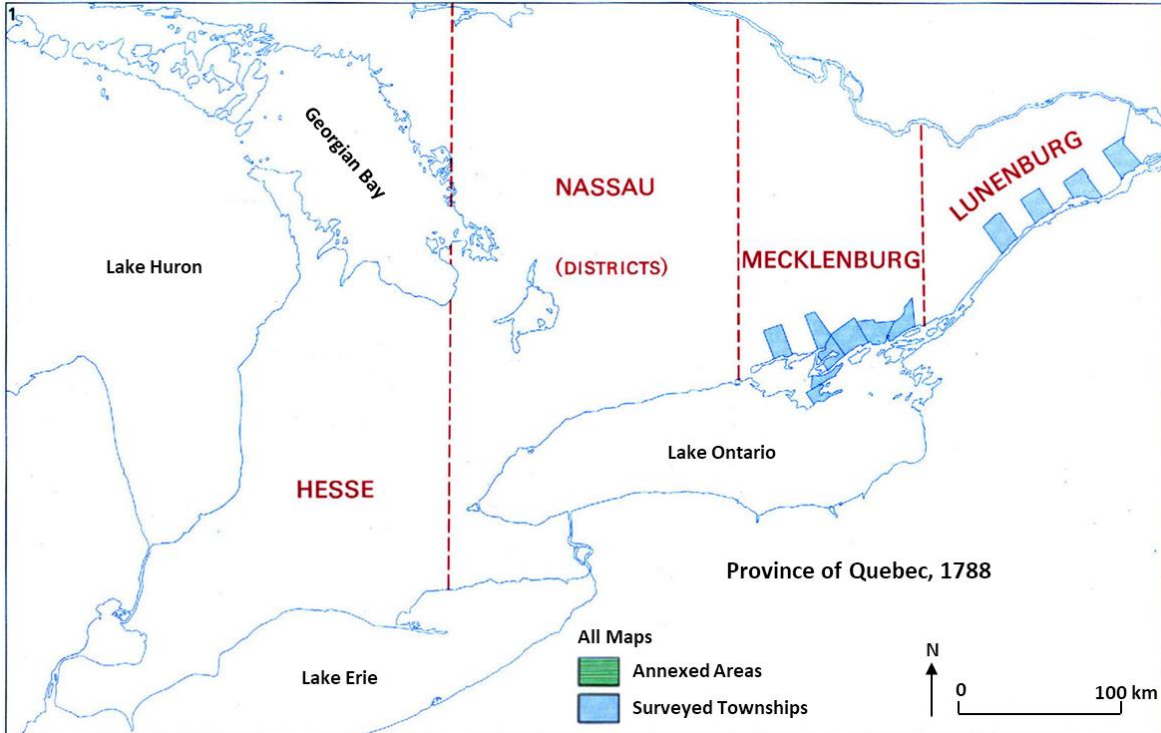
(a)
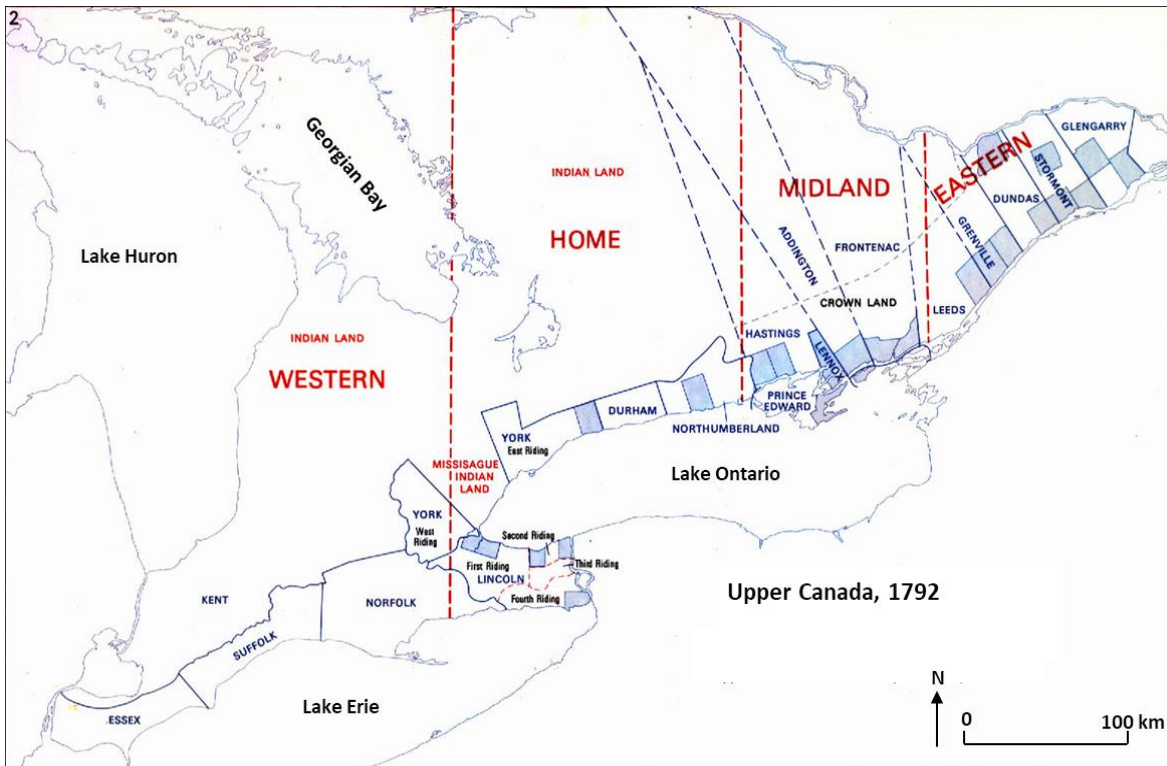
(b)
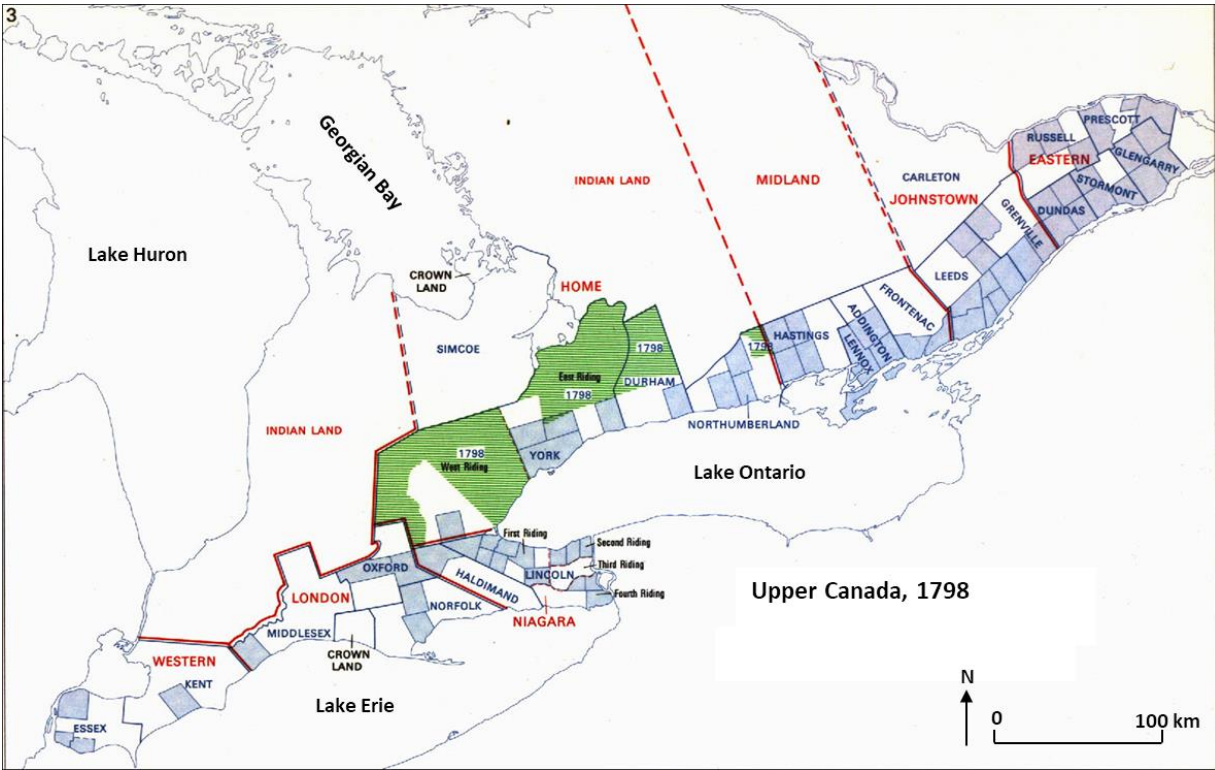
(c)
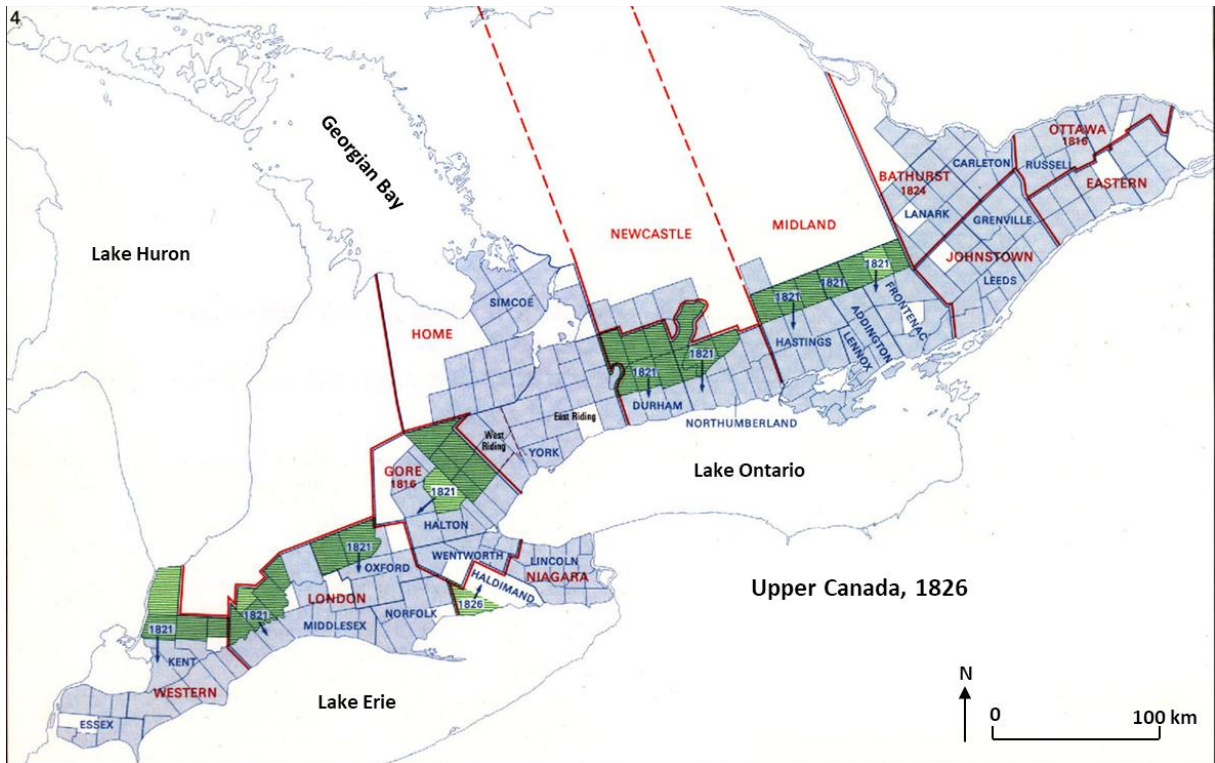
(d)
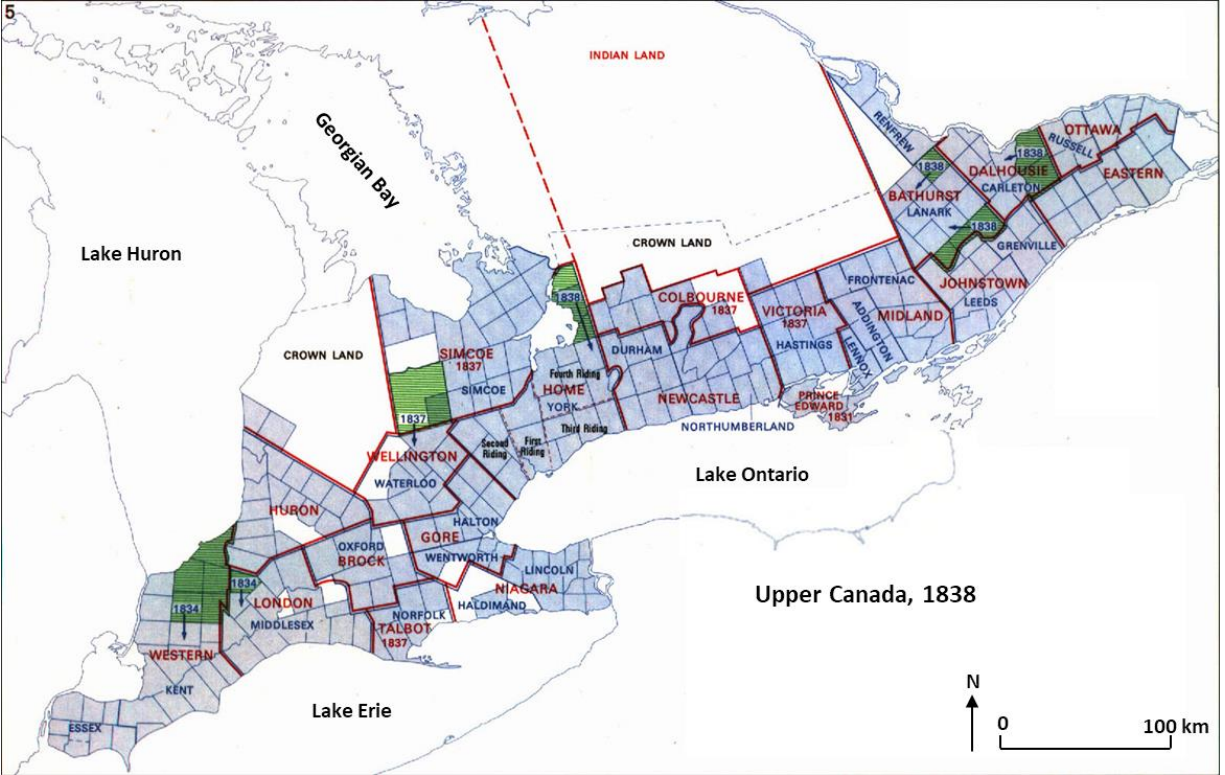
(e)
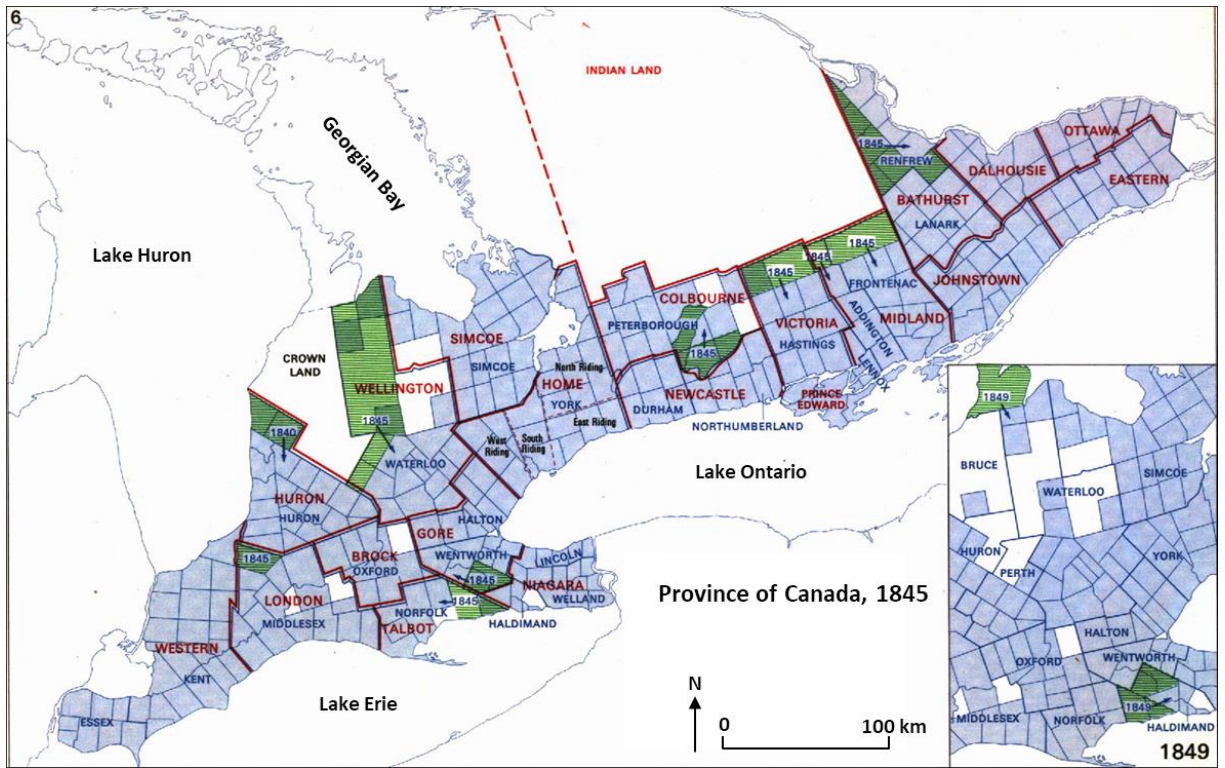
(f)
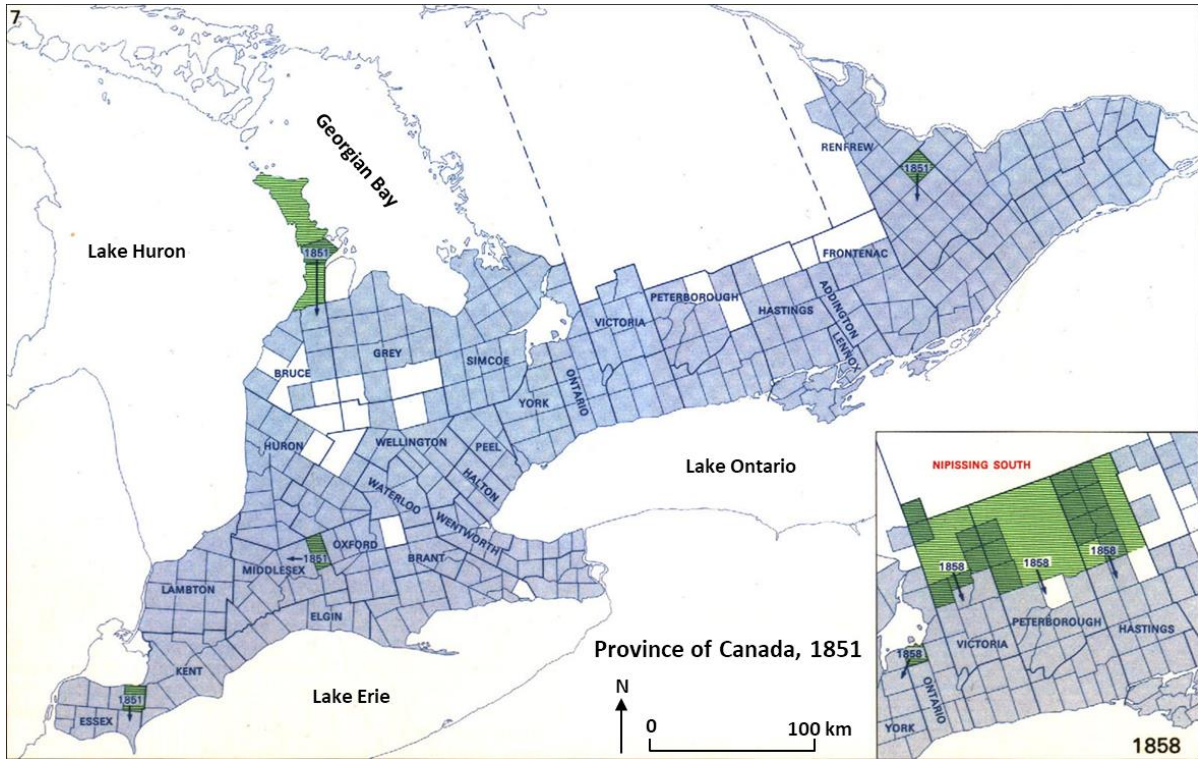
(g)
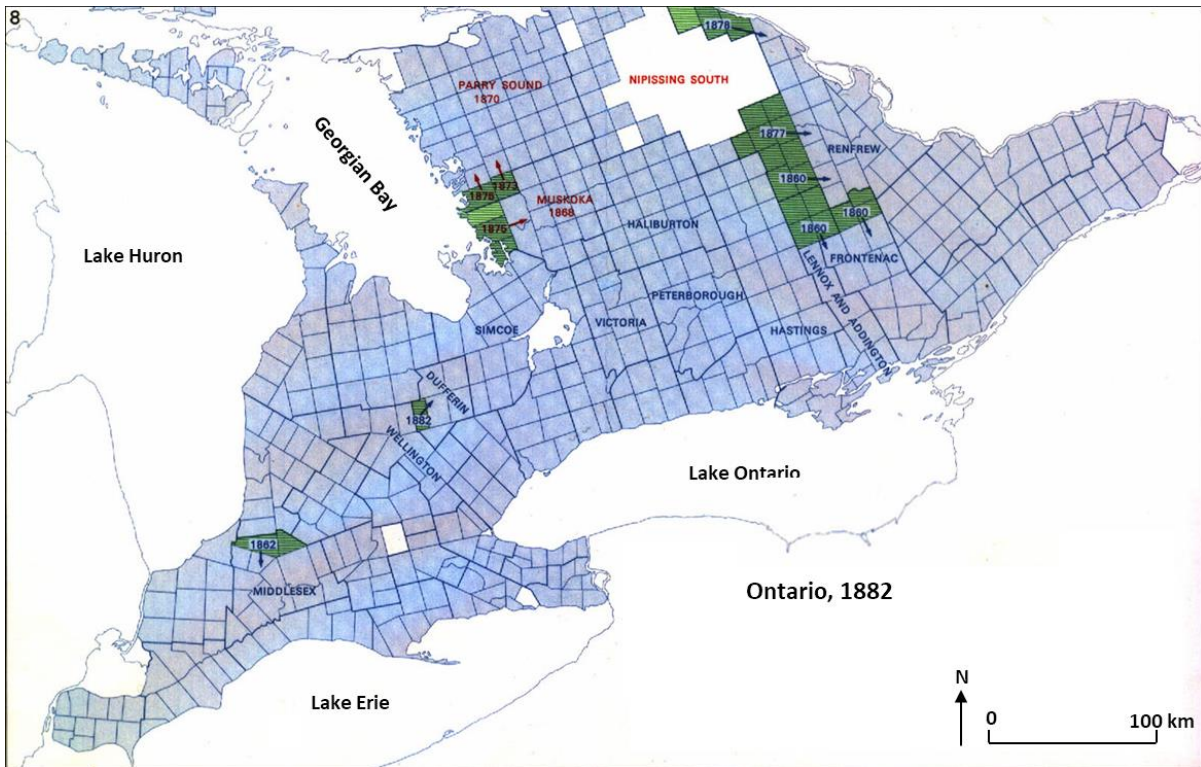
(h)
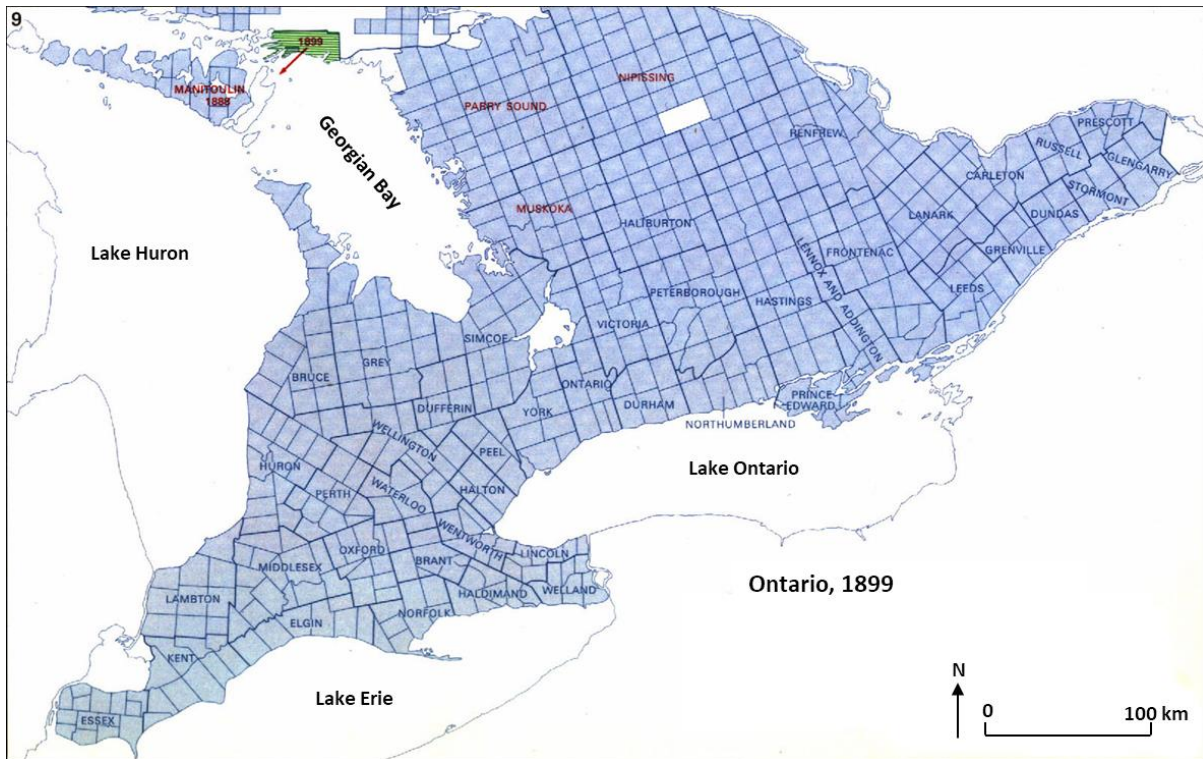
(i)

Figure 5.5. The districts and counties of the Province of Quebec, and its successors Upper Canada, Province of Canada, and Ontario: (a) 1788. (b) 1792. (c) 1798. (d) 1826. (e) 1838. (f) 1845. (g) 1851. (h) 1882. (i) 1899. Modified from Dean and Matthews (1969).
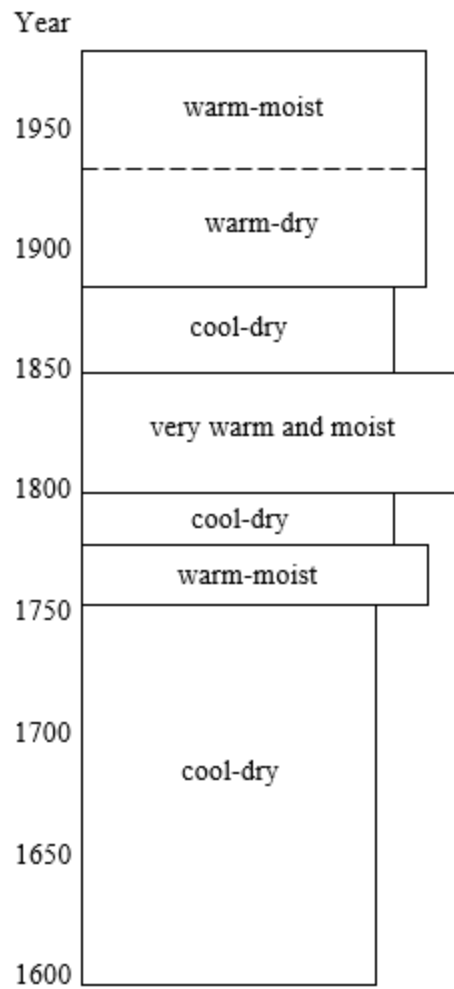
Figure 5.6. Inferred paleoclimate for southwestern Ontario, Canada between 1610 and 1990 CE. Modified from Buhay and Edwards (1995).
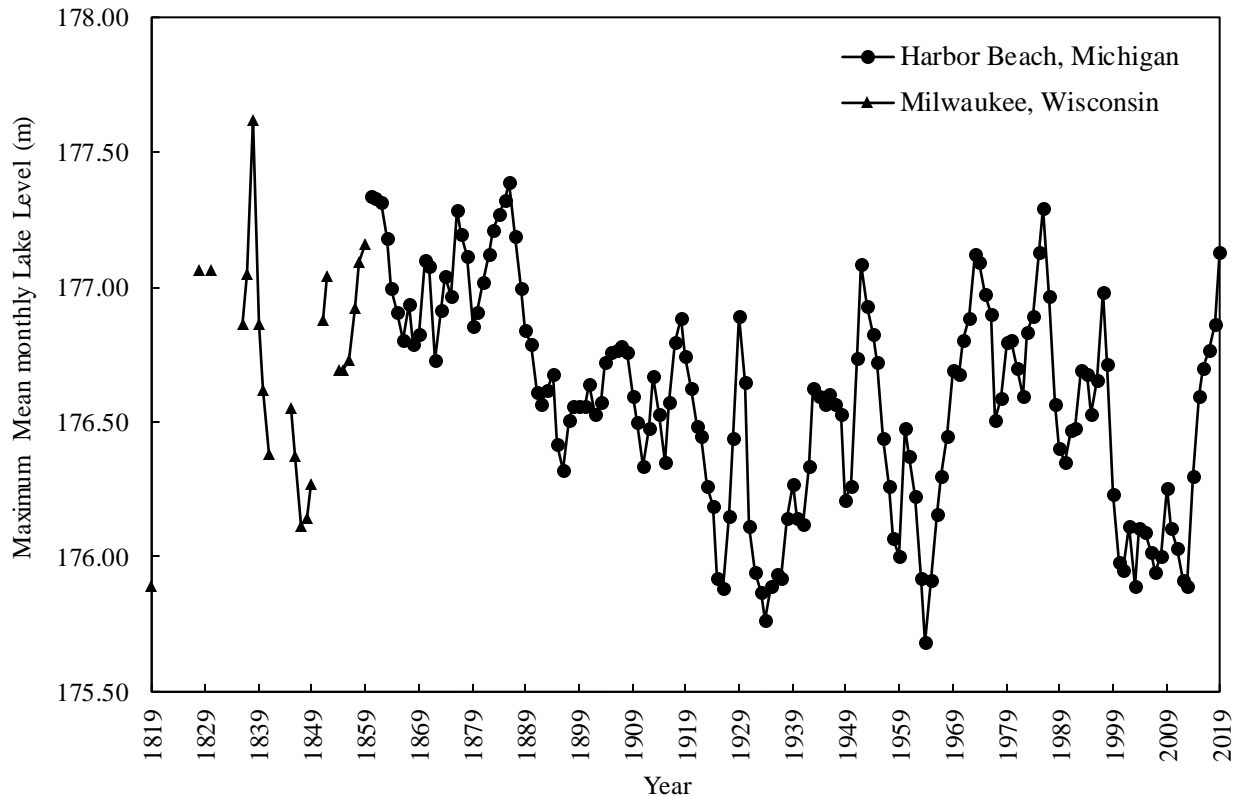
Figure 5.7. Lake Michigan-Huron maximum mean monthly lake levels between 1819 and 2019 CE. Lake level measurements from 1819 to 1859 are from Milwaukee, Wisconsin (Quinn and Sellinger 1990). Lake level measurements between 1860 to present are from Harbor Beach, Michigan (NOAA 2019).

5.2.2 Core 181 (Manitoulin Basin)

Interval I in core 181 (Figure 5.8) spans depths from 100.5 to 40.5 cm and represents 422 to 1776 CE, according to the age-depth model. The Native Anishinaabe people, who are a loose confederation made up of Ojibwe, Odawa and Potawatomi, occupied Manitoulin Island prior to European contact (Pearen 1992). The first European to settle on the island was Father Joseph Poncet, a French Jesuit, in 1648 CE (Zevely 1911). At the same time, the Five Nations of the Iroquois began to raid the island in order to assert control over the fur trade with the French. (Heidenreich 1978). The Anishinaabe and French Jesuits were driven from the island and it remained mostly uninhabited until after the War of 1812.

Overall this interval is characterized by minor variations in the proxies. This suggests that the MWP (800–1100 CE) and the LIA (1600–1850 CE) (PAGES 2k Consortium 2013), which occurred during this interval, did not produce significant changes to the proxies. Small increases and decreases in % TOC are recorded during the MWP and LIA, respectively. This is likely a result of changes in primary production and the flux of allochthonous material into the basin due to warmer and wetter conditions during the MWP, and cooler and dryer conditions during the LIA.

Interval II spans depths from 30.0 to 25.5 cm and represents 1776 to 1876 CE. The Ojibwe and Odawa returned to the island and signed an agreement with the Lieutenant Governor of Upper Canada in 1836 to make the island a refuge for all First Nations. Canadian authorities hoped that native peoples on the mainland would leave their hunting grounds and become farmers on the island. Several hundred did move to the island but maintained their way of life. Farmers and commercial fishermen demanded access to the Manitoulin area, and, in 1862, resident chiefs relinquished the majority of Manitoulin Island to the Crown ("Manitoulin Treaties" n.d.).

This interval is characterized by an increase in % TOC and C/N ratio, a minor increase in % TN, and a decrease followed by a gradual increase in magnetic susceptibility. The warm and moist climate between 1800 and 1850 CE (Buhay and Edwards 1995) would have increased the flux of allochthonous material entering the basin as well as primary production. The observed increase in % TOC is greater than that of % TN because terrestrial plants contain large amounts of carbon-rich cellulose and waxy hydrocarbons and are typically less nitrogen-rich than lacustrine plants. The C/N ratio, however, does not exceed 10, suggesting that although

allochthonous inputs may have increased, algal OM is still the dominate contributor to the total OM. The sudden decrease in magnetic susceptibility suggests that a change in sediment source to one with less magnetic material occurred. High Michigan-Huron water levels (Figure 5.7) may have increased the proportion of sediment sourced from the Michigan basin over the Superior basin, which is likely to contain less magnetic minerals in the surrounding shales and carbonate-rich rocks (Dorr and Eschman 1970). The subsequent gradual increase in magnetic susceptibility reflects the increased flux of terrestrial material into the basin. This pattern is likely a result of increased land clearance following the arrival of Aboriginal and European settlers, coupled with a moist climate.

Interval III spans depths from 25.5 to 11.5 cm and represents 1876 to 1964 CE. This interval is characterized by a gradual increase in $\delta^{13}C_{OM}$, an increase followed by a decrease in $\delta^{15}N_{TN}$, % TOC, and % TN, and an increase in the C/N ratio and magnetic susceptibility. The increase in magnetic susceptibility and the C/N ratio is caused by an increase in the flux of allochthonous material entering the Manitoulin basin. An increase in terrestrial material would have brought in additional magnetic material and terrestrial plant matter. The C/N ratio, however, is not >10, which shows that non-vascular plants such as algae remained the primary contributor of OM. The % TOC and % TN decrease throughout the interval, indicating that there was a reduction in total OM throughout this time period or less preservation of OM. The amount of allochthonous material entering the lake during this time frame may have increased the turbidity within the lake and resulted in a reduction in primary production following the increase observed in *Interval II*. The small increase in Suess-corrected $\delta^{13}C_{OM}$ is the result of a change in isotope composition of the source material due to the larger proportion of terrestrial plant OM

110

contributing to the total OM. Moreover, the climate during this interval was predominantly warm and dry (Buhay and Edwards 1995), and the $\delta^{13}C_{OM}$ of terrestrial C3 plants is known to increase with decreasing mean annual precipitation (Kohn 2010). The $\delta^{15}N_{TN}$ initially gradually increases, likely because of an increase in primary production as seen in *Interval II*. However, following the increase in turbidity and reduction of primary production, the values begin to decrease.

Interval IV spans depths from 11.5 to 0 cm and represents 1964 to 2006 CE. This interval is characterized by an increase in $\delta^{13}C_{OM}$, $\delta^{15}N_{TN}$, % TOC, and % TN, and decreases in the C/N ratio and magnetic susceptibility. The flux of allochthonous material entering the basin appears to have decreased and resulted in a gradual decrease in the C/N ratio and magnetic susceptibility. The C/N ratio decreased because there was less terrestrial plant material, which is rich in carbon, entering the system. The magnetic susceptibility measurements decreased because there was a reduction of magnetic mineral-bearing sediment entering the basin, a reflection of the reduction in land clearance occurring within the watershed. The reduced flux of allochthonous material also would have reduced turbidity, resulting in an increase in primary production. Moreover, urbanization and agricultural runoff may have contributed additional nutrient sources to the basin which would had further increased primary production. Increased temperatures would have also contributed to the increase in primary production. The increase in primary production is reflected in the proxies by the increase in total OM, as shown with the gradual increase of % TOC and % TN. Furthermore, the increases in $\delta^{13}C_{OM}$ and $\delta^{15}N_{TN}$ are consistent with an increase in primary production.
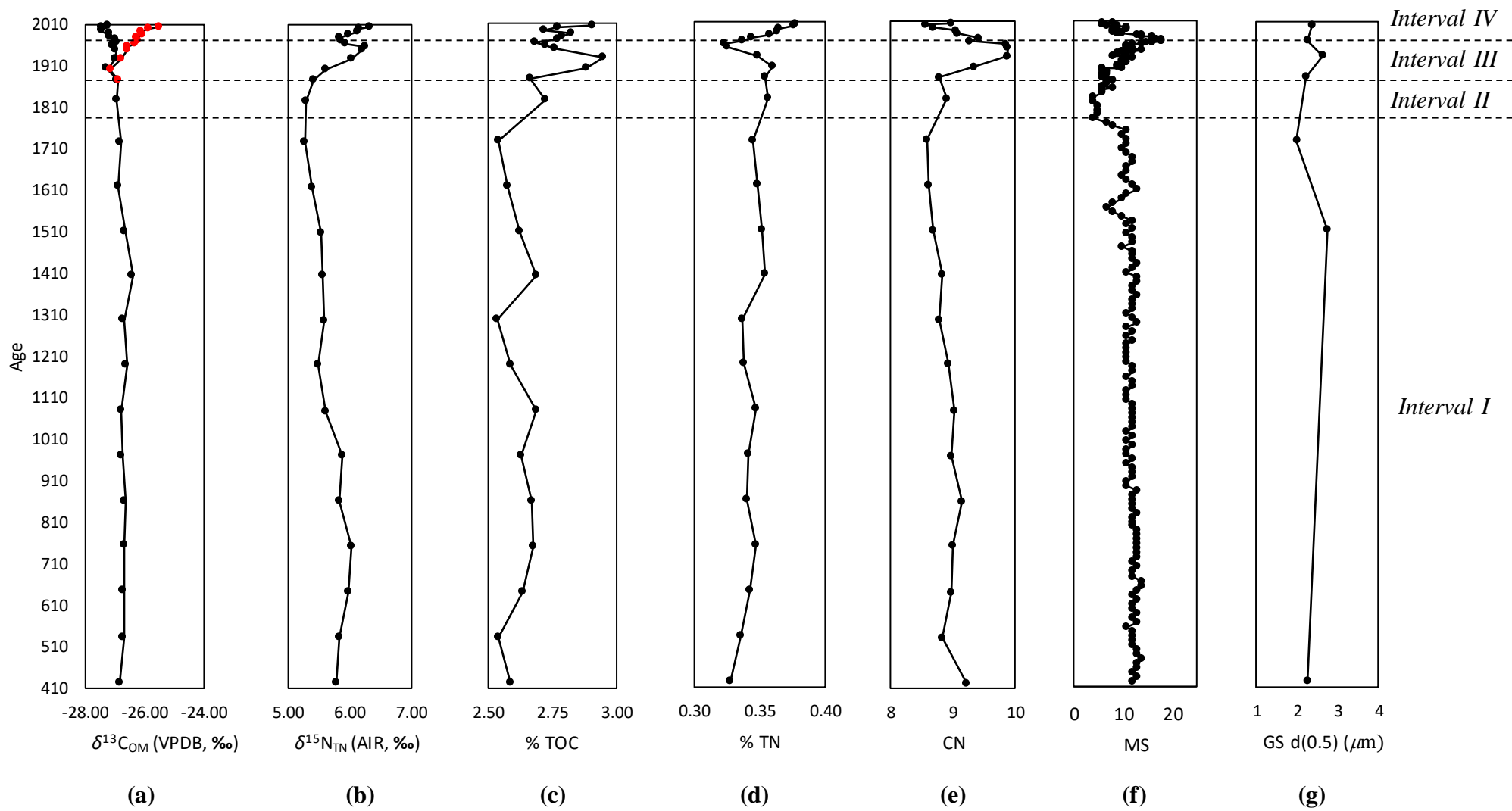
Figure 5.8. Age versus: (a) $\delta^{13}C_{OM}$. Measured $\delta^{13}C_{OM}$ is shown in black, and Suess-corrected $\delta^{13}C_{OM}$ (applied to years after 1850 CE) is shown in red. (b) $\delta^{15}N_{TN}$. (c) Total organic carbon content. (d) Total nitrogen content. (e) C/N ratio. (f) Magnetic susceptibility. (g) Grain size. All curves are from core 181 (Manitoulin basin).

5.2.2   Core 182 (Mackinac Basin)

Interval I spans depths from 100.5 to 9.5 cm and represents 52 to 1871 CE (Figure 5.9). The location of core 182 is south of Cockburn Island where waters are more turbulent, which affects sedimentation rates. As such, there may be large errors in the determined ages, in particular in those pre-1900s CE. Following Samuel de Champlain's voyage to Georgian Bay and Lake Huron in 1615 CE, the French established the North American fur trade. Competition for trade and pelts resulting in the Beaver Wars, and the Iroquois pushed into the Great Lakes territory and displaced the tribes that had settled there. As a result of an Iroquois attack in 1649 CE, the Huron from Southern Ontario settled in Michilimackinac in 1651 (Heidenreich 1978). Michilimackinac is the present-day Mackinac Island and the region around the Straits of Mackinac. Furthermore, in 1836 CE, the Treaty of Washington was signed, and Michigan tribes ceded claims to land in northern Michigan, which opened it to settlement. During the following decades, land was surveyed, and outstanding native land claims were eliminated ("How Michigan Became a State: The Treaty of Washington, 1836" 2017).

This interval is characterized by a gradual increase in % TOC and % TN, a gradual decrease in $\delta^{15}N_{TN}$ in the upper third of the interval, a very gradual decrease in the C/N ratio, and relatively consistent $\delta^{13}C_{OM}$ and magnetic susceptibility measurements. The MWP, where warm conditions were recorded between 800 and 1100 CE, coincides with the period of greatest increase in % TOC and % TN. An increase in primary production, and therefore % TOC and % TN, is expected with increasing temperatures. The gradual decrease is the C/N ratio is also a result of the increase primary production. Initially, the $\delta^{15}N_{TN}$ remained relatively stable before beginning to gradually decrease. The $\delta^{15}N_{TN}$ decrease may be linked to the inferred cooler conditions during the LIA between 1600 to 1750 CE and 1775 to 1800 CE in southwestern

Ontario (Buhay and Edwards 1995). Cold and dry conditions may have decreased the primary production resulting in the decrease in $\delta^{15}N_{TN}$.

Interval II spans depths from 9.5 to 5.5 cm and represents 1871 to 1942 CE. The Homestead Act of 1862 brought Civil War veterans and others to Northern Michigan (Homestead Act, 1862). The amount of land clearance and settlement within the vicinity of the Mackinac basin, however, was less than other locations as it is located near the intersection of Lake Huron and Lake Michigan in a less accessible area. This interval is characterized by a decrease in magnetic susceptibility and the disappearance of calcite. The sharp decrease in magnetic susceptibility measurements suggests that the source material changed to one with less magnetic minerals. Moreover, the disappearance of calcite further suggests that the sediment source has shifted from one that contained calcite to one that was devoid of the mineral. This change coincides with a decrease in lake water levels due to anthropogenic activities such as dredging which lowered lake levels permanently by an estimated 0.20 m in the late 19th century and a further 0.27 m in the early 20th century (Quinn and Croley 1981; Derecki 1982) (Figure 5.7). A lowering of the Michigan-Huron lake level may have increased the proportional contribution of Lake Superior sediment outflow to Lake Huron. Sediments sourced from the Superior basin are less carbonate-rich, and as such, the amount of calcite would decrease (Percival 2007). A lower lake level may have also resulted in decreased bluff erosion, resulting in a decrease in magnetic material entering the basin.

Interval III spans depths from 5.5 to 0 cm and represents 1942 to 2006 CE. This interval is characterized by a significant increase in $\delta^{13}C_{OM}$ and $\delta^{15}N_{TN}$, a sharp increase in the C/N ratio

and magnetic susceptibility, and a stabilization in % TOC and % TN. The increase in the C/N ratio and magnetic susceptibility measurements reflects the increased flux of allochthonous material entering the Mackinac basin during this interval. The increased flux is most likely the result of increased land clearance, deforestation and settlement in and around the vicinity of northern Lake Huron and Lake Michigan. The increase in allochthonous material may have increased the turbidity of the water, which stabilized the gradual increase in % TOC and % TN that occurs throughout the rest of the core. A small decrease in % TOC and % TN does occur coincidentally with the peak of magnetic susceptibility, further implying that the changes in these proxies are related. The increase in the $\delta^{13}C_{OM}$ likely reflects the increased proportion of terrestrial C3 plants to the total OM.
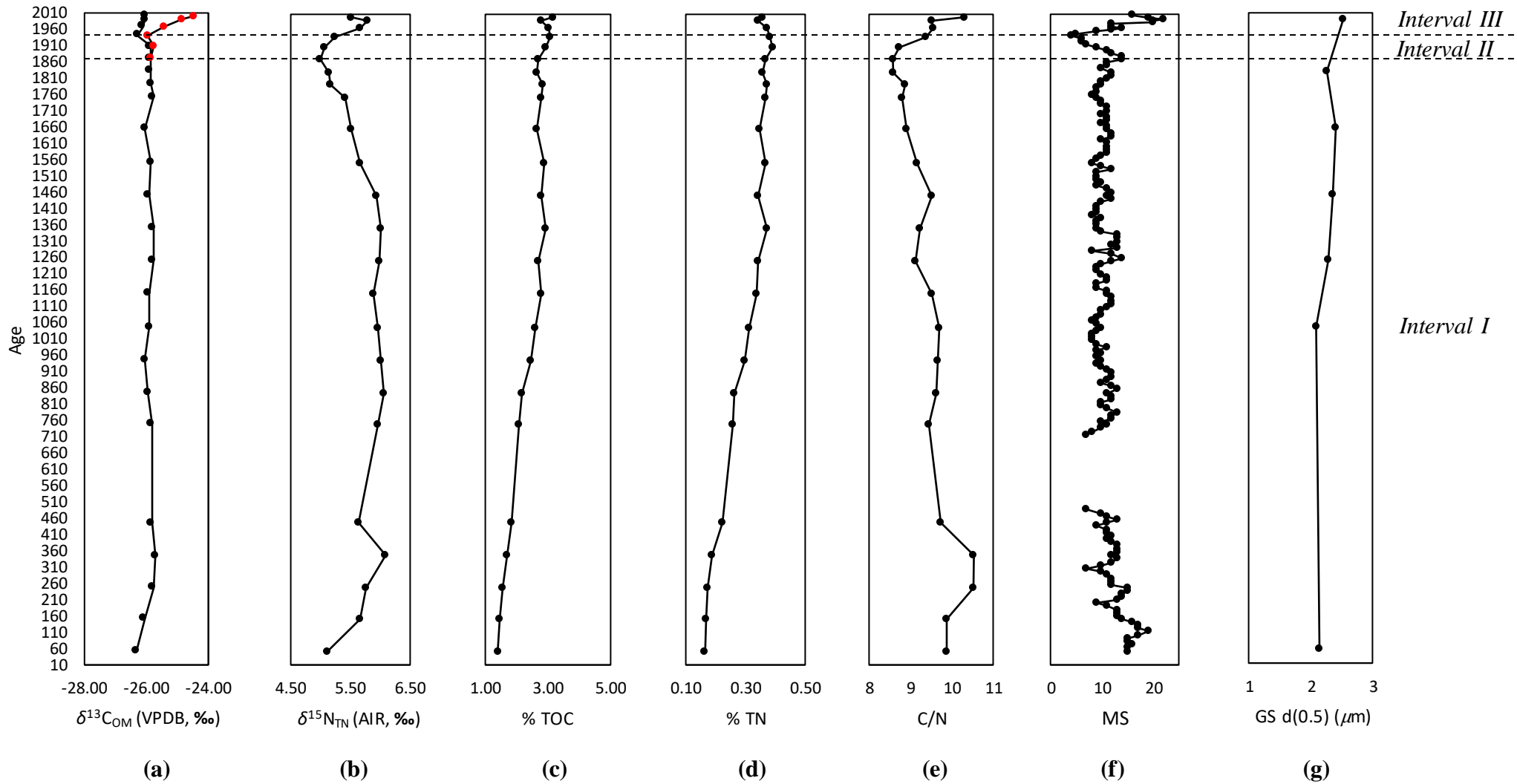
Figure 5.9. Age versus: (a) $\delta^{13}C_{OM}$. Measured $\delta^{13}C_{OM}$ is shown in black, and Suess-corrected $\delta^{13}C_{OM}$ (applied to years after 1850 CE) is shown in red. (b) $\delta^{15}N_{TN}$. (c) Total organic carbon content. (d) Total nitrogen content. (e) C/N ratio. (f) Magnetic susceptibility. (g) Grain size. All curves are from core 182 (Mackinac basin).

5.2.4   Core 821 (Saginaw Basin)

   Interval I in core 821 (Figure 5.10) spans depths from 100.5 to 65.5 cm and represents 537 to 1237 CE. Prior to European contact, the original residents of the Saginaw area were the Sauk and then Ojibwe Native peoples and extensive agriculture and deforestation was not occurring ("Saginaw History" n.d.). This interval is characterized by a very gradual decrease in C/N ratio and gradual increases in $\delta^{13}C_{OM}$ and $\delta^{15}N_{TN}$. The small, gradual decrease in the C/N ratio indicates that the proportion of terrestrial plant material contributing to the total OM was slightly decreasing. A warmer climate, such as the conditions that were recorded between 800 and 1100 CE during the MWP (PAGES 2k Consortium 2013), would have contributed to an increase in algal OM. The likely cause of the increase in $\delta^{13}C_{OM}$ and $\delta^{15}N_{TN}$ was a change in the proportion of lacustrine algae to terrestrial plant-derived OM. The $\delta^{13}C_{OM}$ of C3 terrestrial plants has an average of –28 ‰ (Meyers and Ishiwatari 1993) and algae has an average of –26.8 ‰ (e.g., Meyers 1994). Moreover, the $\delta^{15}N_{TN}$ of C3 land plants and algae are +1 and +8.5 ‰, respectively (Meyers and Lallier-Vergès 1999; Meyers 2003). A greater proportion of algal OM would therefore increase the $\delta^{15}N_{TN}$ and could increase $\delta^{13}C_{OM}$.

   Interval II spans depths from 65.5 to 45.5 cm and represents 1237 to 1637 CE. This interval is characterized by a decrease in $\delta^{13}C_{OM}$ and $\delta^{15}N_{TN}$ followed by a small increase in % TOC and % TN, an increase in the C/N ratio, and a significant increase in calcite and dolomite contents. The presence of carbonates in *Interval I* suggests that the increase in calcite and dolomite was not likely the result of an entirely new source of sediment, but rather an increase in sediment sourced from the Michigan basin, possibly due to a wetter climate prior to the onset of the LIA. Sediment originating from the Michigan basin is likely to be more carbonate-rich than

sediment originating from the Superior basin due to the surrounding carbonate-rich bedrock (Dorr and Eschman 1970). Moreover, sedimentation during this interval was sufficiently high to allow for the burial and preservation of calcite, which is susceptible to dissolution in water. The increase in the C/N ratio to values reaching about 12 is indicative of an increase in terrestrial OM as well. The increase in % TOC and % TN is likely the result of an increased flux of terrestrial plant material. The initial decrease in the $\delta^{13}C_{OM}$ and $\delta^{15}N_{TN}$ is also indicative of a greater proportion of C3 land plants contributing to the total OM. The gradual increase that followed may be the result of an increase in primary production. Warmer and wetter conditions can provide more favorable conditions and nutrient availability for algae by increasing the amount of allochthonous inorganic and organic material that is washed into the lake from the drainage basin.

Interval III spans depths from 45.5 to 35.5 cm and represents 1637 to 1837 CE. This interval is characterized by a decrease in C/N ratio, as well as a decrease in carbonate content. The moderately cooler temperatures between 1600 and 1850 CE during the LIA are likely to have decreased primary production. Buhay and Edwards' (1995) climate model also indicates that the climate was dry in southwestern Ontario from 1600 to 1750 CE, and 1775 to 1800 CE (Figure 5.6). A decrease in the flux of allochthonous material entering the basin, due to less precipitation, would decrease the C/N ratio.

Interval IV spans depths from 35.5 to 15.5 cm and represents 1837 to 1933 CE. A lumber industry emerged in central and eastern Northern Michigan in the 19th century and contributed to the rise of port cities on lake Michigan's eastern shores, including Saginaw. Saginaw Township,

which included the entire county and adjacent land, was organized in 1830 CE and by 1850 CE, the population was 2609 ("Saginaw History" n.d.). By 1880 Michigan produced more lumber than any other state ("A Brief History of Lumbering in Michigan" n.d.). The 1884 CE census recorded a population of 75,813. The year of 1882 CE was the peak of the timber boom, with 1,001,274,905 boardfeet of timber cut in mills along the Saginaw River. By the start of the 20th century, the lumber era had declined and new industries, such as coal mining, were developed ("Saginaw History" n.d.).

This interval is characterized by an initial decrease in $\delta^{13}C_{OM}$ and $\delta^{15}N_{TN}$ followed by relative stability, an increase in % TOC, % TN, C/N ratio, grain size, and quartz content. The increase in C/N ratio from *Interval III* indicates that there was an increase in allochthonous material entering the basin. This increase was likely caused by land clearance and deforestation in the vicinity of the Saginaw basin. The steady increase in % TOC and % TN is also likely the result of an increased flux of terrestrial plant material in the basin due to deforestation. An increase in grain size indicates a shorter transportation distance and an increase in surface runoff. Sediment runoff following land clearance in the vicinity of Saginaw Bay is likely to have contributed to the overall increased flux of allochthonous material, including quartz content. Moreover, as vegetation plays a role in reducing sediment yield from a watershed (Schumm 1965), deforestation would also lead to an increase in allochthonous material entering the basin. The decrease in $\delta^{13}C_{OM}$ and $\delta^{15}N_{TN}$ coincides with the increase in C/N ratio. This suggests that the increased contribution of terrestrial C3 plants to the total OM produced the decrease.

Interval V spans depths from 15.5 to 3.5 cm and represents 1933 to 1991 CE. This interval is characterized by an increase in C/N ratio, a decrease in % TOC and % TN, and a very

large positive spike in magnetic susceptibility. The changes in proxies observed during this interval are the result of an increase in local land disturbance and clearance, which greatly increased the amount of allochthonous material entering the basin. The increase in allochthonous material likely increased the turbidity in the water, which reduces the photosynthesis potential for lacustrine algae. As a result, there is an observed decrease in % TOC and % TN.

Interval VI spans depths from 3.5 to 0 cm and represents 1991 to 2007 CE. This interval is characterized by an increase in $\delta^{13}C_{OM}$ and $\delta^{15}N_{TN}$, a large increase in % TOC, % TN, and grain size, and a decrease in the C/N ratio. The local land clearance that produced changes in the proxies in *Interval V* had abated by this time. As such, the flux of allochthonous material decreased leading to a reduction in the C/N ratio. Moreover, as turbidity decreased, and due to other anthropogenic impacts, such as increasing temperatures (IPCC 2019) and agricultural runoff (e.g., Hodell and Schelske 1988), primary production increased. This led to an increase in $\delta^{13}C_{OM}$ and $\delta^{15}N_{TN}$, as well as % TOC and % TN. The sharp increase in grain size observed during this interval suggests a shorter transportation distance. Water levels during this time period were lower than normal (Figure 5.7), which may have allowed for a shorter transportation distance prior to deposition.
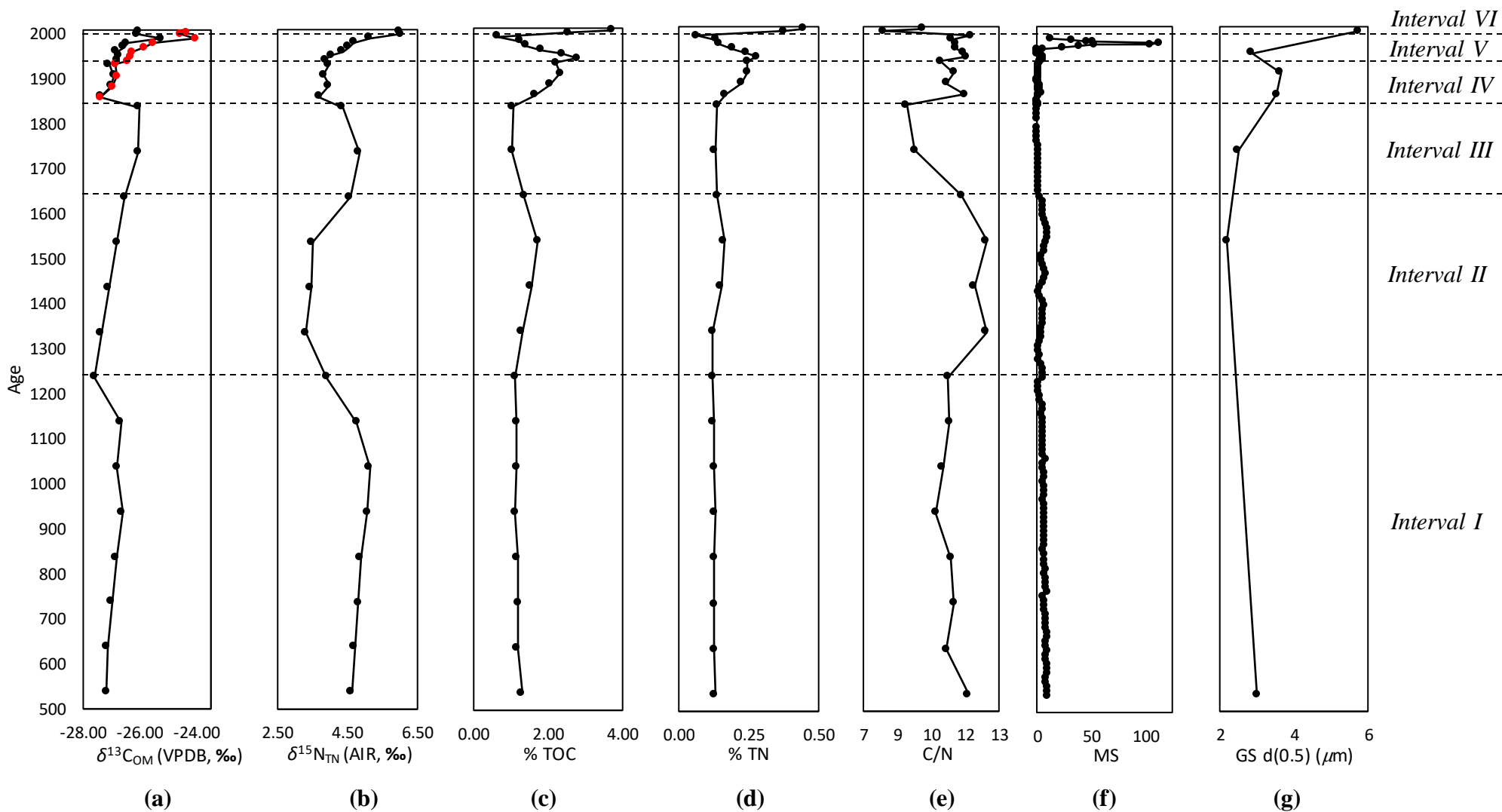
Figure 5.10. Age versus: (a) $\delta^{13}C_{OM}$. Measured $\delta^{13}C_{OM}$ is shown in black, and Suess-corrected $\delta^{13}C_{OM}$ (applied to years after 1850 CE) is shown in red. (b) $\delta^{15}N_{TN}$. (c) Total organic carbon content. (d) Total nitrogen content. (e) C/N ratio. (f) Magnetic susceptibility. (g) Grain size. All curves are from core 821 (Saginaw basin).

5.2.5   Core 817 (Alpena Basin)

Interval I in core 817 (Figure 5.12) spans depths from 100.5 to 30.5 cm and represents 461 to 1861 CE. During this interval, the proxies analyzed do not show substantial variations, suggesting that climatic changes are not represented in the proxies. This interval is characterized by low % TOC and % TN, and the presence of carbonates. The low % TOC and % TN suggest that primary production within the Alpena basin was low during this interval, or that the preservation potential of OM was low. The carbonate content suggests that sediment is being sourced from the carbonate-rich rocks of the Michigan basin. The relatively high magnetic susceptibility compared to what is observed in the Saginaw basin may be due to the location of the Alpena basin. As currents typically move water and entrained sediments counter-clockwise through Lake Huron (Figure 5.11), heavy magnetic minerals may have been deposited in the Alpena basin before they reached the Saginaw basin, which generally shows low magnetic susceptibility.

Interval II spans depths from 30.5 to 11.5 cm and represents 1861 to 1952 CE. The city of Alpena, which is located on an inlet of Lake Huron in northeast Michigan, was first settled in 1835. It was initially a trading post and became incorporated as a city in 1871 ("History of Alpena, Michigan" n.d.). During the logging boom in the late 19th century, Alpena was a significant sawmill town. The first commercial harvest of timber began in the winter of 1858. At its peak, as many as 1500 to 2000 ships docked annually to load logs and lumber productions ("History and Heritage as Told Through our Industry" 2018).

This interval is characterized by a sharp increase in % TOC, % TN, C/N ratio, and quartz content. It is also characterized by a decrease in magnetic susceptibility and dolomite content.

The significant change in all proxies at 30.5 cm indicates that a change in the predominate source of sediment has occurred. The mineralogical signature of the sediments shifts during *Interval II*. Dolomite content decreased and this phase was no longer present at the end of this interval, whereas quartz content increased significantly. This suggests that sediments originating from the Superior basin, which are not carbonate-rich, increasingly contributed to the basin compared to *Interval I* (Percival 2007). The decrease in Michigan-Huron water levels (Figure 5.7) that occurred in the late 19th century due to anthropogenic activities such as dredging may have initiated this change (Quinn and Corley 1981; Derecki 1982). A decrease in bluff erosion due to the lower lake level may have contributed to the decrease in magnetic susceptibility. The increase in the C/N ratio indicates an increase in terrestrial plant material entering the basin. The significant forest clear- cutting that occurred because of the lumber industry in the region would have increased the quantity of terrestrial plant matter entering the basin.

Interval III spans depths of 11.5 to 3.5 cm and represents 1952 to 1991 CE. This interval is characterized by a small decrease in the % TOC, % TN and C/N ratio. Deforestation was not occurring at the same pace as in *Interval II* due to the decline of the lumber industry in Michigan. This likely led to a reduction in allochthonous OM entering the basin, which would reduce the % TOC and % TN, and also the C/N ratio.

Interval IV spans depths of 3.5 to 0 cm and represents 1991 to 2007 CE. This interval is characterized by a small increase in $\delta^{13}C_{OM}$, $\delta^{15}N_{TN}$, % TOC, % TN and C/N ratio. Increased lacustrine primary production due to an increase in summer surface water temperatures by

2.9°C between 1968 and 2002 (Dobiez and Lester 2009), reduced annual lake ice coverage by about 2% per year between 1873 and 2010 (Austin and Colman 2007; Wang et al. 2012), and increase agricultural runoff (e.g., Hodell and Schelske 1988) likely increased the $\delta^{13}C_{OM}$, $\delta^{15}N_{TN}$, % TOC, and % TN. The small increase in the C/N ratio is not significant enough to suggest an increased contribution of terrestrial OM.
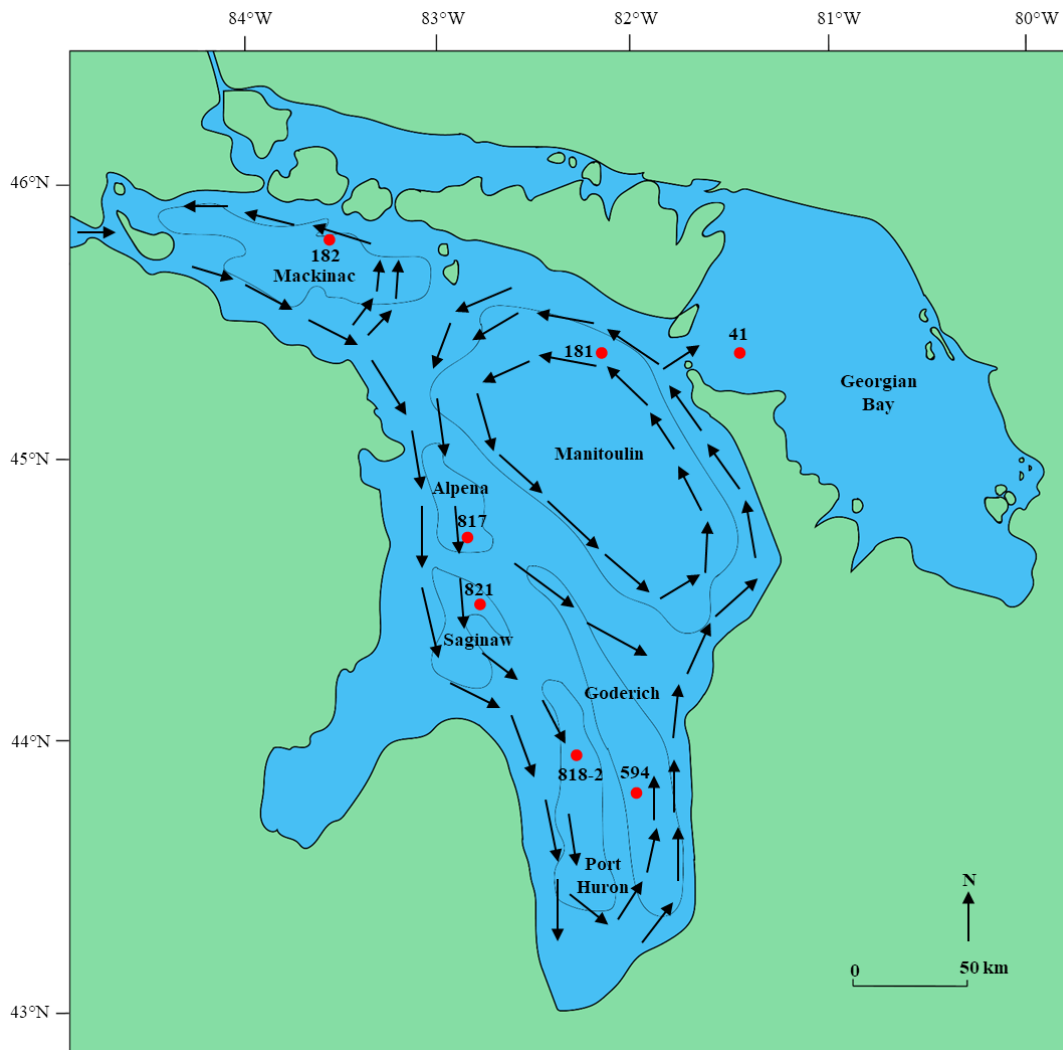
Figure 5.11. Summer-averaged circulation pattern in the epilimnion of Lake Huron. Core locations, Huron basins, and Georgian Bay are also shown. Modified from Sloss and Saylor (1976).
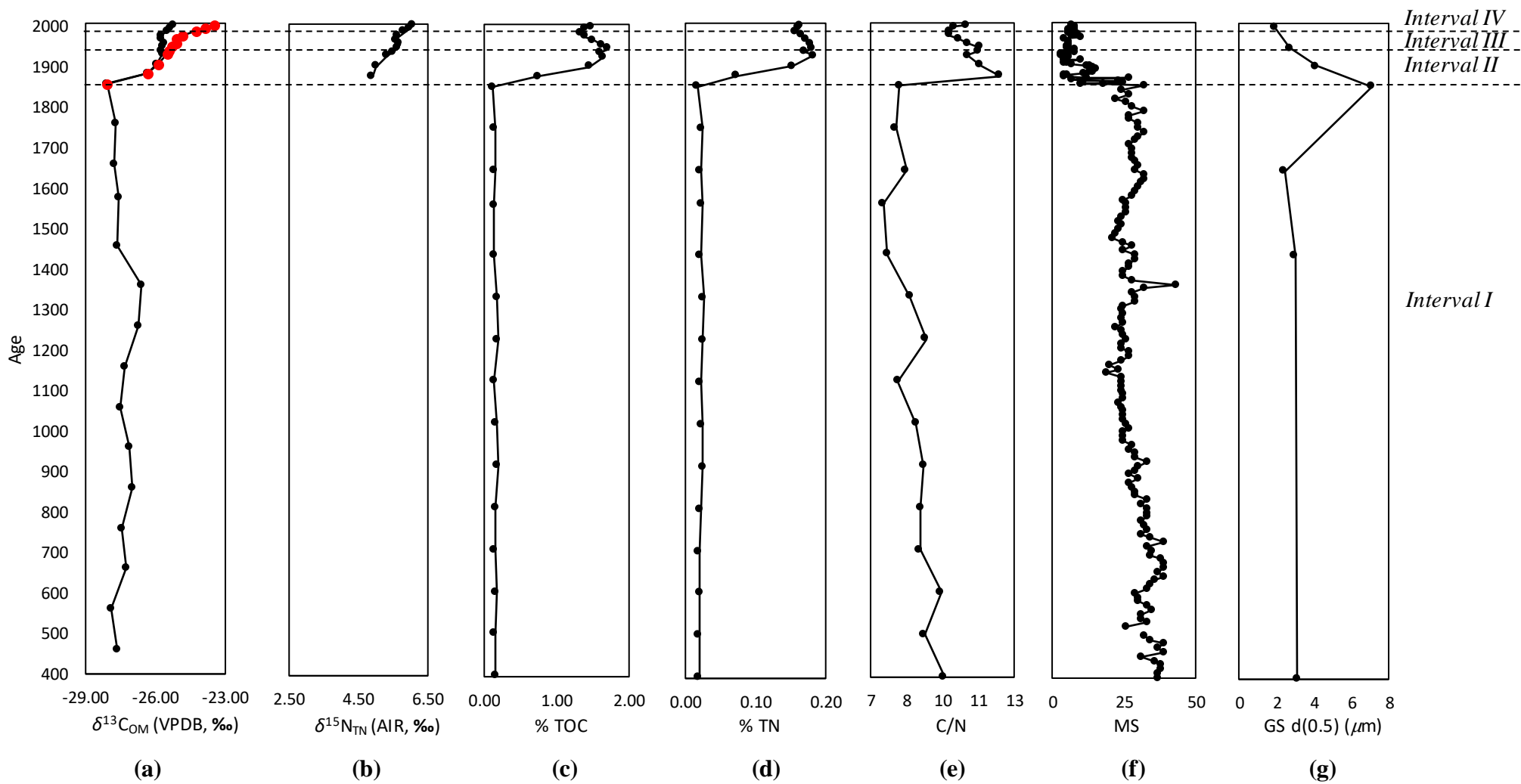
Figure 5.12. Age versus: (a) $\delta^{13}C_{OM}$. Measured $\delta^{13}C_{OM}$ is shown in black, and Suess-corrected $\delta^{13}C_{OM}$ (applied to years after 1850 CE) is shown in red. (b) $\delta^{15}N_{TN}$. (c) Total organic carbon content. (d) Total nitrogen content. (e) C/N ratio. (f) Magnetic susceptibility. (g) Grain size. All curves are from core 817 (Alpena basin).

125

5.2.6   Core 818-2 (Port Huron Basin)

An age-depth model has not been attempted for this core. The age of the missing sediments at the core's top is unknown, and there are no distinct marker horizons suitable for correlation of this core with others.

The upper 16.5 cm of core 818-2 (Figure 5.13) is unconsolidated and no further analysis was conducted on the sediments. From 100.5 to 20.5 cm, there is a gradual increase upwards in $\delta^{13}C_{OM}$, $\delta^{15}N_{TN}$, % TOC and % TN, which suggests increasing lacustrine, primary production. Temperatures have increased in eastern North America since the end of the LIA (e.g., Moore et al. 2001) and have continued to rise due to the anthropogenic increase in atmospheric CO_2 (e.g., Zhang et al. 2000). The increase in temperature has led to an increase in lacustrine primary production. The MS signal does not vary significantly throughout the Port Huron core, suggesting that changes in the source or amount of allochthonous material entering the lake were minimal over this time period.
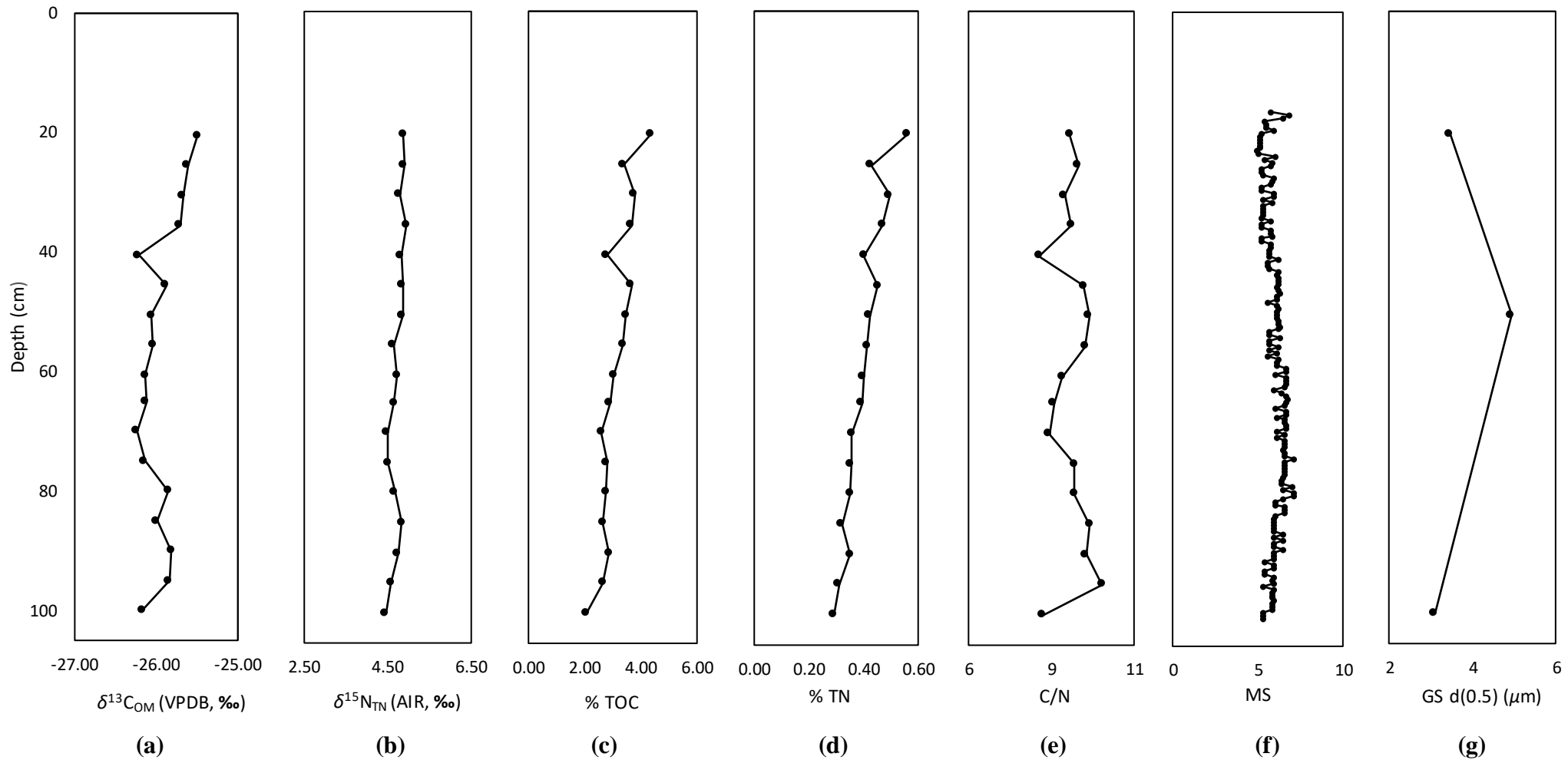
Figure 5.13. Depth versus: (a) $\delta^{13}C_{OM}$. (b) $\delta^{15}N_{TN}$. (c) Total organic carbon content. (d) Total nitrogen content. (e) C/N ratio. (f) Magnetic susceptibility. (g) Grain size. All curves are from core 818-2 (Port Huron basin).

5.2.7   Core 41 (Georgian Bay)

Interval I in core 41 (Figure 5.14) spans depths from 100.5 to 25.5 cm and represents 385 to 1885 CE. Throughout the 17th century, the eastern and southern shores of Georgian Bay and adjacent areas inland were occupied by several Algonquian and Iroquoian Aboriginal groups (Wilson and Urion 1995; Becker 2004). The Algonquian groups likely consisted of the proto-Ottawa, Ottawa and proto-Ojibwa tribes, whereas the Iroquoians consisted of the Huron and Petun tribes (Reimer and Chartrand 2000). The Algonquian peoples practiced a limited form of agriculture prior to European contact, which was likely adopted from the neighboring Iroquoian peoples (Wright 1994). The Huron and Petun tribes lived in villages that were inhabited year-round. It is estimated that agriculture provided up to 80 % of their food (Trigger 1994). Village relocations occurred about every 10–12 years due to soil erosion or depletion of firewood supplies (Trigger 1976; Becker 2004). Europeans first visited the area in the early 16th century. In 1610 CE, Étienne Brûlé, at the behest of French explorer Samuel de Champlain, exchanged places with a young Huron named Savignon (Coyne 1903). The earliest permanent European settlement on the Great Lakes was established at Ste. Marie on the banks of the Wye River near Georgian Bay in 1639 CE by French Jesuit missionaries ("Ste. Marie Among the Hurons" 2005). A series of attacks by the Five Nations Iroquois confederacy between 1648 and 1650 CE forced the Aboriginal groups and French Jesuits from the region (Heidenreich 1978). Huron and Petun refugees fled to various locations including the Mackinac region in Lake Michigan (Heidenreich 1978). The Ottawa tribes living in the Bruce Peninsula area and on the eastern shore of Georgian Bay relocated temporarily to Manitoulin Island, while others relocated to Saginaw Bay and Mackinac (Feest and Feest 1978). Following the forced migration, the region was mostly unoccupied from 1650 to the 1680s CE. During the 1680s and 1690s CE, however, the region

saw battle between the Five Nations Iroquois and an alliance of Algonquian peoples (majority Ojibwa). The Algonquian alliance succeeded in expelling the Iroquois from southern Ontario and then permanently settled in the region (Murray 2013). Estimates of population from the early 18th century suggest that the initial Ojibwe settlement of Georgian Bay and southern Ontario consisted of less than 1,000 people (Rogers 1978). Low sedimentation rates and thin, spatially discontinuous sedimentation in Georgian Bay prior to 150 years ago are the result of: (i) the outcrop of Precambrian igneous and metamorphic rocks of the Canadian Shield with no drift to the east; (ii) sedimentary rocks with thin drift cover to the west; and (iii) the absence of large rivers transporting considerable suspended load to the basin (McCarthy et al. 2007).

This interval is characterized by an initially very gradual decrease in $\delta^{15}N_{TN}$ followed by a larger decrease after 1015 CE (60.5 cm), and relatively stable % TOC and C/N trends that are interrupted by a small increase between 1015 and 1255 CE (60.5 to 50.5 cm). The increase in % TOC and C/N ratio indicates an increase in the influx of allochthonous plant material. Terrestrial plant material has large amounts of carbon-rich cellulose and waxy hydrocarbons and will thus increase the % TOC more readily than the % TN, as well as the C/N ratio. The large decrease in $\delta^{15}N_{TN}$ that coincides with the increase in % TOC and C/N ratio, is also a reflection of the increasing proportion of terrestrial plant material to the total OM. Although there is an increase in terrestrial plant OM, lacustrine OM is still the dominant source of OM, as the C/N ratio is still <10. An increase in precipitation, which would increase the flux of allochthonous material to the basin, is the likely cause of these changes.

Interval II spans depths from 25.5 to 13.5 cm and represents 1855 to 1927 CE. The fur trade dominated the region in the 18th century but began to decline in the early 19th century and

settlers turned to fishing and lumber operations. Penetanguishene was the primary lumbering town in the region, and a sawmill had been built by 1844 (Marchand 1989). Owen Sound is the largest city on Georgian Bay. It began as a settlement called Sydenham in 1840 CE and by 1846 CE it had a population of 150 and an operating sawmill and gristmill. By 1851 CE, a direct road connected Sydenham and Toronto. The community was incorporated as the Town of Owen Sound in 1857 CE and had a population of almost 2000 at the time ("The Founding of Owen Sound" n.d.).

This interval is characterized by the appearance of detrital dolomite, an increase in $\delta^{15}N_{TN}$, % TOC, % TN and C/N ratio, and a gradual increase in magnetic susceptibility. The emergence of dolomite suggests that there is an increase in detrital carbonate from either Manitoulin Island or the Bruce Peninsula entering the lake. This is likely due to land clearance which would introduce detrital grains of dolomite into the basin. The gradual increase in magnetic susceptibility likely reflects an increasing flux of allochthonous material into Georgian Bay that is related to land clearance within the watershed. An increase in the rate of sedimentation due to upland erosion caused by European settlement and increased land clearing was also noted by McAndrews and Power (1973) in Georgian Bay. The gradual increase in C/N ratio is consistent with an increased contribution of terrestrial plant material. The increases in % TOC and % TN arise from both an increase in terrestrial plant OM, and possibly an increase in primary production. Increasing temperatures since the onset of the industrial revolution are likely to have contributed to an increase in algal growth. Moreover, agricultural runoff from farms on Manitoulin Island and the southern shore of Georgian Bay may have also contributed to an increase in primary production. The increase in $\delta^{15}N_{TN}$ is likely a reflection of the increased proportion of algae, which has a $\delta^{15}N_{OM}$ of about +8.5 ‰ (Meyers 2003).

Interval III spans depths from 13.5 to 7.5 cm and represents 1927 to 1963 CE. This interval is characterized by an increase in magnetic susceptibility, a C/N ratio that initially increases then remains steady, and a decrease in % TOC and % TN. The increase in magnetic susceptibility indicates a greater flux of allochthonous material entering the basin during this interval. The high and steady C/N ratio suggests that there is a greater amount of terrestrial OM entering the basin than in previous intervals. The changes in magnetic susceptibility and C/N ratio were probably related to land clearance and urbanization in the region. Increased turbidity within the lake may have also resulted, which could have caused a small decrease in primary production, as indicated by the reduction in % TOC and % TN. The % TOC and % TN are still significantly higher than pre-disturbance values, however, indicating that primary production has still overall increased since the arrival of European settlers. The continued rise of temperature due to the anthropogenic increase in atmospheric CO_2 (e.g., Zhang et al. 2000), as well as nutrient delivery by eutrophication and accompanying rise in pH are evident by the shift in the dominate dinoflagellate cyst assemblages in eastern Georgian Bay (McCarthy et al. 2011). Dinoflagellate species have different degrees of tolerance to eutrophication. The germinating cysts of the freshwater dinoflagellates *Peridinium willei* outcompete *Peridinium wisconsinense* when lakes are impacted anthropogenically (McCarthy et al. 2011).

Interval IV spans depths from 7.5 to 0 cm and represents 1963 to 2007 CE. This interval is characterized by a decrease in magnetic susceptibility, C/N ratio and $\delta^{15}N_{TN}$, and an increase in $\delta^{13}C_{OM}$, % TOC and % TN. The decrease in magnetic susceptibility is most likely related to a reduction of land clearance and urban development around Georgian Bay. Moreover, as there is less terrestrial plant material entering Georgian Bay, the C/N ratio declined to pre-land

disturbance levels. The decreasing C/N ratio and increasing % TOC and % TN suggests that

lacustrine primary production has increased. It has increased to such an extent that the loss of

terrestrial OM input is not apparent in the OM content alone. This is further emphasized by the

increase in $\delta^{13}C_{OM}$. Turbidity is likely to have been reduced with the reduction of land clearance,

which increases the depth to which sunlight can penetrate and allows for photosynthesis to occur

more readily. In addition, rising temperatures would also contribute to a more optimal

environmental for algal growth. The decrease in $\delta^{15}N_{TN}$ is unexpected if primary production is

increasing. Inorganic fertilizers, however, have a $\delta^{15}N$ of about 0 ‰ (Bateman and Kelly 2007)

and may be contributing to a lowering of $\delta^{15}N_{TN}$.
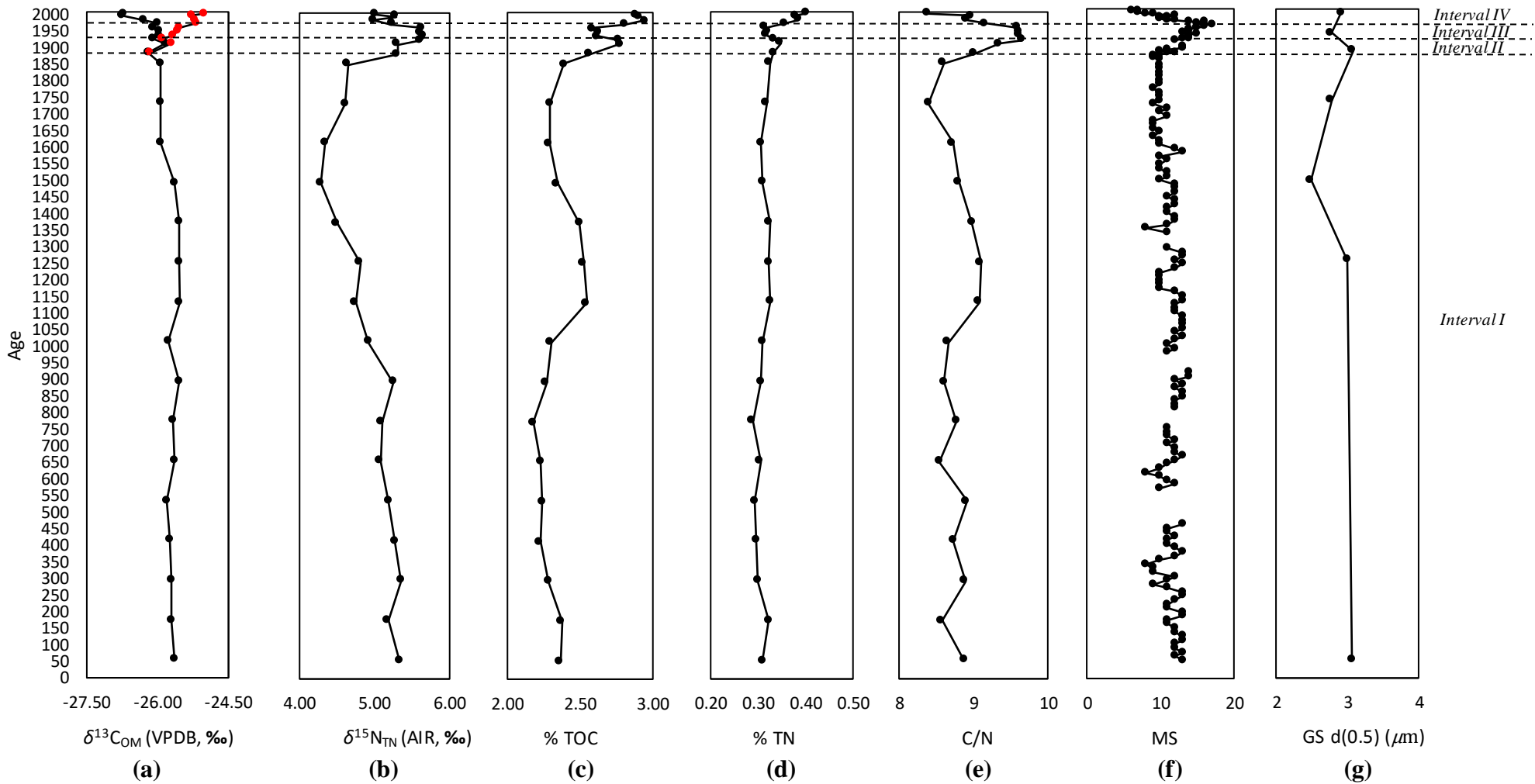
Figure 5.14. Age versus: (a) $\delta^{13}C_{OM}$. Measured $\delta^{13}C_{OM}$ is shown in black, and Suess-corrected $\delta^{13}C_{OM}$ (applied to years after 1850 CE) is shown in red. (b) $\delta^{15}N_{TN}$. (c) Total organic carbon content. (d) Total nitrogen content. (e) C/N ratio. (f) Magnetic susceptibility. (g) Grain size. All curves are from core 41 (Georgian Bay).

5.2.8   Cross-Basin Comparison

There are number of similarities and differences observed among the various benthos cores from Lake Huron (594, 181, 182, 821, 821, and 818-2) and Georgian Bay (41), which collectively span the geographic extent of the Huron basin (Figure 3.1). The $\delta^{13}C_{OM}$ versus CN plot (Figure 4.39) shows that the primary contributor of OM in all cores is lacustrine algae. The plot indicates that cores 821 (Saginaw basin) and 817 (Alpena basin), however, contain a larger contribution of C3 terrestrial plants than the other cores. In particular, deforestation during the 19th century in Michigan led to a greater increase in C3 terrestrial plant material entering the Saginaw and Alpena basins from tributaries in Michigan. Moreover, because of the nature of the movement of currents in Lake Huron (Figure 5.11), the Alpena basin and in particular, the Saginaw basin, are more likely to receive terrestrial plant material from Michigan than the others.

In general, all cores show similar trends in $\delta^{13}C_{OM}$ (Figure 5.15). A common similarity between the cores is a significant gradual increase in Suess-corrected $\delta^{13}C_{OM}$ beginning in the mid- to late- 19th century. For all cores, this is interpreted to be a response to an increase in primary production as a result of increasing temperatures and nutrient input. Temperatures have increased in the eastern North America since the end of the LIA (e.g., Moore et al. 2001), and have continued to increase due to the anthropogenic increase in atmospheric CO_2 (e.g., Zhang et al. 2000). As the rise in temperature is regional, all of the basins have been affected by it.

The Saginaw basin (core 821) $\delta^{13}C_{OM}$ shows high variability throughout the core, with values similar to the Alpena basin during some periods, and similar to the rest of the cores in others. This is likely a reflection of the amount of terrestrial plant material entering the basin as

the changes in $\delta^{13}C_{OM}$ coincide with changes in the C/N ratio. The $\delta^{13}C_{OM}$ of C3 terrestrial plants has an average of –28 ‰ (Meyers and Ishiwatari 1993), whereas algae has an average of –26.8 ‰ (e.g., Meyers 1994). Lower (more negative) $\delta^{13}C_{OM}$ compositions coincide with increases in the C/N ratio throughout much of core 821. An exception occurs between 1933 to 1991 CE, when the increase in $\delta^{13}C_{OM}$ as a result of an increase in primary production counteracts the decrease expected from a larger contribution of terrestrial plant material. The Alpena basin's (core 817) $\delta^{13}C_{OM}$ trend is initially the most negative but shows the largest increase post-mid-19th century. The low $\delta^{13}C_{OM}$ likely reflects low primary production due to low nutrient availability in the Alpena basin. The proportionally larger increase post-mid-19th century is likely because carbon availability was more limited than in the other basins, which leads to a greater increase in $\delta^{13}C_{OM}$. This is further evident in that the % TOC of the Alpena basin is lower than the other cores throughout the record.
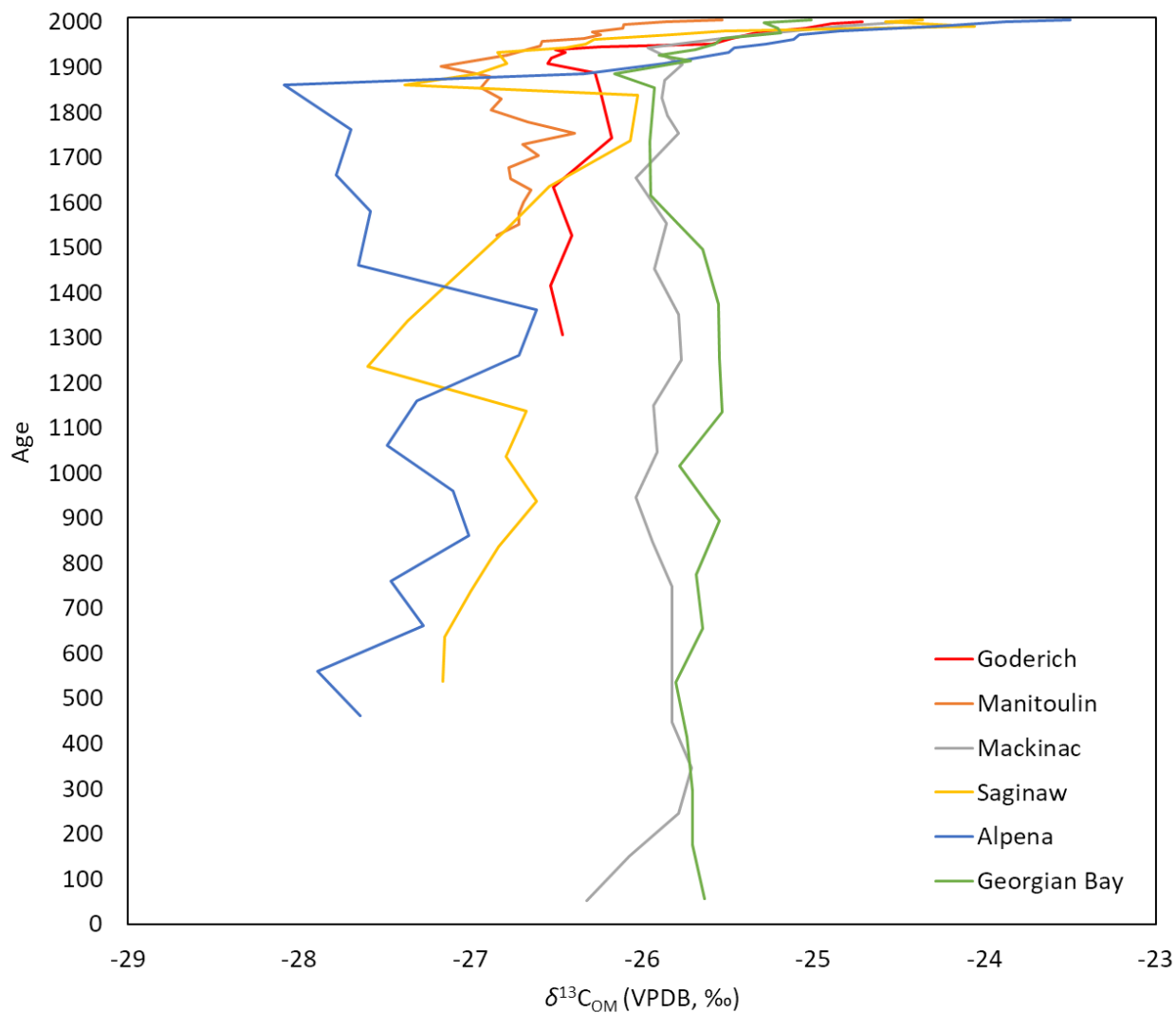
Figure 5.15. Age versus $\delta^{13}C_{OM}$ for cores 594 (Goderich basin), 181 (Manitoulin basin), 182 (Mackinac basin), 821 (Saginaw basin), 817 (Alpena basin), and 41 (Georgian Bay). See Figure 3.1 for core locations.

The trends observed in the $\delta^{15}N_{TN}$ are also similar for the Goderich (core 594), Manitoulin (core 181), Mackinac (core 182), Port Huron (818-2), and Georgian Bay (41) basins, but differ in the magnitude of variations (Figure 5.16). The common trend is relative stability or a very gradual decrease $\delta^{15}N_{TN}$, followed by an increase in the 20th century. An increase in algal matter, due to an increase in primary production following the increase of temperatures and nutrient inputs, is likely the cause of the increases in $\delta^{15}N_{TN}$. The $\delta^{15}N_{OM}$ of C3 terrestrial plants

136

averages about +1 ‰ whereas algae have a $\delta^{15}N_{OM}$ of about +8.5 ‰ (Meyers and Lallier-Vergès 1999; Meyers 2003). Another common feature of the $\delta^{15}N_{TN}$ trend is a small decrease, followed by further increase, that typically occurs in the mid-20th century. This reflects the increased contribution of allochthonous material into Lake Huron due to extensive land clearance in the watershed. In addition to contributing a larger amount of C3 terrestrial plant material, increasing turbidity is likely to have reduced primary production in the basins during this time. Georgian Bay also shows a decrease in $\delta^{15}N_{TN}$ after 1963 CE. This may be due to the use of inorganic fertilizers, which have a $\delta^{15}N$ of about 0 ‰ (Bateman and Kelly 2007).

The Saginaw basin (core 821) and Alpena basin (core 817) cores behave differently than the other cores. The Saginaw basin core shows high variability in $\delta^{15}N_{TN}$. Similarly to the variations observed in $\delta^{13}C_{OM}$, this likely reflects the different amounts of allochthonous versus autocthonous plant material contributing to the total OM. The Saginaw basin may be more susceptible to contributions of terrestrial plant material than the other basins due to its proximity to Michigan and Saginaw Bay. Saginaw Bay and the coast north of the Saginaw basin are fed by numerous tributaries. Moreover, water currents in Lake Huron are more likely to transport material from Lake Michigan to the Saginaw basin than others (Figure 5.11). The Alpena basin core did not contain sufficiently high enough nitrogen content to allow for measurement of $\delta^{15}N_{TN}$ before 1885 CE. Low nutrient availability in the Alpena basin likely resulted in very low primary production. It is also evident that nitrogen is limited in the Alpena basin because of the significant increase in $\delta^{15}N_{TN}$ observed after 1885 CE and very low % TN.
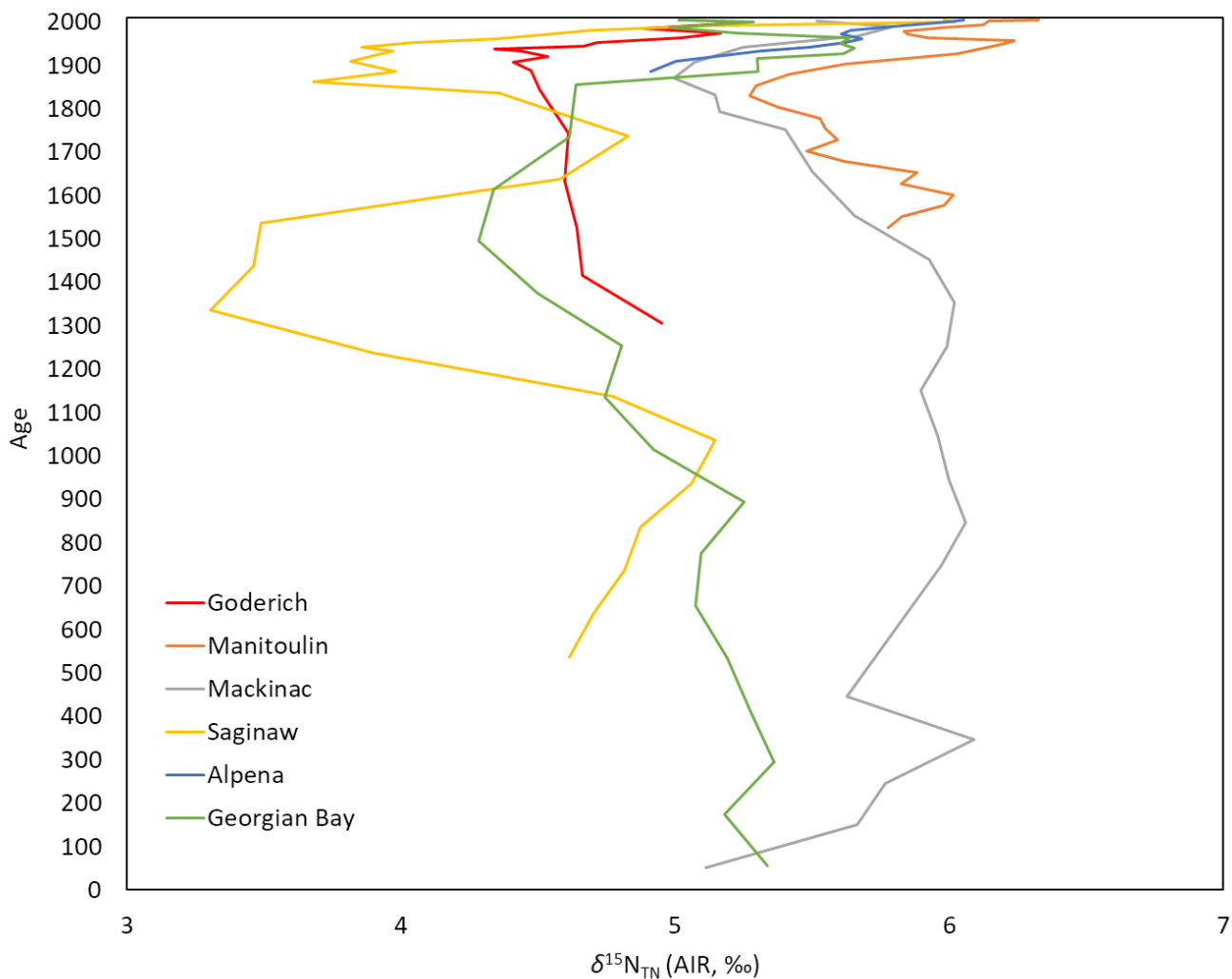
Figure 5.16. Age versus $\delta^{15}N_{TN}$ for cores 594 (Goderich basin), 181 (Manitoulin basin), 182 (Mackinac basin), 821 (Saginaw basin), 817 (Alpena basin), and 41 (Georgian Bay). See Figure 3.1 for core locations.

The patterns shown by the % TOC (Figure 5.17) and % TN (Figure 5.18) curves can be divided into three groups. Firstly, the Manitoulin basin (core 181), Mackinac basin (core 182), and Georgian Bay (core 41) cores have very similar curves. All three basins are situated in the northern portion of the Huron basin, across which climate conditions and anthropogenic impacts are similar. Furthermore, sediment accumulations on either side of the channel connecting Lake Huron and Georgian Bay suggest that water has flowed in both directions through the channel

over the last 7000 years (Dobson et al. 1995). As such, it is expected that there would be similarities between sediment in northern Lake Huron and Georgian Bay. The overall trend observed in these three cores is a gradual increase through time for both % TOC and % TN. Increasing temperatures and nutrient inputs are likely contributing to an increase in total OM.

The second group with similar curves is the cores collected from the Goderich and Port Huron basins (core 594 and 818-2, respectively). The Goderich and Port Huron basin sediments contain higher amounts of % TOC and % TN compared to the northern basins. The lower organic carbon observed in the northern basins is likely a result of the dilution of their sediments by reworked fine-grained glaciolacustrine clay. This clay is rich in quartz and lacking in organic carbon (Thomas et al. 1973). Moreover, the Goderich and Port Huron basins likely experience warmer temperatures due to their more southernly location, leading to greater primary production. The C/N ratio for the northern and southern cores are relatively similar, suggesting that the quantity of algal OM controls the observed difference in % TOC and % TN, rather than terrestrial OM. The sediment texture is also coarser than in the northern Huron basins, due to shallower water that reduces deposition of fine-grained material, which is transported south to the St. Clair River (Thomas et al. 1973).

The cores collected from the Saginaw (core 821) and Alpena (core 817) basins constitute the third group. The two cores are characterized by generally low % TOC and % TN until the mid-19th century, after which a large increase occurs. This increase coincides with a significant increase in the C/N ratio, which indicates that there is a significant contribution of allochthonous material to the basins. Extensive deforestation in Michigan in the mid- to late-19th century is the likely cause of this change. A significant, but temporary, decrease in % TOC and % TN is also observed in both the Saginaw and Alpena cores in the mid-20th century. An increase in turbidity

caused by land clearance and urbanization in Michigan may have caused a reduction in primary production. Smaller magnitude decreases in % TOC and % TN are also observed in the other Huron basin cores, which are also likely caused by an increase in turbidity.
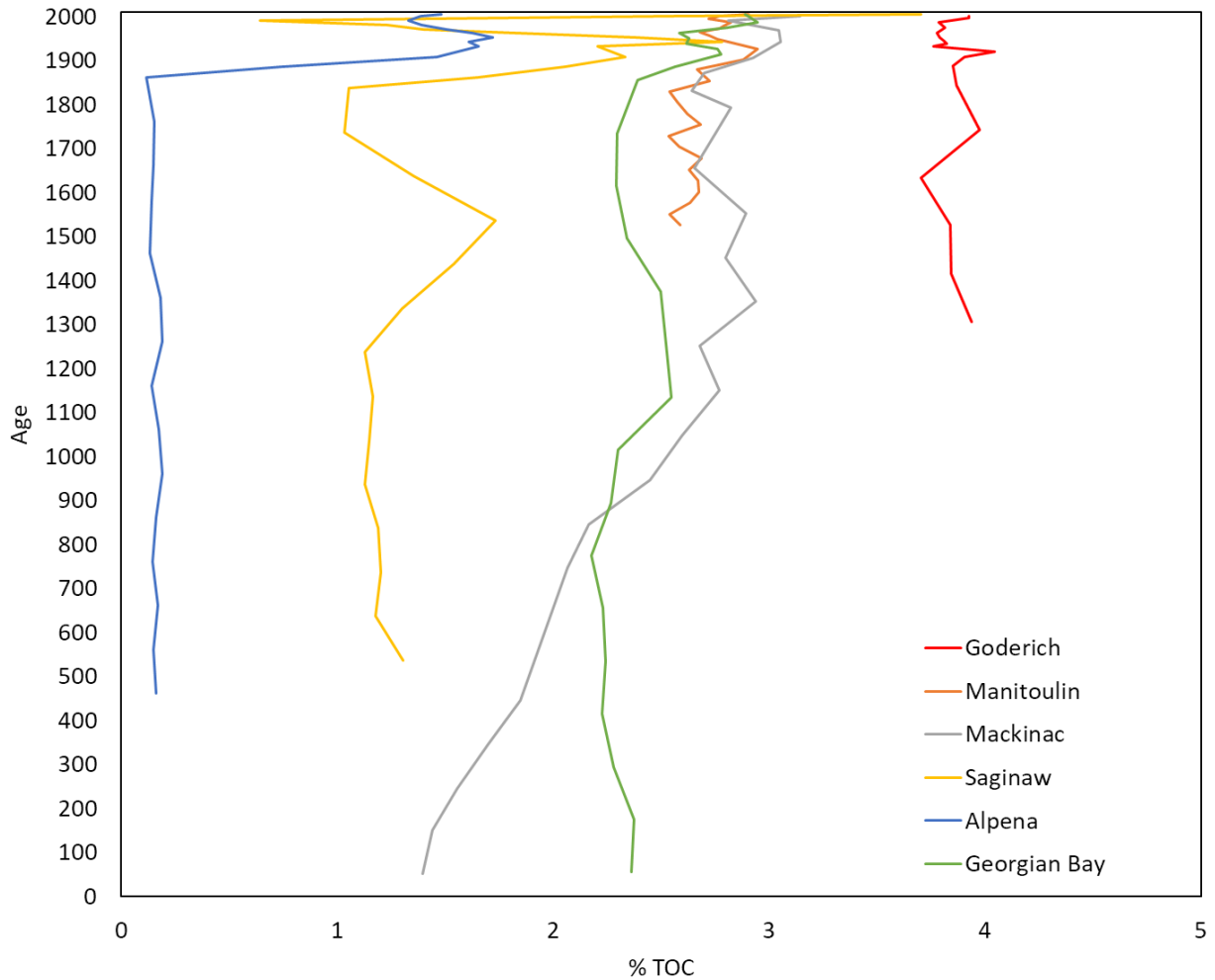
Figure 5.17. Age versus % TOC for cores 594 (Goderich basin), 181 (Manitoulin basin), 182 (Mackinac basin), 821 (Saginaw basin), 817 (Alpena basin), and 41 (Georgian Bay). See Figure 3.1 for core locations.
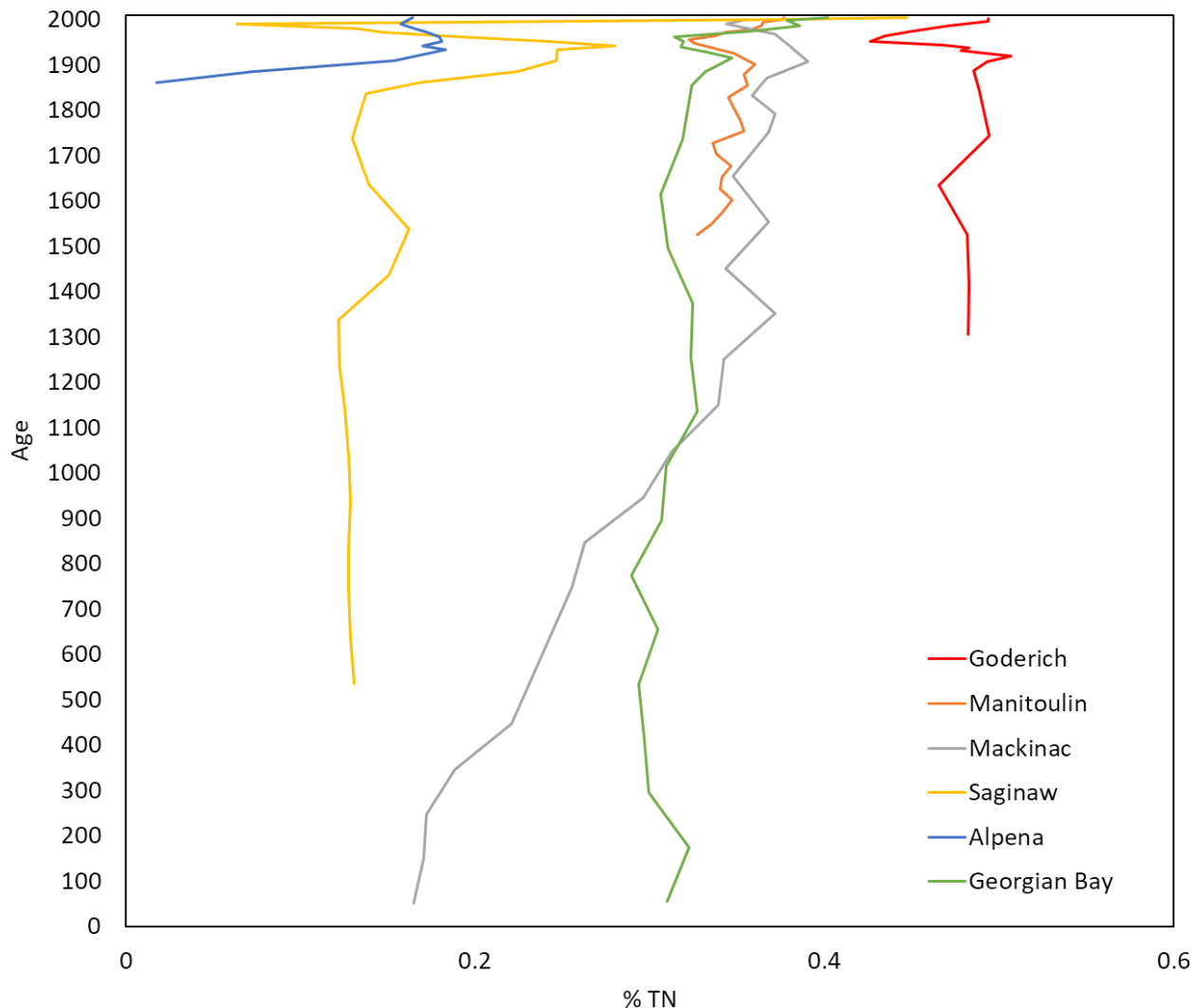
Figure 5.18. Age versus % TN for cores 594 (Goderich basin), 181 (Manitoulin basin), 182 (Mackinac basin), 821 (Saginaw basin), 817 (Alpena basin), and 41 (Georgian Bay). See Figure 3.1 for core locations.

The C/N ratio for the Goderich (core 594), Manitoulin (core 181), and Mackinac (core 182) basins, as well as Georgian Bay (core 41), are generally between 8.5 and 10.5. This is a further indication that the primary source of the OM within the basins is algal matter, which typically has a C/N that ranges between 4 and 10 (Meyers 1994). A common trend among the Goderich, Manitoulin, Mackinac, and Georgian Bay cores is an increase in the C/N ratio during

the mid-19th century. A greater contribution of terrestrial plant material due to anthropogenic activities, such as forest clear-cutting and land disturbance, is the likely cause of this increase. The increase in the C/N ratio after the mid-19th century does not reflect a change in source from primarily algal matter to primarily terrestrial plant material. Instead, the source remains primarily algal matter, but the contribution of terrestrial plant material has increased.

The C/N ratio for the Alpena (core 817) and Saginaw (core 821) basins are more variable than the other cores. Prior to the 19th century, the Alpena basin had the lowest C/N ratios, indicating that the contribution of terrestrial plant material to the basin was lower than in the others. Conversely, the C/N ratios of the Saginaw basin prior to the 19th century were higher than the other cores, indicating that the contribution of terrestrial plant material to the basin was higher than the others. Both the Alpena and Saginaw basins have a larger C/N ratio increase during the 19th century than the other cores. Extensive deforestation during the 19th century in Michigan led to an increase in terrestrial plant material entering the Alpena and Saginaw basins through tributaries in Michigan.
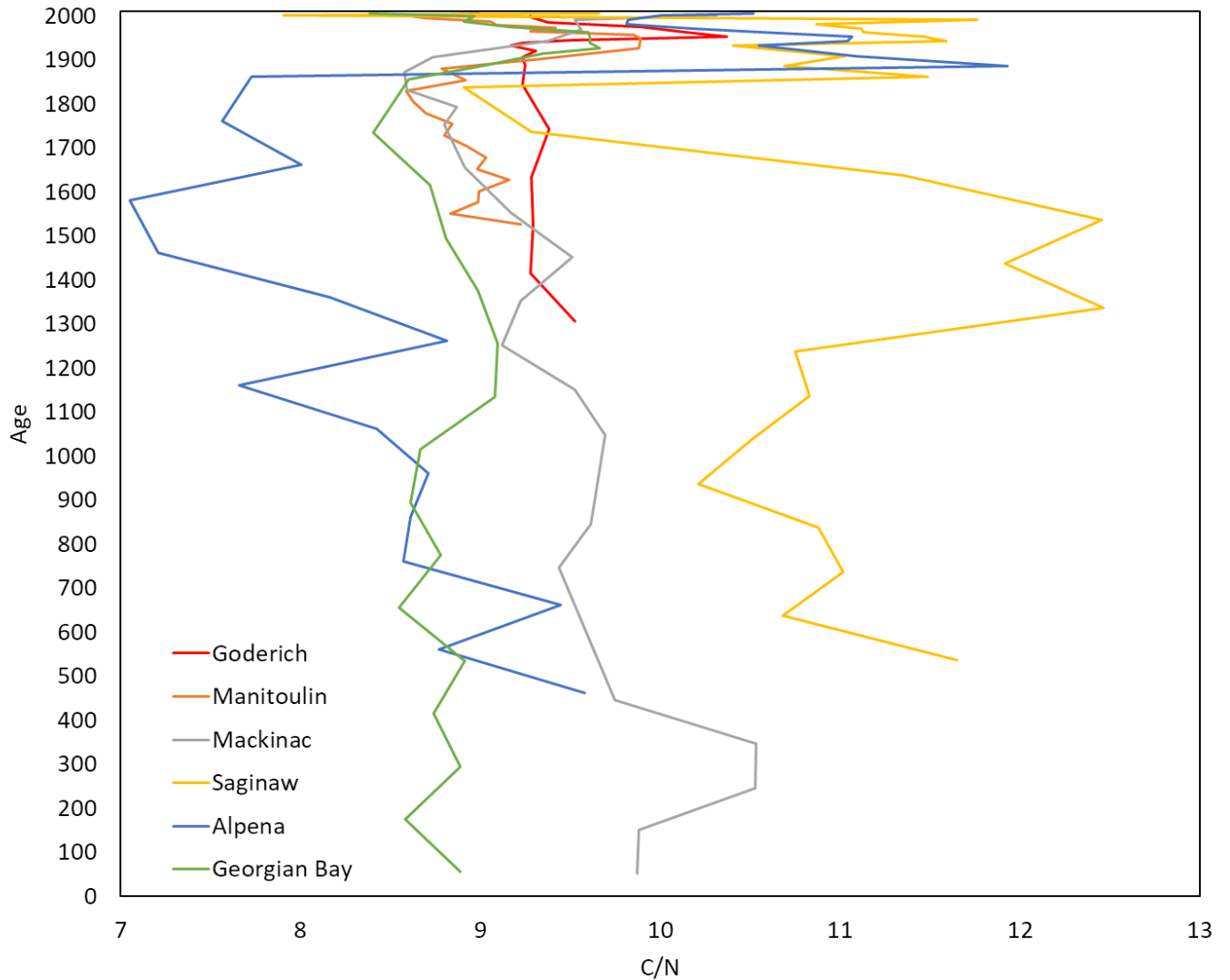
Figure 5.19. Age versus C/N for cores 594 (Goderich basin), 181 (Manitoulin basin), 182 (Mackinac basin), 821 (Saginaw basin), 817 (Alpena basin), and 41 (Georgian Bay). See Figure 3.1 for core locations.

Variations in the magnetic susceptibility curves are influenced by the following factors: (i) land clearance; (ii) Lake Michigan-Huron water levels; and (iii) Lake Huron water currents. A similarity between all cores, except core 817 (Alpena basin) and 818-2 (Port Huron basin) is a large increase in the magnetic susceptibility signal in the early- to mid-20th century. The increase in magnetic susceptibility typically coincides with an increase in the C/N ratio. Land clearance

for settlement, agriculture, and infrastructure increased the amount of allochthonous material entering the lake, which subsequently increased the quantity of magnetic minerals in the sediment. The magnetic susceptibility signal typically decreases in the late-20th century. This reflects the reduction in land clearance.

Shifts in magnetic susceptibility in the Manitoulin (core 181), Mackinac (core 182), and the Alpena (core 817) basins appear related to Michigan-Huron water levels. A sudden decrease in magnetic susceptibility in the Manitoulin basin coincides with a period of very warm and wet climate (Buhay and Edwards 1995) and high water levels (Figure 5.7). The increase in Michigan-Huron water levels may have increased the contribution of Lake Michigan waters to Lake Huron and reduced the amount of water and sediment sourced from Lake Superior. The Canadian Shield rocks that surround portions of Lake Superior are more likely to contribute a greater amount of magnetic minerals to Lake Huron than the Paleozoic carbonate rocks that dominate much of Michigan (Dorr and Eschman 1970; Percival 2007). A decrease in magnetic susceptibility observed in the Mackinac basin at the end of the 20th century may also be related to Michigan-Huron water levels. An approximately 0.5 m permanent decrease in lake level occurred due to anthropogenic activities such as dredging in the St. Clair River in the late 20th and early 21st centuries (Quinn and Croley 1981; Derecki 1982). Lower lake levels decrease the amount of bluff erosion occurring, and subsequently the flux of allochthonous material. Moreover, calcite is present in low amounts throughout the record except after the Michigan-Huron lake level drop when calcite disappears. This suggests that the contribution of sediment sourced from Lake Michigan had decreased.

Although the Saginaw (core 821) and Alpena (core 817) basins are typically expected to have sediments of similar provenance, the Alpena basin is significantly richer in magnetic

material than the Saginaw basin. This may be due to the water currents in Lake Huron, which move water and entrained sediment from north to south in the western portion of the lake. As such, heavy magnetic minerals are more likely to have been deposited prior to reaching the Saginaw basin. A sudden decrease in magnetic susceptibility occurs in core 817 at the end of the 20th century. This is also likely the result of the anthropogenically induced Michigan-Huron water level decrease, which decreased bluff erosion. The Saginaw and Alpena basin are also related in their significant amounts of calcite and dolomite compared to all other cores. The source of the calcite and dolomite are the Paleozoic carbonate rocks in Michigan. The amount of dolomite and calcite, however, decreases after the lake level decreases in the late-20th and early-21st century. This further illustrates that waning influence of Michigan sourced detritus following the lake level decrease.

Chapter 6

6   Conclusions

This study describes aspects of the paleolimnology of Lake Huron and Georgian Bay, with a focus on the last 2000 years. Several proxies preserved within the lacustrine sediments of six benthos cores from Lake Huron, and one from Georgian Bay have been used to investigate variations in climate, lake production, and the sources of OM and sediment, including those arising from anthropogenic activities within the Lake Huron. The proxies measured include total organic carbon (TOC) content, total nitrogen (TN) content, atomic carbon to nitrogen (C/N) ratio, the carbon- and nitrogen-isotope compositions of bulk OM, magnetic susceptibility, mineralogy, and grain size. This chapter summarizes the major findings of the study and provides suggestions for future research.

6.1   Principal Conclusions

1. The source of OM in the Huron basin is predominantly lacustrine algae. This is evident by the C/N ratios that are typically <10 and $\delta^{13}C_{OM}$ compositions. Increases in the C/N ratio occur in the 19th century in the Alpena and Saginaw basins, and the 20th century in the Goderich, Manitoulin, and Mackinac basins, and Georgian Bay. The increases in the C/N ratio are interpreted to be the result of an increase in allochthonous material entering the Huron basin due to deforestation in Michigan and Ontario. The Saginaw and Alpena basins are more likely to receive terrestrial plant material sourced from Michigan than the other cores, and therefore have larger and earlier increases in the C/N ratio. Increases in C/N, however, are not significant enough to suggest that terrestrial plant material has exceeded lacustrine OM as the primary contributor to total OM, only that there is a larger contribution.

2. Prior to the beginning of the 19th century, observable changes in primary production are generally reflected by small increases in the total OM, but not in $\delta^{13}C_{OM}$ and $\delta^{15}N_{TN}$. This occurs because carbon and nitrogen were not limiting nutrients during that period. Increases in primary production may be recorded in the Mackinac and Saginaw basins during the MWP. Due to uncertainties in the age-depth models, however, it is difficult to be certain if the MWP is responsible for the small increases in total OM. Low primary production is observed in the Goderich, Manitoulin, Mackinac, Saginaw, and Alpena basins during the LIA. An increase in primary production as a result of increasing temperatures following the end of the LIA is apparent in all cores. A decrease in primary production occurs in the Goderich, Manitoulin, Mackinac, Saginaw, and Georgian Bay due to an increased flux of allochthonous material into the Huron basin in the early to mid-20th century. The increase in allochthonous material, due to significant land clearance in Michigan and Ontario, increased turbidity to an extent that primary production decreased. The most apparent increase in primary production in all cores occurred during the late 20th and early 21st centuries. This is interpreted to be due to increasing temperature (IPCC 2019) and nutrient inputs (Heaton 1986; Hodell and Schelske 1988) due to anthropogenic activities. The increase in primary production is reflected in significant increases in $\delta^{13}C_{OM}$, $\delta^{15}N_{TN}$, and total OM.

3. The most prominent change in magnetic susceptibility in all cores except 817 (Alpena basin) reflects variations in the flux of allochthonous material entering the Huron basin. A significant increase in the magnetic susceptibility signal begins in Georgian Bay in 1876 CE, the Goderich basin in 1928 CE, the Mackinac basin in 1942 CE, the Manitoulin basin in 1948 CE, and the

147

Saginaw basin in 1962 CE. In general, the magnetic susceptibility signal begins to decrease between the 1960s to 1970s CE and reaches pre-disturbance levels in the 1980s CE. This reflects the increase and eventually decrease in land clearance in the vicinity of the basins. The large increase in magnetic susceptibility observed in the cores typically coincides with an increase in the C/N ratio. This further emphasizes that the changes reflect an increase in allochthonous input.

4. The cores collected from the Goderich, Manitoulin, Mackinac, Port Huron basins and Georgian Bay typically have low calcite and dolomite concentrations. The Saginaw and Alpena cores, however, contain more calcite and dolomite in comparison to the others. This is likely because calcite and dolomite originating from the Michigan basin, which has plentiful carbonate-rich bedrock (Dorr and Eschman 1970), is more likely to be deposited in the Saginaw and Alpena basins than elsewhere in the Huron basin. Changes in the quantity of calcite and dolomite in the cores appear to be related to the amount of precipitation in the watershed and Michigan-Huron lake levels, which can affect the proportion of Michigan and Superior basin sourced water and sediment to the Huron basin. Lower calcite and dolomite contents were observed in the Saginaw basin during the LIA. The lower precipitation amounts during this period (Buhay and Edwards 1995) would have limited delivery of allochthonous material, including detrital calcite and dolomite, to the basin. The calcite and dolomite content disappears entirely in the Mackinac basin and decreases in the Saginaw and Alpena basins following the lowering of water levels due to anthropogenic activities such as dredging in the St. Clair River in the late 19th century and early 20th century. Lower lake levels may have decreased the proportion of Lake Michigan inflow, and increased the proportion of Lake Superior inflow to the Huron basin, which is less likely to contain calcite and dolomite due to the proximal Canadian Shield.

5. Deforestation, predominately during the 19th century, contributed to a rise in total OM in the Goderich, Manitoulin, Mackinac, Saginaw, Alpena basins, and Georgian Bay. The increased contribution of terrestrial plant material to the total OM is most apparent in the Saginaw and Alpena basins. This may suggest that deforestation was more extensive in Northern Michigan and the Saginaw region than in Ontario. Alternatively, it may indicate that primary production is greater in the other basins, and hence the contribution of terrestrial plant material is more apparent in the proxies for the Saginaw and Alpena basins.

6.2   Future Work

There are several future limnological and paleolimnological investigations that should be conducted on these cores from Lake Huron and Georgian Bay.

1. Lead-210 (^{210}Pb) dating should be completed on cores 821, 817, and 41 in order to provide more accurate age-depth models. Efforts to find suitable material for radiocarbon dating should also be continued, so as to better constrain the age of the lower portions of the cores.

2. A new benthos core should be retrieved from the Port Huron basin. This would allow for proper representation of all major basins in the Huron basin.

3. An analysis of *n*-alkanes preserved in the sediment, including their chain lengths, carbon-isotope ($\delta^{13}C_{n\text{-alkane}}$) and hydrogen-isotope ($\delta^2H_{n\text{-alkane}}$) compositions would greatly augment this study. The chain length of *n*-alkanes can provide information regarding their source, given that

terrestrial plants and lacustrine algae have different length chains (e.g., Barnes and Barnes 1978; Ficken et al. 2000). The $\delta^{13}C_{n\text{-alkane}}$ of individual n-alkanes would provide deeper insight into their source, and the environmental conditions leading to changes in lacustrine and terrestrial production (e.g., Rieley et al. 1991; Ishiwatari et al. 1994). The $\delta^{2}H_{n\text{-alkane}}$ of individual n-alkanes would provide information on changes in moisture balance and hence climate in the region over time, by tracking changes in the isotopic compositions of precipitation (terrestrial n-alkanes) and lake-water evaporation (lacustrine n-alkanes) (e.g., Sachse et al. 2004).

4. An examination of palynomorphs and diatoms in these cores would provide key information on environmental change over the time period studied, and in some cases also further support development of more accurate age-depth models for these cores (e.g., Kemp et el. 1974; Smol and Cumming 2000; McCarthy et al. 2011).

REFERENCES

A Brief History of Lumbering in Michigan. n.d. Retrieved December 20, 2019, from http://www.michigan-history.org/lumbering/LumberingBriefHistory.html.

Andresen, J., Hilberg, S., Kunkel, K., and Center, M. R. C. 2012. Historical climate and climate trends in the Midwestern USA. US National Climate Assessment Midwest Technical Input Report, 1-18.

Appleby, P. 2001. Chronostratigraphic techniques in recent sediments. *In* Tracking Environmental Change Using Lake Sediments. *Edited by* Smol, J., Birks, H., and Last, W., Springer Netherlands, 171-203.

Austin, J. A., and Colman, S. M. 2007. Lake Superior summer water temperatures are increasing more rapidly than regional air temperatures: A positive ice-albedo feedback. Geophysical Research Letters, **34**: 6.

Barnes, M. A., and Barnes, W. C. 1978. Organic compounds in lake sediments. *In* Lakes. Springer, New York, NY, 127-152.

Bateman, A. S., and Kelly, S. D. 2007. Fertilizer nitrogen isotope signatures. Isotopes in environmental and health studies, **43**: 237-247.

Becker, M. D. 2004. Farmers and hunters of the eastern woodlands: a regional overview. Native Peoples: The Canadian Experience, 224-228.

Bender, M. M. 1971. Variations in the $^{13}C/^{12}C$ ratios of plants in relation to the pathway of photosynthetic carbon dioxide fixation. Phytochemistry, **10**: 1239-1244.

Bernasconi, S. M., Barbieri, A., and Simona, M. 1997. Carbon and nitrogen isotope variations in sedimenting organic matter in Lake Lugano. Limnology and Oceanography, **42**: 17551765.

Birks, S. J., Edwards, T. W. D., and Remenda, V. H. 2007. Isotopic evolution of Glacial Lake Agassiz: New insights from cellulose and porewater isotopic archives. Palaeogeography, Palaeoclimatology, Palaeoecology, **246**: 8-22.

Bishop, C. T. 1990. Historical variation of water levels in Lakes Erie and Michigan-Huron. Journal of Great Lakes Research, **16**: 406-425.

Brenner, M., Whitmore, T. J., Curtis, J. H., Hodell, D. A., and Schelske, C. L. 1999. Stable isotope ($\delta^{13}C$ and $\delta^{15}N$) signatures of sedimented organic matter as indicators of historic lake trophic state. Journal of Paleolimnology, **22**: 205-221.

Broecker, W. S., and Denton, G. H. 1989. The role of ocean-atmosphere reorganizations in glacial cycles. Geochimica et Cosmochimica Acta, **53**: 2465-2501.

Buhay, W. M., and Betcher, R. N. 1998. Paleohydrologic implications of ^{18}O enriched Lake Agassiz water. Journal of Paleolimnology, **19**: 285-296.

Buhay, W. M., and Edwards, T. W. 1995. Climate in southwestern Ontario, Canada, between AD 1610 and 1885 inferred from oxygen and hydrogen isotopic measurements of wood cellulose from trees in different hydrologic settings. Quaternary Research, **44**: 438-446.

Chambers, R. L., and Eadie, B. J. 1981. Nepheloid and suspended particulate matter in southeastern Lake Michigan. Sedimentology, **28**: 439-447.

Cline, J. D., and Kaplan, I. R. 1975. Isotopic fractionation of dissolved nitrate during denitrification in the eastern tropical North Pacific Ocean. Marine Chemistry, **3**: 271-299.

Colborn T.E., Davidson, A., Green, S.N., Hodge, R.A., Jackson, C.I., Liroff, R.A. 1990. Great Lakes Great Legacy. Washington: The Conservation Foundation.

Coyne, J. H. 1903. Exploration of the Great Lakes, 1669-1670. Ontario Historical Society, Papers and Records, **4**.

Cvancara, A.M. and Melik, J.C. 1961. Bedrock Geology of Lake Huron. *In* Great Lakes Research Division Pub. Institute for Science and Technology, Univ. Michigan, Ann Arbor, MI, **7**: 116–125.

Dean, W. E. and Fouch, T. D. 1983. Lacustrine Carbonate Depositional Environments. American Association of Petroleum Geologists Memoir, **33**: 98-130.

Dean, W. G. and Matthews G. J. 1969. Economic atlas of Ontario. University of Toronto Press.

Derecki, J. A. 1982. Effect of channel changes in the St. Clair River since 1900.

Dickas, A. B. 1986. Comparative Precambrian stratigraphy and structure along the mid-continent rift. American Association of Petroleum Geologists Bulletin, **70**: 225-238.

Dobiesz, N. E., and Lester, N. P. 2009. Changes in mid-summer water temperature and clarity across the Great Lakes between 1968 and 2002. Journal of Great Lakes Research, **35**: 371-384.

Dobson, D. M., Moore, T. C., and Rea, D. K. 1995. The sedimentation history of Lake Huron and Georgian Bay: results from analysis of seismic reflection profiles. Journal of Paleolimnology, **13**: 231-249.

Dorr, J. A., and Eschman, D. F. 1970. Geology of Michigan. University of Michigan Press.

Dyke, A.S., Moore, A., and Robinson, L. 2003. Deglaciation of North America. Geological Survey of Canada, Open File 1574.

Eadie, B. J., and Robbins, J. A. 2005. Composition and accumulation of recent sediments in Lake Michigan. State of Lake Michigan: Ecology, Health and Management, Ecovision World Monogr. Ser, 89-111.

Eadie, B. J., Chambers, R. L., Gardner, W. S., and Bell, G. L. 1984. Sediment trap studies in Lake Michigan: Resuspension and chemical fluxes in the southern basin. Journal of Great Lakes Research, **10**: 307-321.

Environment and Climate Change Canada and the U.S. Environmental Protection Agency. 2018. Lake Huron Lakewide Action and Management Plan, 2017-2021.

Environmental Protection Report. 2018. Environmental Commissioner of Ontario. Retrieved from https://eco.auditor.on.ca/reports/2018-back-to-basics/

Eschman, D. F., and Karrow, P. F. 1985. Huron basin glacial lakes: a review. *In* Quaternary evolution of the Great Lakes. *Edited by* Karrow, P. F., and Calkin, P. E., Geological Association of Canada Special Paper, **30**: 79-93.

Feest, J. E., and Feest, C. F. 1978. "Ottawa,". Handbook of North American Indians, **15**.

Fenneman, N. M. 1938. Physiography of the Eastern United States. McGraw-Hill Book Company, New York.

Fenton, M. M., Moran, S. R., Teller, J. T., and Clayton, L. 1983. Quaternary stratigraphy and history in the southern part of the Lake Agassiz basin. Glacial Lake Agassiz, **26**: 49-74.

Ficken, K. J., Li, B., Swain, D. L., and Eglinton, G. 2000. An *n*-alkane proxy for the sedimentary input of submerged/floating freshwater aquatic macrophytes. Organic geochemistry, **31**: 745-749.

Fisher, T. G., and Lowell, T. V. 2012. Testing northwest drainage from Lake Agassiz using extant ice margin and strandline data. Quaternary International, **260**: 106-114.

Fogel, M. L., and Cifuentes, L. A. 1993. Isotope fractionation during primary production. Organic geochemistry. Springer, Boston, MA, 73-98.

Francey, R. J., C. E. Allison, D. M. Etheridge, C. M. Trudinger, I. G. Enting, M. Leuenberger, R. L. Langenfelds, E. Michel, and L. P. Steele. 1999. A 1000-year high precision record of δ^{13}C in atmospheric CO_2. Tellus B, **51**:170-193.

Friedli, H., Lötscher, H., Oeschger, H., Siegenthaler, U., and Stauffer, B. 1986. Ice core record of the $^{13}C/^{12}C$ ratio of atmospheric CO_2 in the past two centuries. Nature, **324**: 237-238.

Godoy, J. M., Moreira, I., Wanderley, C., Simões Filho, F. F., and Mozeto, A. A. 1998. An alternative method for the determination of excess ^{210}Pb in sediments. Radiation Protection Dosimetry, **75**: 111-115.

Gronewold, A. D., Fortin, V., Lofgren, B., Clites, A., Stow, C. A., and Quinn, F. 2013. Coasts, water levels, and climate change: A Great Lakes perspective. Climatic Change, **120**: 697-711.

Hansel, A. K., Mickelson, D. M., Schneider, A. F., and Larsen, C. E. 1985. Late Wisconsinan and Holocene history of the Lake Michigan basin. *In* Quaternary evolution of the Great Lakes. *Edited by* Karrow, P. F., and Calkin, P. E., Geological Association of Canada Special Paper, **30**: 39-54.

Hayes, J. M. 1993. Factors controlling ^{13}C contents of sedimentary organic compounds: principles and evidence. Marine Geology, **113**: 111-125.

Heaton, T. H. 1986. Isotopic studies of nitrogen pollution in the hydrosphere and atmosphere: a review. Chemical Geology: Isotope Geoscience Section, **59**: 87-102.

Heidenreich, C. E. 1978. Huron. Handbook of North American Indians, **15**: 368-388.

Henderson, P. J., and Last, W. M. 1998. Holocene sedimentation in Lake Winnipeg, Manitoba, Canada: implications of compositional and textural variations. Journal of Paleolimnology, **19**: 265-284.

Hilton, J., and Lishman, J. P. 1985. The effect of redox changes on the magnetic susceptibility of sediments from a seasonally anoxic lake. Limnology and Oceanography, **30**: 907-909.

Hilton, J., Lishman, J. P., and Chapman, J. S. 1986. Magnetic and chemical characterisation of a diagenetic magnetic mineral formed in the sediments of productive lakes. Chemical Geology, **56**: 325-333.

History of Alpena, Michigan. n.d. Retrieved December 20, 2019, from https://www.u-s-history.com/pages/h2438.html.

Hladyniuk, R., and Longstaffe, F. J. 2015. Paleoproductivity and organic matter sources in Late Quaternary Lake Ontario. Palaeogeography, Palaeoclimatology, Palaeoecology, **435**: 1323.

Hodell, D. A., and Schelske, C. L. 1998. Production, sedimentation, and isotopic composition of organic matter in Lake Ontario. Limnology and Oceanography, **43**: 200-214

Hodgkins, G., Dudley, R. W., and Aichele, S. S. 2007. Historical Changes in Precipitation and Streamflow in the US Great Lakes Basin, 1915-2004. US Geological Survey.

Hoefs, J. 1997. Stable isotope geochemistry. Springer, Berlin.

Hollander, D. J., and McKenzie, J. A. 1991. CO_2 control on carbon-isotope fractionation during aqueous photosynthesis: A paleo-pCO_2 barometer. Geology, **19**: 929-932.

Hollander, D. J., McKenzie, J. A., and Ten Haven, H. L. 1992. A 200 year sedimentary record of progressive eutrophication in Lake Greifen (Switzerland): implications for the origin of organic-carbon-rich sediments. Geology, **20**: 825-828.

Homestead Act. 1862. Public Law 37-64 (12 STAT 392), Enrolled Acts and Resolutions of Congress, 1789-2011, General Records of the United States Government, Record Group 11, National Archives Building, Washington, DC.

Hopkins, W.G., Hüner, G., and Norman, P.A. 2004. Introduction to Plant Physiology. John Wiley and Sons Inc., New York.

Hough, J. L. 1958. Geology of the Great lakes. University of Illinois Press.

How Michigan Became a State: The Treaty of Washington, 1836. 2017. Retrieved December 20, 2019, from https://www.mackinacparks.com/how-michigan-became-a-state-the-treaty-of-washington-1836/.

Hyodo, A., and Longstaffe, F. J. 2011. The palaeoproductivity of ancient Lake Superior. Quaternary Science Reviews, **30**: 2988-3000.

International Upper Great Lakes Study Board. 2012. Lake Superior Regulation: Addressing Uncertainty in Upper Great Lakes Water Levels.

IPCC. 2018. Global Warming of 1.5°C. An IPCC Special Report on the impacts of global warming of 1.5°C above pre-industrial levels and related global greenhouse gas emission pathways, in the context of strengthening the global response to the threat of climate change, sustainable development, and efforts to eradicate poverty. Edited by Masson-Delmotte, V., Zhai,, P. , Pörtner, H.-O., Roberts, D., Skea, J., Shukla, P. R., Pirani, A., Moufouma-Okia, W., Péan, C., Pidcock, R., Connors, S., Matthews, J. B. R., Chen, Y., Zhou, X., Gomis, M.I., Lonnoy, E., Maycock, T., Tignor, M., and Waterfield, T. In Press.

Ishiwatari, R., Uzaki, M., and Yamada, K. 1994. Carbon isotope composition of individual *n*-alkanes in recent sediments. Organic Geochemistry, **21**: 801-808.

Johnson, T. C. 1984. Sedimentation in large lakes. Annual Review of Earth and Planetary Sciences, **12**: 179-204.

Karrow, P. F. 1987. Glacial and glaciolacustrine events in northwestern Lake Huron, Michigan and Ontario. Geological Society of America Bulletin, **98**: 113-120.

Karrow, P. F., Dreimanis, A., and Barnett, P. J. 2000. A proposed diachronic revision of late Quaternary time-stratigraphic classification in the eastern and northern Great Lakes area. Quaternary Research, **54**: 1-12.

Keeley, J. E., and Sandquist, D. R. 1992. Carbon: freshwater plants. Plant, Cell and Environment, **15**: 1021-1035.

Keeling, C. D., Mook, W. G., and Tans, P. P. 1979. Recent trends in the $^{13}C/^{12}C$ ratio of atmospheric carbon dioxide. Nature, **277**: 121.

Keeling, C. D., Piper, S. C., Bacastow, R. B., Wahlen, M., Whorf, T. P., Heimann, M., and Meijer, H. A. 2001. Exchanges of atmospheric CO_2 and $^{13}CO_2$ with the terrestrial biosphere and oceans from 1978 to 2000. I. Global aspects. SIO Reference Series, Scripps Institute of Oceangraphy, San Diego, CA.

Kemp, A. L. W., and Harper, N. S. 1977. Sedimentation rates in Lake Huron and Georgian Bay. Journal of Great Lakes Research, **3**: 215-220.

Kemp, A. L. W., and Thomas, R. L. 1976. Impact of man's activities on the chemical composition in the sediments of Lakes Ontario, Erie and Huron. Water, Air, and Soil Pollution, **5**: 469-490.

Kendall, C. 1998. Tracing nitrogen sources and cycling in catchments. *In* Isotope tracers in catchment hydrology. *Edited by* Kendall, C. and McDonnel, J.J. Elsevier, Amsterdam, 519-576.

Kirby, M. E., Lund, S. P., and Poulsen, C. J. 2005. Hydrologic variability and the onset of modern El Niño–Southern Oscillation: a 250-year record from Lake Elsinore, southern California. Journal of Quaternary Science: Published for the Quaternary Research Association, **20**: 239-254.

Kirby, M. E., Lund, S. P., Anderson, M. A., and Bird, B. W. 2007. Insolation forcing of Holocene climate change in Southern California: a sediment study from Lake Elsinore. Journal of Paleolimnology, **38**: 395-417.

Knox, J. C. 1985. Responses of floods to Holocene climatic change in the Upper Mississippi Valley. Quaternary Research, **23**: 287-300.

Kohn, M. J. 2010. Carbon isotope compositions of terrestrial C3 plants as indicators of (paleo) ecology and (paleo) climate. Proceedings of the National Academy of Sciences, **107**: 19691-19695.

Konopka, A., and Brock, T. D. 1978. Effect of temperature on blue-green algae (cyanobacteria) in Lake Mendota. Applied Environmental Microbiology, **36**: 572-576.

Langenfelds, R. L., Francey, R. J., Pak, B. C., Steele, L. P., Lloyd, J., Trudinger, C. M., and Allison, C. E. 2002. Interannual growth rate variations of atmospheric CO_2 and its $\delta^{13}C$, H_2, CH_4, and CO between 1992 and 1999 linked to biomass burning. Global Biogeochemical Cycles, **16**: 21-1.

Larson, G., and Schaetzl, R. 2001. Origin and evolution of the Great Lakes. Journal of Great Lakes Research, 27: 518-546.

Laskar, A., and Mao-Chang, L. 2016. Clumped isotopes in near-surface atmospheric CO_2 over land, coast and ocean in Taiwan and its vicinity. Biogeosciences, **13**: 5297.

Last, W. M. 2002. Geolimnology of salt lakes. Geosciences Journal, **6**: 347-369.

Last, W. M., and Sauchyn, D. J. 1993. Mineralogy and lithostratigraphy of Harris Lake, southwestern Saskatchewan, Canada. Journal of Paleolimnology, **9**: 23-39.

Lewis, C. F. M., and Anderson, T. W. 1989. Oscillations of levels and cool phases of the Laurentian Great Lakes caused by inflows from glacial Lakes Agassiz and Barlow-Ojibway. Journal of Paleolimnology, **2**: 99-146.

Lewis, C. F. M., Heil, C. W., Hubeny, J. B., King, J. W., Moore, T. C., and Rea, D. K. 2007. The Stanley unconformity in Lake Huron basin: evidence for a climate-driven closed lowstand about 7900 ^{14}C BP, with similar implications for the Chippewa lowstand in Lake Michigan basin. Journal of Paleolimnology, **37**: 435-452.

Lewis, C. M., Moore, T. C., Rea, D. K., Dettman, D. L., Smith, A. M., and Mayer, L. A. 1994. Lakes of the Huron basin: their record of runoff from the Laurentide Ice Sheet. Quaternary Science Reviews, **13**: 891-922.

Lick, W. 1982. Entrainment, deposition, and transport of fine-grained sediments in lakes. in Sediment/Freshwater Interaction. Springer, Dordrecht, 31-40.

Macdonald, R.A. 2012. Late Quaternary histories of Lakes Huron and Michigan: A stable isotope investigation of sediment cores and modern biogenic carbonates. PhD Thesis, The University of Western Ontario.

Maher, B. A., and Thompson, R. 1999. Quaternary climates, environments and magnetism. Cambridge University Press.

Manitoulin Treaties. n.d. Retrieved December 20, 2019, from https://web.archive.org/web/20131202224409/http://www.ontarioplaques.com/Plaques_MNO/Plaque_Manitoulin03.html.

Marchand, M. 1989. Les Voyageurs et al Colonisation de Pénétanguishene, 1825-1871. Sudbury: La Société Historique du Nouvel-Ontario.

McAndrews, J. H., and Power, D. M. 1973. Palynology of the Great Lakes: the surface sediments of Lake Ontario. Canadian Journal of Earth Sciences, **10**: 777-792.

McCarthy, F. M., McAndrews, J. H., Blasco, S. M., and Tiffin, S. H. 2007. Spatially discontinuous modern sedimentation in Georgian Bay, Huron Basin, Great Lakes. Journal of Paleolimnology, **37**: 453-470.

McCarthy, F. M., Mertens, K. N., Ellegaard, M., Sherman, K., Pospelova, V., Ribeiro, S., Blasco, S., and Vercauteren, D. 2011. Resting cysts of freshwater dinoflagellates in southeastern Georgian Bay (Lake Huron) as proxies of cultural eutrophication. Review of Palaeobotany and Palynology, **166**: 46-62.

McKenzie, J. A. 1985. Carbon isotopes and productivity in the lacustrine and marine environment. Chemical processes in lakes, 99-118.

Meyers, P. A. 2003. Applications of organic geochemistry to paleolimnological reconstructions: a summary of examples from the Laurentian Great Lakes. Organic geochemistry, **34**: 261-289.

Meyers, P. A., and Teranes, J. L. 2001. Tracking environmental change using lake sediments. Tracking Environmental Change Using Lake Sediments, **2**: 239-270.

Meyers, P. A., and Eadie, B. J. 1993. Sources, degradation and recycling of organic matter associated with sinking particles in Lake Michigan. Organic Geochemistry, **20**: 47-56.

Meyers, P. A., and Ishiwatari, R. 1993. Lacustrine organic geochemistry—an overview of indicators of organic matter sources and diagenesis in lake sediments. Organic geochemistry, **20**: 867-900.

Meyers, P. A. 1994. Preservation of elemental and isotopic source identification of sedimentary organic matter. Chemical geology, **114**: 289-302.

Meyers, P. A., and Lallier-Vergès, E. 1999. Lacustrine sedimentary organic matter records of Late Quaternary paleoclimates. Journal of Paleolimnology, **21**: 345-372.

Meyers, P. A., and Teranes, J. L. 2002. Sediment organic matter. In Tracking environmental change using lake sediments. Edited by Last W. M., and Smol, J. P., Physical and Chemical Techniques, Kluwer, Dordrecht, 239-269.

Meyers, P. A., Leenheer, M. J., and Bourbonniere, R. A. 1995. Diagenesis of vascular plant organic matter components during burial in lake sediments. Aquatic Geochemistry, **1**: 3552.

Moore, J. J., Hughen, K. A., Miller, G. H., and Overpeck, J. T. 2001. Little Ice Age recorded in summer temperature reconstruction from vared sediments of Donard Lake, Baffin Island, Canada. Journal of Paleolimnology, **25**: 503-517.

Moore, T.C., Walker, J. C. G., Rea, D. K., Lewis, C. F. M., Shale, L. C. K., and Smith, A. J. 2000. Younger Dryas interval and outflow from the Laurentide ice sheet. Paleoceanography, **15**: 4-18.

Murray, F. B. 2013. Muskoka and Haliburton, 1615-1875: a collection of documents. Champlain Society.

Murton, J. B., Bateman, M. D., Dallimore, S. R., Teller, J. T., and Yang, Z. 2010. Identification of Younger Dryas outburst flood path from Lake Agassiz to the Arctic Ocean. Nature, **464**: 740.

NOAA. 2019. 1918-Present Coordinated, same as 1860-1917. Retrieved from datahttps://www.glerl.noaa.gov/data/dashboard/data/

O'Beirne, M. D., Werne, J. P., Hecky, R. E., Johnson, T. C., Katsev, S., and Reavie, E. D. 2017. Anthropogenic climate change has altered primary productivity in Lake Superior. Nature Communications, **8**.

O'Leary, M. H. 1988. Carbon isotopes in photosynthesis. Bioscience, **38**: 328-336.

PAGES 2k Consortium. 2013. Continental-scale temperature variability during the past two millennia. Nature Geoscience, **6**: 339-346.

Pearen, S. J. 2001. Exploring Manitoulin. University of Toronto Press.

Percival, J. A. 2007. Geology and metallogeny of the Superior Province, Canada. In Mineral deposits of Canada: A synthesis of major deposit-types, district metallogeny, the evolution of geological provinces, and exploration methods. Geological Association of Canada, Mineral Deposits Division, **5**: 903-928.

Peters, K. E., Sweeney, R. E., and Kaplan, I. R. 1978. Correlation of carbon and nitrogen stable isotope ratios in sedimentary organic matter. Limnology and Oceanography, **23**: 598-604.

Peterson, B. J., and Fry, B. 1987. Stable isotopes in ecosystem studies. Annual review of ecology and systematics, **18**: 293-320.

Pilbeam, D. 2010. The utilization of nitrogen by plants: a whole plant perspective. Annual Plant Reviews, **42**: 305-351.

Quinn, F. H., and Sellinger, C. E. 1990. Lake Michigan record levels of 1838, a present perspective. Journal of Great Lakes Research, **16**: 133-138.

Quinn, F. H., and Croley, T. E. I. I. 1981. The role of precipitation climatology in hydrologic design and planning on the Laurentian Great Lakes. *In* Preprints, 4th Conference on Hydrometeorology, 7-11.

Rea, D. K., Owen, R. M., and Meyers, P. A. 1981. Sedimentary processes in the Great Lakes. Reviews of Geophysics, **19**: 635-648.

Rieck, R.L., and Winters, H.A. 1993. Drift volume in the southern peninsula of Michigan—a prodigious Pleistocene endowment. Physical Geography, **14**: 478–493.

Rieley, G., Collier, R. J., Jones, D. M., Eglinton, G., Eakin, P. A., and Fallick, A. E. 1991. Sources of sedimentary lipids deduced from stable carbon-isotope analyses of individual compounds. Nature, **352**: 425.

Riley, J. L. 2013. The once and future Great Lakes country: an ecological history. McGill-Queen's Press-MQUP.

Rogers, E. S. 1978. Southeastern Ojibwa. Handbook of North American Indians, **15**: 760-771.

Sachse, D., Radke, J., and Gleixner, G. 2004. Hydrogen isotope ratios of recent lacustrine sedimentary n-alkanes record modern climate variability. Geochimica et Cosmochimica Acta, **68**: 4877-4889.

Saginaw History. n.d. Retrieved December 20, 2019, from https://www.saginaw-mi.com/residents/history.php.

Sanchez-Cabeza, J. A., and Ruiz-Fernández, A. C. 2012. ^{210}Pb sediment radiochronology: an integrated formulation and classification of dating models. Geochimica et Cosmochimica Acta, **82**: 183-200.

Sánchez-Cabeza, J., Masqué, P., and Ani-Ragolta, I. 1998. ^{210}Pb and ^{210}Po analysis in sediments and soils by microwave acid digestion. Journal of Radioanalytical and Nuclear Chemistry, **227**: 19-22.

Schelske, C. L., and Hodell, D. A. 1995. Using carbon isotopes of bulk sedimentary organic matter to reconstruct the history of nutrient loading and eutrophication in Lake Erie. Limnology and Oceanography, **40**: 918-929.

Schelske, C. L., Peplow, A., Brenner, M., and Spencer, C. N. 1994. Low-background gamma counting: applications for ^{210}Pb dating of sediments. Journal of Paleolimnology, **10**: 115-128.

Schumm, S. A. 1965. Quaternary paleohydrology. *In* The Quaternary of the United States. *Edited by* Wright Jr, H. E., and Frey, D. G. Princeton University Press, 783-794.

Sharp, Z. 2007. Principles of Stable Isotope Geochemistry. Pearson Education, Upper Saddle River, NJ.

Sloss, P. W., and Saylor, J. H. 1976. Large-scale current measurements in Lake Huron. Journal of Geophysical Research, **8**: 3069-3078.

Smol, J. P., and Cumming, B. F. 2000. Tracking long-term changes in climate using algal indicators in lake sediments. Journal of Phycology, **36**: 986-1011.

Smoot, J. P., and Benson, L. V. 2004. Mechanical mixing of climate proxies by sediment focusing in Pyramid Lake, Nevada: a cautionary tale. *In* Geological Society of America Abstracts with Programs.

Soller, D.R. 1998. Map showing the thickness and character of Quaternary sediments in the glaciated United States east of the Rocky Mountains: northern Great Lakes States and Central Mississippi Valley States, the Great Lakes, and southern Ontario (80°31′ to 93° West Longitude). U.S. Geological Survey Miscellaneous Series Map I-1970-B, 1:1,000,000.

Sournia, A. 1986. La Cyanophyceae Oscillatoria dans le plancton marin: Taxanomic, et observations dans le canae de Mozambique. Nova Hedwigia **15**: 1-12.

Ste. Marie Among the Hurons. 2005. Retrieved December 20, 2019, from https://www.collectionscanada.gc.ca/settlement/kids/021013-2051.3-e.html.

Szpak, P., White, C., Longstaffe, F., Millaire, J., and Vasquez Sanchez, V. 2013. Carbon and nitrogen isotopic survey of northern Peruvian plants: baselines for paleodietary and paleoecological studies. PloS one, **8**: e53763.

Talbot, M. 2001. Nitrogen isotopes in palaeolimnology. *In* Tracking Environmental Change Using Lake Sediments. *Edited by* Smol, J., Birks, H. and Last, W., Springer Netherlands, 401-439.

Talbot, M., and Laerdal, T. 2000. The late Pleistocene-Holocene paleolimnology of Lake Victoria, east Africa, based upon elemental and isotopic analyses of sedimentary organic matter. Journal of Paleolimnology, **23**: 141-164.

Teller, J. T. 1985. Glacial Lake Agassiz and its influence on the Great Lakes. Quaternary Evolution of the Great Lakes. Geological Association of Canada, Special Paper, **30**: 1-16.

Teller, J. T. 1995. History and drainage of large ice-dammed lakes along the Laurentide Ice Sheet. Quaternary International, **28**: 83-92.

Teller, J. T., and Last, W. M. 1990. Paleohydrological indicators in playas and salt lakes, with examples from Canada, Australia, and Africa. Palaeogeography, Palaeoclimatology, Palaeoecology, **76**: 215-240.

Teranes, J., and Bernasconi, S. 2000. The record of nitrate utilization and productivity limitation provided by δ^{15}N values in lake organic matter–a study of sediment trap and core sediments from Baldeggersee, Switzerland. Limnology and Oceanography, **45**: 801-813.

The Founding of Owen Sound. n.d. Retrieved December 20, 2019, from http://www.ontarioplaques.com/Plaques/Plaque_Grey10.html.

Thomas, R. L., Kemp, A. L., and Lewis, C. F. 1973. The surficial sediments of Lake Huron. Canadian Journal of Earth Sciences, **10**: 226-271.

Thompson, R., Battarbee, R. W., O'sullivan, P. E., and Oldfield, F. 1975. Magnetic susceptibility of lake sediments. Limnology and Oceanography, **20**: 687-698.

Trigger, B. 1994. The Original Iroquoians: Huron, Petun, and Neutral. Aboriginal Ontario: Historical Perspectives on the First Nations, 41-63.

Turekian, K. K., Nozaki, Y., and Benninger, L. K. 1977. Geochemistry of atmospheric radon and radon products. Annual Review of Earth and Planetary Sciences, **5**: 227-255.

Upper Canada Land Surrenders and the Williams Treaties (1764-1862/1923). 2013. Retrieved December 20, 2019, from https://www.rcaanccirnac.gc.ca/eng/1360941656761/1544619778887.

Vajda, N., LaRosa, J., Zeisler, R., Danesi, P., and Kis-Benedek, G. Y. 1997. A novel technique for the simultaneous determination of ^{210}Pb and ^{210}Po using a crown ether. Journal of Environmental Radioactivity, **37**: 355-372.

Verburg, P. 2007. The need to correct for the Suess-effect in the application of δ^{13}C in sediment of autotrophic Lake Tanganyika, as a productivity proxy in the Anthropocene. Journal of Paleolimnology, **37**: 591-602.

Wada, E., and Hattori, A. 1991. Nitrogen in the sea: forms, abundance, and rate processes. CRC Press, Boca Raton, FL.

Wang, J., Bai, X., Hu, H., Clites, A., Colton, M., and Lofgren, B. 2012. Temporal and spatial variability of Great Lakes ice cover, 1973–2010. Journal of Climate, **25**: 1318-1329.

Wetzel, R. G. 2001. Limnology: lake and river ecosystems. Academic Press, San Diego, CA.

Wilson, C. R., and Urion, C. 1995. First Nations prehistory and Canadian history. Native Peoples: The Canadian Experience, 2nd ed. Toronto: McClelland and Stewart, 22-66.

Wold, R.J., Paull, R.A., Wolosin, C.A., and Friedel, R.J. 1981. Geology of central Lake Michigan. American Association Petroleum Geology, **65**: 1621–1632.

Wolfe, B. B., Edwards, T. W., Elgood, R. J., and Beuning, K. R. 2002. Carbon and oxygen isotope analysis of lake sediment cellulose: methods and applications. *In* Tracking environmental change using lake sediments. *Edited by* Last, W. M., and Smol, J. P., Physical and Chemical Techniques, Dordrecht, Kluwer, 373-400.

Woszczyk, M., Grassineau, N., Tylmann, W., Kowalewski, G., Lutynska, M., and Bechtel, A. 2014. Stable C and N isotope record of short term changes in water level in lakes of different morphometry: Lake Anastazewo and Lake Skulskie, central Poland. Organic Geochemistry, **76**: 278-287.

Xiao, J., Chang, Z., Si, B., Qin, X., Itoh, S., and Lomtatidze, Z. 2009. Partitioning of the grain-size components of Dali Lake core sediments: evidence for lake-level changes during the Holocene. Journal of Paleolimnology, **42**: 249-260.

Yoneyama, T., Ito, O., and Engelaar, W. 2003. Uptake, metabolism and distribution of nitrogen in crop plants traced by enriched and natural ^{15}N: progress over the last 30 years. Phytochemistry Reviews, **2**: 121-132.

Zevely, J. 1911. Joseph Anthony de la Rivière Poncet. *In* The Catholic Encyclopedia, Robert Appleton Company, New York.

Zhang, X., Vincent, L. A., Hogg, W. D., and Niitsoo, A. 2000. Temperature and precipitation trends in Canada during the 20th century. Atmosphere-ocean, **38**: 395-429.

Appendices

Appendix I: Digital images of each core (594 – Goderich basin; 181 – Manitoulin basin; 182 Mackinac basin; 821 – Saginaw basin; 817 – Alpena basin; 818-2 – Port Huron basin; 41 – Georgian Bay). Core descriptions include general commentary and Munsell Soil Colour Charts (2000) classifications.

Core 594 – Goderich basin

- Fine-grained silt and clay throughout the core

- Massive, very dark grey (10YR 3/1) sediment in the top 12 cm

- Massive, very dark greyish brown (10YR 3/2) in remainder of core

Core 181 – Manitoulin basin

- Fine-grained silt and clay throughout the core

- Massive, generally brown (10YR 3/3) sediment in the top 20 cm

- Massive, very dark greyish brown (10YR 3/2) in remainder of core

- Black oxides on outer surface
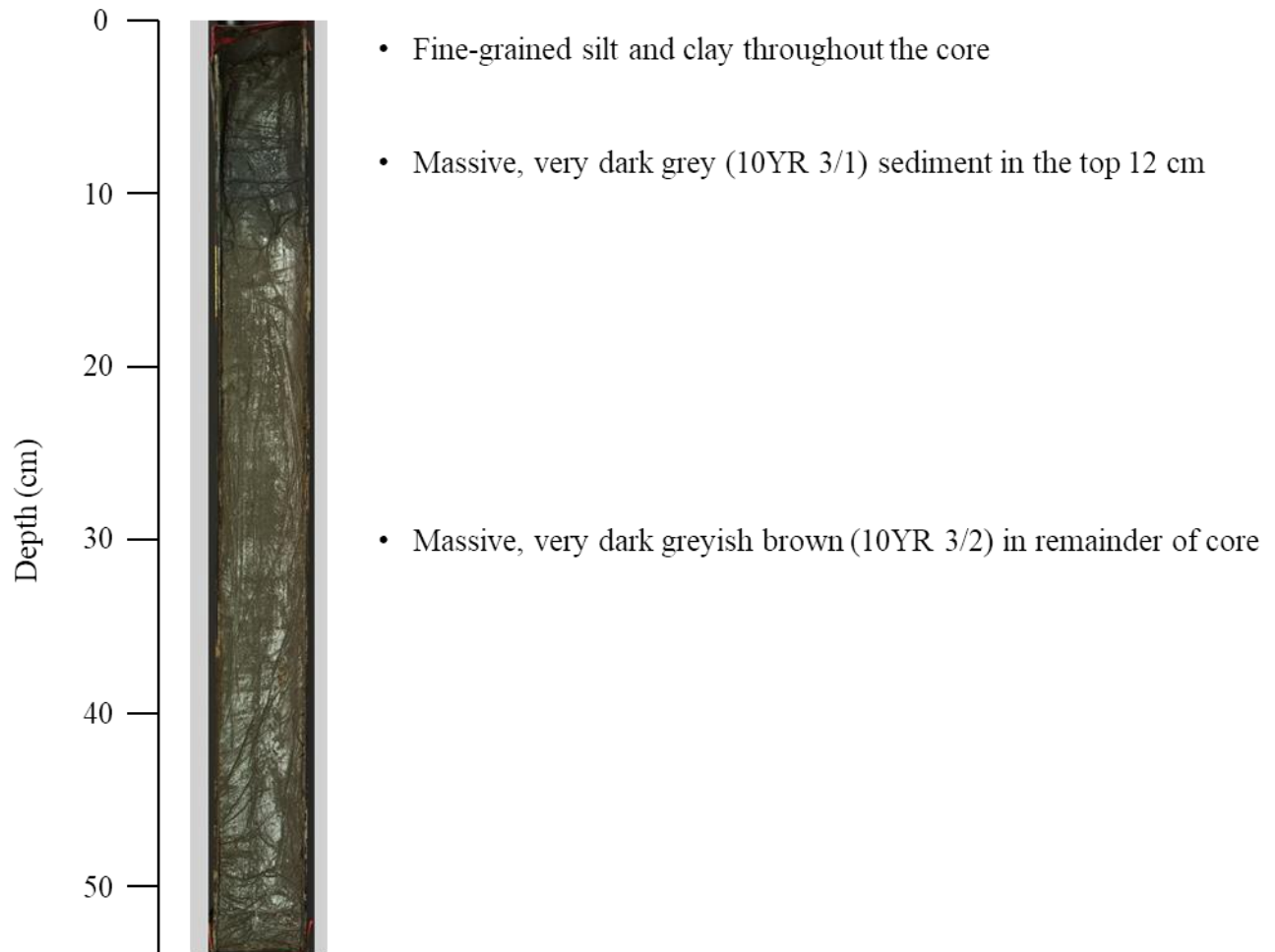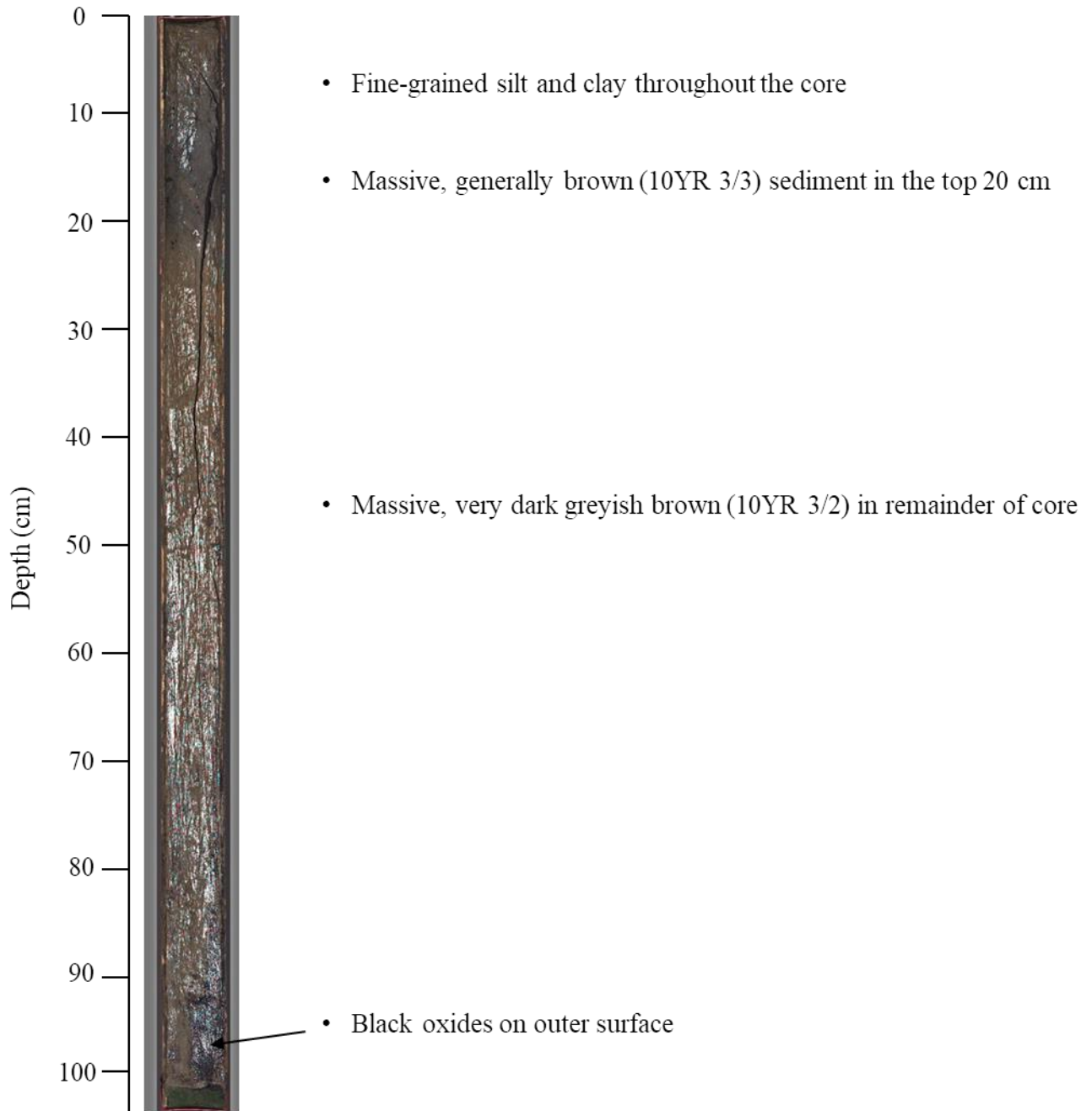
Core 182 – Mackinac basin

- Fine-grained silt and clay throughout the core

- Massive, very dark greyish brown (10YR 3/2) sediment in the top 2 cm

- Massive, dark greyish brown (10YR 4/2) throughout most of the core

- Large vertical crack throughout

- Sediment missing due to previous sampling

- Sediment gradually transitions to brown (10YR 5/3) at the bottom of the core

Core 821 – Saginaw basin
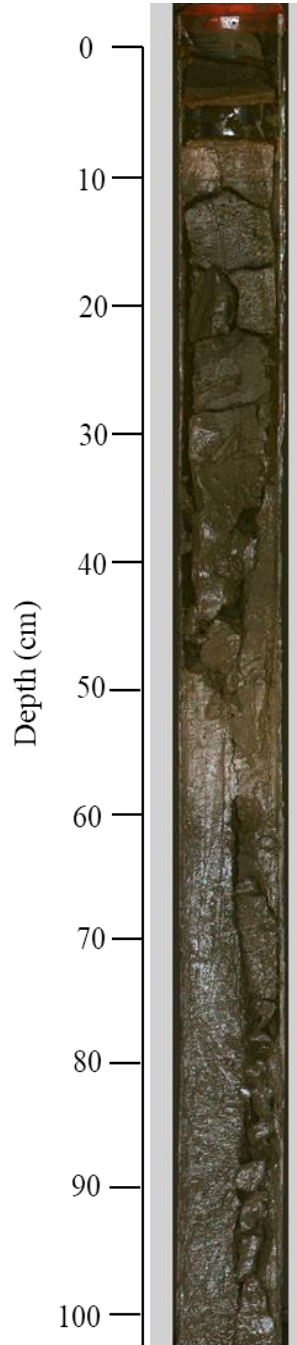
- Fine-grained silt and clay throughout the core

- Massive, very dark greyish brown (10YR 3/2) sediment in the top 2 cm

- Massive, dark greyish brown (10YR 4/2) between 2 – 20 cm

- Massive, brown (10YR 5/3) between 20 – 50 cm

- Massive, brown (10YR 5/3) to pale brown (10YR 6/3) between 50 – 60 cm

- Massive, dark grey (10YR 4/1) to dark greyish brown (10YR 4/2) from 60 cm to the bottom of the core

Core 817 – Alpena basin
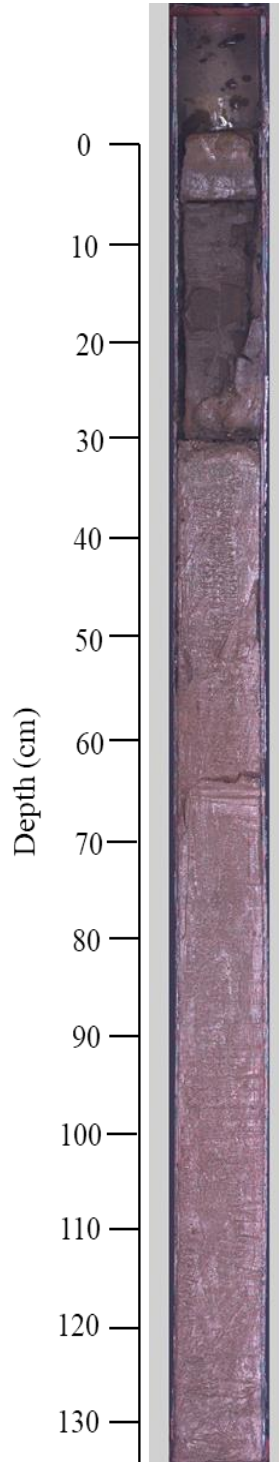
- Fine-grained silt and clay throughout majority of the core

- Dark greyish brown (10YR 4/2) in top 26 cm

- Coarse-grained sand and shelly material present between 29 – 32 cm

- Massive, brown (10YR 5/3) to pale brown (10YR 6/3) throughout the remainder of the core

Core 818-2 – Port Huron basin
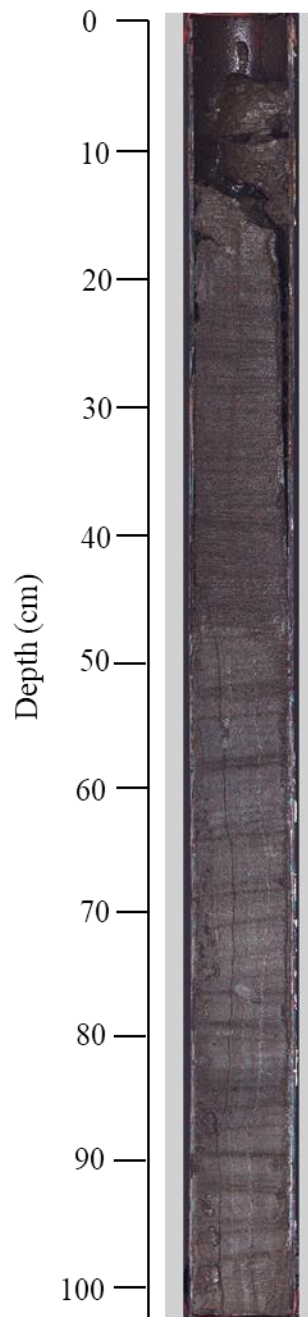
- Top ~16.5 cm are generally unconsolidated sediment

- Fine-grained silt and clay throughout the core

- Massive, dark greyish brown (10YR 3/2) throughout the core

- Lamination-like appearance is an artifact of core splitting

Core 41 – Georgian Bay
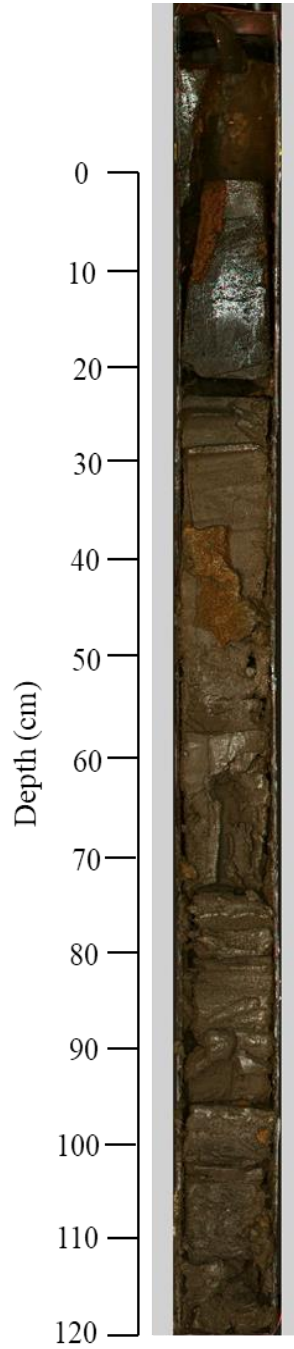
- Fine-grained silt and clay throughout the core

- Massive, very dark grey (10YR 3/1) in top 22 cm

- Massive, dark greyish brown (10YR 4/2) throughout the remainder of the core

Appendix II: Results obtained for isotopic and elemental standard.

Bulk organic matter

Standard	$\delta^{13}C_{OM}$ (‰, VPDB)	Standard	$\delta^{13}C_{OM}$ (‰, VPDB)	Standard	$\delta^{13}C_{OM}$ (‰, VPDB
Keratin	–24.00	Keratin	–23.98	USGS-40	–26.48
Keratin	–24.05	Keratin	–23.89	USGS-40	–26.28
Keratin	–23.91	Keratin	–23.88	USGS-40	–26.40
Keratin	–24.05	Keratin	–24.04	USGS-40	–26.38
Keratin	–24.01	Keratin	–24.09	USGS-40	–26.41
Keratin	–24.03	Keratin	–24.05	USGS-40	–26.53
Keratin	–24.13	Keratin	–24.08	USGS-40	–26.27
Keratin	–24.09	Keratin	–24.14	USGS-40	–26.39
Keratin	–23.92	IAEA-CH-6	–10.72	USGS-40	–26.49
Keratin	–23.98	IAEA-CH-6	–10.68	USGS-40	–26.29
Keratin	–24.18	IAEA-CH-6	–10.89	USGS-40	–26.41
Keratin	–23.99	IAEA-CH-6	–10.84	USGS-40	–26.46
Keratin	–23.95	IAEA-CH-6	–10.85	USGS-41a	+36.31
Keratin	–23.98	IAEA-CH-6	–10.90	USGS-41a	+36.38
Keratin	–23.98	IAEA-CH-6	–10.48	USGS-41a	+36.96
Keratin	–24.06	IAEA-CH-6	–10.39	USGS-41a	+36.46
Keratin	–23.91	IAEA-CH-6	–10.56	USGS-41a	+36.44
Keratin	–23.94	IAEA-CH-6	–10.40	USGS-41a	+36.76
Keratin	–24.02	IAEA-CH-6	–10.91	USGS-41a	+36.44
Keratin	–23.98	IAEA-CH-6	–10.57	USGS-41a	+36.67
Keratin	–24.02	IAEA-CH-6	–10.55	USGS-41a	+36.54
Keratin	–24.06	IAEA-CH-6	–10.24	USGS-41a	+36.49
Keratin	–24.26	IAEA-CH-6	–10.59	USGS-41a	+36.48
Keratin	–24.45	IAEA-CH-6	–10.42	USGS-41a	+36.59
Keratin	–24.28	IAEA-CH-6	–10.57	USGS-41a	+36.65
Keratin	–24.22	USGS-40	–26.49	USGS-41a	+36.58
Keratin	–24.21	USGS-40	–26.30	USGS-41a	+36.52
Keratin	–24.30	USGS-40	–26.30	USGS-41a	+36.52
Keratin	–23.80	USGS-40	–26.28	USGS-41a	+36.68
Keratin	–23.86	USGS-40	–26.30	USGS-41a	+36.48
Keratin	–24.22	USGS-40	-26.44	USGS-41a	+36.52

*USGS-40 and USGS-41 carbon-isotope compositions are defined by the calibration curve.
*IAEA-CH-6 and keratin carbon-isotope compositions provide tests of the calibration curve.

Bulk organic matter

Standard	$\delta^{15}N_{TN}$ (‰, AIR)	Standard	$\delta^{15}N_{TN}$ (‰, AIR)
Keratin	+6.46	USGS-40	–4.48
Keratin	+6.36	USGS-40	–4.56
Keratin	+6.40	USGS-40	–4.52
Keratin	+6.35	USGS-40	–4.58
Keratin	+6.38	USGS-40	–4.5
Keratin	+6.49	USGS-40	–4.47
Keratin	+6.15	USGS-40	–4.46
Keratin	+6.34	USGS-40	–4.58
Keratin	+6.43	USGS-40	–4.5
Keratin	+6.48	USGS-40	–4.57
Keratin	+6.48	USGS-40	–4.49
Keratin	+6.46	USGS-41a	+47.85
Keratin	+6.39	USGS-41a	+47.45
Keratin	+6.31	USGS-41a	+47.35
Keratin	+6.34	USGS-41a	+47.35
Keratin	+6.34	USGS-41a	+47.43
Keratin	+6.49	USGS-41a	+47.91
Keratin	+6.44	USGS-41a	+47.51
Keratin	+6.37	USGS-41a	+47.12
Keratin	+6.41	USGS-41a	+47.98
Keratin	+6.55	USGS-41a	+47.14
Keratin	+6.39	USGS-41a	+47.50
Keratin	+6.44	USGS-41a	+47.99
Keratin	+6.38	USGS-41a	+47.57
GG-Hatch	+16.23		
GG-Hatch	+16.17		
GG-Hatch	+16.12		
GG-Hatch	+16.39		
GG-Hatch	+16.38		
GG-Hatch	+15.42		
GG-Hatch	+15.51		

*USGS-40 and USGS-41a nitrogen-isotope compositions are defined by the calibration curve.
*GG-Hatch and keratin nitrogen-isotope composition provide tests of the calibration curve.

Appendix III: Grain size measurements of all cores (594 – Goderich basin; 181 – Manitoulin basin; 182 Mackinac basin; 821 – Saginaw basin; 817 – Alpena basin; 818-2 – Port Huron basin; 41 – Georgian Bay).

Core 594 – Goderich Basin

Depth (cm)	d(10) (μm)	d(50) (μm)	d(90) (μm)
1.5	0.74	3.77	19.84
11.5	0.72	3.9	21.97
20.5	0.83	4.61	20.43
30.5	0.76	5.44	140.52
40.5	0.78	5.25	53.02
50.5	0.73	4.24	25.36
60.5	0.73	4.61	42.79

Core 181 – Manitoulin Basin

Depth (cm)	d(10) (μm)	d(50) (μm)	d(90) (μm)
1.5	0.58	2.37	14.75
11.5	0.58	2.27	11.92
20.5	0.61	2.63	13.45
30.5	0.57	2.24	13.64
40.5	0.54	1.99	13.66
50.5	0.6	2.76	21.02
100.5	0.56	2.25	14.72

Core 182 – Mackinac Basin

Depth (cm)	d(10) (μm)	d(50) (μm)	d(90) (μm)
1.5	0.6	2.53	12.12
11.5	0.57	2.27	13.25
20.5	0.59	2.42	14.59
30.5	0.59	2.35	12.35
40.5	0.58	2.3	13.03
50.5	0.55	2.09	11.87
100.5	0.58	2.16	13.27

Core 821 – Saginaw Basin

Depth (cm)	d(10) (μm)	d(50) (μm)	d(90) (μm)
1.5	0.85	5.74	36.82
11.5	0.68	2.87	13.91
20.5	0.69	3.64	21.5
30.5	0.67	3.55	18.3
40.5	0.51	2.51	11.43
50.5	0.59	2.19	11.83
100.5	0.49	3.01	14.65

Core 817 – Alpena Basin

Depth (cm)	d(10) (μm)	d(50) (μm)	d(90) (μm)
1.5	0.39	1.93	7.89
11.5	0.63	2.71	14.87
20.5	0.81	4.13	16.3
30.5	0.82	7.1	213.8
40.5	0.6	2.43	13.12
50.5	0.63	3	16.61
100.5	0.73	3.13	13.64

Core 818-2 – Port Huron Basin

Depth (cm)	d(10) (μm)	d(50) (μm)	d(90) (μm)
20.5	0.94	3.47	16.54
50.5	0.82	4.95	27.78
100.5	0.64	3.11	35.8

Core 41 – Georgian Bay

Depth (cm)	d(10) (μm)	d(50) (μm)	d(90) (μm)
1.5	0.65	2.91	16.1
11.5	0.61	2.78	14.15
20.5	0.65	3.08	17.06
30.5	0.62	2.78	16.73
40.5	0.59	2.49	16.37
50.5	0.63	3.01	19.45
100.5	0.64	3.07	19.38

Appendix IV: Mineral percentages of sediments in all cores (594 – Goderich basin; 181 – Manitoulin basin; 182 Mackinac basin; 821 – Saginaw basin; 817 – Alpena basin; 818-2 – Port Huron basin; 41 – Georgian Bay) as determined by powder X-ray diffraction (p-XRD).

Core 594 – Goderich Basin

Weighted peak height (%)

Depth	Quartz	Plagioclase	Potassium-Feldspar	Kaolinite (0.7 nm)	Illite (1.0 nm)	Chlorite (1.4 nm)	Calcite	Dolomite	Amphibole
1.5	66	6	5	4	8	8	0	3	1
11.5	62	6	4	5	10	7	0	5	0
20.5	62	9	5	5	8	8	0	3	1
30.5	59	7	5	5	11	8	0	3	2
40.5	60	6	6	7	9	9	0	2	0
50.5	60	8	5	6	9	8	0	3	0
60.5	61	9	5	5	8	7	0	2	5

Core 181 – Manitoulin Basin

Weighted peak height (%)

Depth	Quartz	Plagioclase	Potassium-Feldspar	Kaolinite (0.7 nm)	Illite (1.0 nm)	Chlorite (1.4 nm)	Calcite	Dolomite	Amphibole
1.5	52	9	6	6	11	11	3	0	2
11.5	56	9	7	6	9	10	2	0	2
20.5	54	8	6	7	10	11	2	0	2
30.5	54	9	6	6	10	11	2	0	2
40.5	51	8	6	7	11	10	3	0	2
50.5	54	8	7	6	10	11	3	0	2
60.5	55	9	6	6	9	10	3	0	2
70.5	51	9	6	6	11	11	3	0	2
80.5	53	9	6	7	10	10	3	0	2
90.5	50	9	7	7	12	10	4	0	2
100.5	51	8	6	6	11	10	3	2	2

Core 182 – Mackinac Basin

Weighted peak height (%)

Depth	Quartz	Plagioclase	Potassium-Feldspar	Kaolinite (0.7 nm)	Illite (1.0 nm)	Chlorite (1.4 nm)	Calcite	Dolomite	Amphibole
1.5	57	9	6	6	11	10	0	0	2
11.5	57	9	6	5	11	10	0	0	2
20.5	57	9	5	5	9	9	3	0	2
30.5	54	11	6	7	8	8	3	0	2
40.5	58	9	5	5	9	8	3	0	2
50.5	54	9	6	5	10	11	3	0	2
60.5	52	9	6	6	10	11	3	0	3
80.5	54	9	6	6	10	10	3	0	2
90.5	55	8	6	6	11	10	2	0	2
100.5	60	8	7	5	8	9	3	0	1

Core 821 – Saginaw Basin

Weighted peak height (%)

Depth	Quartz	Plagioclase	Potassium-Feldspar	Kaolinite (0.7 nm)	Illite (1.0 nm)	Chlorite (1.4 nm)	Calcite	Dolomite	Amphibole
1.5	72	6	3	2	7	8	0	0	1
11.5	55	10	6	5	10	9	0	4	2
20.5	55	7	5	5	10	10	3	2	2
30.5	41	6	5	4	7	6	2	27	2
40.5	34	9	7	9	18	12	3	3	3
50.5	34	4	3	4	9	5	23	16	1
60.5	30	5	4	5	10	6	26	12	2
70.5	38	9	7	10	13	12	3	4	3
80.5	37	9	7	9	15	14	3	3	3
90.5	39	9	6	9	14	13	3	3	4
100.5	38	10	6	8	14	12	4	4	4

Core 817 – Alpena Basin

Weighted peak height (%)

Depth	Quartz	Plagioclase	Potassium-Feldspar	Kaolinite (0.7 nm)	Illite (1.0 nm)	Chlorite (1.4 nm)	Calcite	Dolomite	Amphibole
1.5	58	12	7	4	11	8	0	0	0
11.5	64	7	6	4	8	9	0	0	2
20.5	56	6	6	4	6	7	3	12	0
30.5	66	5	2	2	4	8	5	7	0
40.5	39	12	5	6	9	9	2	15	2
50.5	42	9	6	5	11	8	2	16	2
60.5	39	10	5	6	6	9	3	20	2
70.5	44	9	6	4	9	7	2	16	2
80.5	44	8	5	6	8	7	2	18	2
90.5	43	10	5	4	7	7	2	19	2
100.5	41	8	5	4	9	8	3	20	2

Core 818-2 – Port Huron Basin

Weighted peak height (%)

Depth	Quartz	Plagioclase	Potassium-Feldspar	Kaolinite (0.7 nm)	Illite (1.0 nm)	Chlorite (1.4 nm)	Calcite	Dolomite	Amphibole
20.5	69	7	5	4	5	8	0	0	1
30.5	64	6	5	5	7	9	0	3	2
40.5	66	11	6	4	4	8	0	0	1
50.5	66	6	4	4	8	8	2	0	2
60.5	59	9	5	5	9	7	2	2	2
70.5	69	6	4	4	7	7	0	2	1
80.5	65	5	5	4	8	8	0	4	2
90.5	68	5	4	4	9	7	0	3	1
100.5	58	6	4	5	9	8	3	5	2

Core 41 – Georgian Bay

Weighted peak height (%)

Depth	Quartz	Plagioclase	Potassium-Feldspar	Kaolinite (0.7 nm)	Illite (1.0 nm)	Chlorite (1.4 nm)	Calcite	Dolomite	Amphibole
1.5	50	10	6	7	12	12	0	0	3
11.5	47	9	6	7	10	11	3	3	3
20.5	46	9	6	7	10	12	4	3	3
30.5	46	10	7	6	13	12	4	0	3
40.5	46	10	7	8	12	11	4	0	3
50.5	45	11	7	7	14	10	4	0	3
60.5	50	10	6	6	12	10	4	0	2
70.5	49	10	6	6	12	11	4	0	3
80.5	45	15	6	7	10	11	3	0	3
90.5	48	10	6	6	11	13	3	0	2
100.5	44	10	7	6	11	16	3	0	2

Appendix V: Magnetic susceptibility measurements of all cores (594 – Goderich basin; 181 – Manitoulin basin; 182 Mackinac basin; 821 – Saginaw basin; 817 – Alpena basin; 818-2 – Port Huron basin; 41 – Georgian Bay).

Point Sensor Magnetic Susceptibility

Depth (cm)	Core 594 MS	Core 181 MS	Core 182 MS	Core 821 MS	Core 817 MS	Core 818-2 MS	Core 41 MS
0.5	15	6	16	1	7		6
1	21	8	19	13	8		7
1.5	28	6	22	32	8		7
2	25	6	20	46	8		8
2.5	24	7	20	51	8		9
3		9	12	112	6		12
3.5	32	11	12	104	6		11
4	35	11	14	53	6		10
4.5	36	11	12	39	6		10
5	36	11	9	24	9		11
5.5	35	9	5	6	9		12
6	33	8	4	0	7		14
6.5	32	8	6	0	10		16
7	31	9	6	-1	4		15
7.5	33	9	7	0			17
8	31	10	9	2			16
8.5	30	13	11	4			16
9	28	14	12	6	6		15
9.5	26	14	14	6	6		15
10	26	16	14	5	6		14
10.5	24	16	11	5	6		14
11	24	16	11	3	5		14
11.5	22	17	10	3	6		13
12	23	18	12	3	5		15
12.5	21	18	12	2	8		14
13	20	18	11	1	7		14
13.5	21	16	10	1	7		14
14	20	15	10	2	8		14
14.5	18	14	9	2	5		14
15	17	12	9	2	3		13
15.5	17	11	8	2	3		12
16	17	11	9	1	6		
16.5	17	11	10	2	6	11	
17	17	11	10	1	4	11	
17.5	17	12	11	1	4	11	
18	18	14	11	2	10	11	
18.5	18	12	10	1	5	11	13
19	17	10	11	1	4	10	13
19.5	16	9	11	0	5	8	13
20	15	11	10	0	7	8	11

Loop Sensor Magnetic Susceptibility

Depth (cm)	Core 821 MS	Core 817 MS	Core 41 MS
0.5	24	7	13
1	22	4	11
1.5	23	5	11
2	23	5	15
2.5	23	5	15
3	26	5	17
3.5	40	6	17
4	81	5	19
4.5	32	6	19
5	18	6	20
5.5	14	6	21
6	12	6	19
6.5	10	5	16
7	8	7	16
7.5	7		14
8	7		12
8.5	5	6	12
9	5	2	12
9.5	4	3	13
10	3	2	13
10.5	3	2	12
11	3	3	13
11.5	3	3	12
12	3	3	12
12.5	3	3	
13	3	4	12
13.5	3	3	11
14	2	3	11
14.5	2	3	12
15	2	4	12
15.5	2	4	12
16	2	4	11
16.5	2	4	11
17	3	4	10
17.5	2	5	10
18	2	4	11
18.5	2	5	13
19	2	5	11
19.5	2	5	10
20	2	6	10

Point Sensor Magnetic Susceptibility

Depth (cm)	Core 594 MS	Core 181 MS	Core 182 MS	Core 821 MS	Core 817 MS	Core 818-2 MS	Core 41 MS
20.5	17	11	11	1	12	9	10
21	16	8	11	1	13	9	11
21.5	16	11	12	2	14	9	11
22	17	12	12	3	15	10	12
22.5	16	11	10	3	14	11	10
23	16	11	11	2	14	12	10
23.5	16	10	11	2	13	24	9
24	15	11	11	3	14	11	9
24.5	15	11	11	2	11	12	10
25	18	10	10	3	5	13	10
25.5	17	10	9	4	4	10	
26	16	9	8	3	4	10	10
26.5	16	9	10	1	12	11	10
27	16	10	12	1	27	12	10
27.5	16	6	9	1	7	13	10
28	17	6	9	-1	11	11	10
28.5	16	7	9	-1	23	10	10
29	16	7	10	0	25	9	9
29.5	16	7	9	0	10	8	10
30	16	6	11	0	18	10	10
30.5	16	7	12	1	32	10	10
31	16	6	11	2	24	11	9
31.5	16	7	12	0	27	10	11
32	15	8	10	0	22	10	10
32.5	15	7	9	0	26	9	11
33	15	7	9	0	28	11	9
33.5	15	6	9	-1	32	11	9
34	15	8	8	0	27	10	9
34.5	15	6	10	0	27	10	10
35	16	6	9	0	30		9
35.5	16	6	9	0	30	10	10
36	15	4	9	2	32	9	10
36.5	15	4	10	2	30	9	12
37	17	5	13	2	29	10	13
37.5	16	5	13	1	27	10	10
38	16	5	13	2	28	10	11
38.5	15	4	12	1	28	10	10
39	16	7	13	2	28	10	10
39.5	15	8	8	1	29	11	11
40	16	11	12	1	30	11	11

Loop Sensor Magnetic Susceptibility

Depth (cm)	Core 821 MS	Core 817 MS	Core 41 MS
20.5	2	7	9
21	1	7	10
21.5	5	7	9
22		8	9
22.5	3	8	9
23	1	8	9
23.5	2	9	9
24	1	9	9
24.5	2	9	9
25	1	11	8
25.5	2	11	8
26	2	11	9
26.5	2	12	8
27	2	12	8
27.5	2	13	8
28	2	13	8
28.5	2	13	9
29	2	15	8
29.5	2	15	8
30	3	15	8
30.5	3	14	8
31	3	17	8
31.5	3	19	8
32	3	16	8
32.5	4	17	8
33	3	18	8
33.5	3	20	9
34	4	21	8
34.5	3	21	8
35	4	21	8
35.5	5	21	8
36	5	21	7
36.5	4	22	8
37	4	21	8
37.5	5	21	7
38	3	21	8
38.5	4	21	10
39	4	21	11
39.5	5	21	9
40	4	22	9

Point Sensor Magnetic Susceptibility

Depth (cm)	Core 594 MS	Core 181 MS	Core 182 MS	Core 821 MS	Core 817 MS	Core 818-2 MS	Core 41 MS
40.5	15	10	14	1	29	13	10
41	15	11	12	2	32	12	12
41.5	15	11	10	3	32	11	12
42	16	10	9	5	31	11	12
42.5	15	11	9	5	30	11	11
43	17	12	10	6	29	11	12
43.5	16	12	11	6	28	10	12
44	17	11	11	7	25	11	11
44.5	17	11	9	8	26	11	11
45	15	10	9	9	26	11	12
45.5	16	11	11	9	26	10	12
46	17	12	11	9	24	10	11
46.5	17	13	12	8	23	12	8
47	17	11	12	7	24	11	11
47.5	16	10	12	7	23	10	
48	17	8	11	4	22	11	
48.5	17	7	10	4	21	10	
49	16	8	10	6	25	10	11
49.5	17	10	9	7	28	12	13
50	17	12	8	8	25	11	13
50.5	16	11	9	7	29	10	12
51	17	12	10	6	29	10	13
51.5	16	11	9	3	27	9	12
52	16	12	8	1	27	10	10
52.5	14	12	8	3	25	9	10
53	15	10	8	5	25	9	10
53.5	16	12	9	7	28	9	10
54	16	12	11	6	43	9	10
54.5	16	12	9	6	32	10	12
55	16	13	10	6	28	9	13
55.5	17	12	9	5	29	9	13
56	16	11	10	4	29	9	12
56.5	16	13	9	4	25	10	12
57	17	13	10	4	24	11	12
57.5	16	12	11	3	25	10	13
58	15	12	12	2	24	9	13
58.5	16	13	12	2	25	10	13
59	15	12	11	3	22	9	13
59.5	16	12	10	2	24	10	12
60	18	12	12	4	25	10	13

Loop Sensor Magnetic Susceptibility

Depth (cm)	Core 821 MS	Core 817 MS	Core 41 MS
40.5	5	21	9
41	5	21	9
41.5	5	21	8
42	4	21	8
42.5	5	21	8
43	5	21	8
43.5	5	21	9
44	5	22	8
44.5	5	21	9
45	5	21	8
45.5	5	20	8
46	5	20	8
46.5	5	20	9
47	4	20	8
47.5	5	20	8
48	5	20	8
48.5	4	20	7
49	4	19	8
49.5	4	20	8
50	4	20	9
50.5	4	20	8
51	4	20	9
51.5	4	20	8
52	4	20	9
52.5	4	20	10
53	4	21	9
53.5	4	21	9
54	3	21	8
54.5	3	21	8
55	3	21	7
55.5	4	22	8
56	3	21	8
56.5	3	21	9
57	3	21	8
57.5	4	22	7
58	3	21	7
58.5	4	22	8
59	3	22	7
59.5	4	22	7
60	4	22	7

Point Sensor Magnetic Susceptibility								Loop Sensor Magnetic Susceptibility			
	Core 594	Core 181	Core 182	Core 821	Core 817	Core 818-2	Core 41		Core 821	Core 817	Core 41
Depth (cm)	MS	MS	MS	MS	MS	MS	MS	Depth (cm)	MS	MS	MS
60.5	16	11	13	6	26	10	12	60.5	4	22	7
61		12	11	6	24	10	11	61	4	23	8
61.5		13	12	5	24	12	12	61.5	4	23	8
62		11	12	1	27	12	11	62	4	22	7
62.5		12	10	2	27	13		62.5	5	22	8
63		11	10	2	24	11		63	4	22	8
63.5		12	11	3	20	9		63.5	4	22	8
64		11	13	3	23	11		64	5	23	8
64.5		11	12	5	19	13	14	64.5	5	22	9
65		11	12	5	24	11	14	65	6	22	7
65.5		11	10	4	24	11	12	65.5	5	22	8
66		11	11	6	24	10	13	66	5	22	8
66.5		12	10	5	24	10	12	66.5	6	22	8
67		12	8	6	25	12	13	67	6	22	7
67.5		11	7	5	25	11	13	67.5	6	21	7
68		12		6	23	10	12	68	6	22	7
68.5		12		5	24	11	12	68.5	6	22	7
69		11		6	25	9	12	69	6	22	7
69.5		11		6	25	11		69.5	6	23	7
70		11		6	25	11		70	6	22	6
70.5		12		8	26	12		70.5	6	23	7
71		12		6	27	11		71	6	22	
71.5		12		6	25	10	11	71.5	7	22	7
72		12		7	25	11	11	72	7	22	7
72.5		12		7	25	11	11	72.5	5	22	7
73		12		5	28	11	12	73	6	22	7
73.5		11		7	27	11	11	73.5	6	23	7
74		12		7	29	12	12	74	6	23	6
74.5		11		7	29	10	12	74.5	6	23	7
75		12		6	33	12	13	75	5	23	7
75.5		11		7	30	11	12	75.5	6	22	6
76		11		7	29	12	11	76	5	23	7
76.5		12		7	27	13	10	76.5	6	23	6
77		11		7	30	14	8	77	6	23	6
77.5		12		7	27	15	10	77.5	6	24	6
78		12		7	28	13	11	78	5	23	7
78.5		12		7	29	12	12	78.5	6	23	7
79		11	7	7	29	12	10	79	5	23	7
79.5		11	10	7	33	11		79.5	6	23	7
80		13	11	7	31	11		80	5	23	7

Point Sensor Magnetic Susceptibility

Depth (cm)	Core 594 MS	Core 181 MS	Core 182 MS	Core 821 MS	Core 817 MS	Core 818-2 MS	Core 41 MS
80.5		12	13	6	33	11	
81		12	11	7	33	11	
81.5		12	9	7	33	12	
82		12	11	7	31	10	
82.5		13	11	8	32	11	
83		12	12	7	33	11	
83.5		12	11	8	31	9	13
84		12	12	8	34	11	11
84.5		13	13	8	39	11	11
85		13	13	9	33	12	12
85.5		13	13	6	35	13	11
86		13	12	7	34	10	11
86.5		13	13	7	38	11	12
87		13	12	7	39	11	13
87.5		13	10	8	39	12	12
88		12	7	8	37	10	10
88.5		13	10	8	39	11	8
89		12	11	8	36	11	9
89.5		12	12	9	34	10	9
90		14	12	9	33	11	12
90.5		14	12	8	29	11	11
91		13	15	8	30	11	9
91.5		12	15	9	30	10	11
92		13	14	8	33	11	13
92.5		12	14	8	35	9	13
93		12	13	9	31	10	12
93.5		13	9	9	31	10	11
94		12	11	10	33	10	11
94.5		13	13	8	26	10	13
95		11	13	8		10	13
95.5		12	13	9	32	10	11
96		12	14	9	34	10	11
96.5		12	16	9	39	10	12
97		12	17	8	37	11	12
97.5		13	17	8	39	11	13
98		13	19	8	31	11	13
98.5		14	17	9	36	9	12
99		13	15	9	38	9	12
99.5		13	15	9	38	10	13
100		12	16	10	37	10	12
100.5		13	15	11	37	11	13

Loop Sensor Magnetic Susceptibility

Depth (cm)	Core 821 MS	Core 817 MS	Core 41 MS
80.5	5	23	7
81	6	23	7
81.5	6	24	7
82	6	24	8
82.5	6	24	7
83	6	24	7
83.5	5	24	7
84	6	25	7
84.5	5	25	7
85	6	25	7
85.5	5	25	7
86	6	25	7
86.5	6	26	8
87	6	25	8
87.5	5	25	8
88	6	25	7
88.5	6	26	7
89	6	25	8
89.5	6	25	7
90	6		7
90.5	6	24	7
91	6	25	7
91.5	6	25	7
92	7	25	8
92.5	6	24	8
93	6	24	7
93.5	7	24	8
94	6	23	7
94.5	6	24	7
95	6	24	7
95.5	7	22	8
96	6	23	7
96.5	6	23	7
97	6	23	7
97.5	6	23	7
98	6	24	7
98.5	7	25	8
99	7	25	7
99.5	6	25	8
100	7	25	7
100.5	7	25	7

Appendix VI: Bulk organic matter carbon and nitrogen elemental and isotope compositions including calculated molar carbon to nitrogen ratios.

594 - Goderich Basin

Depth (cm)	$\delta^{13}C_{OM}$ (‰, VPDB)	TOC (%)	$\delta^{15}N_{TN}$ (‰, AIR)	TN (%)	C/N
0.5	–24.71	3.93	+5.17	0.49	9.3
1.5	–24.89	3.86	+5.06	0.48	9.3
3.5	–25.05	3.78	+4.89	0.47	9.4
5.5	–25.33	3.81	+5.17	0.45	9.9
7.5	–25.48	3.78	+5.02	0.43	10.1
9.5	–25.59	3.79	+4.72	0.43	10.4
11.5	–26.24	3.81	+4.66	0.47	9.5
13.5	–26.51	3.82	+4.34	0.48	9.2
15.5	–26.45	3.76	+4.44	0.48	9.2
20.5	–26.53	4.05	+4.54	0.51	9.3
25.5	–26.55	3.90	+4.48	0.49	9.2
30.5	–26.27	3.85	+4.47	0.49	9.2
35.5	–26.24	3.87	+4.50	0.49	9.2
40.5	–26.17	3.98	+4.61	0.49	9.4
45.5	–26.52	3.70	+4.60	0.47	9.3
50.5	–26.41	3.84	+4.64	0.48	9.3
55.5	–26.53	3.84	+4.66	0.48	9.3
60.5	–26.46	3.94	+4.95	0.48	9.5

181 - Manitoulin Basin

Depth (cm)	$\delta^{13}C_{OM}$ (‰, VPDB)	TOC (%)	$\delta^{15}N_{TN}$ (‰, AIR)	TN (%)	C/N
0.5	–25.53	2.90	+6.33	0.38	9.0
1.5	–25.86	2.77	+6.14	0.38	8.6
3.5	–26.11	2.72	+6.12	0.36	8.7
5.5	–26.10	2.82	+5.98	0.36	9.1
7.5	–26.28	2.79	+5.84	0.36	9.1
9.5	–26.25	2.77	+5.85	0.34	9.4
11.5	–26.34	2.68	+5.92	0.34	9.3
13.5	–26.58	2.72	+6.24	0.32	9.9
15.5	–26.58	2.76	+6.19	0.33	9.9
20.5	–26.78	2.95	+6.03	0.35	9.9
25.5	–27.17	2.88	+5.62	0.36	9.3
30.5	–26.89	2.67	+5.41	0.35	8.8
35.5	–26.94	2.72	+5.30	0.36	8.9
40.5	–26.82	2.54	+5.27	0.34	8.6
45.5	–26.88	2.58	+5.38	0.35	8.6
50.5	–26.66	2.62	+5.53	0.35	8.7
55.5	–26.39	2.68	+5.55	0.35	8.8
60.5	–26.70	2.54	+5.59	0.34	8.8
65.5	–26.61	2.58	+5.48	0.34	8.9
70.5	–26.78	2.69	+5.62	0.35	9.0
75.5	–26.76	2.63	+5.88	0.34	9.0
80.5	–26.64	2.67	+5.82	0.34	9.2
85.5	–26.69	2.68	+6.01	0.35	9.0
90.5	–26.72	2.63	+5.98	0.34	9.0
95.5	–26.71	2.54	+5.83	0.34	8.8
100.5	–26.84	2.59	+5.78	0.33	9.2

182 - Mackinac Basin

Depth (cm)	$\delta^{13}C_{OM}$ (‰, VPDB)	TOC (%)	$\delta^{15}N_{TN}$ (‰, AIR)	TN (%)	C/N
0.5	–24.45	3.14	+5.51	0.36	10.3
1.5	–24.85	2.81	+5.79	0.34	9.5
3.5	–25.45	3.04	+5.67	0.37	9.6
5.5	–25.96	3.05	+5.25	0.38	9.4
7.5	–25.76	2.92	+5.07	0.39	8.7
9.5	–25.87	2.70	+5.00	0.37	8.6
11.5	–25.88	2.64	+5.15	0.36	8.6
13.5	–25.85	2.82	+5.16	0.37	8.9
15.5	–25.79	2.78	+5.40	0.37	8.8
20.5	–26.03	2.65	+5.50	0.35	8.9
25.5	–25.85	2.89	+5.66	0.37	9.2
30.5	–25.92	2.80	+5.93	0.34	9.5
35.5	–25.79	2.94	+6.02	0.37	9.2
40.5	–25.77	2.68	+5.99	0.34	9.1
45.5	–25.93	2.77	+5.90	0.34	9.5
50.5	–25.91	2.60	+5.96	0.31	9.7
55.5	–26.03	2.45	+6.00	0.30	9.7
60.5	–25.94	2.16	+6.06	0.26	9.6
65.5	–25.82	2.07	+5.97	0.26	9.4
80.5	–25.82	1.85	+5.63	0.22	9.7
85.5	–25.71	1.70	+6.09	0.19	10.5
90.5	–25.79	1.55	+5.77	0.17	10.5
95.5	–26.07	1.44	+5.66	0.17	9.9
100.5	–26.32	1.40	+5.11	0.16	9.9

821 - Saginaw Basin

Depth (cm)	$\delta^{13}C_{OM}$ (‰, VPDB)	TOC (%)	$\delta^{15}N_{TN}$ (‰, AIR)	TN (%)	C/N
0.5	–24.36	3.70	+5.98	0.45	9.7
1.5	–24.58	2.56	+6.02	0.38	7.9
3.5	–24.06	0.64	+5.13	0.06	11.8
5.5	–25.52	1.23	+4.69	0.13	10.9
7.5	–25.83	1.40	+4.54	0.15	11.1
9.5	–26.28	1.83	+4.35	0.19	11.1
11.5	–26.32	2.38	+4.05	0.24	11.5
13.5	–26.45	2.78	+3.86	0.28	11.6
15.5	–26.84	2.21	+3.97	0.25	10.4
20.5	–26.79	2.33	+3.82	0.25	11.0
25.5	–26.96	2.05	+3.98	0.22	10.7
30.5	–27.39	1.65	+3.68	0.17	11.5
35.5	–26.03	1.05	+4.36	0.14	8.9
40.5	–26.07	1.03	+4.83	0.13	9.3
45.5	–26.54	1.35	+4.58	0.14	11.4
50.5	–26.80	1.73	+3.49	0.16	12.5
55.5	–27.08	1.54	+3.46	0.15	11.9
60.5	–27.37	1.30	+3.31	0.12	12.5
65.5	–27.60	1.13	+3.90	0.12	10.7
70.5	–26.67	1.16	+4.77	0.13	10.8
75.5	–26.79	1.15	+5.14	0.13	10.5
80.5	–26.61	1.13	+5.06	0.13	10.2
85.5	–26.84	1.19	+4.87	0.13	10.9
90.5	–27.00	1.20	+4.81	0.13	11.0
95.5	–27.15	1.18	+4.70	0.13	10.7
100.5	–27.16	1.30	+4.61	0.13	11.6

817 - Alpena Basin

Depth (cm)	$\delta^{13}C_{OM}$ (‰, VPDB)	TOC (%)	$\delta^{15}N_{TN}$ (‰, AIR)	TN (%)	C/N
0.5	–23.50	1.48	+6.05	0.16	10.5
1.5	–23.88	1.39	+5.99	0.16	10.0
3.5	–24.28	1.33	+5.83	0.16	9.8
5.5	–24.85	1.39	+5.64	0.17	9.8
7.5	–25.08	1.51	+5.61	0.17	10.2
9.5	–25.11	1.62	+5.68	0.18	10.6
11.5	–25.28	1.72	+5.62	0.18	11.1
13.5	–25.46	1.61	+5.49	0.17	11.0
15.5	–25.49	1.65	+5.31	0.18	10.5
20.5	–25.87	1.46	+5.00	0.15	11.1
25.5	–26.34	0.74	+4.91	0.07	11.9
30.5	–28.09	0.12		0.02	7.7
35.5	–27.70	0.15		0.02	7.6
40.5	–27.78	0.15		0.02	8.0
45.5	–27.58	0.14		0.02	7.0
50.5	–27.65	0.13		0.02	7.2
55.5	–26.61	0.18		0.03	8.2
60.5	–26.72	0.19		0.03	8.8
65.5	–27.31	0.14		0.02	7.7
70.5	–27.49	0.17		0.02	8.4
75.5	–27.10	0.19		0.03	8.7
80.5	–27.01	0.16		0.02	8.6
85.5	–27.46	0.14		0.02	8.6
90.5	–27.27	0.17		0.02	9.4
95.5	–27.89	0.15		0.02	8.8
100.5	–27.64	0.16		0.02	9.6

818-2 - Port-Huron Basin

Depth (cm)	$\delta^{13}C_{OM}$ (‰, VPDB)	TOC (%)	$\delta^{15}N_{TN}$ (‰, AIR)	TN (%)	C/N
20.5	–25.50	4.35	+4.88	0.56	9.1
25.5	–25.61	3.41	+4.89	0.43	9.3
30.5	–25.68	3.79	+4.78	0.50	8.9
35.5	–25.71	3.68	+4.94	0.47	9.1
40.5	–26.21	2.80	+4.82	0.40	8.1
45.5	–25.87	3.68	+4.85	0.45	9.5
50.5	–26.60	3.48	+4.86	0.42	9.6
55.5	–26.04	3.38	+4.64	0.41	9.5
60.5	–26.13	3.03	+4.73	0.40	8.8
65.5	–26.12	2.90	+4.66	0.39	8.6
70.5	–26.23	2.60	+4.49	0.36	8.4
75.5	–26.14	2.80	+4.50	0.35	9.2
80.5	–25.85	2.77	+4.67	0.35	9.2
85.5	–26.00	2.67	+4.83	0.32	9.7
90.5	–25.81	2.89	+4.75	0.35	9.6
95.5	–25.84	2.66	+4.59	0.31	10.0
100	–26.17	2.06	+4.46	0.29	8.2

41 - Georgian Bay

Depth (cm)	$\delta^{13}C_{OM}$ (‰, VPDB)	TOC (%)	$\delta^{15}N_{TN}$ (‰, AIR)	TN (%)	C/N
0.5	–25.01	2.89	+5.01	0.40	8.4
1.5	–25.29	2.91	+5.29	0.38	9.0
3.5	–25.20	2.95	+4.98	0.39	8.9
5.5	–25.19	2.80	+5.23	0.36	9.2
7.5	–25.53	2.58	+5.64	0.31	9.6
9.5	–25.58	2.63	+5.60	0.32	9.6
11.5	–25.69	2.62	+5.65	0.32	9.6
13.5	–25.90	2.76	+5.61	0.33	9.7
15.5	–25.71	2.78	+5.30	0.35	9.3
20.5	–26.16	2.57	+5.30	0.33	9.0
25.5	–25.92	2.39	+4.64	0.32	8.6
30.5	–25.95	2.30	+4.62	0.32	8.4
35.5	–25.95	2.29	+4.34	0.31	8.7
40.5	–25.64	2.34	+4.28	0.31	8.8
45.5	–25.55	2.50	+4.50	0.32	9.0
50.5	–25.54	2.52	+4.80	0.32	9.1
55.5	–25.53	2.55	+4.74	0.33	9.1
60.5	–25.78	2.30	+4.92	0.31	8.7
65.5	–25.55	2.27	+5.25	0.31	8.6
70.5	–25.68	2.18	+5.09	0.29	8.8
75.5	–25.64	2.23	+5.07	0.30	8.5
80.5	–25.80	2.24	+5.19	0.29	8.9
85.5	–25.73	2.23	+5.27	0.30	8.7
90.5	–25.70	2.28	+5.36	0.30	8.9
95.5	–25.70	2.37	+5.18	0.32	8.6
100.5	–25.63	2.36	+5.34	0.31	8.9

Curriculum Vitae

Name: Jamal Nigim

Post-secondary Education and Degrees:

The University of Western Ontario
London, Ontario, Canada
2017–present; M.Sc. Geology

The University of Western Ontario
London, Ontario, Canada
2010–2015; B.Sc. (Honours) Geology

Honours and Awards:

Arcangelo Rea Family Foundation Graduate Scholarship
2019
Robert W. Hodder Travel Bursary
2019
Ontario Graduate Scholarship
2018
Mary Ann Underwood Small Global Opportunities Award
2017
Aleksis Dreimanis Prize
2014
AMBI Undergraduate Research Award Recipient
2014
J.P. Bickell Foundation Mining Scholarship
2014
Robert and Ruth Lumsden Undergraduate Award in Earth Science
2013, 2014
Laurene Paterson Estate Scholarship
2013
Roma Fence Group of Companies Scholarship in Mining and Mineral
Exploration
2013

Related Work Experience:

Teaching and Research Assistant
The University of Western Ontario
2017 – 2019

Research Assistant
Surface Science Western
Sept. – Dec. 2015

Research Assistant
The University of Western Ontario
May – Aug. 2014